Title
Metric Algebraic Geometry

Permalink
https://escholarship.org/uc/item/06x8f0mg

Author
Weinstein, Madeleine Aster

Publication Date
2021

Peer reviewed|Thesis/dissertation

Metric Algebraic Geometry

by

Madeleine Aster Weinstein

A dissertation submitted in partial satisfaction of the

requirements for the degree of

Doctor of Philosophy

in

Mathematics

in the

Graduate Division

of the

University of California, Berkeley

Committee in charge:

Professor Bernd Sturmfels, Chair
Associate Professor Adityanand Guntuboyina
Professor David Nadler

Spring 2021

Metric Algebraic Geometry

Abstract

Metric Algebraic Geometry

by

Madeleine Aster Weinstein

Doctor of Philosophy in Mathematics

University of California, Berkeley

Professor Bernd Sturmfels, Chair

Algebraic geometry is the study of algebraic varieties, zero sets of systems of polynomial equations. Metric algebraic geometry concerns properties of real algebraic varieties that depend on a distance metric. Applications are seen in distance optimization and the geometry of data.

Algebraic geometry provides a useful perspective on distance optimization. We study variations of the *nearest point problem*, which is stated as follows: given a subset $S \subset \mathbb{R}^n$ and point $p \notin S$, find a point in S of minimal distance to p. An inverse to the nearest point problem can be stated as follows: Suppose now that $p \in S$. Describe the subset of $\mathbb{R}^n$ consisting of points that are closer to p than to any other point of S. This subset is called the *Voronoi cell* of p with respect to S. We study its algebraic boundary. Voronoi cells enable us to create algorithms to approximate several metric features of varieties S. *Bottlenecks* are pairs of points on an algebraic variety that are critical points of the distance function between pairs of distinct points on the variety. We study the *bottleneck variety* consisting of such points and prove a formula for its degree.

Algebraic geometry informs the computational study of data. We study the algebraic geometry of the *offset hypersurface*, the locus of all points at some fixed distance from a given variety. The offset hypersurface allows us to prove the algebraicity of two quantities central to the computation of persistent homology, a method at the heart of topological data analysis. Conversely, numerical and symbolic computational methods yield insight in the analysis of algebraic varieties. We use numerical methods to show that the degree of the Zariski closure of the orbit of a general cubic surface under the action of the projective linear group is 96120. We pair representation theory and numerical algebraic geometry to investigate the real algebraic variety of real symmetric matrices with eigenvalue multiplicities specified by a given partition.

Taken together, the results show the power of combining algebraic geometry and numerical methods to produce insights for problems related to distance and metrics.

To Pumpkin π

Contents

Acknowledgments

Many people have supported me throughout my time in graduate school. I would like to thank my academic family for giving me a research community. At every step of graduate school, I have relied on the example and support of my academic sister Maddie Brandt. Thank you to Bernd Sturmfels for inspiring and cultivating a mathematical community that nurtures young researchers. Thank you to my coauthors: Maddie Brandt, Paul Breiding, Laura Brustenga i Moncusí, Diego Cifuentes, Sandra Di Rocco, David Eklund, Emil Horobeţ, Sara Kalisnik, Kristian Ranestad, Bernd Sturmfels, and Sascha Timme. In particular, I am grateful to my senior coauthors Paul Breiding, David Eklund, and Kristian Ranestad for being so generous with their time as they educated me in their areas of expertise. I am grateful to my peer coauthors for bringing fun and energy to our collaborations. Thank you to the members of the Noetherian Ring, who go above and beyond any reasonable requirements of their jobs to improve the climate and culture of the mathematics community and work towards equity and inclusion. I have been particularly inspired and uplifted by the efforts of Maddie Brandt and Mariel Supina. I am also deeply grateful to the woman mathematicians who paved the way for our cohort. Thank you to Judie Filomeo, Vicky Lee, and Marsha Snow for enabling the math department at UC Berkeley to function, and Saskia Gutzschebauch for doing the same at MPI Leipzig. Thank you to the math department at Harvey Mudd College, and in particular Dagan Karp and Talithia Williams, for guiding me on my journey from calculus student to graduate student. Thank you to the AAAS Ambassador community for amazing me every day. Thank you to my roommates Esme, Maddie, and Mariel for helping turn Berkeley into my home. Thank you to my family for supporting me in all of my pursuits. Thank you to Hailey, Kathryn, Kayla, and Shifrah for holding the door open for me to the world outside of mathematics. Thank you to my canine companions: Dolce Galileo, Fido, William, Chenille, Bean, and Pumpkin. No matter how short our time together, each of you has a special place in my heart.

Chapter 1

Introduction

Metric algebraic geometry arose out of a desire to bring the perspective and tools of algebraic geometry to the objects of differential geometry that arise in applications concerning the geometry of data. The necessity of bringing together such tools can be understood through the story of the reach of an algebraic variety.

First introduced by Federer in 1959, the reach is an invariant of a subset $S \subset \mathbb{R}^n$ that characterizes the difficulty of performing calculations in computational geometry [97]. The reach of S is the maximum distance from S such that every point of $\mathbb{R}^n$ within this distance has a unique nearest point in S. Sets with nonzero reach are close to being differential.

In Section 4.2, we prove that the reach of an algebraic variety is a number algebraic over the field of definition of the variety. With this knowledge comes the hope of finding an algebraic characterization of the reach; that is, given an algebraic variety, can we find equations for the subvariety of points critical to the computation of the reach? It can be shown that the reach of a variety is the minimum of two quantities: the minimal radius of curvature of a geodesic of the variety and half of the narrowest *bottleneck distance* on the variety. Thus, we set out to provide algebraic characterizations of these two quantities. Finding an algebraic characterization of curvature is the subject of Chapter 3. To obtain an algebraic characterization of bottlenecks, as we do in Section 2.2, we follow the lead of the paper [86], which lays out a framework for finding critical points of distance optimization problems on algebraic varieties by defining the *Euclidean distance degree*. This is the subject of Section 1.1.

Once we have algebraic characterizations of curvature and bottlenecks, we ask for the degree of the associated algebraic varieties. The degree is a measure of algebraic complexity, which is a proxy for computational difficulty. The field of *intersection theory* provides methods for finding the degree of an algebraic variety. This is the topic of Section 1.2.

Having found equations for these varieties and characterized the difficulty of computations, we wish to perform these computations and find specific points on given algebraic varieties. For this, we turn to the field of *numerical algebraic geometry*, the topic of Section 1.3.

Reach exemplifies the spirit of metric algebraic geometry because it plays an important role in the geometry of data analysis. It determines the sampling density required for the method of *persistent homology* to successfully characterize the topology of a manifold. We provide background

information on persistent homology in Section 1.4.

1.1 Euclidean Distance Degree

Let $X \subset \mathbb{R}^n$ be a variety and $u \in \mathbb{R}^n$. The nearest point problem asks what point or points of X are closest to u. Algebraic conditions are unable to distinguish between types of critical points, so we reformulate the problem as follows. Define a function $d_u(x) : X \longrightarrow \mathbb{R}$ by

$$d_u(x) = (x_1 - u_1)^2 + \cdots + (x_n - u_n)^2.$$

Then $d_u(x)$ is the square of the Euclidean distance from u to x. We seek to find the critical points of the function d_u. We now describe the construction of the ideal whose variety consists of these critical points. We follow [86].

Let $I_X = \langle f_1, \ldots, f_s \rangle \subset \mathbb{R}[x_1, \ldots, x_n]$ and $X = V(I_X) \subset \mathbb{C}^n$. We denote by $J(f)$ the $s \times n$ Jacobian matrix whose entry in row i and column j is the partial derivative $\partial f_i / \partial x_j$. Let c be the codimension of X. The singular locus X_{sing} of X is defined by

$$I_{X_{\text{sing}}} = I_X + \langle c \times c - \text{minors of } J(f) \rangle.$$

We exclude the singular locus of X from our analysis.

To characterize the idea of criticality, we use Lagrange multipliers. Lagrange multipliers is a method for finding optimal values of a function subject to constraints. Here, we wish to optimize d_u given that $x \in X \setminus X_{sing}$. The key insight of Lagrange multipliers is that at a critical point, the gradient of d_u will be contained in the normal space of X. Up to scaling, the gradient of d_u is $u - x$. So at a critical value of x, the vector $u - x$ is in the span of the matrix $J(f)$. The *critical ideal* for $u \in \mathbb{C}^n$ is the ideal obtained from the following saturation:

$$\left(I_X + \left\langle (c+1) \times (c+1) - \text{minors of } \begin{pmatrix} u - x \\ J(f) \end{pmatrix} \right\rangle \right) : (I_{X_{\text{sing}}})^\infty$$

In [86], it is proved that for general $u \in \mathbb{C}^n$, the variety of the critical ideal contains a finite number of complex solutions and that this number is independent of a choice of $u \in \mathbb{C}^n$. It is called the *Euclidean distance degree* of X.

So far, we have defined the Euclidean distance degree in affine space. However, in algebraic geometry it is often preferable to work with projective varieties. The concept of Euclidean distance does not translate well to projective space. See Section 4.1 for a discussion of metrics in projective space. The Euclidean distance degree of a projective variety is defined as the Euclidean distance degree of its affine cone.

1.2 Intersection Theory

Intersection theory is the study of how varieties intersect. In the case where two varieties intersect in finitely many points, we may wish to know how many points. One of the first examples of intersection theory that students encounter is the Fundamental Theorem of Algebra, which states that

a polynomial of degree d over an algebraically closed field has d roots, counted with multiplicity. Later in our mathematical studies, we generalize this to Bézout's Theorem, which states that curves of degree d and degree e in general position in the projective plane over an algebraically closed field intersect in de points, again counted with multiplicity.

In this section we will encounter a far-reaching generalization of Bézout. The *Chow ring* will enable us to turn geometric questions about intersections into algebraic ones; in particular, intersection will correspond to multiplication. *Chern classes* will generalize degree as a way to encode the invariants of a variety relevant to its intersection properties. We apply the Chow ring and Chern classes to present Porteous' formula, which is used to obtain the degree of determinantal varieties.

Chow ring

Let X be an algebraic variety over an algebraically closed field k of characteristic 0. We will now define the Chow ring of X, following [92, Section 1.2].

The *group of cycles* on X, denoted $Z(X)$, is the free abelian group generated by the set of subvarieties of X. The group $Z(X)$ is graded by dimension: we write $Z_k(X)$ for the group of cycles that are formal linear combinations of subvarieties of dimension k (these are called *k-cycles*), so that $Z(X) = \bigoplus_k Z_k(X)$. A cycle $Z = \sum n_i Y_i$, where the Y_i are subvarieties, is *effective* if the coefficients n_i are all nonnegative. A *divisor* (sometimes called a *Weil divisor*) is an $(n-1)$-cycle on a pure n-dimensional variety.

Let $\mathrm{Rat}(X) \subset Z(X)$ be the group generated by differences of the form

$$\langle \Phi \cap (t_0 \times X) \rangle - \langle \Phi \cap (t_1 \times X) \rangle,$$

where $t_0, t_1 \in \mathbb{P}^1$ and Φ is a subvariety of $\mathbb{P}^1 \times X$ not contained in any fiber $\{t\} \times X$. We say that two cycles are rationally equivalent if their difference is in $\mathrm{Rat}(X)$. The *Chow group* of X is the quotient

$$A(X) = Z(X)/\mathrm{Rat}(X),$$

the group of rational equivalence classes of cycles on X. If $Y \in Z(X)$ is a cycle, we write $[Y] \in A(X)$ for its equivalence class.

It can be shown that $A(X)$ is graded by dimension; that is,

$$A(X) = \oplus A_k(X),$$

where $A_k(X)$ is the group of rational equivalence classes of k-cycles.

The subvarieties A, B of a variety X *intersect transversely* at a point p if A, B and X are all smooth at p and

$$\mathrm{codim}(T_p A \cap T_p B) = \mathrm{codim}(T_p A) + \mathrm{codim}(T_p B).$$

The subvarieties $A, B \subset X$ are *generically transverse*, or *intersect generically transversely*, if they meet transversely at a general point of each component C of $A \cap B$. Two cycles $A = \sum n_i A_i$ and $B = \sum m_j B_j$ are generically transverse if each A_i is generically transverse to each B_j.

The following theorem enables us to define the Chow ring. It is a generalization of Bézout's theorem.

Theorem 1.2.1. *If X is a smooth quasi-projective variety, then there is a unique product structure on $A(X)$ such that if two subvarieties A, B of X are generically transverse, then*

$$[A][B] = [A \cap B].$$

This structure makes

$$A(X) = \bigoplus_{c=0}^{\dim(X)} A^c(X)$$

into an associative, commutative ring, graded by codimension, called the Chow ring of X.

The main idea in the proof is the Moving Lemma, which states the following: For every two subvarieties A and B, we can find a subvariety A' that is rationally equivalent to A and intersects B generically transversally. The class $[A' \cap B]$ is independent of our choice of A'.

The Chow ring enables a new interpretation of Bézout's theorem. Namely, Bézout's theorem computes the Chow ring of the projective plane: $A(\mathbb{P}^2) = \mathbb{Z}[h]/\langle h^3 \rangle$, where $h = [\mathbb{P}^1]$ is the class of a line. In other words, a curve of degree d is rationally equivalent to the cycle defined by a union of d lines, and two curves of degree d and e intersect in de points, just as a union of d lines and a union of e lines.

Chern classes

Let $\mathscr{E}$ be a vector bundle of rank r on a variety X of dimension n. In most of our examples, we take $\mathscr{E}$ to be the tangent bundle on X. Corresponding to the vector bundle $\mathscr{E}$ are certain special classes in the Chow ring of X: we now define the Chern classes $c_i(\mathscr{E}) \in A_{n-i}(X)$. Our exposition follows [91][Section 5.2].

We first consider the case $r = 1$, that is $\mathscr{E} = \mathscr{L}$ is a line bundle on X. We define

$$c_1(\mathscr{L}) = [\mathrm{Div}(\tau)] \in A_{n-1}(X)$$

where τ is any rational section of $\mathscr{L}$ and $c_i(\mathscr{L}) = 0$ for $i \geq 2$.

Now let $r > 1$. Let $\tau_0, \ldots, \tau_{r-1}$ be general sections of $\mathscr{E}$. For any i, consider the scheme where $r - i$ general sections of $\mathscr{E}$ fail to be dependent, defined by the vanishing of

$$\tau_0 \wedge \cdots \wedge \tau_{r-i} \in \bigwedge^{r-i+1} \mathscr{E}.$$

This is called the *degeneracy locus* of the sections $\tau_0, \ldots, \tau_{r-i}$.

We now characterize the Chern classes $c_i(\mathscr{E}) \in A^i(X)$ for vector bundles $\mathscr{E}$ on smooth varieties X and integers $i \geq 0$:

Theorem 1.2.2. *There is a unique way of assigning to each vector bundle $\mathscr{E}$ on a smooth quasi-projective variety X a class $c(\mathscr{E}) = 1 + c_1(\mathscr{E}) + c_2(\mathscr{E}) + \cdots \in A(X)$ such that:*

(a) If $\mathscr{L}$ is a line bundle on X, then the Chern class of $\mathscr{L}$ is $1 + c_1(\mathscr{L})$, where $c_1(\mathscr{L}) \in A^1(X)$ is the class of the divisor of zeros minus the divisor of poles of any rational section of $\mathscr{L}$.

(b) If $\tau_0, \ldots, \tau_{r-i}$ are global sections of $\mathscr{E}$, and the degeneracy locus D where they are dependent has codimension i, then $c_i(\mathscr{E}) = [D] \in A^i(X)$.

(c) If

$$0 \longrightarrow \mathscr{E} \longrightarrow \mathscr{F} \longrightarrow \mathscr{G} \longrightarrow 0$$

is a short exact sequence of vector bundles on X, then

$$c(\mathscr{F}) = c(\mathscr{E})c(\mathscr{G}) \in A(X).$$

(d) If $\phi : Y \longrightarrow X$ is a morphism of smooth varieties, then

$$\phi^*(c(\mathscr{E})) = c(\phi^*(\mathscr{E})).$$

In future chapters, we make frequent use of Chow rings and Chern classes to determine formulas for the degrees of varieties.

Porteous' formula

We now describe an application of intersection theory to find the degree of a determinantal variety. We follow [91, Chapter 12].

As we just saw, when a vector bundle $\mathscr{F}$ of rank f on a smooth variety X is generated by global section, the Chern class $c_i(\mathscr{F})$ is the class of the scheme where $e = f - i + 1$ general sections of $\mathscr{F}$ become dependent. Specifically, if the locus where a map

$$\phi : \mathscr{O}_X^e \longrightarrow \mathscr{F}$$

fails to have maximal rank has the expected codimension i, then $c_i(\mathscr{F})$ is the class of the scheme that is locally defined by the $e \times e$ minors of a matrix representing ϕ. Let $\mathscr{E}$ be a vector bundle of rank e. Let $k \leq \min(e, f)$. We now consider the more general case of the class of the scheme $M_k(\phi)$ where a map of vector bundles $\phi : \mathscr{E} \longrightarrow \mathscr{F}$ has rank $\leq k$, locally defined by the ideal of the $(k+1) \times (k+1)$ minors of a matrix representation. If X is an affine space of dimension ef and ϕ_{gen} is the map defined by an $f \times e$ matrix of variables, the codimension of the locus $M_k(\phi_{\text{gen}})$ is $(e-k)(f-k)$.

We first establish notation required to state the next theorem. For any sequence of elements $\gamma := (\gamma_0, \gamma_1, \ldots)$ in a commutative ring and any natural numbers e, f, we set $\Delta_f^e(\gamma) = \det \mathbb{D}_f^e(\gamma)$, where

$$\mathbb{D}_f^e(\gamma) := \begin{pmatrix} \gamma_f & \gamma_{f+1} & \cdots & \cdots & \gamma_{e+f-1} \\ \gamma_{f-1} & \gamma_f & \cdots & \cdots & \gamma_{e+f-2} \\ \vdots & \vdots & \ddots & & \vdots \\ \vdots & \vdots & & \ddots & \vdots \\ \gamma_{f-e+1} & \gamma_{f-e+2} & \cdots & \cdots & \gamma_f \end{pmatrix}.$$

Let $a(t) = 1 + a_1 t + \cdots + a_e t^e$ and $b(t) = 1 + b_1 t + \cdots + b_f t^f$ be polynomials with constant coefficient 1. We denote by $\frac{a(t)}{b(t)}$ the sequence of coefficients $(1, c_1, c_2, \dots)$ of the formal power series $a(t)/b(t) = 1 + c_1 t + c_2 t^2 + \cdots$.

Theorem 1.2.3. *(Porteous' formula). Let $\phi : \mathscr{E} \rightarrow \mathscr{F}$ be a map of vector bundles of ranks e and f on a smooth variety X. If the scheme $M_k(\phi) \subset X$ has codimension $(e-k)(f-k)$, then its class is given by*

$$[M_k(\phi)] = \Delta_{f-k}^{e-k} \left[\frac{c(\mathscr{F})}{c(\mathscr{E})} \right].$$

We use Theorem 1.2.3 to compute the degree of determinantal varieties. We are often able to characterize geometric conditions in terms of linear dependence of forms, using Lagrange multipliers as explained in Section 1.1 of this dissertation. Thus this formula is an important tool.

1.3 Numerical Algebraic Geometry

Numerical algebraic geometry concerns numerical computations of objects describing algebraic sets defined over subfields of the complex numbers. The most basic of these objects are the *solution sets*, a data structure for representing solutions to polynomial systems. The term "numerical" refers to computations which are potentially inexact (e.g., floating-point arithmetic). However, this does not necessarily mean that the results obtained are unreliable. The certification of solutions plays an important role in the field. For a more in-depth definition and a brief history of numerical algebraic geometry see [113]. A comprehensive introduction to the subject is available in [176]. This section is adapted from [46] which is joint work with Laura Brustenga i Moncusí and Sascha Timme.

We now introduce tools from numerical algebraic geometry needed to compute and certify the degree of an algebraic variety. We fix a system of polynomials $F = (F_1, \dots, F_m)$ in n variables and assume that it has l isolated solutions $p_1, \dots, p_l \in \mathbb{C}^n$.

Homotopy continuation. Numerical homotopy continuation [176, Section 8.4.1] is a fundamental method that underlies most of numerical algebraic geometry. The general idea is as follows. Suppose we want to compute the isolated solutions of F. We build a homotopy $H(x,t) : \mathbb{C}^n \times \mathbb{C} \rightarrow \mathbb{C}^m$ which deforms a system of polynomials $G(x) = H(x,0)$ whose isolated solutions are known or easily computable into the system $F(x) = H(x,1)$. A well-defined homotopy requires that G has at least as many isolated solutions as F so that we are able to compute *all* isolated solutions of F. Given a solution x_0 of G, there is a solution path $x(t) : \mathbb{C} \rightarrow \mathbb{C}^n$, which is a curve implicitly defined by the conditions $x(0) = x_0$ and $H(x(t),t) = 0$ for $t \in U \subseteq \mathbb{C}$ where U is the flat locus of the projection $\mathbb{C}^n \times \mathbb{C} \rightarrow \mathbb{C}$ restricted to $H = 0$, which is dense in $\mathbb{C}$ by generic flatness. In particular, a well-defined homotopy requires $0 \in U$. The solution path is usually tracked using a predictor-corrector scheme. As t approaches 1 the solution path either diverges or converges to a solution of F.

A standard homotopy for the case $m = n$ is the *total degree homotopy*. Bézout's theorem gives $N = \prod_{i=1}^{m} \deg(F_i)$ as an upper bound for the the number of isolated solutions of F. A total degree homotopy uses a start system G with N isolated solutions and the homotopy $H(x,t) = (1-t)G(x) + tF(x)$. As the Bézout bound may be very high, for large computations the total degree homotopy is impractical and other methods are necessary.

Monodromy method. Monodromy (see [70, 89]) is an alternative method for finding isolated solutions to parameterized polynomial systems which is advantageous if the number of solutions is substantially lower than the Bézout bound. Embed our polynomial system F in a family of polynomial systems $\mathscr{F}_Q$, parameterized by a connected open set $Q \subseteq \mathbb{C}^k$. Let l be the number of solutions of $F_q \in \mathscr{F}_Q$ for $q \in U$, where $U \subseteq Q$ is the flat locus of the family $\mathscr{F}_Q$.

Consider the incidence variety

$$Y := \left\{ (x,q) \in \mathbb{C}^n \times Q \mid F_q(x) = 0 \right\}.$$

Let π be the projection from $\mathbb{C}^n \times Q$ onto the second argument restricted to Y. For every $q \in Q \backslash \Delta$, the fiber $Y_q = \pi^{-1}(q)$ has exactly l points. Given a loop O in U based at q, the preimage $\pi^{-1}(O)$ is a union of paths starting and ending at (possibly different) points of Y_q. So, giving a direction to the loop O, we may associate to each point y of Y_q the endpoint of the path starting at y. This defines an action, the *monodromy action*, of the fundamental group of U on the fiber Y_q, which in turn defines a map from the fundamental group of U to the symmetric group S_l. The *monodromy group* of our family at q is the image of such a map. This action is transitive if and only if Y is irreducible, which we assume.

Fix $q_0 \in U$ such that $F = F_{q_0} \in \mathscr{F}_Q$. Suppose a *start pair* (x_0, q_0) is given, that is, x_0 is a solution to the instance F_{q_0}. The start solution x_0 is numerically tracked along a directed loop in $Q \backslash \Delta$, yielding a solution p_0' at the end. If $p_0 \neq p_0'$, then p_0' is tracked along the *same* loop, possibly yielding again a new solution. Then, all solutions are tracked along a *new* loop, and the process is repeated until some stopping criterion is fulfilled.

We note that this method requires us to know one solution of our polynomial system to use as a start pair. Various strategies exist to find such a solution. We will describe one strategy in Section .

Certifying solutions. The above methods yield numerical approximations of solutions of our polynomial system F. How can we certify that the obtained approximations correspond to actual solutions of F and that they are all distinct? For systems F with an equal number n of polynomials and variables, Smale introduced the notion of an *approximate zero*, the α-number and the α-theorem, see [175]. In short, an approximate zero of F is any point $p \in \mathbb{C}^n$ such that Newton's method, when applied to p, converges quadratically towards a zero of F. This means that the number of correct significant digits roughly doubles with each iteration of Newton's method.

Definition 1.3.1 (Approximate zero)**.** Let J_F be the $n \times n$ Jacobian matrix of F. A point $p \in \mathbb{C}^n$ is an *approximate zero* of F if there exists a zero $\zeta \in \mathbb{C}^n$ of F such that the sequence of Newton

iterates

$$z_{k+1} = z_k - J_F(z_k)^{-1}F(z_k)$$

starting at $z_0 = p$ satisfies for all $k \geq 1$ that

$$\|z_{k+1} - \zeta\| \leq \frac{1}{2}\|z_k - \zeta\|^2.$$

If this holds, then we call ζ the *associated zero* of p. Here $\|x\|$ is the standard Euclidean norm in $\mathbb{C}^n$, and the zero ζ is assumed to be nonsingular (that is, $\det(J_F(\zeta)) \neq 0$ since F).

To check whether a point $p \in \mathbb{C}^n$ is an approximate zero of F from Definition 1.3.1 requires infinitely many steps, one for each iteration of the Newton method. Nevertheless, when p is close enough to its associated zero, it is possible to certify that p is an approximate zero with only finitely many computations, as we now see. Smale's α-theorem (see [28, Theorem 4 in Chapter 8]) is an essential ingredient. The theorem uses the γ- and α-numbers

$$\gamma(F,x) = \sup_{k \geq 2} \left\|\frac{1}{k!}J_F(x)^{-1}D^kF(x)\right\|^{\frac{1}{k-1}} \quad \text{and}$$
$$\alpha(F,x) = \|J_F(x)^{-1}F(x)\| \cdot \gamma(F,x),$$

where D^kF is the tensor of order-k derivatives of F and the tensor $J_F^{-1}D^kF$ is understood as a multilinear map $A : (\mathbb{C}^n)^k \rightarrow \mathbb{C}^n$ with norm $\|A\| := \max_{\|v\|=1}\|A(v,\ldots,v)\|$.

Theorem 1.3.2 (Smale's α-theorem)**.** *If $\alpha(F,x) < 0.03$, then x is an approximate zero of F. Furthermore, if $y \in \mathbb{C}^n$ is any point with $\|y - x\|$ less than $(20\,\gamma(F,x))^{-1}$, then y is also an approximate zero of F with the same associated zero ζ as x.*

Smale's α-theorem is in fact more general than is stated above. The numbers 0.03 and 20 can be replaced by any pair of positive numbers satisfying certain constraints.

To avoid the computation of the γ-number, Shub and Smale [174] derived an upper bound for $\gamma(F,x)$ which can be computed exactly and efficiently. Hence, one can decide algorithmically whether x is an approximate zero using only the data of the point x itself and F. Hauenstein and Sottile [114] implemented these ideas in an algorithm, called `alphaCertified`, which decides both whether a point $x \in \mathbb{C}^n$ is an approximate zero and whether two approximate zeros have distinct associated zeros. A new implementation of a method for certifying solutions called the "interval-arithmetic method" was introduced by Breiding, Rose, and Timme in [41].

Trace test.   The certification process explained above establishes a *lower* bound for the number of isolated solutions of F. The trace test can be used for polynomial systems satisfying certain conditions to show that *all* solutions have been found. See [141] for a more detailed explanation.

We first establish definitions of concepts used in the trace test. A *pencil of linear spaces* is a family M_t for $t \in \mathbb{C}$ of linear spaces that depends affinely on the parameter t. Each M_t is the span of a linear space L and a point t on a line l that is disjoint from L. Suppose that $W \subset \mathbb{C}^n$ is an

irreducible variety of dimension m and that M_t for $t \in \mathbb{C}$ is a general pencil of linear subspaces of codimension m such that W and M_0 intersect transversally. Consider a fixed subset $W' \subseteq W \cap M_0$ and denote by $W_t' \subseteq W \cap M_t$ the points obtained by tracking W' along the pencil. Denote by $w(t)$ the sum of the points of W_t'. If $W_t' = W \cap M_t$ then $w(t)$ is the *trace* of $W \cap M_t$. A $\mathbb{C}$-valued function w is called an *affine linear function* of t if there exist $a, b \in \mathbb{C}$ such that $w(t) = a + bt$. A $\mathbb{C}^n$-valued function w is called an affine linear function of t if for a nonconstant path $\gamma : [0, 1] \to \mathbb{C}$ with $\gamma(0) = 0$, we have that $w(\gamma(s))$ is an affine linear function of $\gamma(s)$. The trace is an affine linear function of t [141, Prop. 3]. It can be shown that no proper subset of the points in $W \cap M_t$ defines an affine linear function of t.

This leads to the idea of the trace test: Let $t_1 \in \mathbb{C} \setminus \{0\}$, fix $W' \subseteq W \cap M_0$ and compute $\mathrm{tr}(t_1) := (w(t_1) - w(0)) - (w(0) - w(-t_1))$. Note that $\mathrm{tr}(t_1)$ is identically zero if and only if w is an affine linear function of t, which is true if and only if the cardinality of W' corresponds to the degree of W. Due to the generality assumption on M_t, it is sufficient to compute $\mathrm{tr}(t_1)$ for only *one* $t_1 \in \mathbb{C} \setminus \{0\}$.

1.4 Persistent Homology

Topological data analysis is a growing field that brings the mathematical structures of topology to the analysis of data. Persistent homology, a method central to topological data analysis, adapts the concept of homology to point clouds. We now provide an abbreviated introduction to persistent homology. This section is adapted from [120], which is joint work with Emil Horobeţ. For further background, we refer the reader to [52].

The persistent homology of a finite subset of $\mathbb{R}^n$ at parameter ε is defined as the homology of a simplicial complex, called the Čech complex, associated to a covering of the point cloud by hyperballs of radius ε. By the nerve theorem, the Čech complex has the same homology as the covering.

Definition 1.4.1. Let $X \subset \mathbb{R}^n$ and $\varepsilon > 0$ a parameter. Let σ be a finite subset of X. The *Čech complex* of X at radius ε is

$$C_X(\varepsilon) = \left\{ \sigma \subset X \text{ s.t. } \bigcap_{x \in \sigma} B_\varepsilon(x) \neq 0 \right\},$$

an abstract simplicial complex where the *n*-faces are the subsets of size n of X with nonempty *n*-wise intersection.

From these simplicial complexes, we obtain a filtration for which we can define persistent homology. Following [91], consider a simplicial complex, K, and a function $f : K \to \mathbb{R}$. We require that f be *monotonic* by which we mean it is non-decreasing along chains of faces, that is, $f(\sigma) \leq f(\tau)$ whenever σ is a face of τ. Monotonicity implies that the sublevel set, $K(a) = f^{-1}(-\infty, a]$, is a subcomplex of K for every $a \in \mathbb{R}$. Letting m be the number of simplices in K, we get $n + 1 \leq m + 1$ different subcomplexes, which we arrange as an increasing sequence,

$$\emptyset = K_0 \subseteq K_1 \subseteq \cdots \subseteq K_n = K.$$

In other words, if $a_1 < a_2 < \cdots < a_n$ are the function values of the simplices in K and $a_0 = -\infty$ then $K_i = K(a_i)$ for each i. We call this sequence of complexes the *filtration* of f.

For every $i \leq j$ we have an inclusion map from the underlying space of K_i to that of K_j and therefore an induced homomorphism, $f_q^{i,j} : H_q(K_i) \rightarrow H_q(K_j)$, for each dimension q.

Definition 1.4.2. The *q-th persistent homology groups* are the images of the homomorphisms induced by inclusion, $H_q^{i,j} = \operatorname{im} f_q^{i,j}$, for $0 \leq i \leq j \leq n$. The corresponding *q-th persistent Betti numbers* are the ranks of these groups, $\beta_q^{i,j} = \operatorname{rank} H_q^{i,j}$.

As a consequence of the Structure Theorem for PIDs, the family of modules $H_q(K_i)$ and homomorphisms $f_q^{i,j} : H_q(K_i) \rightarrow H_q(K_j)$ over a field F yields a decomposition

$$H_q(K_i; F) \cong \bigoplus_i x^{t_i} \times F[x] \bigoplus \left(\bigoplus_j x^{r_j} \cdot (F[x]/(x^{s_j} \cdot F[x])) \right), \tag{1.1}$$

where t_i, r_j, and s_j are values of the persistence parameter ε [104].

The free portions of Equation 1.1 are in bijective correspondence with those homology generators which appear at parameter t_i and persist for all $\varepsilon > t_i$, while the torsional elements correspond to those homology generators which appear at parameter r_j and disappear at parameter $r_j + s_j$.

To encode the information given by this decomposition, we create a graphical representation of the q-th persistent homology group called a *barcode* [104]. For each parameter interval $[r_j, r_j + s_j]$ corresponding to a homology generator, there is a horizontal line segment (bar), arbitrarily ordered along a vertical axis. The persistent Betti number $\beta_q^{i,j}$ equals the number of intervals in the barcode of $H_q(K_i; F)$ spanning the parameter interval $[i, j]$.

Persistent homology is defined using the Čech complex, but it is hard to compute using the Čech complex because this requires storing simplices is many dimensions. In practice, persistent homology is often computed using the Vietoris-Rips complex, a simplicial complex determined entirely by its edge information. The Vietoris-Rips complex is defined as follows.

Definition 1.4.3. Let $X \subset \mathbb{R}^n$ and $\varepsilon > 0$ a parameter. Let σ be a finite subset of X. The *Vietoris-Rips complex* of X at radius ε is

$$VR_X(\varepsilon) = \{\sigma \subset X \text{ s.t. } B_\varepsilon(x) \cap B_\varepsilon(y) \neq 0 \text{ for all pairs}(x,y) \in \sigma\},$$

an abstract simplicial complex where the *n*-faces are the subsets of size n of X such that every pair of points in the subset has nonempty pairwise intersection.

Using Jung's theorem, one can show that $C_X(\varepsilon) \subseteq VR_X(\sqrt{2}\varepsilon) \subset C_X(\sqrt{2}\varepsilon)$, so that the Vietoris-Rips complex can indeed be used to approximate persistent homology [104].

We include here an example of the real variety defined by the Trott curve and a barcode representing its persistent homology, computed by taking a sample of points on the variety.

Example 1.4.4 (**The barcodes of the Trott curve**). In dimension 1, the first four bars correspond to the cycles in each of the four components of the real variety. As epsilon increases, these cycles

fill in, and then the components join together in one large circle. This demonstrates how persistent homology can detect the global arrangement of the components of a variety. The barcodes were computed using Ripser, which uses the Vietoris-Rips complex [22].
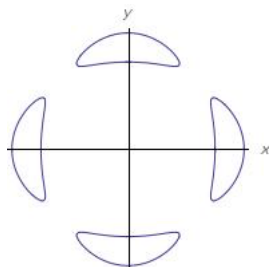
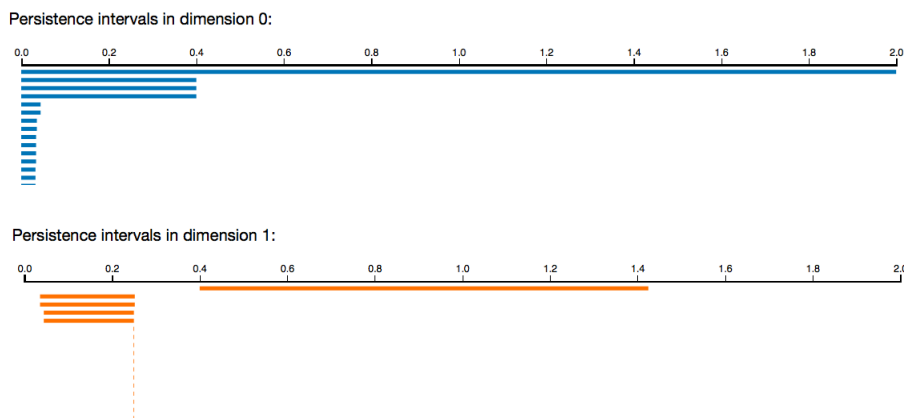

Figure 1.1: The Trott curve.

Figure 1.2: Barcodes for the Trott curve in homological dimensions 0 and 1.

1.5 Contributions in this Dissertation

This dissertation addresses several topics in metric algebraic geometry, starting with distance optimization and curvature, then turning to data analysis and numerical methods.

In Chapter 2, I explore algebraic varieties underlying distance optimization. The original work in this chapter comes from the following sources. Section 2.1 is based on the paper [60], joint with Diego Cifuentes, Kristian Ranestad, and Bernd Sturmfels. It is published in the Journal of Symbolic Computation. Section 2.2 is based on the paper [79], joint with David Eklund and Sandra Di Rocco. It is published in the SIAM Journal on Applied Algebra and Geometry.

Every finite subset X of $\mathbb{R}^n$ defines a *Voronoi decomposition* of the ambient space. The *Voronoi cell* of a point $y \in X$ consists of all points in $\mathbb{R}^n$ for which the closest point in X is y. In Section 2.1, we generalize these definitions to allow X to be any real algebraic variety. We compute and prove formulas for the degree of the algebraic boundary of the Voronoi cell of a point on a variety. We apply these results to low-rank matrix approximation.

A *bottleneck* of a smooth algebraic variety $X \subset \mathbb{R}^n$ is a pair (x, y) of distinct points $x, y \in X$ such that the line containing x and y is orthogonal to X at both x and y. Such a pair of points gives a critical value of the distance function between pairs of distinct points on the variety. The narrowness of bottlenecks is a fundamental complexity measure in the algebraic geometry of data. For instance, it is one of two factors that determine the sampling density required for persistent homology, a method central to topological data analysis, to obtain the desired results. The number of bottlenecks, or the *bottleneck degree*, of a variety is a measure of the complexity of computing all bottlenecks. In Section 2.2, we prove a formula for the bottleneck degree as a function of classical invariants such as Chern classes and polar classes, providing the formula explicitly in low dimension and giving an algorithm to compute it in the general case.

In Chapter 3, I explore the intersections of algebraic geometry and differential geometry. The original work in this chapter comes from the paper [35], joint with Madeline Brandt, and the paper [40], joint with Paul Breiding and Kristian Ranestad. We find systems of polynomial equations such that their zeros are the points on a variety where the curvature exhibits a special property. For example, we find points where one of the principal curvatures is critical and points where all principal curvatures agree. By bringing the structure of an algebraic variety to features defined in abstract differential geometric terms, we are able to use numerical algebraic geometry to compute these features and intersection theory to analyze the complexity of the computations by determining the degrees of the relevant subvarieties.

In Chapter 4, I use algebro-geometric formulations to inform the computational study of data. The original work in this chapter comes from three papers. Section 4.1 is based on [37], a joint paper with Paul Breiding, Sara Kališnik, and Bernd Sturmfels published in Revista Mathematica Complutense. Section 4.2 is based on the paper [120], joint with Emil Horobeţ and published in Computer Aided Geometric Design. Section 4.3 is based on the paper [35], joint with Madeline Brandt.

In Section 4.1, we model finite sets of points in $\mathbb{R}^n$ as real algebraic varieties, finding a defining system of polynomial equations and estimates for the dimension and degree. We test our algorithms on a range of data sets and implement them in Julia. We also analyze these data sets using persistent homology. Persistent homology involves studying the homology of a simplicial complex obtained from a set of points by noting the intersections of neighborhoods of the points. The homology of the complex is studied for a range of neighborhood radii. Topological features that persist over a large range of radii are deemed significant. We demonstrate how algebraic geometry can benefit persistent homology. The neighborhoods traditionally used in persistent homology are spheres. We propose a variant using elliptical neighborhoods with axis orientation determined by the tangent space of the variety and axis length determined by a metric algebraic geometry feature called *local reach*. In examples, this method improved the accuracy of persistent homology techniques.

Algebraic geometry can provide theoretical guarantees of the accuracy of data analysis meth-

ods. In Section 4.2, we define a version of persistent homology for algebraic varieties using the *offset hypersurface*, the locus of all points at some fixed distance from a given variety. This algebraic formulation enables us to use Hardt's theorem from real algebraic geometry to prove the algebraicity of two quantities central to the computation of persistent homology.

We can also use algebraic geometry to guarantee estimation methods for metric features of plane curves. Recall from above that a finite point set in $\mathbb{R}^n$ determines a Voronoi decomposition of $\mathbb{R}^n$ into Voronoi cells defined by their nearest point in the set. In Section 2.1, we modify this definition so that the finite point set is replaced with a real algebraic variety of any dimension. One might ask whether the Voronoi decomposition of a finite point sample of a positive dimensional variety converges to the Voronoi decomposition of the variety as the number of points sampled increases. In Section 4.3, we prove that such convergence, as defined with respect to an appropriate metric, does occur for plane curves. Using this result, we provide and implement algorithms to approximate metric features of plane curves, including the medial axis, curvature, evolute, bottlenecks, and reach.

In Chapter 5, I use numerical and symbolic computational methods to analyze algebraic varieties. The original work in this chapter comes from two papers. Section 5.1 comes from the paper [46], which is joint work with Laura Brustenga i Moncusí and Sascha Timme. It is published in Le Matematiche. Section 5.2 comes from the paper [185].

The projective linear group $\mathrm{PGL}(\mathbb{C}, 4)$ acts on cubic surfaces, considered as points of $\mathbb{P}^{19}_{\mathbb{C}}$ via the coefficients of their defining polynomials. In Section 5.1, we compute that the degree of the 15-dimensional projective variety defined by the Zariski closure of the orbit of a general cubic surface is 96120. This computation demonstrates the power of numerical algebraic geometry to find and certify solutions to systems of polynomial equations, producing numerical theorems for degrees that are difficult to prove using intersection theory.

In Section 5.2, we study the real algebraic variety of real symmetric matrices with eigenvalue multiplicities determined by a partition. We present formulas for the dimension and Euclidean distance degree. We give a parametrization by rational functions. For small matrices, we provide equations; for larger matrices, we explain how to use representation theory to find equations. We describe the ring of invariants under the action of the special orthogonal group. For the subvariety of diagonal matrices, we give the degree.

Chapter 2

Optimizing Distances with Algebraic Varieties

Given a variety $X \subset \mathbb{R}^n$ and a point $p \in \mathbb{R}^n$, a standard question is to ask for a point of X at minimal distance to p. In Section 1.1, we saw how this question is studied algebraically in the context of the Euclidean distance degree. In this chapter, we will explore two variations of this "nearest point problem." The first variation can be considered an inverse to the standard nearest point problem: Given a point $p \in X$, characterize the locus of $\mathbb{R}^n$ consisting of all points that are closer to p than to any other point of X. This locus is called the *Voronoi cell* of p. In the second variation, we seek all pairs of points on X that provide a critical value of the distance function between pairs of points. These critical points are called *bottlenecks* of the variety.

Section 2.1 is based on the paper [60], joint with Diego Cifuentes, Kristian Ranestad, and Bernd Sturmfels. It is published in the Journal of Symbolic Computation. Section 2.2 is based on the paper [79], joint with David Eklund and Sandra Di Rocco. It is published in the SIAM Journal on Applied Algebra and Geometry.

2.1 Voronoi Cells

Every finite subset X of $\mathbb{R}^n$ defines a Voronoi decomposition of the ambient Euclidean space. The *Voronoi cell* of a point $y \in X$ consists of all points whose closest point in X is y, i.e.

$$\text{Vor}_X(y) \; := \; \big\{ u \in \mathbb{R}^n : y \in \arg\min_{x \in X} \|x - u\|^2 \big\}. \tag{2.1}$$

This is a convex polyhedron with at most $|X| - 1$ facets. The study of these cells, and how they depend on X, is ubiquitous in computational geometry and its numerous applications.

In what follows we assume that X is a real algebraic variety of codimension c and that y is a smooth point on X. The ambient space is $\mathbb{R}^n$ with its Euclidean metric. The Voronoi cell $\text{Vor}_X(y)$ is a convex semialgebraic set of dimension c. It lives in the *normal space*

$$N_X(y) \; = \; \big\{ u \in \mathbb{R}^n : u - y \text{ is perpendicular to the tangent space of } X \text{ at } y \big\}.$$

The topological boundary of $\mathrm{Vor}_X(y)$ in $N_X(y)$ is denoted by $\partial\,\mathrm{Vor}_X(y)$. It consists of the points in X that have at least two closest points in X, including y. We study the *algebraic boundary* $\partial_{\mathrm{alg}}\mathrm{Vor}_X(y)$. This is the hypersurface in the complex affine space $N_X(y)_{\mathbb{C}} \simeq \mathbb{C}^c$ obtained as the Zariski closure of $\partial\,\mathrm{Vor}_X(y)$ over the field of definition of X. The degree of this hypersurface is denoted $\delta_X(y)$ and called the *Voronoi degree* of X at y. If X is irreducible and y is a general point on X, then this degree does not depend on y.

Example 2.1.1 (Surfaces in 3-space). Fix a general inhomogeneous polynomial $f \in \mathbb{Q}[x_1, x_2, x_3]$ of degree $d \geq 2$ and let $X = V(f)$ be its surface in $\mathbb{R}^3$. The normal space at a general point $y \in X$ is the line $N_X(y) = \{y + \lambda(\nabla f)(y) : \lambda \in \mathbb{R}\}$. The Voronoi cell $\mathrm{Vor}_X(y)$ is a line segment (or ray) in $N_X(y)$ that contains the point y. The boundary $\partial\,\mathrm{Vor}_X(y)$ consists of ≤ 2 points from among the zeros of an irreducible polynomial in $\mathbb{Q}[\lambda]$. We shall see that this polynomial has degree $d^3 + d - 7$. Its complex zeros form the algebraic boundary $\partial_{\mathrm{alg}}\mathrm{Vor}_X(y)$. Thus, the Voronoi degree of the surface X is $d^3 + d - 7$. For example, let $d = 2$ and fix $y = (0,0,0)$ and $f = x_1^2 + x_2^2 + x_3^2 - 3x_1x_2 - 5x_1x_3 - 7x_2x_3 + x_1 + x_2 + x_3$. Then $\partial_{\mathrm{alg}}\mathrm{Vor}_X(y)$ consists of the three zeros of $\langle u_1 - u_3, u_2 - u_3, 368u_3^3 + 71u_3^2 - 6u_3 - 1 \rangle$. The Voronoi cell is the segment $\mathrm{Vor}_X(y) = \{(\lambda, \lambda, \lambda) \in \mathbb{R}^3 : -0.106526\ldots \leq \lambda \leq 0.12225\ldots\}$.
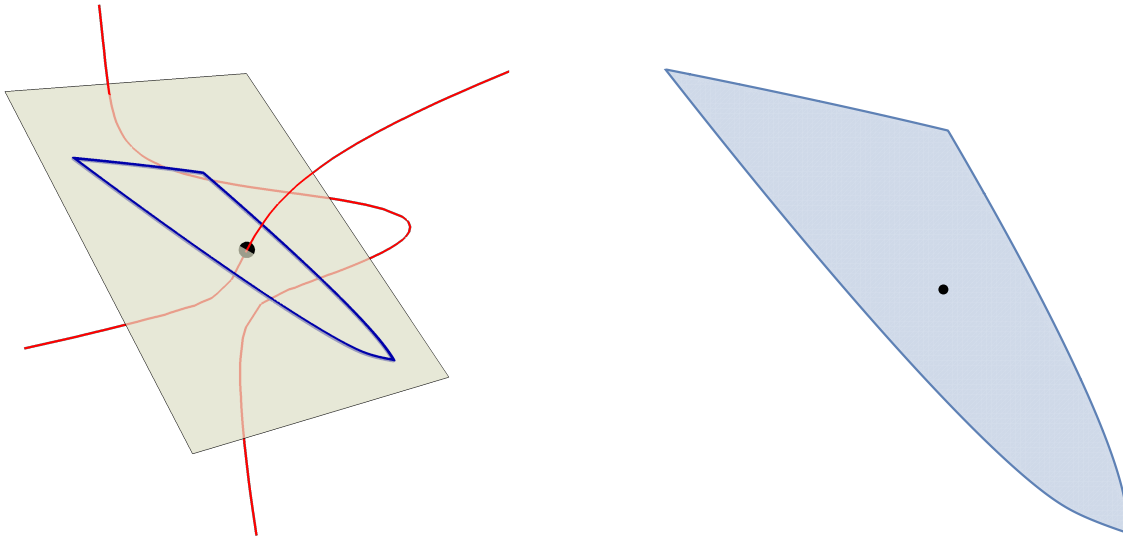

Figure 2.1: A quartic space curve, shown with the Voronoi cell in one of its normal planes.

Example 2.1.2 (Curves in 3-space). Let X be a general algebraic curve in $\mathbb{R}^3$. For $y \in X$, the Voronoi cell $\mathrm{Vor}_X(y)$ is a convex set in the normal plane $N_X(y) \simeq \mathbb{R}^2$. Its algebraic boundary $\partial_{\mathrm{alg}}\mathrm{Vor}_X(y)$ is a plane curve of degree $\delta_X(y)$. This Voronoi degree can be expressed in terms of the degree and genus of X. Specifically, if X is the intersection of two general quadrics in $\mathbb{R}^3$, then the Voronoi degree is 12. Figure 2.1 shows one such quartic space curve X together with the normal

plane at a point $y \in X$. The Voronoi cell $\mathrm{Vor}_X(y)$ is the planar convex region highlighted on the right. Its boundary is an algebraic curve of degree $\delta_X(y) = 12$.

This section is organized as follows. First, we describe the exact symbolic computation of the Voronoi boundary at y from the equations that define X. We present a Gröbner-based algorithm whose input is y and the ideal of X and whose output is the ideal defining $\partial_{\mathrm{alg}} \mathrm{Vor}_X(y)$. Next we consider the case when y is a low rank matrix and X is the variety of these matrices. Here, the Eckart-Young Theorem yields an explicit description of $\mathrm{Vor}_X(y)$ in terms of the spectral norm. We then consider inner approximations of the Voronoi cell $\mathrm{Vor}_X(y)$ by spectrahedral shadows. This is derived from the Lasserre hierarchy in polynomial optimization. Next we present formulas for the degree of the Voronoi boundary $\partial_{\mathrm{alg}} \mathrm{Vor}_X(y)$ when X, y are sufficiently general and $\dim(X) \leq 2$. These formulas are proved at the end of this section using tools from intersection theory.

Computing with Ideals

We now describe Gröbner basis methods for finding the Voronoi boundaries of a given variety. We start with an ideal $I = \langle f_1, f_2, \ldots, f_m \rangle$ in $\mathbb{Q}[x_1, \ldots, x_n]$ whose real variety $X = V(I) \subset \mathbb{R}^n$ is assumed to be nonempty. One often further assumes that I is real radical and prime, so that $X_{\mathbb{C}}$ is an irreducible variety in $\mathbb{C}^n$ whose real points are Zariski dense. Our aim is to compute the Voronoi boundary of a given point $y \in X$. In our examples, the coordinates of the point y and the coefficients of the polynomials f_i are rational numbers. Under these assumptions, the following computations are done in polynomial rings over $\mathbb{Q}$.

Fix the polynomial ring $R = \mathbb{Q}[x_1, \ldots, x_n, u_1, \ldots, u_n]$ where $u = (u_1, \ldots, u_n)$ is an additional unknown point. The *augmented Jacobian* of X at x is the following matrix of size $(m+1) \times n$ with entries in R. It contains the n partial derivatives of the m generators of I:

$$J_I(x, u) \quad := \quad \begin{bmatrix} u - x \\ (\nabla f_1)(x) \\ \vdots \\ (\nabla f_m)(x) \end{bmatrix}$$

Let N_I denote the ideal in R generated by I and the $(c+1) \times (c+1)$ minors of the augmented Jacobian $J_I(x, u)$, where c is the codimension of the given variety $X \subset \mathbb{R}^n$. The ideal N_I in R defines a subvariety of dimension n in $\mathbb{R}^{2n}$, namely the *Euclidean normal bundle* of X. Its points are pairs (x, u) where x is a point in X and u lies in the normal space of X at x.

Example 2.1.3 (Cuspidal cubic). Let $n = 2$ and $I = \langle x_1^3 - x_2^2 \rangle$, so $X = V(I) \subset \mathbb{R}^2$ is a cubic curve with a cusp at the origin. The ideal of the Euclidean normal bundle of X is

$$N_I = \left\langle x_1^3 - x_2^2, \det \begin{pmatrix} u_1 - x_1 & u_2 - x_2 \\ 3x_1^2 & -2x_2 \end{pmatrix} \right\rangle.$$

Let $N_I(y)$ denote the linear ideal that is obtained from N_I by replacing the unknown point x by the given point $y \in \mathbb{R}^n$. For instance, for $y = (4, 8)$ we obtain $N_I(y) = \langle u_1 + 3u_2 - 28 \rangle$. We now

define the *critical ideal* of the variety X at the point y as

$$C_I(y) \quad = \quad I + N_I + N_I(y) + \langle \, \|x - u\|^2 - \|y - u\|^2 \, \rangle \quad \subset \quad R.$$

The variety of $C_I(y)$ consists of pairs (u, x) such that x and y are equidistant from u and both are critical points of the distance function from u to X. The *Voronoi ideal* is the following ideal in $\mathbb{Q}[u_1, \ldots, u_n]$. It is obtained from the critical ideal by saturation and elimination:

$$\mathrm{Vor}_I(y) \quad = \quad \big(C_I(y) : \langle x - y \rangle^\infty \big) \cap \mathbb{Q}[u_1, \ldots, u_n]. \tag{2.2}$$

The geometric interpretation of each step in our construction implies the following result:

Proposition 2.1.4. *The affine variety in $\mathbb{C}^n$ defined by the Voronoi ideal $\mathrm{Vor}_I(y)$ contains the algebraic Voronoi boundary $\partial_{\mathrm{alg}} \mathrm{Vor}_X(y)$ of the given real variety X at its point y.*

Example 2.1.5. For the point $y = (4, 8)$ on the cuspidal cubic X in Example 2.1.3, we have $N_I(y) = \langle u_1 + 3u_2 - 28 \rangle$. Going through the steps above, we find that the Voronoi ideal is

$$\mathrm{Vor}_I(y) \quad = \quad \langle u_1 - 28, u_2 \rangle \cap \langle u_1 + 26, u_2 - 18 \rangle \cap \langle u_1 + 3u_2 - 28, \, 27u_2^2 - 486u_2 + 2197 \rangle.$$

The third component has no real roots and is hence extraneous. The Voronoi boundary consists of two points: $\partial \mathrm{Vor}_X(y) = \{(28, 0), (-26, 18)\}$. The Voronoi cell $\mathrm{Vor}_X(y)$ is the line segment connecting these points. This segment is shown in green in Figure 2.2. Its right endpoint $(28, 0)$ is equidistant from y and the point $(4, -8)$. Its left endpoint $(-26, 18)$ is equidistant from y and the point $(0, 0)$, whose Voronoi cell is discussed in Remark 2.1.6.

The cuspidal cubic X is very special. If we replace X by a general cubic (defined over $\mathbb{Q}$) in the affine plane, then $\mathrm{Vor}_I(y)$ is generated modulo $N_I(y)$ by an irreducible polynomial of degree eight in $\mathbb{Q}[u_2]$. Thus, the expected Voronoi degree of (affine) plane cubics is $\delta_X(y) = 8$.

Remark 2.1.6 (Singularities). Voronoi cells at singular points can be computed with the same procedure as above. However, these Voronoi cells generally have higher dimensions. For an illustration, consider the cuspidal cubic, and let $y = (0, 0)$ be the cusp. A Gröbner basis computation yields the Voronoi boundary $27u_2^4 + 128u_1^3 + 72u_1u_2^2 + 32u_1^2 + u_2^2 + 2u_1$. The Voronoi cell is the two-dimensional convex region bounded by this quartic, shown in blue in Figure 2.2. The Voronoi cell might also be empty at a singularity. This happens for instance for $V(x_1^3 + x_1^2 - x_2^2)$, which has an ordinary double point at $y = (0, 0)$. In general, the cell dimension depends on both the embedding dimension and the branches of the singularity.

In this work we restrict ourselves to Voronoi cells at points y that are nonsingular in the given variety $X = V(I)$. Proposition 2.1.4 gives an algorithm for computing the Voronoi ideal $\mathrm{Vor}_I(y)$. We implemented it in `Macaulay2` [107] and experimented with numerous examples. For small enough instances, the computation terminates and we obtain the defining polynomial of the Voronoi boundary $\partial_{\mathrm{alg}} \mathrm{Vor}_X(y)$. This polynomial is unique modulo the linear ideal of the normal
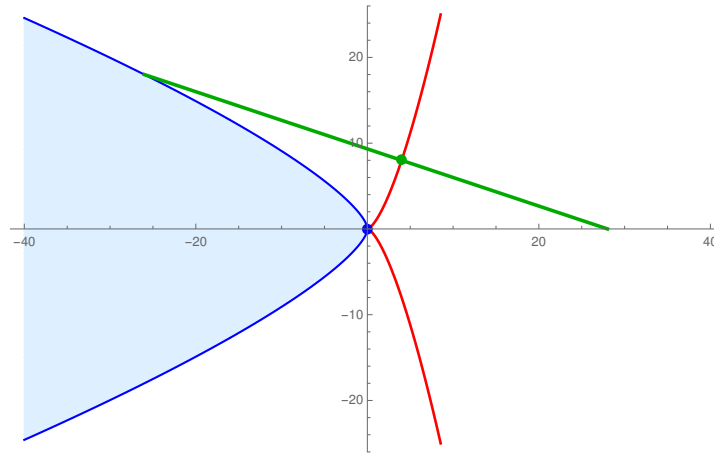
Figure 2.2: The cuspidal cubic is shown in red. The Voronoi cell of a smooth point is a green line segment. The Voronoi cell of the cusp is the convex region bounded by the blue curve.

space $N_I(y)$. For larger instances, we can only compute the degree of $\partial_{\mathrm{alg}} \mathrm{Vor}_X(y)$ but not its equation. This is done by working over a finite field and adding $c-1$ random linear equations in $u_1, \ldots, u_n$ in order to get a zero-dimensional polynomial system.

Our experiments were most extensive for the case of hypersurfaces $(c = 1)$. We sampled random polynomials f of degree d in $\mathbb{Q}[x_1, \ldots, x_n]$, both inhomogeneous and homogeneous. These were chosen among those that vanish at a preselected point y in $\mathbb{Q}^n$. In each iteration, the resulting Voronoi ideal $\mathrm{Vor}_I(y)$ from (2.2) was found to be zero-dimensional. In fact, $\mathrm{Vor}_I(y)$ is a maximal ideal in $\mathbb{Q}[u_1, \ldots, u_n]$, and $\delta_X(y)$ is the degree of the associated field extension. We summarize our results in Tables 2.1 and 2.2, and we extract conjectural formulas.

$n \backslash d$	2	3	4	5	6	7	8	$\delta_X(y) = \mathrm{degree}(\mathrm{Vor}_{\langle f \rangle}(y))$
1	1	2	3	4	5	6	7	$d-1$
2	2	8	16	26	38	52	68	d^2+d-4
3	3	23	61	123	215	343		d^3+d-7
4	4	56	202	520	1112			$d^4-d^3+d^2+d-10$
5	5	125	631					$d^5-2d^4+2d^3+d-13$
6	6	266	1924					$d^6-3d^5+4d^4-2d^3+d^2+d-16$
7	7	551						$d^7-4d^6+7d^5-6d^4+3d^3+d-19$

Table 2.1: The Voronoi degree of an inhomogeneous polynomial f of degree d in $\mathbb{R}^n$.

Conjecture 2.1.7. *The Voronoi degree of a generic hypersurface of degree d in $\mathbb{R}^n$ equals*

$$(d-1)^n + 3(d-1)^{n-1} + \tfrac{4}{d-2}\left((d-1)^{n-1} - 1\right) - 3n.$$

$n\backslash d$	2	3	4	5	6	7	8	$\delta_X(y) = \text{degree}(\text{Vor}_{\langle f\rangle}(y))$
2	2	4	6	8	10	12	14	$2d-2$
3	3	13	27	45	67	93	123	$2d^2-5$
4	4	34	96	202				$2d^3-2d^2+2d-8$
5	5	79	309					$2d^4-4d^3+4d^2-11$
6	6	172						$2d^5-6d^4+8d^3-4d^2+2d-14$
7	7	361						$2d^6-8d^5+14d^4-12d^3+6d^2-17$

Table 2.2: The Voronoi degree of a homogeneous polynomial f of degree d in $\mathbb{R}^n$.

The Voronoi degree of the cone of a generic homogeneous polynomial of degree d in $\mathbb{R}^n$ is

$$2(d-1)^{n-1} + \frac{4}{d-2}((d-1)^{n-1} - 1) - 3n + 2.$$

We shall prove both parts of this conjecture for $n \leq 3$ in Section 2.1, where we develop the geometric theory of Voronoi degrees of low-dimensional varieties. The case $d = 2$ was analyzed in [58, Proposition 5.8]. In general, for $n \geq 4$ and $d \geq 3$, the problem is still open.

Low Rank Matrices

There are several natural norms on the space $\mathbb{R}^{m \times n}$ of real $m \times n$ matrices. We focus on two of these norms. First, we have the *Frobenius norm* $\|U\|_F := \sqrt{\sum_{ij} U_{ij}^2}$. And second, we have the *spectral norm* $\|U\|_2 := \max_i \sigma_i(U)$ which extracts the largest singular value.

Let X denote the variety of real $m \times n$ matrices of rank $\leq r$. Fix a rank r matrix V in X. This is a nonsingular point in X. We consider the Voronoi cell $\text{Vor}_X(V)$ with respect to the Frobenius norm. This is consistent with the previous sections because the Frobenius norm agrees with Euclidean norm on $\mathbb{R}^{m \times n}$. This identification will no longer be valid after Remark 2.1.10 when we restrict to the subspace of symmetric matrices.

Let $U \in \text{Vor}_X(V)$, i.e. the closest point to U in the rank r variety X is the matrix V. By the Eckart-Young Theorem, the matrix V is derived from U by computing the singular value decomposition $U = \Sigma_1 D \Sigma_2$. Here Σ_1 and Σ_2 are orthogonal matrices of size $m \times m$ and $n \times n$ respectively, and D is a nonnegative diagonal matrix whose entries are the singular values. Let $D^{[r]}$ be the matrix that is obtained from D by replacing all singular values except for the r largest ones by zero. Then, according to Eckart-Young, we have $V = \Sigma_1 \cdot D^{[r]} \cdot \Sigma_2$.

Remark 2.1.8. The Eckart-Young Theorem works for both the Frobenius norm and the spectral norm. This means that $\text{Vor}_X(V)$ is also the Voronoi cell for the spectral norm.

The following is the main result in this section.

Theorem 2.1.9. *Let V be an $m \times n$-matrix of rank r. The Voronoi cell $\text{Vor}_X(V)$ is congruent up to scaling to the unit ball in the spectral norm on the space of $(m-r) \times (n-r)$-matrices.*

Before we present the proof, let us first see why the statement makes sense. The determinantal variety X has dimension $rm + rn - r^2$ in an ambient space of dimension mn. The dimension of the normal space at a point is the difference of these two numbers, so it equals $(m-r)(n-r)$. Every Voronoi cell is a full-dimensional convex body in the normal space. Next consider the case $m = n$ and restrict to the space of diagonal matrices. Now X is the set of vectors in $\mathbb{R}^n$ having at most r nonzero coordinates. This is a reducible variety with $\binom{n}{r}$ components, each a coordinate subspace. For a general point y in such a subspace, the Voronoi cell $\text{Vor}_X(y)$ is a convex polytope. It is congruent to a regular cube of dimension $n-r$, which is the unit ball in the L^∞-norm on $\mathbb{R}^{n-r}$. Theorem 2.1.9 describes the orbit of this picture under the action of the two orthogonal groups on $\mathbb{R}^{m \times n}$. For example, consider the special case $n = 3, r = 1$. Here, X consists of the three coordinate axes in $\mathbb{R}^3$. The Voronoi decomposition of this curve decomposes $\mathbb{R}^3$ into squares, each normal to a different point on the three lines. The image of this picture under orthogonal transformations is the Voronoi decomposition of $\mathbb{R}^{3 \times 3}$ associated with the affine variety of rank 1 matrices. That variety has dimension 5, and each Voronoi cell is a 4-dimensional convex body in the normal space.

Proof of Theorem 2.1.9. The Voronoi cell is invariant under orthogonal transformations. We may therefore assume that the matrix $V = (v_{ij})$ satisfies $v_{11} \geq v_{22} \geq \cdots \geq v_{rr} = u > 0$ and $v_{ij} = 0$ for all other entries. The Voronoi cell of the diagonal matrix V consists of matrices U whose block-decomposition into $r + (m-r)$ rows and $r + (n-r)$ columns satisfies

$$\begin{pmatrix} I & 0 \\ 0 & T_1 \end{pmatrix} \cdot \begin{pmatrix} U_{11} & U_{12} \\ U_{21} & U_{22} \end{pmatrix} \cdot \begin{pmatrix} I & 0 \\ 0 & T_2 \end{pmatrix} = \begin{pmatrix} V_{11} & 0 \\ 0 & V_{22} \end{pmatrix}.$$

Here $V_{11} = \text{diag}(v_{11}, \ldots, v_{rr})$ agrees with the upper $r \times r$-block of V, and V_{22} is a diagonal matrix whose entries are bounded above by u in absolute value. This implies $U_{11} = V_{11}$, $U_{12} = 0$, $U_{21} = 0$, and U_{22} is an arbitrary $(m-r) \times (n-r)$ matrix with spectral norm at most u. Hence the Voronoi cell of V is congruent to the set of all such matrices U_{22}. This convex body equals u times the unit ball in $\mathbb{R}^{(m-r) \times (n-r)}$ under the spectral norm. $\square$

Remark 2.1.10. It is instructive to compare the Voronoi degree with the *Euclidean distance degree* (ED degree). Assume $m \leq n$ in Theorem 2.1.9. According to [86, Example 2.3], the ED degree of the determinantal variety X equals $\binom{m}{r}$. On the other hand, the Voronoi degree of X is $2(m-r)$. Indeed, we have shown that the Voronoi boundary is isomorphic to the hypersurface $\{\det(WW^T - I_{m-r}) = 0\}$, where W is an $(m-r) \times (n-r)$ matrix of unknowns.

Our problem becomes even more interesting when we restrict to matrices in a linear subspace. To see this, let X denote the variety of symmetric $n \times n$ matrices of rank $\leq r$. We can regard X either as a variety in the ambient matrix space $\mathbb{R}^{n \times n}$ or in the space $\mathbb{R}^{\binom{n+1}{2}}$ whose coordinates are the upper triangular entries of a symmetric matrix. On the latter space we have both the *Euclidean norm* and the *Frobenius norm*. These are now different!

The Frobenius norm on $\mathbb{R}^{\binom{n+1}{2}}$ is the restriction of the Frobenius norm on $\mathbb{R}^{n \times n}$ to the subspace of symmetric matrices. For instance, if $n = 2$, we identify the vector (a, b, c) with the symmetric matrix $\begin{pmatrix} a & b \\ b & c \end{pmatrix}$. The Frobenius norm is $\sqrt{a^2 + 2b^2 + c^2}$, whereas the Euclidean norm is $\sqrt{a^2 + b^2 + c^2}$. The two norms have dramatically different properties with respect to low rank approximation. The Eckart-Young Theorem remains valid for the Frobenius norm on $\mathbb{R}^{\binom{n+1}{2}}$, but this is not true for the Euclidean norm (cf. [86, Example 3.2]). In what follows we elucidate this by comparing the Voronoi cells with respect to the two norms.
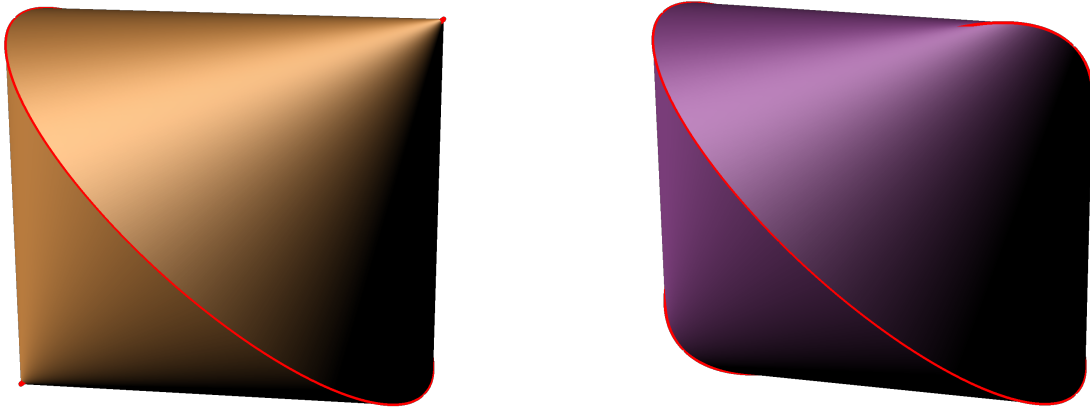

Figure 2.3: The Voronoi cell of a symmetric 3×3 matrix of rank 1 is a convex body of dimension 3. It is shown for the Frobenius norm (left) and for the Euclidean norm (right).

Example 2.1.11. Let X be the variety of symmetric 3×3 matrices of rank ≤ 1. For the Euclidean metric, X lives in $\mathbb{R}^6$. For the Frobenius metric, X lives in a 6-dimensional subspace of $\mathbb{R}^{3 \times 3}$. Let V be a regular point in X, i.e. a symmetric 3×3 matrix of rank 1. The normal space to X at V has dimension 3. Hence, in either norm, the Voronoi cell $\mathrm{Vor}_X(V)$ is a 3-dimensional convex body. Figure 2.3 illustrates these bodies for our two metrics.

For the Frobenius metric, the Voronoi cell is isomorphic to the set of matrices $\begin{pmatrix} a & b \\ b & c \end{pmatrix}$ with eigenvalues between -1 and 1. This semialgebraic set is bounded by the surfaces defined by the singular quadrics $\det \begin{pmatrix} a+1 & b \\ b & c+1 \end{pmatrix}$ and $\det \begin{pmatrix} a-1 & b \\ b & c-1 \end{pmatrix}$. The Voronoi ideal is of degree 4, defined by the product of these two determinants (modulo the normal space). The Voronoi cell is shown on the left in Figure 2.3. It is the intersection of two quadratic cones. The cell is the convex hull of the circle in which the two quadrics meet, together with the two vertices.

For the Euclidean metric, the Voronoi boundary at a generic point V in X is defined by an irreducible polynomial of degree 18 in a, b, c. In some cases, the Voronoi degree can drop. For instance, consider the special rank 1 matrix $V = \begin{pmatrix} 1 & 0 & 0 \\ 0 & 0 & 0 \\ 0 & 0 & 0 \end{pmatrix}$. For this point, the degree of the Voronoi boundary is only 12. This particular Voronoi cell is shown on the right in Figure 2.3. This cell is the convex hull of two ellipses, which are shown in red in the diagram.

Spectrahedral Approximations of Voronoi Cells

Computing Voronoi cells of varieties is computationally hard. In this section we introduce some tractable approximations to the Voronoi cell based on semidefinite programming (SDP). More precisely, for a point $y \in X$ we will construct convex sets $\{S_X^d(y)\}_{d \geq 1}$ such that

$$S_X^1(y) \subset S_X^2(y) \subset S_X^3(y) \subset \cdots \subset \text{Vor}_X(y). \tag{2.3}$$

Here each $S_X^d(y)$ is a spectrahedral shadow. The construction is based on the sum-of-squares (SOS) hierarchy, also known as Lasserre hierarchy, for polynomial optimization problems [26]. This section is to be understood as a continuation of the studies undertaken in [57, 58].

Let $\mathscr{S}^n$ denote the space of real symmetric $n \times n$ matrices. Given $A, B \in \mathscr{S}^n$, the notation $A \preceq B$ means that the matrix $B - A$ is positive semidefinite (PSD). A *spectrahedron* is the intersection of the cone of PSD matrices with an affine-linear space. Spectrahedra are the feasible sets of SDP. In symbols, a spectrahedron has the following form for some $C_i \in \mathscr{S}^n$:

$$S := \{y \in \mathbb{R}^m : y_1 C_1 + \cdots + y_m C_m \preceq C_0\}.$$

A *spectrahedral shadow* is the image of an spectrahedron under an affine-linear map. Using SDP one can efficiently maximize linear functions over a spectrahedral shadow.

Our goal is to describe inner spectrahedral approximations of the Voronoi cells. We first consider the case of *quadratically defined varieties*. This is the setting of [58] which we now follow. Let $\mathbf{f} = (f_1, \ldots, f_m)$ be a list of inhomogeneous quadratic polynomials in n variables. We fix $X = V(\mathbf{f}) \subset \mathbb{R}^n$ and we assume that y is a nonsingular point in X. Let $A_i \in \mathscr{S}^n$ denote the Hessian matrix of the quadric f_i. Consider the following spectrahedron:

$$S_{\mathbf{f}} := \{\lambda \in \mathbb{R}^m : \lambda_1 A_1 + \cdots + \lambda_m A_m \preceq I_n\}.$$

This was called the *master spectrahedron* in [58]. Let $\text{Jac}_{\mathbf{f}}$ be the Jacobian matrix of $\mathbf{f}$. This is the $n \times m$ matrix with entries $\partial f_j / \partial x_i$. The specialized Jacobian matrix $\text{Jac}_{\mathbf{f}}(y)$ defines a linear map $\mathbb{R}^m \longrightarrow \mathbb{R}^n$ whose range is the normal space of the variety at y. We define the set

$$S_{\mathbf{f}}^1(y) := y - \tfrac{1}{2} \text{Jac}_{\mathbf{f}}(y) \cdot S_{\mathbf{f}} \subset \mathbb{R}^n.$$

By construction, this is a spectrahedral shadow. The following result was established in [58].

Lemma 2.1.1. *The spectrahedral shadow $S_{\mathbf{f}}^1(y)$ is contained in the Voronoi cell $\text{Vor}_X(y)$.*

Proof. We include the proof to better explain the situation. Let $u \in S_{\mathbf{f}}^1(y)$, so there exists $\lambda \in S_{\mathbf{f}}$ with $u = y - \tfrac{1}{2} \text{Jac}(y)\lambda$. We need to show that y is the nearest point from u to the variety X. Let $L(x, \lambda) = \|x - u\|^2 - \sum_i \lambda_i f_i(x)$ be the Lagrangian function, and let $L_\lambda(x)$ be the quadratic function obtained by fixing the value of λ. Observe that $L_\lambda(x)$ is convex, and its minimum is attained at y. Indeed, $\lambda \in S_{\mathbf{f}}$ means that the Hessian of this function is positive semidefinite, and $u = y - \tfrac{1}{2} \text{Jac}_{\mathbf{f}}(y)\lambda$ implies that $\nabla L_\lambda(y) = 0$. Therefore,

$$\|y - u\|^2 = L_\lambda(y) = \min_x L_\lambda(x) \leq \min_{x \in X} \|x - u\|^2 \leq \|y - u\|^2.$$

We conclude that y is the minimizer of the squared distance function $x \mapsto \|x - u\|^2$ on X. $\qquad\square$

Example 2.1.12 ([58, Example 6.1]). Let $X \subset \mathbb{R}^3$ be the twisted cubic curve, defined by the two equations $x_2 = x_1^2$ and $x_3 = x_1 x_2$. Both $\text{Vor}_X(0)$ and $S_{\mathbf{f}}^1(0)$ lie in the normal space at the origin, which is the plane $u_1 = 0$. The Voronoi cell is the planar convex set bounded by the quartic curve $27u_3^4 + 128u_2^3 + 72u_2u_3^2 - 160u_2^2 - 35u_3^2 + 66u_2 = 9$. The inner approximation $S_{\mathbf{f}}^1(0)$ is bounded by the parabola $2u_2 = 1 - u_3^2$. The two curves are tangent at the point $(0, \frac{1}{2}, 0)$.

Example 2.1.13. Let $X \subset \mathbb{R}^3$ be the quartic curve in Figure 2.1. The Voronoi boundary is a plane curve of degree 12. The master spectrahedron $S_{\mathbf{f}}$ is bounded by a cubic curve, as seen in [58, Example 5.2]. The convex set $S_{\mathbf{f}}^1(y)$ is affinely isomorphic to $S_{\mathbf{f}}$, so it is also bounded by a cubic curve. Figure 2.4 shows the Voronoi cell and its inner spectrahedral approximation. Note that their boundaries are tangent.
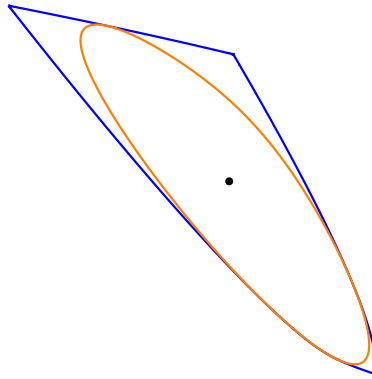

Figure 2.4: The spectrahedral approximation $S_{\mathbf{f}}^1(0)$ of the Voronoi cell $\text{Vor}_X(0)$ shown in Figure 2.1. The boundaries of these two convex sets – curves of degree 3 and 12 – are tangent.

The above examples motivate the following open problem.

Problem 2.1.14. Fix a quadratically defined variety $X = V(\mathbf{f})$ in $\mathbb{R}^n$. Let $\partial_{\text{alg}} \text{Vor}_X(y)$ be the algebraic boundary of the Voronoi cell at $y \in X$ and let $\partial_{\text{alg}} S_{\mathbf{f}}^1(y)$ be its first spectrahedral approximation. Investigate the tangency behavior of these two hypersurfaces.

This problem was studied in [58] for complete intersections of n quadrics in $\mathbb{R}^n$. Here, X is a finite set, and it was proved in [58, Theorem 4.5] that the Voronoi walls are tangent to the spectrahedral approximations. It would be desirable to better understand this fact.

We now shift gears, by allowing $\mathbf{f} = (f_1, \ldots, f_m)$ to be an arbitrary tuple of polynomials in $x = (x_1, \ldots, x_n)$. Fix $d \in \mathbb{N}$ such that $\deg(()f_i) \leq 2d$ for all i. We will construct a spectrahedral shadow $S_{\mathbf{f}}^d(y) \subset \mathbb{R}^n$ that is contained in $\text{Vor}_X(y)$. The idea is to perform a change of variables that makes the constraints $\mathbf{f}$ quadratic, and use the construction above.

Let $\mathscr{A} := \{\alpha \in \mathbb{N}^n : 0 < \sum_i \alpha_i \leq d\}$. This set consists of $N := \binom{n+d}{d} - 1$ nonnegative integer vectors. We consider the d-th Veronese embedding of affine n-space into affine N-space:

$$\nu_d : \mathbb{R}^n \longrightarrow \mathbb{R}^N, \quad x = (x_1, \ldots, x_n) \mapsto z = (z_\alpha)_{\alpha \in \mathscr{A}}, \quad \text{where } z_\alpha := x^\alpha = x_1^{\alpha_1} \cdots x_n^{\alpha_n}.$$

Among the entries of z are the variables $x_1, \ldots, x_n$. We list these at the beginning in the vector z. The image of ν_d is the Veronese variety. It is defined by the quadratic equations

$$z_{\alpha_1} z_{\alpha_2} = z_{\beta_1} z_{\beta_2} \qquad \forall \alpha_1, \alpha_2, \beta_1, \beta_2 \text{ such that } \alpha_1 + \alpha_2 = \beta_1 + \beta_2. \tag{2.4}$$

Since the polynomial $f_i(x)$ has degree $\leq 2d$, there is a quadratic function $q_i(z)$ such that $f_i(x) = q_i(\nu_d(x))$. The Veronese image $\nu_d(X)$ is defined by the quadratic equations $q_i(z) = 0$ together with those in (2.4). We write $\mathbf{q} \subset \mathbb{R}[z]$ for the (finite) set of all of these quadrics.

Each $q \in \mathbf{q}$ is a quadratic polynomial in N variables. Let $A_q \in \mathscr{S}^N$ be its Hessian matrix. Let $C := \left(\begin{smallmatrix} I_n & 0 \\ 0 & 0 \end{smallmatrix} \right) \in \mathscr{S}^N$ be the Hessian of the function $z \mapsto x^T x$. The master spectrahedron is

$$S_{\mathbf{q}} := \{\lambda \in \mathbb{R}^{|\mathbf{q}|} : \sum_{q \in \mathbf{q}} \lambda_q A_q \preceq C\}.$$

Let $J_{\mathbf{q}}(y) := \mathrm{Jac}_{\mathbf{q}}(\nu_d(y))$ be the Jacobian matrix of $\mathbf{q}$ evaluated at the point $\nu_d(y) \in \mathbb{R}^N$. This matrix has N rows. Let $J_{\mathbf{q}}^n(y)$ be the submatrix of $J_{\mathbf{q}}(y)$ that is given by the n rows corresponding to the variables x_i, and let $J_{\mathbf{q}}^{N-n}(y)$ be the submatrix given by the remaining $N-n$ rows. We now consider the spectrahedral shadow

$$S_{\mathbf{f}}^d(y) := y - \tfrac{1}{2} J_{\mathbf{q}}^n(y) \cdot (S_{\mathbf{q}} \cap \ker J_{\mathbf{q}}^{N-n}(y)) \subset \mathbb{R}^n.$$

This is obtained by intersecting the spectrahedron $S_{\mathbf{q}}$ with a linear subspace and then taking the image under an affine-linear map. One can show the inclusions in (2.3) using ideas similar to those in Lemma 2.1.1. An alternative argument is given in the proof of Corollary 2.1.17.

Example 2.1.15. Consider the cardioid curve $X = V((x_1^2 + x_2^2 + x_1)^2 - x_1^2 - x_2^2)$ in $\mathbb{R}^2$, shown in red in Figure 2.5. See also [86, Figure 1]. We compare the Voronoi cells with the spectrahedral relaxation of degree $d = 2$. The Voronoi cell at the origin, a singular point, is the interior of the circle $C : \{u_1^2 + u_2^2 + u_1 = 0\}$. The Voronoi cell at a smooth point y is contained in the normal line to X at y. It is either a ray emanating from the circle C, or a line segment from C to the x-axis. The spectrahedral shadow $S_{\mathbf{f}}^2(y)$ is the subset of the Voronoi cell outside of the cardioid. For instance, the Voronoi cell at $y = (0,1)$ is the ray $\mathrm{Vor}_X(y) = \{(t, t+1) : t \geq -\tfrac{1}{2}\}$, and its spectrahedral approximation is the strictly smaller ray $S_{\mathbf{f}}^2(y) = \{(t, t+1) : t \geq 0\}$.

Fix $u \in \mathbb{R}^n$, and let y be its nearest point on the variety X. Though computing this nearest point y is hard in general, we can do it efficiently if u lies in the interior of the spectrahedral shadow $S_{\mathbf{f}}^d(y)$ for some fixed d. Indeed, this is done by solving a certain SDP.

Proposition 2.1.16. *Consider the d-th level of the SOS hierarchy for the optimization problem* $\min_{x \in V(\mathbf{f})} \|x - u\|^2$. *A point u lies in the interior of the spectrahedral shadow $S_{\mathbf{f}}^d(y)$ if and only if the d-th SOS relaxation exactly recovers y (i.e. the moment matrix has rank one).*
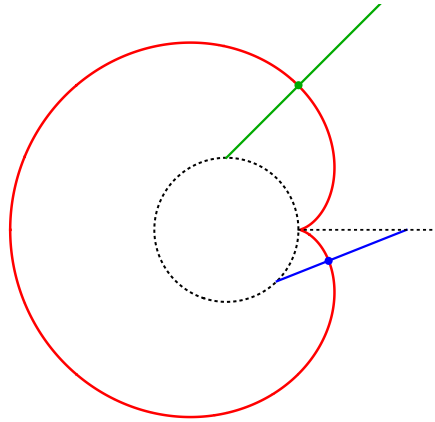
Figure 2.5: The red curve is the cardioid. The inner circle is the Voronoi cell of its singular point. Other Voronoi cells are either rays or line segments. These emanate from the circle. As they exit the cardioid, they enter the spectrahedral approximation to the Voronoi cell.

Proof. The d-th level of the relaxation is obtained by taking the Lagrangian dual of the quadratic optimization problem given by the quadrics in the set $\mathbf{q}$ above; see [26]. The SDP-exact region in quadratic programming was formally defined in [58, Definition 3.2]. It is straightforward to verify that this definition agrees with our description of $S_{\mathbf{f}}^d(y)$. □

Corollary 2.1.17. *The inclusions $S_{\mathbf{f}}^d(y) \subset S_{\mathbf{f}}^{d+1}(y) \subset \mathrm{Vor}_X(y)$ hold.*

Proof. If the SOS relaxation recovers a point u, then it must lie in the Voronoi cell $\mathrm{Vor}_X(y)$. And if the d-th SOS relaxation is exact then the $(d+1)$-st relaxation is also exact. □

Example 2.1.18. Consider the problem of finding the nearest point from a point $u \in \mathbb{R}^2$ to the cardioid. By [86, Example 1.1], the ED degree is 3. Here we consider the second SOS relaxation of the problem. We characterized the sets $S_{\mathbf{f}}^2(y)$ above. It follows that the second SOS relaxation solves the problem exactly if and only if u lies on the outside of the cardioid.

Formulas for Curves and Surfaces

The algebraic boundary of the Voronoi cell $\mathrm{Vor}_X(y)$ is a hypersurface in the normal space to a variety $X \subset \mathbb{R}^n$ at a point $y \in X$. We study the degree of that hypersurface when X is a curve or a surface. We denote this degree by $\delta_X(y)$ and refer to it as the Voronoi degree. We identify X and $\partial_{\mathrm{alg}}\mathrm{Vor}_X(y)$ with their Zariski closures in complex projective space $\mathbb{P}^n$.

Theorem 2.1.19. *Let $X \subset \mathbb{P}^n$ be a curve of degree d and geometric genus g with at most ordinary multiple points as singularities. The Voronoi degree at a general point $y \in X$ equals*

$$\delta_X(y) = 4d + 2g - 6,$$

provided X is in general position in $\mathbb{P}^n$.

Example 2.1.20. If X is a smooth curve of degree d in the plane, then $2g - 2 = d(d - 3)$, so

$$\delta_X(y) = d^2 + d - 4.$$

This confirms our experimental results in the row $n = 2$ of Table 2.1.

Example 2.1.21. If X is a rational curve of degree d, then $g = 0$ and hence $\delta_X(y) = 4d - 6$. If X is an elliptic curve, so the genus is $g = 1$, then we have $\delta_X(y) = 4d - 4$. A space curve with $d = 4$ and $g = 1$ was studied in Example 2.1.2. Its Voronoi degree equals $\delta_X(y) = 12$.

The proof of Theorem 2.1.19 appears in the next section. We will then see what general position means. For example, let X be the twisted cubic curve in $\mathbb{P}^3$, with affine parameterization $t \mapsto (t, t^2, t^3)$. Here $g = 0$ and $d = 3$, so the expected Voronoi degree is 6. But in Example 2.1.12 we saw $\delta_X(y) = 4$. This is explained by the fact that the plane at infinity in $\mathbb{P}^3$ intersects the curve X in a triple point. After a general linear change of coordinates in $\mathbb{P}^3$, which amounts to a linear fractional transformation in $\mathbb{R}^3$, we correctly find $\delta_X(y) = 6$.

We next present a formula for the Voronoi degree of a surface X which is smooth and irreducible in $\mathbb{P}^n$. Our formula is in terms of its degree d and two further invariants. The first, denoted $\chi(X) := c_2(X)$, is the topological Euler characteristic. This is equal to the degree of the second Chern class of the tangent bundle. The second invariant, denoted $g(X)$, is the genus of the curve obtained by intersecting X with a general smooth quadratic hypersurface in $\mathbb{P}^n$. Thus, $g(X)$ is the quadratic analogue to the usual sectional genus of the surface X.

Theorem 2.1.22. *Let $X \subset \mathbb{P}^n$ be a smooth surface of degree d. Then its Voronoi degree equals*

$$\delta_X(y) = 3d + \chi(X) + 4g(X) - 11,$$

provided the surface X is in general position in $\mathbb{P}^n$ and y is a general point on X.

The proof of Theorem 2.1.22 will also be presented in the next section. At present we do not know how to generalize these formulas to the case when X is a variety of dimension ≥ 3.

Example 2.1.23. If X is a smooth surface in $\mathbb{P}^3$ of degree d, then $\chi(X) = d(d^2 - 4d + 6)$, by [101, Example 3.2.12]. A smooth quadratic hypersurface section of X is an irreducible curve of degree (d, d) in $\mathbb{P}^1 \times \mathbb{P}^1$. The genus of such a curve is $g(X) = (d - 1)^2$. We conclude that

$$\delta_X(y) = 3d + d(d^2 - 4d + 6) + 4(d - 1)^2 - 11 = d^3 + d - 7.$$

This confirms our experimental results in the row $n = 3$ of Table 2.1.

Example 2.1.24. Let X be the Veronese surface of order e in $\mathbb{P}^{\binom{e+1}{2}-1}$, taken after a general linear change of coordinates in that ambient space. The degree of X equals $d = e^2$. We have $\chi(X) =$

$\chi(\mathbb{P}^2) = 3$, and the general quadratic hypersurface section of X is a curve of genus $g(X) = \binom{2e-1}{2}$. We conclude that the Voronoi degree of X at a general point y equals

$$\delta_X(y) \;=\; 3e^2 + 3 + 2(2e-1)(2e-2) - 11 \;=\; 11e^2 - 12e - 4.$$

For instance, for the quadratic Veronese surface in $\mathbb{P}^5$ we have $e = 2$ and hence $\delta_X(y) = 16$. This is smaller than the number 18 found in Example 2.1.11, since back then we were dealing with the cone over the Veronese surface in $\mathbb{R}^6$, and not with the Veronese surface in $\mathbb{R}^5 \subset \mathbb{P}^5$.

We finally consider affine surfaces defined by homogeneous polynomials. Namely, let $X \subset \mathbb{R}^n$ be the affine cone over a general smooth curve of degree d and genus g in $\mathbb{P}^{n-1}$.

Theorem 2.1.25. *Let $X \subset \mathbb{R}^n$ be the cone over a smooth curve in $\mathbb{P}^{n-1}$. Its Voronoi degree is*

$$\delta_X(y) \;=\; 6d + 4g - 9$$

provided that the curve is in general position and y is a general point.

The proof of Theorem 2.1.25 will be presented in the next section.

Example 2.1.26. If $X \subset \mathbb{R}^3$ is the cone over a smooth curve of degree d in $\mathbb{P}^2$, then $2g - 2 = d(d-3)$. Hence the Voronoi degree of X is

$$\delta_X(y) \;=\; 2d^2 - 5.$$

This confirms our experimental results in the row $n = 3$ of Table 2.2.

To conclude, we comment on the assumptions made in our theorems. We assumed that the variety X is in general position in $\mathbb{P}^n$. If this is not satisfied, then the Voronoi degree may drop. Nonetheless, the technique introduced in the next section can be adapted to determine the correct value. As an illustration, we consider the affine Veronese surface (Example 2.1.24).

Example 2.1.27. Let $X \subset \mathbb{P}^5$ be the Veronese surface with affine parametrization $(s,t) \mapsto (s,t,s^2,st,t^2)$. The hyperplane at infinity intersects X in a double conic, so X is not in general position. In the next section, we will show that the true Voronoi degree is $\delta_X(y) = 10$. For the Frobenius norm, the Voronoi degree drops further. For this, we shall derive $\delta_X(y) = 4$.

Euler Characteristic of a Fibration

We now develop the geometry and the proofs for the degree formulas. Let $X \subset \mathbb{P}^n$ be a smooth projective variety defined over $\mathbb{R}$. We assume that $y \in X$ is a general point, and that we fixed an affine space $\mathbb{R}^n \subset \mathbb{P}^n$ containing y such that the hyperplane at infinity $\mathbb{P}^n \backslash \mathbb{R}^n$ is in general position with respect to X. We use the Euclidean metric in this $\mathbb{R}^n$ to define the normal space to X at y. This can be expressed equivalently as follows. After a projective transformation in $\mathbb{P}^n$, we can assume that $\mathbb{R}^n = \{x_0 = 1\}$, that $y = [1 : 0 : \cdots : 0]$ is a point in X, and that the tangent space

to X at y is contained in the hyperplane $\{x_n = 0\}$. The normal space to X at y contains the line $\{x_1 = \ldots = x_{n-1} = 0\}$.

The sphere through y with center $[1 : 0 : \cdots : 0 : u]$ on this normal line is

$$Q_u \;=\; \{x_1^2 + \cdots + x_{n-1}^2 + (x_n - u)^2 - u^2 = 0\} \quad \subset \mathbb{R}^n.$$

As u varies, this is a linear pencil that extends to a $\mathbb{P}^1$ family of quadric hypersurfaces

$$Q_{(t:u)} \;=\; \{t(x_1^2 + \cdots + x_{n-1}^2 + x_n^2) - 2ux_0 x_n = 0\} \quad \subset \mathbb{P}^n.$$

Note that $Q_{(t:u)}$ is tangent to X at y. Assuming the normal line to be general, we observe:

Remark 2.1.28. The Voronoi degree $\delta_X(y)$ is the number of quadratic hypersurfaces $Q_{(t:u)}$ with $t \neq 0$ that are tangent to X at a point in the affine space $\{x_0 = 1\}$ distinct from y.

We shall compute this number by counting tangency points of all quadrics in the pencil. In particular we need to consider the special quadric $Q_{(0:1)} = \{x_0 x_n = 0\}$. This quadric is reducible: it consists of the tangent hyperplane $\{x_n = 0\}$ and the hyperplane at infinity $\{x_0 = 0\}$. It is singular along a codimension two linear space $\{x_0 = x_n = 0\}$ at infinity. Any point of X on this linear space is therefore also a point of tangency between X and $Q_{(0:1)}$.

To count the tangent quadrics, we consider the map $X \dashrightarrow \mathbb{P}^1, x \mapsto (t : u)$ whose fibers are the intersections $X_{(t:u)} = Q_{(t:u)} \cap X$. By Remark 2.1.28, we need to count its ramification points. However, this map is not a morphism. Its base locus is $X \cap Q_{(1:0)} \cap Q_{(0:1)}$. We blow up that base locus to get a morphism which has the intersections $X_{(t:u)}$ for its fibers:

$$q : \tilde{X} \longrightarrow \mathbb{P}^1.$$

The topological Euler characteristic (called *Euler number*) of the fibers of q depends on the singularities. We shall count the tangencies indirectly, by computing the Euler number $\chi(\tilde{X})$ of the blow-up $\tilde{X}$ in two ways, first directly as a variety, and secondly as a fibration over $\mathbb{P}^1$.

Euler numbers have the following two fundamental properties. The first property is *multiplicativity*. It is found in topology books, e.g. [177, Chapter 9.3]. Namely, if $W \rightarrow Z$ is a surjection of topological spaces, Z is connected and all fibers are homeomorphic to a topological space Y, then $\chi(W) = \chi(Y) \cdot \chi(Z)$. The second property is *additivity*. It applies to complex varieties, as seen in [100, Section 4.5]. To be precise, if Z is a closed algebraic subset of a complex variety W with complement Y, then $\chi(W) = \chi(Y) + \chi(Z)$.

For the fibration $q : \tilde{X} \rightarrow \mathbb{P}^1$, the first property may be applied to the set of fibers that are smooth, hence homeomorphic, while the second may be used when adding the singular fibers. Assuming that singular fibers (except the special one) have a quadratic node as its singular point, the Voronoi degree $v := \delta_X(y)$ satisfies the equation

$$\chi(\tilde{X}) \;=\; (1 - v)\chi(X_{gen}) + \chi(X_{(0:1)}) + v\,\chi(X_s). \tag{2.5}$$

Here X_{gen} is a smooth fiber of the fibration, $X_{(0:1)}$ is the special fiber over $(0 : 1)$, and X_s is a fiber with one quadratic node as singular point. The factor $1 - v$ is the Euler number of $\mathbb{P}^1 \setminus \{v+1 \text{ points}\}$. We will use (2.5) to derive the degree formulas from Section 5, and refer to [101, Examples 3.2.12-13] for Euler numbers of smooth curves, surfaces and hypersurfaces.

Proof of Theorem 2.1.19. Let $\bar{X} \to X$ be a resolution of singularities. As above, we assume that y is a smooth point on X and that $\{x_n = x_0 = 0\} \cap X = \emptyset$. We may pull back the pencil of quadrics $Q_{(t:u)}$ to $\bar{X}$. This gives a map $\bar{q} : \bar{X} \dashrightarrow \mathbb{P}^1$. All quadrics in the pencil have multiplicity at least 2 at y, so we remove the divisor $2[y]$ from each divisor in the linear system $\{X_{(t:u)}\}_{(u:t)\in\mathbb{P}^1}$. Thus we obtain a pencil of divisors of degree $2d - 2$ on X that defines a morphism $q : \bar{X} \to \mathbb{P}^1$. The Euler number of $\bar{X}$ is $\chi(\bar{X}) = 2 - 2g$. The Euler number of a fiber is now simply the number of points in the fiber, i.e. $\chi(X_{gen}) = 2d - 2$ and $\chi(X_s) = 2d - 3$ for the singular fibers, the fibers where one point appear with multiplicity two. Also $\chi(X_{(0:1)}) = 2d - 2$, since $X_{(0:1)}$ consists of $2d - 2$ points. Plugging into (2.5) we get:

$$2 - 2g = (1 - v)(2d - 2) + (2d - 2) + v(2d - 3) = 4d - 4 - v.$$

We now obtain Theorem 2.1.19 by solving for v. □

The above derivation can also be seen as an application of the Riemann-Hurwitz formula.

Proof of Theorem 2.1.22. The curves $\{X_{(t:u)}\}_{(u:t)\in\mathbb{P}^1}$ have a common intersection. This is our base locus $X_{(1:0)} \cap X_{(0:1)}$. By Bézout's Theorem, the number of intersection points is at most $2 \cdot 2 \cdot d = 4d$. All curves are singular at y, the general one a simple node, so this point counts with multiplicity 4 in the intersection. We assume that all other base points are simple. We thus have $4d - 4$ simple points. We blow up all the base points, $\pi : \tilde{X} \to X$, with exceptional curve E_0 over y and $E_1, \ldots, E_{4d-4}$ over the remaining base points. The strict transforms of the curves $X_{(t:u)}$ on $\tilde{X}$ are then the fibers of a morphism $q : \tilde{X} \to \mathbb{P}^1$ for which we apply (2.5).

The Euler number $\chi(X)$ equals the degree of the Chern class $c_2(X)$ of the tangent bundle of X. Since π blows up $4d - 3$ points, there are $4d - 3$ points on X that are replaced by $\mathbb{P}^1$s on $\tilde{X}$. Since $\chi(\mathbb{P}^1) = 2$, we get $\chi(\tilde{X}) = \chi(X) + 4d - 3$. If the genus of a smooth hyperquadric intersection with X is g, the general fiber of q is a smooth curve of genus $g - 1$, since it is the strict transform of a curve that is singular at y. We conclude that $\chi(X_{gen}) = 4 - 2g$.

To compute $\chi(X_s)$ we remove first the singular point of X_s and obtain a smooth curve of genus $g - 2$ with two points removed. This curve has Euler number $-2(g - 2)$. Adding the singular point, the additivity of the Euler number yields

$$\chi(X_s) = -2(g - 2) + 1 = 5 - 2g.$$

The special curve $X_{(0:1)}$ has two components, one in the tangent plane that is singular at the point of tangency, and one in the hyperplane at infinity. Assume that the two components are smooth outside the point of tangency and that they meet transversally, i.e., in d points. We then compute $\chi(X_{(0:1)})$, as above, by first removing the d points of intersection to get a smooth curve of genus $g - 1 - d$ with $2d$ points removed, and we next use the addition property to add the d points back. Thus

$$\chi(X_{(0:1)}) = 2 - 2(g - d - 1) - 2d + d = d + 4 - 2g.$$

Substituting into the formula (2.5) gives

$$\chi(X) + 4d - 3 = (1 - v)(4 - 2g) + d + 4 - 2g + v(5 - 2g).$$

From this we obtain the desired formula $v = 3d + \chi(X) + 4g - 11$. $\qquad\square$

Details for Example 2.1.27. The given Veronese surface X intersects the hyperplane at infinity in a double conic instead of a smooth curve. We explain how to compute the Voronoi degree in this case. For the Euclidean metric, the general curve $X_{(t:u)} = Q_{(t:u)} \cap X$ is transverse at four points on this conic. Then $X_{(0:1)}$ has seven components, $\chi(X_{(0:1)}) = 8$ and $\delta_X(y) = 10$.

For the Frobenius metric, the curves $X_{(t:u)}$ are all singular at two distinct points on this conic. The three common singularities of the curves $X_{(t:u)}$ are part of the base locus of the pencil. Outside these three points, the pencil has 4 additional basepoints, so the map $\tilde{X} \to X$ blows up 7 points. Hence $\chi(\tilde{X}) = 10$. The curve X_{gen} is now rational, so $\chi(X_{gen}) = 2$ and $\chi(X_s) = 1$. The reducible curve $X_{(0:1)}$ has two components from the tangent hyperplane, and only the conic from the hyperplane at infinity. Therefore $X_{(0:1)}$ has three components, all $\mathbb{P}^1$s, two that are disjoint and one that meets the other two in one point each, and so $\chi(X_{(0:1)}) = 4$. Equation (2.5) gives $10 = (1-v) \cdot 2 + 4 + v \cdot 1$, and hence $v = \delta_X(y) = 4$. $\qquad\square$

Proof of Theorem 2.1.25. The closure of the affine cone X in $\mathbb{P}^n$ is a projective surface as above. We need to blow up also the vertex of the cone to get a morphism from a smooth surface $q : \tilde{X} \to \mathbb{P}^1$. The Euler number of the blown up cone is $\chi(C) \cdot \chi(\mathbb{P}^1) = 2(2 - 2g)$, so

$$\chi(\tilde{X}) = 2(2 - 2g) + 4d - 3 = 1 + 4d - 4g.$$

The genus of a smooth quadratic hypersurface section $X \cap Q$ is then $g(X \cap Q) = 2g - 1 + d$. Hence the strict transform of each one nodal quadratic hypersurface section X_{gen} has genus $2g - 2 + d$. The Euler number equals $\chi(X_{gen}) = 4 - 2d - 4g$, while $\chi(X_s) = 3 - 2d - 4g$.

The tangent hyperplane at y is tangent to the line L_0 in the cone through y, and it intersects the surface X in $d - 2$ further lines $L_1, \ldots, L_{d-2}$. Therefore,

$$X_{(0:1)} = C_0 + L_0 + L_1 + \cdots + L_{d-2} + C_\infty,$$

where C_0 is the exceptional curve over the vertex of the cone, C_∞ is the strict transform of the curve at infinity, and the L_i are the strict transforms of the lines through y. We conclude

$$\begin{aligned}
\chi(X_{(0:1)}) &= \chi(C_0 \backslash (d-1) \text{ points}) + \chi(C_\infty \backslash (d-1) \text{ points}) + (d-1) \cdot \chi(\mathbb{P}^1) \\
&= 2(2 - 2g - (d-1)) + 2(d-1) = 4 - 4g.
\end{aligned}$$

From (2.5) we get

$$\begin{aligned}
\chi(\tilde{X}) &= (1-v)\chi(X_{gen}) + \chi(X_{(0:1)}) + v \cdot \chi(X_s), \\
1 + 4d - 4g &= (1-v) \cdot (4 - 2d - 4g) + 4 - 4g + v \cdot (3 - 2d - 4g)) = v - 8g - 2d + 10.
\end{aligned}$$

This means that the Voronoi degree is $\delta_X(y) = v = 4g + 6d - 9$. $\qquad\square$

2.2 Bottlenecks

In this section, we compute and count *bottlenecks* of an algebraic variety $X \subset \mathbb{R}^n$. This is the study of lines in $\mathbb{R}^n$ orthogonal to X at two or more points. Such lines contribute to the computation of the *reach* and may be found by solving a polynomial system (2.8). To be able to use the appropriate tools from algebraic geometry we often have to move from the real numbers to the algebraically closed field of complex numbers $\mathbb{C}$, as we illustrate below. We will see that classical invariants such as polar classes appear naturally and turn out to be essential to obtaining a closed formula for the number of bottlenecks. In our opinion, the following results provide yet one more illustration that classical algebraic geometry and in particular intersection theory are useful and often necessary in applications such as data science.

Bottlenecks and Optimization

Finding lines orthogonal at two or more points is an optimization problem with algebraic constraints. The focus of this section is to determine, or bound, the number of critical points for this optimization problem.

Example 2.2.1. Consider the ellipse $C \subset \mathbb{R}^2$ defined by $f = x^2 + y^2/2 - 1 = 0$. A bottleneck on C is a pair of points $p, q \in C$ that span a line orthogonal to C at both points. The only such lines are the x-axis and the y-axis, that is the principal axes of the ellipse, see Figure 2.6. A line l is
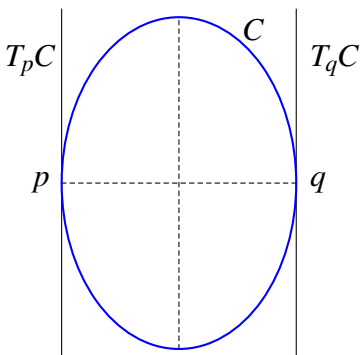

Figure 2.6: An ellipse with tangent lines and principal axes.

orthogonal to C at a point $p \in C$ if l is orthogonal to the tangent line T_pC at p. In other words l is the normal line N_pX at p. The direction of the normal line is given by the gradient $\nabla f = (2x, y)$. Consider a pair of points $p = (x, y) \in C$ and $q = (z, w) \in C$. The claim that (p, q) is a bottleneck

may then be expressed as

$$
\begin{aligned}
x - z &= 2\lambda x, \\
y - w &= \lambda y, \\
x - z &= 2\mu z, \\
y - w &= \mu w,
\end{aligned}
$$

for some $\lambda, \mu \in \mathbb{R}$. These equations, together with $x^2 + y^2/2 = 1$ and $z^2 + w^2/2 = 1$, constitute a polynomial system for computing bottlenecks on the curve C. Note that this is also the system we get if we apply the Lagrange multiplier method to the problem of optimizing the squared distance function $(x - z)^2 + (y - w)^2$ subject to the constraints $x^2 + y^2/2 - 1 = z^2 + w^2/2 - 1 = 0$. This is thus a polynomial optimization problem and we are asking for the critical points of the distance between pairs of points on C.

Consider again an arbitrary variety $X \subset \mathbb{R}^n$. For convenience, we will restrict to the case where X is *smooth*, that is every point of X is a manifold point. A line is orthogonal to X if it is orthogonal to the tangent space $T_x X \subset \mathbb{R}^n$ at x.

Definition 2.2.2. Let $X \subset \mathbb{R}^n$ be a smooth variety. The bottlenecks of X are pairs (x, y) of distinct points $x, y \in X$ such that the line spanned by x and y is normal to X at both points.

Equivalently one can define bottlenecks as the critical points of the squared distance function

$$
\mathbb{R}^n \times \mathbb{R}^n : (x, y) \mapsto ||x - y||^2, \tag{2.6}
$$

subject to the constraints $x, y \in X$ as well as the non-triviality condition $x \neq y$.
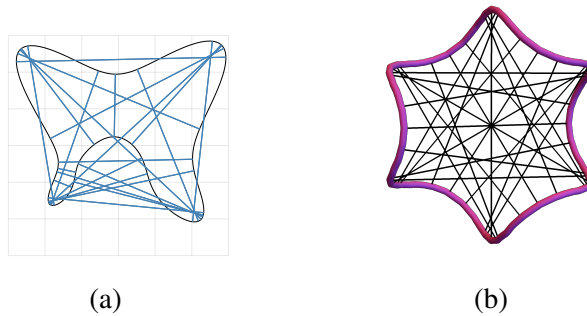

(a)   (b)

Figure 2.7: Two curves and their bottlenecks.

Example 2.2.3. Figure 2.7a shows a quartic curve in $\mathbb{R}^2$ and its 22 bottleneck lines. The curve is defined by $x^4 + y^4 + 1 - 4y - x^2 y^2 - 4x^2 - x - 2y^2 = 0$. The figure was produced by Paul Breiding and Sascha Timme using the Julia package *HomotopyContinuation.jl* [44].

As another example consider the space curve in $\mathbb{R}^3$ defined by

$$
\begin{aligned}
x^3 - 3xy^2 - z &= 0, \\
x^2 + y^2 + 3z^2 - 1 &= 0.
\end{aligned}
$$

(a) Connected components

(b) Sampling of a torus

Figure 2.8

Figure 2.7b shows this curve and its 24 bottleneck lines.

Equations for Bottlenecks

We will now formulate a system of equations for bottlenecks that does not introduce auxiliary variables as in the Lagrange multiplier method. Both of these formulations are useful and the latter will be developed further in Remark 2.2.24.

Let $X \subset \mathbb{R}^n$ be a smooth m-dimensional variety defined by polynomials $f_1, \ldots, f_k$. Note that for $x \in X$, $\dim(T_x X) = \dim(X) = m$. Here we are considering the embedded tangent space which passes through the point x. The corresponding linear space through the origin is $(T_x X)_0 = T_x X - x$. The orthogonal complement $N_x X = \{z \in \mathbb{R}^n : (z - x) \perp (T_x X)_0\}$ is the normal space at x and has the complementary dimension $n - m$. As in the case of the ellipse in Example 2.2.1, the normal space is the span of the gradients $\langle \nabla f_1, \ldots, \nabla f_k \rangle$. More precisely $N_x X = x + \langle \nabla f_1(x), \ldots, \nabla f_k(x) \rangle$. Now, if $x, y \in X$ are distinct then (x, y) is a bottleneck precisely when $(y - x) \in \langle \nabla f_1(x), \ldots, \nabla f_k(x) \rangle$ and $(y - x) \in \langle \nabla f_1(y), \ldots, \nabla f_k(y) \rangle$. To formulate the equations we define the *augmented Jacobian* to be the following matrix of size $(k + 1) \times n$:

$$
J(x, y) = \begin{bmatrix} y - x \\ \nabla f_1(x) \\ \vdots \\ \nabla f_k(x) \end{bmatrix},
\tag{2.7}
$$

where $y - x$ is viewed as a row vector. The condition that $y - x$ is in the span of $\nabla f_1(x), \ldots, \nabla f_k(x)$ is equivalent to saying that the matrix $J(x, y)$ has rank less than or equal to $n - m$, or in other words that all $(n - m + 1) \times (n - m + 1)$-minors of $J(x, y)$ vanish. There is a similar rank condition given by the $(n - m + 1) \times (n - m + 1)$-minors of the augmented Jacobian $J(y, x)$ with x and y reversed. In summary, the bottlenecks of X are the non-trivial $(x \neq y)$ solutions to the following system of

equations:

$$
\begin{aligned}
&(n-m+1) \times (n-m+1)\text{-minors of } J(x,y) = 0,\\
&(n-m+1) \times (n-m+1)\text{-minors of } J(y,x) = 0,\\
&f_1(x) = \cdots = f_k(x) = 0,\\
&f_1(y) = \cdots = f_k(y) = 0.
\end{aligned}
\tag{2.8}
$$

Counting Roots, Complex Numbers and Projective Space

In this subsection we will motivate the study of complex and projective bottlenecks. Let $f_1, \ldots, f_k \in \mathbb{R}[x_1, \ldots, x_n]$ with corresponding variety $X_{\mathbb{R}}$. The system of equations $f_1(x) = \cdots = f_k(x) = 0$ may have non-real solutions $x \in \mathbb{C}^n$. The complex solutions are very relevant for solving polynomial systems. We can define a complex variety $X_{\mathbb{C}} \subset \mathbb{C}^n$ given by $X_{\mathbb{C}} = \{x \in \mathbb{C}^n : f_1(x) = \cdots = f_k(x) = 0\}$. Note that $X_{\mathbb{C}}$ contains the real solutions $X_{\mathbb{R}} \subseteq X_{\mathbb{C}}$.

As practitioners we need tools to numerically approximate solutions to polynomial systems. A useful approach we would like to mention here is numerical homotopy methods, as introduced in Section 1.3. These are predictor/corrector routines based on Newton's method but with probabilistic guarantees that all complex isolated solutions will be found. If a system has only finitely many solutions then the number of complex roots is an upper bound on the number of real roots. A naive approach to finding the real roots is of course to compute all complex roots and filter out the real ones. We stress this point because it illustrates how the number of complex bottlenecks (if finite) provides upper bounds on the computational complexity of real bottlenecks. It is therefore natural to explore the concept of bottlenecks in the complex setting even if one is only interested in real solutions.

An alternative approach to homotopy methods is symbolic computations via Gröbner bases, see for example [178]. Whether homotopy methods or Gröbner bases is appropriate depends on the particular system of equations at hand. See [18] for a comparison of numerical and symbolic methods for equation solving.

Let $X \subset \mathbb{C}^n$ be a smooth variety, defined by $f_1, \ldots, f_k \in \mathbb{C}[x_1, \ldots x_n]$, with $\dim(X) = m > 0$. A *bottleneck* of X is defined to be a pair of distinct points $x, y \in X$ such that the line $\overline{xy}$ joining x and y is normal to X at both x and y. The orthogonality relation $a \perp b$ involved in the definition of bottlenecks is given by $\sum_{i=1}^n a_i b_i = 0$ for $a = (a_1, \ldots, a_n) \in \mathbb{C}^n$ and $b = (b_1, \ldots, b_n) \in \mathbb{C}^n$. For a point $x \in X$, let $(T_x X)_0$ denote the embedded tangent space of X translated to the origin. Then the *Euclidean normal space* of X at x is defined as $N_x X = \{z \in \mathbb{C}^n : (z - x) \perp (T_x X)_0\}$. A pair of distinct points $(x, y) \in X \times X$ is thus a bottleneck exactly when $\overline{xy} \subseteq N_x X \cap N_y X$. Note that this is the case if and only if $y \in N_x X$ and $x \in N_y X$. The *bottleneck variety* in $\mathbb{C}^{2n}$ consists of the bottlenecks of X together with the diagonal $\{(x, y) \in X \times X : x = y\} \subset \mathbb{C}^n \times \mathbb{C}^n$. Just as for real varieties, the augmented Jacobian is defined by (2.7) and the system (2.8) defines the bottleneck variety of X.

In a similar manner we will define bottlenecks for projective varieties in complex projective space $\mathbb{P}^n$. Recall that projective space $\mathbb{P}^n$ is obtained by gluing a hyperplane at infinity to the affine space $\mathbb{C}^n$. For example, the projective plane $\mathbb{P}^2$ is the complex plane $\mathbb{C}^2$ with an added line at infinity.

Counting the number of roots to a system of polynomials is a highly challenging problem. The simplest case is counting roots in $\mathbb{P}^n$. Counting roots in $\mathbb{C}^n$ is harder and even harder is to count real roots. Consider for example a univariate polynomial $f \in \mathbb{R}[x]$ of degree d. In this case there are always d complex roots counted with multiplicity while the number of real roots depends on the coefficients of f. Consider now the next step of two equations $f_1, f_2 \in \mathbb{R}[x_1, x_2]$ of degrees d_1 and d_2 and the corresponding intersection of two curves in $\mathbb{C}^2$. If the intersection is finite there can be at most $d_1 d_2$ complex solutions. This is also the number of roots for almost all f_1 and f_2 of degrees d_1 and d_2. In the case of real curves in $\mathbb{R}^2$ there is no such generic root count. Also, the number of complex intersection points may be smaller than $d_1 d_2$ as illustrated by the example of two disjoint lines defined by $x_1 = 0$ and $x_1 = 1$. In contrast, the intersection of two curves in $\mathbb{P}^2$ of degrees d_1 and d_2 with finite intersection always consists of $d_1 d_2$ points counted with multiplicity. This fact is known as Bézout's theorem and it can be generalized to a system of n equations in n variables [101, Proposition 8.4]. This might seem to solve the problem, at least in $\mathbb{P}^n$. However, the system we want to solve might be *overdetermined* and have *excess components* of higher dimension. Both of these complications are present in the system (2.8). The excess component in this case consists of the discarded trivial solutions on the diagonal $\{(x, y) \in \mathbb{C}^n \times \mathbb{C}^n : x = y\}$. Amazingly, intersection theory provides tools to deal with these issues under certain circumstances. These tools are however often confined to the complex projective setting.

Bottlenecks for projective varieties turn out to be essential for counting bottlenecks on affine varieties. In fact, in Proposition 2.2.21 we reduce the affine case to the projective case by considering bottlenecks at infinity.

Polar Geometry

Consider the ellipse C defined by $x^2 + y^2/2 = 1$ in Example 2.2.1. For a point $p \in \mathbb{R}^2$ outside the region bounded by C there are exactly two lines through p tangent to C. The two tangent points $x, y \in C$ define what we call the first polar locus $P_1(X, p) = \{x, y\}$, see Figure 2.9. The polar locus depends on the choice of p but two polar loci $P_1(X, p)$ and $P_1(X, p')$ can be seen as deformations of each other by letting p' approach p along a curve. In this sense, the polar loci all represent the same *polar class* p_1 on C.

Polar loci, also known as polar varieties, can be generalized to varieties of higher dimension and play an important role in applications of non-linear algebra. Examples include real equation solving [15], computational complexity [49], computing invariants [19, 76, 77, 94], Euclidean distance degree [86] and optimization [165].

Here we use polar varieties to count bottlenecks. This is done in the complex projective setting. For a smooth projective variety $X \subset \mathbb{P}^n$ polar loci are defined using the projective tangent space $\mathbb{T}_x X \subset \mathbb{P}^n$ at points $x \in X$. Consider first the case where X is a smooth hypersurface defined by a homogeneous polynomial $f \in \mathbb{C}[x_0, \ldots, x_n]$ and let $x \in X$. Then the hyperplane $\mathbb{T}_x X \subset \mathbb{P}^n$ is defined by the equation $\sum_{i=0}^{n} x_i \frac{\partial f}{\partial x_i}(x) = 0$. In general, if X is a smooth variety defined by an ideal generated by homogeneous polynomials $f_1, \ldots, f_k \in \mathbb{C}[x_0, \ldots, x_n]$, then $\mathbb{T}_x X \subseteq \mathbb{P}^n$ is the subspace defined by the kernel of the Jacobian matrix $\{\frac{\partial f_i}{\partial x_j}(x)\}_{i,j}$.
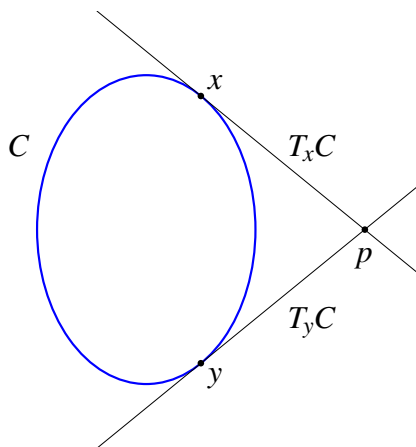
Figure 2.9: Polar locus of an ellipse.

For a smooth surface $X \subset \mathbb{P}^3$ we have two polar varieties. Let $p \in \mathbb{P}^3$ be a general point and $l \subset \mathbb{P}^3$ a general line. Then $P_1(X, p)$ is the set of points x such that the projective tangent plane $\mathbb{T}_x X \subset \mathbb{P}^3$ contains p. This is a curve on X. Similarly, $P_2(X, l) = \{x \in X : l \subseteq \mathbb{T}_x X\}$, which is finite. We also let $P_0(X) = X$. More generally, an m-dimensional variety has $m + 1$ polar varieties defined by exceptional tangent loci as follows. Let $X \subset \mathbb{P}^n$ be a smooth variety of dimension m. For $j = 0, \ldots, m$ and a general linear space $V \subseteq \mathbb{P}^n$ of dimension $n - m - 2 + j$ we define the polar locus

$$P_j(X, V) = \{x \in X : \dim(\mathbb{T}_x X \cap V) \geq j - 1\}.$$

If X has codimension 1 and $j = 0$, then V is the empty set using the convention $\dim(\emptyset) = -1$. By [101, Example 14.4.15] , $P_j(X, V)$ is either empty or of pure codimension j.

In order to link bottlenecks and polar varieties we employ the tools of intersection theory and pass from polar varieties to polar classes. For each polar variety $P_j(X, V)$ there is a corresponding polar class $[P_j(X, V)] = p_j$ which represents $P_j(X, V)$ up to *rational equivalence*. For example, $P_j(X, V)$ represents the same polar class p_j, independently of the general choice of linear space V. In a similar manner, any subvariety $Z \subset \mathbb{P}^n$ has a corresponding rational equivalence class $[Z]$. We refer to Section 1.2 for background on intersection theory. For more details on polar classes see for example [161, 162] and [101, Example 14.4.15]. An important point is that there is a well defined multiplication of polar classes corresponding to intersection of polar varieties. This means that $p_i p_j = [P_i(X, V) \cap P_j(X, W)]$ for $0 \leq i, j \leq m$. Here $V \subset \mathbb{P}^n$ and $W \subset \mathbb{P}^n$ are general linear spaces of dimension $n - m - 2 + i$ and $n - m - 2 + j$, respectively. To express the number of bottlenecks of a variety in terms of polar classes we also need the notion of *degree of a class*. If $Z \subset \mathbb{P}^n$ is a subvariety, $\deg(Z)$ is the number of points of $Z \cap L$, where $L \subset \mathbb{P}^n$ is a general linear space of dimension $n - \dim(Z)$. For the class $[Z]$ we let $\deg([Z]) = \deg(Z)$.

Results

Let $X \subset \mathbb{C}^n$ be a smooth variety and consider the closure $\bar{X} \subset \mathbb{P}^n$ in projective space. For the purpose of counting bottlenecks we introduce the *bottleneck degree* of an algebraic variety. Under suitable genericity assumptions (see Definition 2.2.9), the bottleneck degree coincides with the number of bottlenecks.

The orthogonality relation on $\mathbb{P}^n$ is defined via the *isotropic quadric* $Q \subset \mathbb{P}^n$ given in homogeneous coordinates by $\sum_0^n x_i^2 = 0$. Varieties which are tangent to Q are to be considered degenerate in this context and we say that a smooth projective variety is in *general position* if it intersects Q transversely.

Our main result, Theorem 2.2.13, is a proof that the bottleneck degree of a smooth variety $\bar{X} \subset \mathbb{P}^n$ in general position can be computed via the polar classes $p_0, \ldots, p_m$. The arguments in the proof directly give an algorithm for expressing the bottleneck degree in terms of polar classes. We have implemented this algorithm in Macaulay2 [107] and the script is available at [78]. We give the formula for projective curves, surfaces and threefolds, with the following notation: h denotes the hyperplane class in the intersection ring of $\bar{X}$, $d = \deg(\bar{X})$ and $\varepsilon_i = \sum_{j=0}^{m-i} \deg(p_j)$. We also use $\mathrm{BND}(\bar{X})$ to denote the bottleneck degree of $\bar{X}$.

Curves in $\mathbb{P}^2$:
$$\mathrm{BND}(\bar{X}) = d^4 - 4d^2 + 3d.$$

Curves in $\mathbb{P}^3$:
$$\mathrm{BND}(\bar{X}) = \varepsilon_0^2 + d^2 - \deg(2h + 5p_1).$$

Surfaces in $\mathbb{P}^5$:
$$\mathrm{BND}(\bar{X}) = \varepsilon_0^2 + \varepsilon_1^2 + d^2 - \deg(3h^2 + 6hp_1 + 12p_1^2 + p_2).$$

Threefolds in $\mathbb{P}^7$:
$$\mathrm{BND}(\bar{X}) = \varepsilon_0^2 + \varepsilon_1^2 + \varepsilon_2^2 + d^2 - \deg(4h^3 + 11h^2 p_1 + 4hp_1^2 + 24p_1^3 + 2hp_2 - 12p_1 p_2 + 17p_3).$$

Notice that $\varepsilon_0 = \deg(p_0) + \cdots + \deg(p_m)$ is equal to the Euclidean Distance Degree of the variety.

Now consider the smooth affine variety $X \subset \mathbb{C}^n \subset \mathbb{P}^n$ and let $H_\infty = \mathbb{P}^n \setminus \mathbb{C}^n$ be the hyperplane at infinity. The formulas for projective varieties above have to be modified to yield the bottleneck degree $\mathrm{BND}(X)$ of the affine variety X. Namely, there is a contribution to $\mathrm{BND}(\bar{X})$ from the hyperplane section $X \cap H_\infty$ at infinity. More precisely, we show in Proposition 2.2.21 that

$$\mathrm{BND}(X) = \mathrm{BND}(\bar{X}) - \mathrm{BND}(\bar{X} \cap H_\infty).$$

Here we have assumed that $X \subset \mathbb{C}^n$ is in general position in the following sense: $\bar{X}$ and $X \cap H_\infty$ are smooth and in general position. In the case of a plane curve $X \subset \mathbb{C}^2$ in general position the hyperplane section $\bar{X} \cap H_\infty$ consists of d points on the line at infinity. This results in

$$\mathrm{BND}(X) = d^4 - 4d^2 + 3d - d(d-1) = d^4 - 5d^2 + 4d. \tag{2.9}$$

We end this introduction with an example illustrating the above formula for affine curves $X \subset \mathbb{C}^2$. Before looking at a concrete example it is worth pointing out that by convention bottlenecks are counted as ordered pairs $(x, y) \in X \times X$. Since (y, x) is also a bottleneck if (x, y) is a bottleneck, each unordered bottleneck pair contributes twice to the bottleneck degree.

Example. Consider the Trott curve $X \subset \mathbb{C}^2$ defined by the equation

$$144(x_1^4 + x_2^4) - 225(x_1^2 + x_2^2) + 350x_1^2x_2^2 + 81.$$

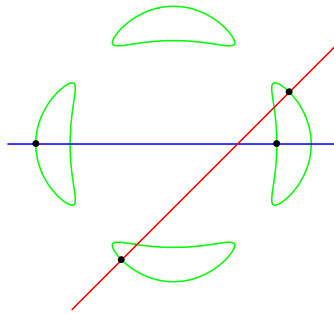This nonsingular quartic curve is notable because all 28 bitangents are real.

Figure 2.10: The quartic Trott curve depicted with two bottleneck pairs and their corresponding normal lines.

The bottleneck pairs $\{(x_1, x_2), (y_1, y_2)\}$ are the off-diagonal solutions to the following set of four equations, which are the equations of the bottleneck ideal described in (2.8). The first two imply that each point is on the curve and the second two imply that each point is on the normal line to the curve at the other point:

$$144(x_1^4 + x_2^4) - 225(x_1^2 + x_2^2) + 350x_1^2x_2^2 + 81 = 0$$
$$144(y_1^4 + y_2^4) - 225(y_1^2 + y_2^2) + 350y_1^2y_2^2 + 81 = 0$$
$$x_1(-576x_1^2 - 700x_2^2 + 450)(y_2 - x_2) = x_2(576x_2^2 + 700x_1^2 - 450)(x_1 - y_1)$$
$$y_1(-576y_1^2 - 700y_2^2 + 450)(x_2 - y_2) = y_2(576y_2^2 + 700y_1^2 - 450)(y_1 - x_1).$$

For a general enough affine plane curve of degree 4, (2.9) gives a bottleneck degree of 192. This is in fact the number of bottlenecks of the Trott curve. It was verified in Macaulay2 by creating the ideal of the four equations above and then saturating to remove the diagonal.

In this example, the 192 bottlenecks correspond to 192/2=96 bottleneck pairs. In particular, the real part of the Trott curve intersects the *x*- and *y*-axis each 4 times and in each case the relevant axis is the normal line to the curve at the intersection, leading to six bottleneck pairs on each axis.

Notation and Background in Intersection Theory

Below we introduce the Chow group of a subscheme of complex projective space $\mathbb{P}^n$ and present the double point formula from intersection theory. The reason for considering schemes and not only algebraic varieties is that isolated bottlenecks are counted with multiplicity and similar considerations should be made for higher dimensional bottleneck components. Specifically, the double point class defined below is a push forward of the double point scheme and the latter carries multiplicity information. In the end we only study bottlenecks on algebraic varieties and little is lost if the reader wishes to think of varieties in place of schemes.

The notation used here will closely follow that of Fulton's book [101]. Let $X \subseteq \mathbb{P}^n$ be a closed m-dimensional subscheme. We use $A_k(X)$ to denote the group of k-cycles on X up to rational equivalence and $A_*(X) = \bigoplus_{k=0}^{m} A_k(X)$ denotes the Chow group of X. For a subscheme $Z \subseteq X$ we have an associated cycle class $[Z] \in A_*(X)$. Also, for a zero cycle class $\alpha \in A_0(X)$ we have the notion of degree, denoted $\deg(\alpha)$, which counts the number of points with multiplicity of a 0-cycle representing α.

Suppose now that $X \subseteq \mathbb{P}^n$ is a smooth variety of dimension m. In this case we will also consider the intersection product on $A_*(X)$ which makes it into a ring. For $\alpha, \beta \in A_*(X)$ we denote their intersection product by $\alpha\beta$ or $\alpha \cdot \beta$. Now let $\alpha \in A_k(X)$ with $k > 0$ and consider the hyperplane class $h \in A_{m-1}(X)$ induced by the embedding $X \subseteq \mathbb{P}^n$. Here, we define $\deg(\alpha) = \deg(h^k \alpha)$. This means that if α is represented by a subvariety $Z \subseteq X$, then $\deg(\alpha)$ is the degree of Z. For a cycle class $\alpha \in A_*(X)$, we will use $(\alpha)_k$ to denote the homogeneous piece of α of codimension k, that is $(\alpha)_k$ is the projection of α to $A_{m-k}(X)$. Finally, for $i = 0, \ldots, m$, $c_i(T_X)$ denotes the i-th Chern class of the tangent bundle of X and $c(T_X) = c_0(T_X) + \cdots + c_m(T_X)$ denotes the total Chern class.

Now let X and Y be subschemes of projective space. A map $f : X \longrightarrow Y$ gives rise to a push forward group homomorphism $f_* : A_*(X) \longrightarrow A_*(Y)$ and if X and Y are smooth varieties we also have a pull-back ring homomorphism $f^* : A_*(Y) \longrightarrow A_*(X)$.

Let $f : X \longrightarrow Y$ be a morphism of smooth projective varieties. Let $x \in A_k(X)$, $y \in A_l(Y)$ satisfy $k + l = \dim(Y)$. By the projection formula [101, Proposition 8.3 (c)], $f_*(f^*(y) \cdot x) = y \cdot f_*(x)$. In particular $\deg(y \cdot f_*(x)) = \deg(f_*(f^*(y) \cdot x)) = \deg(f^*(y) \cdot x)$. This relation is used many times in the sequel.

Now let $f : X \longrightarrow Y$ be a map of smooth projective varieties with $\dim(X) = k$ and $\dim(Y) = 2k$. Let $f \times f : X \times X \longrightarrow Y \times Y$ be the induced map, let $\mathrm{Bl}_{\Delta_X}(X \times X)$ be the blow-up of $X \times X$ along the diagonal $\Delta_X \subset X \times X$ and let $bl : \mathrm{Bl}_{\Delta_X}(X \times X) \longrightarrow X \times X$ be the blow-up map. Consider the map $h = (f \times f) \circ bl : \mathrm{Bl}_{\Delta_X}(X \times X) \longrightarrow Y \times Y$ and the inverse image scheme $h^{-1}(\Delta_Y)$ of the diagonal $\Delta_Y \subset Y \times Y$. Then the exceptional divisor $bl^{-1}(\Delta_X)$ is a subscheme of $h^{-1}(\Delta_Y)$ and its residual scheme in $h^{-1}(\Delta_Y)$ is called the *double point scheme* of f and is denoted $\tilde{D}(f)$. The exceptional divisor $bl^{-1}(\Delta_X)$ may be interpreted as the projectivized tangent bundle $\mathbb{P}(T_X)$. The support of the double point scheme $\tilde{D}(f)$ consists of the pairs of distinct points $(x,y) \in X \times X \subset \mathrm{Bl}_{\Delta_X}(X \times X) \setminus bl^{-1}(\Delta_X)$ such that $f(x) = f(y)$ together with the tangent directions in $\mathbb{P}(T_X)$ where the differential $df : T_X \to T_Y$ vanishes, see [132, Remark 14]. There is also an associated residual intersection class $\bar{\mathbb{D}}(f) \in A_0(\tilde{D}(f))$ defined in [101, Theorem 9.2]. If $\tilde{D}(f)$ has dimension 0, as expected, then $\mathbb{D}(f) = [\tilde{D}(f)]$. Let $\eta : \tilde{D}(f) \longrightarrow X$ be the map induced by bl and the projection $X \times X \longrightarrow X$ onto

the first factor. Then the *double point class* $\mathbb{D}(f) \in A_0(X)$ is defined by $\mathbb{D}(f) = \eta_*(\bar{\mathbb{D}}(f))$. By the double point formula, [101, Theorem 9.3],

$$\mathbb{D}(f) = f^* f_*[X] - (c(f^* T_Y) c(T_X)^{-1})_k. \tag{2.10}$$

The Conormal Variety

Let $X \subset \mathbb{P}^n$ be a smooth variety of dimension m. Recall that $H^0(X, \mathscr{O}_X(1)) \cong \mathbb{C}^{n+1}$ is the vector space parameterizing the hyperplane sections of the embedding $X \subseteq \mathbb{P}^n \cong \mathbb{P}(H^0(X, \mathscr{O}_X(1)))$. Consider the surjective linear map:

$$\mathrm{jet}_x : H^0(X, \mathscr{O}_X(1)) \longrightarrow H^0(\mathscr{O}_X(1) \otimes \mathscr{O}_X/m_x^2) \cong \mathbb{C}^{m+1},$$

where m_x is the maximal ideal at x. Roughly speaking this map assigns to a global section s the $(m+1)$-tuple $(s(x), \ldots, \frac{\partial s}{\partial x_i}(x), \ldots)$, where $(x_1, \ldots, x_m)$ is a system of coordinates around x. We also have that

$$\mathbb{T}_x X = \mathbb{P}(\mathrm{im}(\mathrm{jet}_x)) \cong \mathbb{P}^m.$$

Let $N_{X/\mathbb{P}^n}$ be the normal bundle of X in $\mathbb{P}^n$ and let $N_{X/\mathbb{P}^n}^\vee$ be its dual. The fibers of the dual normal bundle at x are given by the kernel of the map $\mathrm{jet}_x : \ker(\mathrm{jet}_x) \cong N_{X/\mathbb{P}^n}^\vee{}_x \otimes \mathscr{O}_X(1)_x$. The projective tangent spaces at points $x \in X$ glue together to form the first jet bundle $\mathbb{J}$ with fiber $\mathbb{J}_x = H^0(\mathscr{O}_X(1) \otimes \mathscr{O}_X/m_x^2)$, inducing the exact sequence of vector bundles:

$$0 \longrightarrow N_{X/\mathbb{P}^n}^\vee \otimes \mathscr{O}_X(1) \longrightarrow X \times H^0(\mathscr{O}_X(1)) \longrightarrow \mathbb{J} \longrightarrow 0 \tag{2.11}$$

The projectivized bundle of the conormal bundle is called the *conormal variety*:

$$\mathscr{C}_X = \mathbb{P}(N_{X/\mathbb{P}^n}^\vee) \cong \mathbb{P}(N_{X/\mathbb{P}^n}^\vee \otimes \mathscr{O}_X(1)) \subset \mathbb{P}^n \times (\mathbb{P}^n)^*$$

where $\mathbb{P}(N_{X/\mathbb{P}^n}^\vee)$ denotes the projectivized conormal bundle of X in $\mathbb{P}^n$, see [101, Example 3.2.21] for more details. From the exact sequence (2.11) it follows that the conormal variety consists of pairs of points $x \in X$ and hyperplanes in $\mathbb{P}^n$ that contain the projective tangent space $\mathbb{T}_x X$.

Bottleneck Degree

Let $X \subset \mathbb{P}^n$ be a smooth variety of dimension $m < n$ and consider the conormal variety $\mathscr{C}_X = \mathbb{P}(N_{X/\mathbb{P}^n}^\vee) \subset \mathbb{P}^n \times (\mathbb{P}^n)^*$ introduced above. We use $\mathscr{O}(1)$ to denote the dual of the tautological line bundle on $\mathscr{C}_X$, see [101, Appendix B.5.1 and B.5.5], and $\xi = c_1(\mathscr{O}(1))$ denotes the first Chern class of $\mathscr{O}(1)$. Also, let $\pi : \mathscr{C}_X \to X$ be the projection. Note that $\dim(\mathscr{C}_X) = n - 1$.

Remark 2.2.4. In the sequel we will compute the degrees of zero cycle classes in $A_0(\mathbb{P}(N_{X/\mathbb{P}^n}^\vee))$. By [101, Theorem 3.3 (b)], $A_0(X) \cong A_0(\mathbb{P}(N_{X/\mathbb{P}^n}^\vee))$ via the map $\alpha \mapsto \xi^{n-m-1} \pi^* \alpha$. This means that every element of $A_0(\mathbb{P}(N_{X/\mathbb{P}^n}^\vee))$ can be written uniquely in the form $\xi^{n-m-1} \pi^* \alpha$ where $\alpha \in A_0(X)$, leading to a degree formula:

$$\deg(\xi^{n-m-1} \pi^* \alpha) = \deg(\alpha).$$

Also, by [101, Remark 3.2.4]

$$\xi^{n-m} + c_1(\pi^* N^\vee_{X/\mathbb{P}^n})\xi^{n-m-1} + \cdots + c_{n-m}(\pi^* N^\vee_{X/\mathbb{P}^n}) = 0. \tag{2.12}$$

Hence, given a zero cycle class $Z \in A_0(\mathbb{P}(N^\vee_{X/\mathbb{P}^n}))$ of the form $Z = \xi^i \pi^* \beta$ where $i > n - m - 1$ and $\beta \in A_{i-(n-m-1)}(X)$ we may use (2.12) to write Z as $\xi^{n-m-1}\pi^*\alpha$ for some $\alpha \in A_0(X)$. More generally, consider a 0-cycle class $Z \in A_0(\mathbb{P}(N^\vee_{X/\mathbb{P}^n}))$ which is a polynomial in ξ and pull-backs of classes on X, $Z = \sum_{i=0}^l \xi^i \pi^* \beta_i$. Then $\xi^i \pi^* \beta_i = 0$ for $i < n - m - 1$ and $\beta_i \in A_{i-(n-m-1)}(X)$ for $i \geq n - m - 1$. Again we can use the relation (2.12) to write Z as $\xi^{n-m-1}\pi^*\alpha$ for some $\alpha \in A_0(X)$. This may be done in practice by applying the function `pseudoRemainder` in Macaulay2 [107] to Z and the left hand side of (2.12). We will make use of this to compute bottleneck degrees in Algorithm 1.

We will consider $\mathscr{C}_X$ as a subvariety of $\mathbb{P}^n \times \mathbb{P}^n$ as follows. Fix coordinates on $\mathbb{P}^n$ induced by the standard basis of $\mathbb{C}^{n+1}$. Then identify $\mathbb{P}^n$ with $(\mathbb{P}^n)^*$ via the isomorphism $L : \mathbb{P}^n \longrightarrow (\mathbb{P}^n)^*$ which sends a point $(a_0, \ldots, a_n) \in \mathbb{P}^n$ to the hyperplane $\{(x_0, \ldots, x_n) \in \mathbb{P}^n : a_0 x_0 + \cdots + a_n x_n = 0\}$. Define $a \perp b$ by $\sum_{i=0}^n a_i b_i = 0$ for $a = (a_0, \ldots, a_n), b = (b_0, \ldots, b_n) \in \mathbb{P}^n$. For a point $p \in X$ we denote by $(\mathbb{T}_p X)^\perp$ the orthogonal complement of the projective tangent space of X at p. The span $\langle p, (\mathbb{T}_p X)^\perp \rangle$ of p and $(\mathbb{T}_p X)^\perp$ is called the Euclidean normal space of X at p and is denoted $N_p X$. The Euclidean normal space is intrinsically related to the conormal variety as:

$$\mathscr{C}_X = \{(p,q) \in \mathbb{P}^n \times \mathbb{P}^n : p \in X, q \in (\mathbb{T}_p X)^\perp\}.$$

Definition 2.2.5. We say that a smooth variety $X \subset \mathbb{P}^n$ is in *general position* if $\mathscr{C}_X$ is disjoint from the diagonal $\Delta \subset \mathbb{P}^n \times \mathbb{P}^n$.

Let $Q \subset \mathbb{P}^n$ be the *isotropic quadric*, which is defined by $\sum_{i=0}^n x_i^2 = 0$. If $p \in X \cap Q$ is that such that $\mathbb{T}_p X \subseteq \mathbb{T}_p Q$, then $(p,p) \in \mathscr{C}_X$. Conversely, if $(p,p) \in \mathscr{C}_X$, then $p \in X \cap Q$ and $\mathbb{T}_p X \subseteq \mathbb{T}_p Q$. In other words, X is in general position if and only if X intersects the isotropic quadric transversely.

Suppose that X is in general position. We then have a map

$$f : \mathscr{C}_X \to \mathrm{Gr}(2, n+1) : (p,q) \mapsto \langle p, q \rangle, \tag{2.13}$$

from $\mathscr{C}_X$ to the Grassmannian of lines in $\mathbb{P}^n$. The map sends a pair (p,q) to the line spanned by p and q. For the remainder of this section, f will be used to denote this map associated to a variety X. To simplify notation we will also let $G = \mathrm{Gr}(2, n+1)$.

Note that for $p \in X$, the map f restricted to the fiber $\{(p',q') \in \mathscr{C}_X : p' = p\}$ parameterizes lines in the Euclidean normal space $N_p X$ passing through p.

Example 2.2.6. In the case where $X \subset \mathbb{P}^n$ is a smooth hypersurface, $\mathscr{C}_X \cong X$ via the projection on the first factor of $\mathbb{P}^n \times (\mathbb{P}^n)^*$. Consider a general curve $X \subset \mathbb{P}^2$ of degree d defined by a polynomial $F \in \mathbb{C}[x,y,z]$. For $u \in \{x,y,z\}$, let $F_u = \frac{\partial F}{\partial u}$. In this case $G = (\mathbb{P}^2)^*$ and the map $f : X \longrightarrow (\mathbb{P}^2)^*$ defined above is given by $(x,y,z) \mapsto (yF_z - zF_y, zF_x - xF_z, xF_y - yF_x)$. Note that $f(p) = N_p X$ is the Euclidean normal line to X at p.

Returning to a smooth m-dimensional variety $X \subset \mathbb{P}^n$ in general position, consider the projection $\eta : \mathscr{C}_X \times \mathscr{C}_X \longrightarrow X \times X$ and the incidence correspondence

$$I(X) = \eta(\{(u,v) \in \mathscr{C}_X \times \mathscr{C}_X : f(u) = f(v)\}).$$

Pairs $(x,y) \in I(X) \subset X \times X$ with $x \neq y$ are called *bottlenecks* of X. The following lemma relates this definition of bottlenecks to the one given for affine varieties in the introduction. For $x \in X$, recall the definition of the Euclidean normal space $N_x X = \langle x, (\mathbb{T}_x X)^\perp \rangle$, where $\mathbb{T}_x X$ denotes the projective tangent space of X at x.

Lemma 2.2.7. *Let $X \subset \mathbb{P}^n$ be a smooth variety in general position. For a pair of distinct points $x, y \in X$, (x,y) is a bottleneck if and only if $y \in N_x X$ and $x \in N_y X$.*

Proof. By definition $(x,q) \in \mathscr{C}_X \subset \mathbb{P}^n \times \mathbb{P}^n$ if and only if $x \in X$ and $q \in (\mathbb{T}_x X)^\perp$. Hence, for $(x,q) \in \mathscr{C}_X$, the line $\langle x, q \rangle$ is contained in $N_x X$. Now, if $(x,y) \in X \times X$ is a bottleneck, then $(x,q), (y,q') \in \mathscr{C}_X$ for some $q, q' \in \mathbb{P}^n$ with $\langle x, q \rangle = \langle y, q' \rangle$. Hence $y \in \langle x, q \rangle \subseteq N_x X$. In the same way $x \in N_y X$. To see the converse let $x, y \in X$ be distinct points such that $y \in N_x X$ and $x \in N_y X$. Since $y \in N_x X$, $y \in \langle x, q \rangle$ for some $q \in (\mathbb{T}_x X)^\perp$. Then $(x,q) \in \mathscr{C}_X$ and $q \neq x$ since X is in general position. This implies that $\langle x, y \rangle = \langle x, q \rangle$. In the same way, $x \in N_y X$ implies that $(y,q') \in \mathscr{C}_X$ for some $q' \in \mathbb{P}^n$ with $\langle x, y \rangle = \langle y, q' \rangle$. Since $\langle x, q \rangle = \langle y, q' \rangle$, (x,y) is a bottleneck. $\square$

Applying the double point formula (2.10) to the map f we obtain

$$\mathbb{D}(f) = f^* f_* [\mathscr{C}_X] - (c(f^* T_G) c(T_{\mathscr{C}_X})^{-1})_{n-1},$$

where $\mathbb{D}(f)$ is the double point class of f.

Definition 2.2.8. Let $X \subset \mathbb{P}^n$ be a smooth variety in general position. We call $\deg(\mathbb{D}(f))$ the *bottleneck degree* of X and denote it by $\mathrm{BND}(X)$.

The bottleneck degree is introduced to count bottlenecks on X but there are some issues that need to be considered. The first issue is that there might be higher dimensional components worth of bottlenecks. In this case the bottleneck degree assigns multiplicities to these components which contribute to the bottleneck degree. We will not pursue this aspect of bottlenecks even though it is an interesting topic. Consider now a smooth variety $X \subset \mathbb{P}^n$ in general position with only finitely many bottlenecks. As mentioned above, the double point scheme of f contains not only bottlenecks but also the tangent directions in $\mathbb{P}(T_{\mathscr{C}_X})$ where the differential of f vanishes. This motivates the following definition of *bottleneck regular* varieties. As we shall see in Proposition 2.2.11, the bottleneck degree is equal to the number of bottlenecks counted with multiplicity in this case.

Definition 2.2.9. We will call a smooth variety $X \subset \mathbb{P}^n$ *bottleneck regular* (BN-regular) if

1. X is in general position,

2. X has only finitely many bottlenecks and

3. the differential $df_p : T_p \mathscr{C}_X \longrightarrow T_{f(p)} G$ of the map f has full rank for all $p \in \mathscr{C}_X$.

Proposition 2.2.10. *Assume X is BN-regular. Let $X \subset \mathbb{P}^a \subseteq \mathbb{P}^b$ be a smooth variety where $\mathbb{P}^a \subseteq \mathbb{P}^b$ is a coordinate subspace. If X is in general position with respect to $\mathbb{P}^a$ then X is in general position with respect to $\mathbb{P}^b$ and the bottleneck degree is independent of the choice of ambient space.*

Proof. For $c = a, b$, let $\mathscr{C}^c$ denote the conormal variety with respect to the embedding $X \subset \mathbb{P}^c$. The embedding $\mathbb{P}^a \subseteq \mathbb{P}^b$ induces an embedding $\mathscr{C}^a \subseteq \mathscr{C}^b$. Similarly for $c = a, b$, let $f_c : \mathscr{C}^c \longrightarrow$ $\mathrm{Gr}(2, c+1)$ be the map given by $(p, q) \mapsto \langle p, q \rangle$ and let $\Delta_c \subset \mathbb{P}^c \times \mathbb{P}^c$ be the diagonal. Suppose that $(p, q) \in \mathscr{C}^b \cap \Delta_b$. Since $p \in X \subset \mathbb{P}^a$, we have that $q = p \in \mathbb{P}^a$ and $(p, q) \in \mathscr{C}^a \cap \Delta_a = \emptyset$. Hence X is in general position with respect to $\mathbb{P}^b$.

We will consider $\mathbb{D}(f_a)$ as a cycle class on $\mathscr{C}^b$ via the inclusion $\mathscr{C}^a \subseteq \mathscr{C}^b$. We will show that $\tilde{D}(f_a) = \tilde{D}(f_b)$. Since X is BN-regular $[\tilde{D}(f_c)] = \mathbb{D}(f_c)$ for $c = a, b$. It follows that $\mathbb{D}(f_a) = \mathbb{D}(f_b)$, which in turn implies that the bottleneck degree is independent of the choice of ambient space. Note that $\tilde{D}(f_a) \subseteq \tilde{D}(f_b)$.

We will first show that the differential $df_b : T_{\mathscr{C}^b} \longrightarrow T_G$ has full rank outside $T_{\mathscr{C}^a}$. This implies that $\tilde{D}(f_b) \setminus \tilde{D}(f_a)$ consists of pairs $x, y \in \mathscr{C}^b$ with $x \neq y$ and $f_b(x) = f_b(y)$. Suppose that $x = (p, q) \in \mathscr{C}^b$ and $v \in T_x \mathscr{C}^b$ is a non-zero tangent vector such that $(df_b)_x(v) = 0$. Let $D \subset \mathbb{C}$ be the unit disk and let $P, Q : D \longrightarrow \mathbb{C}^{b+1} \setminus \{0\}$ be smooth analytic curves such that the induced curve $D \longrightarrow \mathbb{P}^n \times \mathbb{P}^n$ is contained in $\mathscr{C}^b$, passes through $x = (p, q)$ at $0 \in D$ and has tangent vector v there. In other words $P(0) \in p$ and $Q(0) \in q$ are representatives of p and q. We need to show that $Q(0), Q'(0) \in \mathbb{C}^{a+1}$. Since $(df_b)_x(v) = 0$, we have by [111, Example 16.1] that $P'(0), Q'(0) \in \langle P(0), Q(0) \rangle$. Suppose first that $P'(0)$ and $P(0)$ are independent. Then $Q(0), Q'(0) \in \langle P(0), P'(0) \rangle$ and $\langle P(0), P'(0) \rangle \subseteq \mathbb{C}^{a+1}$ since $X \subset \mathbb{P}^a$. Now suppose that $P'(0)$ is a multiple of $P(0)$. Since $v \neq 0$, $Q(0)$ and $Q'(0)$ are independent and $Q'(0)$ corresponds to a point $q' \in \mathbb{P}^n$. That $P(0)$ and $P'(0)$ are dependent implies that $(p, q') \in \mathscr{C}^b$. Moreover, $P(0) \in \langle Q(0), Q'(0) \rangle$ by above and hence $p \in \langle q, q' \rangle$. It follows that $(p, p) \in \mathscr{C}^b$, which contradicts that X is in general position.

Now let $(x, y) \in \tilde{D}(f_b)$ with $x \neq y$ and $f_b(x) = f_b(y)$. If $x, y \in \mathscr{C}^a$ then $(x, y) \in \tilde{D}(f_a)$ so assume that $x \notin \mathscr{C}^a$. Let $x = (p_1, q_1)$ and $y = (p_2, q_2)$ with $(p_i, q_i) \in X \times \mathbb{P}^b$. Since $\langle p_1, q_1 \rangle = \langle p_2, q_2 \rangle$ and because this line intersects $\mathbb{P}^a$ in exactly one point $p \in \mathbb{P}^a$, we have that $p_1 = p_2 = p$. Moreover, $p \in \langle q_1, q_2 \rangle$ and hence $(p, p) \in \mathscr{C}^a$ contradicting that X is in general position. This means that $\tilde{D}(f_b) \subseteq \tilde{D}(f_a)$ and hence $\tilde{D}(f_a) = \tilde{D}(f_b)$. $\qquad \square$

If $X \subset \mathbb{P}^n$ is BN-regular, then the double point scheme $\tilde{D}(f)$ is finite and in one-to-one correspondence with the bottlenecks of X through the projection $\eta : \mathscr{C}_X \times \mathscr{C}_X \longrightarrow X \times X$. Using the scheme-structure of $\tilde{D}(f)$ we assign a multiplicity to each bottleneck. With notation as above, $[\tilde{D}(f)] = \bar{\mathbb{D}}(f)$ and we therefore have the following.

Proposition 2.2.11. *If $X \subset \mathbb{P}^n$ is BN-regular, then $\mathrm{BND}(X)$ is equal to the number of bottlenecks of X counted with multiplicity.*

Remark 2.2.12. Recalling the notation from above, $\mathscr{O}(1)$ denotes the dual of the tautological line bundle on the conormal variety $\mathscr{C}_X$, $\pi : \mathscr{C}_X \longrightarrow X$ is the projection and $\xi = c_1(\mathscr{O}(1))$. The bottleneck degree depends on the Chern classes of $\mathscr{C}_X$ and below we shall relate these to the Chern

classes of X, the hyperplane class and ξ. By [101, Example 3.2.11] we have that $c(T_{\mathscr{C}_X}) = c(\pi^* T_X) c(\pi^* N_{X/\mathbb{P}^n}^\vee \otimes \mathscr{O}(1))$. Since the rank of $N_{X/\mathbb{P}^n}^\vee$ is $n - m$ we have by [101, Remark 3.2.3] that

$$
\begin{aligned}
c(\pi^* N_{X/\mathbb{P}^n}^\vee \otimes \mathscr{O}(1)) &= \sum_{i=0}^{n-m} c_i(\pi^* N_{X/\mathbb{P}^n}^\vee)(1+\xi)^{n-m-i} \\
&= \sum_{i=0}^{n-m} (-1)^i \pi^* c_i(N_{X/\mathbb{P}^n})(1+\xi)^{n-m-i}.
\end{aligned}
$$

Note also that $c_i(N_{X/\mathbb{P}^n}) = 0$ for $i > m = \dim(X)$. Moreover, the normal bundle $N_{X/\mathbb{P}^n}$ is related to the tangent bundles T_X and $T_{\mathbb{P}^n}$ by the exact sequence

$$0 \longrightarrow T_X \longrightarrow i^* T_{\mathbb{P}^n} \longrightarrow N_{X/\mathbb{P}^n} \longrightarrow 0,$$

where $i : X \longrightarrow \mathbb{P}^n$ is the inclusion. It follows that $c(N_{X/\mathbb{P}^n}) = c(i^* T_{\mathbb{P}^n}) c(T_X)^{-1}$. Also, $c(T_{\mathbb{P}^n}) = (1+H)^{n+1}$ where $H \in A_{n-1}(\mathbb{P}^n)$ is the hyperplane class.

For $n - 1 \geq a \geq b \geq 0$, define the Schubert class $\sigma_{a,b} \in A_*(G)$ as the class of the locus $\Sigma_{a,b} = \{l \in G : l \cap A \neq \emptyset, l \subset B\}$ where $A \subset B \subseteq \mathbb{P}^n$ is a general flag of linear spaces with $\operatorname{codim}(A) = a+1$ and $\operatorname{codim}(B) = b$. In the case $b = 0$ we use the notation $\sigma_{a,0} = \sigma_a$. See [92] for basic properties of Schubert classes. In particular we will make use of the relations $\sigma_1^2 = \sigma_{1,1} + \sigma_2$ if $n \geq 3$ and $\sigma_{a+c,b+c} = \sigma_{c,c}\sigma_{a,b}$ for $n-1 \geq a \geq b \geq 0$ and $0 \leq a+c \leq n-1$. Also, $\sigma_{n-1-i,i} \cdot \sigma_{n-1-j,j} = 0$ for $0 \leq i,j \leq \lfloor \frac{n-1}{2} \rfloor$ if $i \neq j$ and $\sigma_{n-1-i,i}^2$ is the class of a point. In Algorithm 1 below we will need to express the total Chern class $c(T_G)$ of the Grassmannian as a polynomial in Schubert classes. To do this we apply the routine `chern` from the Macaulay2 package *Schubert2* [106].

We will recall the definition of the polar classes $p_0, \ldots, p_m \in A_*(X)$ of X. For a general linear space $V \subseteq \mathbb{P}^n$ of dimension $n - m - 2 + j$ we have that p_j is the class represented by the polar locus

$$P_j(X, V) = \{x \in X : \dim(\mathbb{T}_x X \cap V) \geq j - 1\}.$$

If X has codimension 1 and $j = 0$, then V is the empty set using the convention $\dim(\emptyset) = -1$. By [101, Example 14.4.15], $P_j(X, V)$ is either empty or of pure codimension j and

$$p_j = \sum_{i=0}^{j} (-1)^i \binom{m-i+1}{j-i} h^{j-i} c_i(T_X), \tag{2.14}$$

where $h \in A_{n-1}(X)$ is the hyperplane class. Moreover, the polar loci $P_j(X, V)$ are reduced, see [161]. Inverting the relationship between polar classes and Chern classes we get

$$c_j(T_X) = \sum_{i=0}^{j} (-1)^i \binom{m-i+1}{j-i} h^{j-i} p_i. \tag{2.15}$$

We will examine an alternative interpretation of polar classes via the conormal variety $\mathscr{C}_X$. This will help us to determine the class of $\mathscr{C}_X$ in $A_*(\mathbb{P}^n \times \mathbb{P}^n)$. Recall that the polar loci $P_j(X, V)$ are either empty or of codimension j. It follows that for a generic point $x \in P_j(X, V)$, $\mathbb{T}_x X$ intersects V in exactly dimension $j - 1$, that is $\dim(\mathbb{T}_x X \cap V) = j - 1$. Let $0 \leq i \leq m$ and let $\hat{V}, W \subseteq \mathbb{P}^n$ be general linear spaces with $\dim(\hat{V}) = i+1$ and $\dim(W) = n-i$. Recall the fixed isomorphism $L : \mathbb{P}^n \longrightarrow (\mathbb{P}^n)^*$

and let $V \subset \mathbb{P}^n$ be the intersection of all hyperplanes in $L(\hat{V})$. Note that $\dim(V) = n - 2 - i$. Now consider the intersection $J = \mathscr{C}_X \cap (W \times \hat{V}) \subseteq \mathbb{P}^n \times \mathbb{P}^n$. Then J is finite and we have the projection map $\pi_{|J} : J \longrightarrow P_{m-i}(X, V) \cap W$. Now, $\pi_{|J}$ is bijective onto $P_{m-i}(X, V) \cap W$ because given $x \in P_{m-i}(X, V) \cap W$, $\dim(\mathbb{T}_x X \cap V) = m - i - 1$ and therefore the span of $\mathbb{T}_x X$ and V is the unique hyperplane containing $\mathbb{T}_x X$ and V. Let $\alpha, \beta \in A_{2n-1}(\mathbb{P}^n \times \mathbb{P}^n)$ be the pullbacks of the hyperplane class of $\mathbb{P}^n$ under the two projections and consider $[\mathscr{C}_X]$ as an element of $A_*(\mathbb{P}^n \times \mathbb{P}^n)$. Then $[W \times \hat{V}] = \alpha^i \beta^{n-1-i}$ and $\deg([\mathscr{C}_X] \cdot \alpha^i \beta^{n-1-i}) = \deg(J) = \deg(p_{m-i})$. Note that $[\mathscr{C}_X] \cdot \alpha^i = 0$ if $i > m$ since α is the pullback of a divisor on $\mathbb{P}^n$.

Theorem 2.2.13. *Let $X \subset \mathbb{P}^n$ be a smooth m-dimensional variety in general position. Let $h = \pi^*(h_X) \in A_*(\mathscr{C}_X)$ where $h_X \in A_*(X)$ is the hyperplane class and $\pi : \mathscr{C}_X \longrightarrow X$ is the projection. We use $\mathscr{O}(1)$ to denote the dual of the tautological line bundle on $\mathscr{C}_X$ and ξ to denote its first Chern class. Also $\alpha, \beta \in A_{2n-1}(\mathbb{P}^n \times \mathbb{P}^n)$ denote the pullbacks of the hyperplane class of $\mathbb{P}^n$ under the two projections. Let $k = \min\{\lfloor \frac{n-1}{2} \rfloor, m\}$ and for $i = 0, \ldots, k$, put $\varepsilon_i = \sum_{j=r_i}^{m-i} \deg(p_j)$ where $r_i = \max\{0, m - n + 1 + i\}$. Then the following holds:*

$$[\mathscr{C}_X] = \sum_{i=0}^{m} \deg(p_{m-i}) \alpha^{n-i} \beta^{1+i}, \tag{2.16}$$

$$f^*(\sigma_{a,b}) = \sum_{i=0}^{a-b} h^{b+i}(\xi - h)^{a-i}, \tag{2.17}$$

$$f_*[\mathscr{C}_X] = \sum_{i=0}^{k} \varepsilon_i \sigma_{n-1-i,i}, \tag{2.18}$$

$$\deg(f^* f_*[\mathscr{C}_X]) = \sum_{i=0}^{k} \varepsilon_i^2. \tag{2.19}$$

Hence

$$\mathrm{BND}(X) = \sum_{i=0}^{k} \varepsilon_i^2 - \deg(B_{m,n}),$$

for some polynomial $B_{m,n}$ in the polar classes and the hyperplane class of X.

Proof. To show (2.16), note that $\mathrm{codim}(\mathscr{C}_X) = 2n - (n-1) = n + 1$ and write $[\mathscr{C}_X] = \sum_{i=0}^{n-1} d_i \alpha^{n-i} \beta^{1+i}$ for some $d_i \in \mathbb{Z}$. Let $0 \leq i \leq n - 1$. Because $d_i = \deg([\mathscr{C}_X] \cdot \alpha^i \beta^{n-1-i})$, it follows that:

$$d_i = \deg(p_{m-i}) \text{ if } 0 \leq i \leq m \text{ and } d_i = 0 \text{ if } i > m.$$

Let $bl : \mathrm{Bl}_\Delta(\mathbb{P}^n \times \mathbb{P}^n) \longrightarrow \mathbb{P}^n \times \mathbb{P}^n$ be the blow-up of $\mathbb{P}^n \times \mathbb{P}^n$ along the diagonal $\Delta \subset \mathbb{P}^n \times \mathbb{P}^n$ and let $E = bl^{-1}(\Delta)$, the exceptional divisor. The map $\mathbb{P}^n \times \mathbb{P}^n \setminus \Delta \longrightarrow \mathrm{Gr}(2, n+1)$, which sends a pair of points (p, q) to the line spanned by p and q, extends to a map $\gamma : \mathrm{Bl}_\Delta(\mathbb{P}^n \times \mathbb{P}^n) \longrightarrow \mathrm{Gr}(2, n+1)$, see [125]. The theorem in the third paragraph of [125, Appendix B], with $X = \mathbb{P}^N$ in the notation used there, states that

$$\gamma^*(\sigma_a) = \sum_{i=0}^{a} bl^* \alpha^i bl^* \beta^{a-i} + \sum_{i=0}^{a-1} (-1)^{i+1} \binom{a+1}{i+2} bl^* \alpha^{a-1-i}[E]^{i+1}.$$

Consider $\mathscr{C}_X$ as a subvariety of $\mathrm{Bl}_\Delta(\mathbb{P}^n \times \mathbb{P}^n)$ and let $i : \mathscr{C}_X \longrightarrow \mathrm{Bl}_\Delta(\mathbb{P}^n \times \mathbb{P}^n)$ be the embedding. Then $i^* bl^* \alpha = h$ and by [101, Example 3.2.21], $\xi - h = i^* bl^* \beta$. Moreover, since X is in general position, $i^*[E] = 0$. Using $f = \gamma \circ i$, we get that $f^*(\sigma_a) = i^* \gamma^*(\sigma_a) = \sum_{i=0}^{a} h^i(\xi - h)^{a-i}$. In particular, $f^*(\sigma_1) = \xi$, which proves (2.17) in the case $n = 2$. If $n \geq 3$, we have by above that $f^*(\sigma_2) = \xi^2 - h\xi + h^2$. Moreover $\sigma_{1,1} = \sigma_1^2 - \sigma_2$, and hence $f^*(\sigma_{1,1}) = h(\xi - h)$. Since $\sigma_{b,b} = \sigma_{1,1}^b$ we get $f^*(\sigma_{b,b}) = h^b(\xi - h)^b$. Finally, using $\sigma_{a,b} = \sigma_{b,b}\sigma_{a-b}$ we get that $f^*(\sigma_{a,b}) = h^b(\xi - h)^b \sum_{i=0}^{a-b} h^i(\xi - h)^{a-b-i}$, which gives (2.17).

For (2.18), note first that

$$\gamma^*(\sigma_{a,b}) = \gamma^*(\sigma_{b,b})\gamma^*(\sigma_{a-b}) = \sum_{i=0}^{a-b} bl^* \alpha^{b+i} bl^* \beta^{a-i} + R, \tag{2.20}$$

where $R = [E] \cdot \delta$ for some $\delta \in A_*(\mathrm{Bl}_\Delta(\mathbb{P}^n \times \mathbb{P}^n))$. Also, $f_*[\mathscr{C}_X] = \sum_{i=0}^{s} e_i \sigma_{n-1-i,i}$ where $e_i = \deg(f_*[\mathscr{C}_X] \cdot \sigma_{n-1-i,i})$ and $s = \lfloor \frac{n-1}{2} \rfloor$. Since γ restricts to f on $\mathscr{C}_X$, $f_*[\mathscr{C}_X] = \gamma_*[\mathscr{C}_X]$ and $e_i = \deg(\gamma_*[\mathscr{C}_X] \cdot \sigma_{n-1-i,i}) = \deg([\mathscr{C}_X] \cdot \gamma^* \sigma_{n-1-i,i})$ by the projection formula. Here $[\mathscr{C}_X]$ denotes the class of $\mathscr{C}_X$ on $\mathrm{Bl}_\Delta(\mathbb{P}^n \times \mathbb{P}^n)$ and $[\mathscr{C}_X] \cdot R = 0$ since X is in general position. Moreover, by (2.16) we have that $[\mathscr{C}_X] = bl^*(\sum_{l=0}^{m} \deg(p_{m-l})\alpha^{n-l}\beta^{l+1})$. Using (2.20) we get

$$[\mathscr{C}_X] \cdot \gamma^* \sigma_{n-1-i,i} = bl^*(\sum_{l=0}^{m} \deg(p_{m-l})\alpha^{n-l}\beta^{l+1}) \cdot bl^*(\sum_{j=0}^{n-1-2i} \alpha^{i+j}\beta^{n-1-i-j}).$$

It follows that $[\mathscr{C}_X] \cdot \gamma^* \sigma_{n-1-i,i} = 0$ if $i > m$. For $i \leq m$, we get

$$[\mathscr{C}_X] \cdot \gamma^* \sigma_{n-1-i,i} = bl^*(\alpha^n \beta^n) \sum_{j=0}^{t} \deg(p_{m-(i+j)}),$$

where $t = \min\{m-i, n-1-2i\}$. Hence $e_i = 0$ for $i > m$ and $e_i = \varepsilon_i$ otherwise, which gives (2.18).

To show (2.19), let $0 \leq i \leq k$ and note that by the projection formula

$$\varepsilon_i = \deg(f_*[\mathscr{C}_X] \cdot \sigma_{n-1-i,i}) = \deg([\mathscr{C}_X] \cdot f^* \sigma_{n-1-i,i}) = \deg(f^* \sigma_{n-1-i,i}).$$

Hence applying f^* to (2.18) gives (2.19).

Since the intersection ring of $\mathrm{Gr}(2, n+1)$ is generated by $\sigma_{a,b}$ as a group, we may express $c(f^* T_G)$ as a polynomial in ξ and h by (2.17). Moreover, $c(T_{\mathscr{C}_X})$ is a polynomial in pullbacks of polar classes, h and ξ by (2.15) and Remark 2.2.12. It follows from Remark 2.2.4 that $(c(f^* T_G)c(T_{\mathscr{C}_X})^{-1})_{n-1} = \xi^{n-m-1}\pi^* B_{m,n}$ for some polynomial $B_{m,n}$ in polar classes and the hyperplane class of X. Also by Remark 2.2.4, $\deg(\xi^{n-m-1}\pi^* B_{m,n}) = \deg(B_{m,n})$. $\qquad\square$

Note that the polynomials $B_{m,n}$ in Theorem 2.2.13 only depend on n and m. Combining Theorem 2.2.13, Remark 2.2.12 and Remark 2.2.4 gives an algorithm to compute polynomials $B_{m,n}$ as in Theorem 2.2.13. We will now give a high level description of this algorithm. It has been implemented in Macaulay2 [107] and is available at [78].

We will use the notation in Theorem 2.2.13. In addition, we use $p_1, \ldots, p_m$ to denote the polar classes of X and $c_1, \ldots, c_m$ to denote the Chern classes of X. Also $i : X \longrightarrow \mathbb{P}^n$ denotes the inclusion and h_X is the hyperplane class on X. The algorithm makes use of the routines `pseudoRemainder` from [107] and `chern` from [106].

The input to the algorithm are integers $0 < m < n$ and the output is a polynomial $B_{m,n}$ in $p_1, \ldots, p_m, h_X$ such that $(c(f^*T_G)c(T_{\mathscr{C}_X})^{-1})_{n-1} = \xi^{n-m-1}\pi^*B_{m,n}$.

Algorithm 1 Algorithm to compute polynomial $B_{m,n}$ in $p_1, \ldots, p_m, h_X$ as in Theorem 2.2.13

Input: Integers $0 < m < n$.
Output: Polynomial $B_{m,n}$.

Invert $c(T_X)$: $c(T_X)^{-1} = 1 - \delta + \delta^2 + \cdots + (-1)^m \delta^m$ where $\delta = c(T_X) - 1$.
Let $c(i^*T_{\mathbb{P}^n}) = (1 + h_X)^{n+1}$.
Compute $c(N_{X/\mathbb{P}^n}) = c(i^*T_{\mathbb{P}^n})c(T_X)^{-1}$.
Compute $c(\pi^*N_{X/\mathbb{P}^n}^\vee \otimes \mathscr{O}(1)) = \sum_{j=0}^{n-m}(-1)^j\pi^*c_j(N_{X/\mathbb{P}^n})(1+\xi)^{n-m-j}$.
Compute $c(T_{\mathscr{C}_X}) = c(\pi^*T_X)c(\pi^*N_{X/\mathbb{P}^n}^\vee \otimes \mathscr{O}(1))$.
Invert $c(T_{\mathscr{C}_X})$: $c(T_{\mathscr{C}_X})^{-1} = 1 - \delta + \delta^2 + \cdots + (-1)^{n-1}\delta^{n-1}$ where $\delta = c(T_{\mathscr{C}_X}) - 1$.
Apply `chern` to express $c(T_G)$ as a polynomial in Schubert classes $\sigma_{a,b}$.
Apply the substitution (2.17) to express $c(f^*T_G) = f^*c(T_G)$ as a polynomial in ξ and π^*h_X.
Compute $(c(f^*T_G)c(T_{\mathscr{C}_X})^{-1})_{n-1}$.
Let $R = \xi^{n-m} - c_1(\pi^*N_{X/\mathbb{P}^n})\xi^{n-m-1} + \cdots + (-1)^{n-m}c_{n-m}(\pi^*N_{X/\mathbb{P}^n})$.
Let P be the output of `pseudoRemainder` applied to $(c(f^*T_G)c(T_{\mathscr{C}_X})^{-1})_{n-1}$ and R.
Let $\hat{B}_{m,n}$ be P divided by ξ^{n-m-1} and with $\pi^*c_1, \ldots, \pi^*c_m, \pi^*h_X$ replaced by $c_1, \ldots, c_m, h_X$.
Replace $c_1, \ldots, c_m$ by $p_1, \ldots, p_m$ using (2.15) on $\hat{B}_{m,n}$ to acquire $B_{m,n}$.

Corollary 2.2.14. *Let $X \subset \mathbb{P}^n$ be a smooth variety in general position. Let $d = \deg(X) = \deg(p_0)$, $\varepsilon_i = \sum_{j=0}^{m-i}\deg(p_j)$ with $m = \dim(X)$ and $h \in A_{m-1}(X)$ the hyperplane class. The following holds:*

1. *If X is a curve in $\mathbb{P}^2$ then*
$$\mathrm{BND}(X) = d^4 - 4d^2 + 3d.$$

2. *If X is a curve in $\mathbb{P}^3$ then*
$$\mathrm{BND}(X) = \varepsilon_0^2 + d^2 - 5\deg(p_1) - 2d,$$
   where $\varepsilon_0 = d + \deg(p_1)$ is the Euclidean distance degree of X.

3. *If X is a surface in $\mathbb{P}^5$ then*
$$\mathrm{BND}(X) = \varepsilon_0^2 + \varepsilon_1^2 + d^2 - \deg(3h^2 + 6hp_1 + 12p_1^2 + p_2).$$

4. *If X is a threefold in $\mathbb{P}^7$ then*
$$\mathrm{BND}(X) = \varepsilon_0^2 + \varepsilon_1^2 + \varepsilon_2^2 + d^2 - \deg(4h^3 + 11h^2p_1 + 4hp_1^2 + 24p_1^3 + 2hp_2 - 12p_1p_2 + 17p_3).$$

Proof. The formulas are acquired by applying Algorithm 1, which has been implemented in Macaulay2 [107] and is available at [78].

For illustrative purposes we will carry out the computation for curves in $\mathbb{P}^3$. By the double point formula

$$\mathbb{D}(f) = f^* f_*[\mathscr{C}_X] - (c(f^* T_G) c(T_{\mathscr{C}_X})^{-1})_2,$$

and using Theorem 2.2.13 we get that $\deg(f^* f_*[\mathscr{C}_X]) = \varepsilon_0^2 + \varepsilon_1^2 = \varepsilon_0^2 + d^2$. Moreover, $c(f^* T_G) = f^* c(T_G) = 1 + 4 f^* \sigma_1 + 7(f^* \sigma_2 + f^* \sigma_{1,1})$ and $f^* \sigma_1 = \xi$, $f^* \sigma_2 = \xi^2 - \xi h + h^2 = \xi^2 - \xi h$ and $f^* \sigma_{1,1} = h\xi$ by Theorem 2.2.13.

Let c_1 denote the first Chern class of X. To compute $c(T_{\mathscr{C}_X})$ we follow the steps of Remark 2.2.12. First of all $\pi^* c(N_{X/\mathbb{P}^n}^\vee) = 1 - 4h + \pi^* c_1$. Hence we get that $c(\pi^* N_{X/\mathbb{P}^n}^\vee \otimes \mathscr{O}(1)) = (1 + \xi)^2 + (1 + \xi)(-4h + \pi^* c_1)$. Moreover, by (2.12), $\xi^2 = -\pi^* c_1 (N_{X/\mathbb{P}^n}^\vee)\xi = (4h - \pi^* c_1)\xi$ and hence $c(\pi^* N_{X/\mathbb{P}^n}^\vee \otimes \mathscr{O}(1)) = 1 + 2\xi + (-4h + \pi^* c_1)$. This means that

$$
\begin{aligned}
c(T_{\mathscr{C}_X}) = c(\pi^* N_{X/\mathbb{P}^n}^\vee \otimes \mathscr{O}(1)) c(\pi^* T_X) &= (1 + 2\xi - 4h + \pi^* c_1)(1 + \pi^* c_1) \\
&= 1 + 2\xi - 4h + 2\pi^* c_1 + 2\xi \pi^* c_1.
\end{aligned}
$$

Hence $c(T_{\mathscr{C}_X})^{-1} = 1 - 2\xi + 4h - 2\pi^* c_1 + 2\xi \pi^* c_1$. It follows that:

$$(c(f^* T_G) c(T_{\mathscr{C}_X})^{-1})_2 = ((1 + 4 f^* \sigma_1 + 7(f^* \sigma_2 + f^* \sigma_{1,1}))(1 - 2\xi + 4h - 2\pi^* c_1 + 2\xi \pi^* c_1))_2.$$

Multiplying out and using the expressions for $f^* \sigma_2$ and $f^* \sigma_{1,1}$ above we get

$$
\begin{aligned}
(c(f^* T_G) c(T_{\mathscr{C}_X})^{-1})_2 &= 7 f^* \sigma_2 + 7 f^* \sigma_{1,1} + 4 f^* \sigma_1(-2\xi + 4h - 2\pi^* c_1) + 2\xi \pi^* c_1 \\
&= 7(\xi^2 - \xi h) + 7h\xi + 4\xi(-2\xi + 4h - 2\pi^* c_1) + 2\xi \pi^* c_1.
\end{aligned}
$$

Simplifying the last expression results in the following formulas:

$$
\begin{aligned}
(c(f^* T_G) c(T_{\mathscr{C}_X})^{-1})_2 &= -\xi^2 + 16\xi h - 6\xi \pi^* c_1 \\
&= -(4h - \pi^* c_1)\xi + 16\xi h - 6\xi \pi^* c_1 \\
&= \xi(12h - 5\pi^* c_1).
\end{aligned}
$$

Finally, using Remark 2.2.4, we get $\deg((c(f^* T_G) c(T_{\mathscr{C}_X})^{-1})_2) = 12d - 5\deg(c_1) = 2d + 5\deg(p_1)$, since $\deg(p_1) = 2d - \deg(c_1)$. This shows the claim about $\mathrm{BND}(X)$ for a smooth curve $X \subset \mathbb{P}^3$ in general position.

In the case of a general plane curve $X \subset \mathbb{P}^2$ we have that $\deg(c_1) = 2 - 2g$ where $g = (d-1)(d-2)/2$ is the genus of X. It follows that $\deg(p_1) = d^2 - d$ and $\varepsilon_0 = d^2$ and $\mathrm{BND}(X) = d^4 - 4d^2 + 3d$. $\qquad \square$

Remark 2.2.15. The formulas in Corollary 2.2.14 are given for specific ambient dimensions n. For example, Corollary 2.2.14 (2) is for curves in $\mathbb{P}^3$ and one may ask if the same formula is valid for curves in $\mathbb{P}^4$. For the formulas given in Corollary 2.2.14 we have checked that they are valid for any ambient dimension $n \leq 30$ (excluding the case $X = \mathbb{P}^n$). This was done using the Macaulay2 implementation [78].

Consider now the general case of a smooth m-dimensional variety $X \subset \mathbb{P}^n$. Combining Algorithm 1 and Theorem 2.2.13 we get an algorithm that, for any given m and n, computes the bottleneck degree of a smooth m-dimensional variety $X \subset \mathbb{P}^n$ in general position. The result is a formula that expresses the bottleneck degree in terms of polar classes of X. Now, if we let $n = 2m + 1$ we get a formula for each m. It is our belief that through projection arguments one can show that this formula is in fact valid in any ambient dimension $n > m$. Thus we conjecture that the formula in terms of polar classes only depends on the dimension m.

The Affine Case

We now define bottlenecks for affine varieties and show how they may be counted using the bottleneck degrees of projective varieties.

Let $X \subset \mathbb{C}^n$ be a smooth affine variety of dimension m. Consider coordinates $x_0, \ldots, x_{n-1}$ given by the standard basis on $\mathbb{C}^n$ and the usual embedding $\mathbb{C}^n \subset \mathbb{P}^n$ with coordinates $x_0, \ldots, x_n$ on $\mathbb{P}^n$. Let $H_\infty = \mathbb{P}^n \setminus \mathbb{C}^n$ be the hyperplane at infinity defined by $x_n = 0$. Also consider the closure $\bar{X} \subset \mathbb{P}^n$ and the intersection $\bar{X}_\infty = \bar{X} \cap H_\infty$. We consider $\bar{X}_\infty$ a subvariety of $\mathbb{P}^{n-1} \cong H_\infty$.

Definition 2.2.16. A smooth affine variety $X \subset \mathbb{C}^n$ is in *general position* if $\bar{X}_\infty$ is smooth and both $\bar{X}$ and $\bar{X}_\infty$ are in general position.

Assume that X is in general position. Let $v : \mathbb{P}^n \setminus \{o\} \longrightarrow H_\infty$ be the projection from the point $o = (0, \ldots, 0, 1)$. If $(p, q) \in \mathscr{C}_{\bar{X}}$ then $q \neq o$ since $\bar{X}_\infty$ is smooth. Also, $p \neq v(q)$ since $\bar{X}_\infty$ is in general position. Therefore we can define a map

$$g : \mathscr{C}_{\bar{X}} \to \mathrm{Gr}(2, n+1) : (p, q) \mapsto \langle p, v(q) \rangle,$$

mapping a pair $(p, q) \in \mathscr{C}_{\bar{X}}$ to the line spanned by p and $v(q)$. For the remainder of this section we will use g to denote this map associated to a variety X. In the following lemma we show that for $x \in X$ the fiber $F_x = \{(x', q) \in \mathscr{C}_{\bar{X}} : x' = x\}$ together with the map g parameterize lines in the Euclidean normal space $N_x X$ passing through x. Recall that for $x \in X \subset \mathbb{C}^n$, $(T_x X)_0$ denotes the embedded tangent space translated to the origin and the Euclidean normal space at x is given by $N_x X = \{z \in \mathbb{C}^n : (z - x) \in (T_x X)_0^\perp\}$.

Lemma 2.2.17. *Let $X \subset \mathbb{C}^n$ be a smooth variety in general position. As above we consider $\mathbb{C}^n \subset \mathbb{P}^n$ and $X \subset \bar{X} \subset \mathbb{P}^n$. Let $x \in X$ and $F_x = \{(x', q) \in \mathscr{C}_{\bar{X}} : x' = x\}$. Then the map $u \mapsto g(u) \cap \mathbb{C}^n$ on F_x defines a one-to-one correspondence between F_x and the set of lines in $N_x X$ passing through x.*

Proof. Let $(x, q) \in \mathscr{C}_{\bar{X}}$ with $q = (q_1, \ldots, q_{n+1})$ and $x = (x_1, \ldots, x_n, 1)$ where $(x_1, \ldots, x_n) \in X \subset \mathbb{C}^n$. The line $\langle x, v(q) \rangle \cap \mathbb{C}^n$ expressed in coordinates on $\mathbb{C}^n$ is given by $\{(x_1, \ldots, x_n) + a(q_1, \ldots, q_n) : a \in \mathbb{C}\}$. To show that this line is normal to X at x we need to show that $(q_1, \ldots, q_n) \in (T_x X)_0^\perp \subset \mathbb{C}^n$. Let $(v_1, \ldots, v_n) \in (T_x X)_0$. Then $(x_1 + v_1, \ldots, x_n + v_n) \in T_x X$ where $T_x X \subset \mathbb{C}^n$ is the embedded tangent space of X at x. This means that $(x_1 + v_1, \ldots, x_n + v_n, 1) \in \mathbb{T}_x \bar{X} \subset \mathbb{P}^n$ and hence $\sum_{i=1}^n (x_i + v_i) q_i + q_{n+1} = 0$. Since $(x_1, \ldots, x_n, 1) \in \mathbb{T}_x \bar{X}$ we have that $\sum_{i=1}^n x_i q_i + q_{n+1} = 0$. It follows that $\sum_{i=1}^n v_i q_i = 0$ and we have shown $(q_1 \ldots, q_n) \in (T_x X)_0^\perp$.

Now let $x \in X \subset \bar{X}$ with $x = (x_1, \ldots, x_n, 1)$ and consider a line in $N_x X$ through x. In coordinates on $\mathbb{C}^n$ the line is given by $\{(x_1, \ldots, x_n) + a(q_1, \ldots, q_n) : a \in \mathbb{C}\}$ for some $0 \neq (q_1, \ldots, q_n) \in (T_x X)_0^\perp \subseteq \mathbb{C}^n$. Note that $(q_1, \ldots, q_n)$ is unique up to scaling. We need to show that there is a unique $q_{n+1} \in \mathbb{C}$ such that $(x, q) \in \mathscr{C}_{\bar{X}}$ where $q = (q_1, \ldots, q_n, q_{n+1})$. Since $x \in \mathbb{T}_x \bar{X}$, a necessary condition on $q_{n+1} \in \mathbb{C}$ is that $\sum_{i=1}^n x_i q_i + q_{n+1} = 0$. Accordingly we let $q_{n+1} = -\sum_{i=1}^n x_i q_i$. It remains to show $(x, q) \in \mathscr{C}_{\bar{X}}$. Since $\{(v_1, \ldots, v_n, v_{n+1}) \in \mathbb{T}_x \bar{X} : v_{n+1} \neq 0\} \subset \mathbb{T}_x \bar{X}$ is a dense subset, it is enough to show that for all $(v_1, \ldots, v_n, 1) \in \mathbb{T}_x \bar{X}$ we have that $\sum_{i=1}^n v_i q_i + q_{n+1} = 0$. Note that $(v_1, \ldots, v_n) \in T_x X \subset \mathbb{C}^n$ and $(v_1 - x_1, \ldots, v_n - x_n) \in (T_x X)_0$. Hence $\sum_{i=1}^n (v_i - x_i) q_i = 0$. It follows that $\sum_{i=1}^n v_i q_i + q_{n+1} = \sum_{i=1}^n x_i q_i + q_{n+1} = 0$. $\square$

Consider the projection $\mathfrak{p} : \mathscr{C}_{\bar{X}} \longrightarrow \bar{X}$. A *bottleneck* of the affine variety X is a pair of distinct points $x, y \in X \subset \bar{X}$ such that there exists $u, v \in \mathscr{C}_{\bar{X}}$ with $\mathfrak{p}(u) = x$, $\mathfrak{p}(v) = y$ and $g(u) = g(v)$. We will now show that this definition of bottlenecks is equivalent to the definition given in the introduction in terms of Euclidean normal spaces.

Lemma 2.2.18. *Let $X \subset \mathbb{C}^n$ be a smooth variety in general position. A pair of distinct points $(x, y) \in X \times X$ is a bottleneck if and only if the line in $\mathbb{C}^n$ joining x and y is contained in $N_x X \cap N_y X$.*

Proof. If $(x, y) \in X \times X$ is a bottleneck, then there are $u, v \in \mathscr{C}_{\bar{X}}$ with $g(u) = g(v)$, $\mathfrak{p}(u) = x$ and $\mathfrak{p}(v) = y$. The line $g(u) \cap \mathbb{C}^n$ in $\mathbb{C}^n$ thus contains x and y and it is contained in $N_x X \cap N_y X$ by Lemma 2.2.17. For the converse, let $x, y \in X$ be distinct such that the line $l \subset \mathbb{C}^n$ joining x and y is contained in $N_x X \cap N_y X$. By Lemma 2.2.17 there are $u, v \in \mathscr{C}_{\bar{X}}$ with $l = g(u) \cap \mathbb{C}^n$, $l = g(v) \cap \mathbb{C}^n$, $\mathfrak{p}(u) = x$ and $\mathfrak{p}(v) = y$. It follows that $g(u) = g(v)$ and (x, y) is a bottleneck. $\square$

The map g can have double points that do not correspond to actual bottlenecks of X since we require that $x, y \in X$ lie in the affine part. Note however that if $u, v \in \mathscr{C}_{\bar{X}}$ with $g(u) = g(v)$ and $\mathfrak{p}(u) \in \bar{X}_\infty$, then $\mathfrak{p}(v) \in \bar{X}_\infty$ as well. Therefore the extraneous double point pairs of g are in one-to-one correspondence with double point pairs of the map

$$ g_\infty : \mathscr{C}_{\bar{X}_\infty} \to \mathrm{Gr}(2, n) : (p, q) \mapsto \langle p, q \rangle. $$

Here $\mathscr{C}_{\bar{X}_\infty}$ is defined with respect to the embedding $\bar{X}_\infty \subset \mathbb{P}^{n-1}$. This leads us to consider the double point classes $\mathbb{D}(g)$, $\mathbb{D}(g_\infty)$ of g and g_∞ and define the bottleneck degree of X as the difference of the degrees of these classes.

Definition 2.2.19. Let $X \subset \mathbb{C}^n$ be a smooth variety in general position. The *bottleneck degree* of X is $\deg(\mathbb{D}(g)) - \deg(\mathbb{D}(g_\infty))$ and is denoted by $\mathrm{BND}(X)$.

Example 2.2.20. Consider a general plane curve $X \subset \mathbb{C}^2$ of degree d defined by a polynomial $F \in \mathbb{C}[x, y]$. Then $\bar{X} \subset \mathbb{P}^2$ is defined by the homogenization $\bar{F} \in \mathbb{C}[x, y, z]$ of F with respect to z. We may assume that $\bar{X}$ is smooth. The map $g : \bar{X} \longrightarrow (\mathbb{P}^2)^*$ is given by $(x, y, z) \mapsto (-z\bar{F}_y, z\bar{F}_x, x\bar{F}_y - y\bar{F}_x)$. It maps a point $p \in X$ to the closure of the normal line $N_p X \subset \mathbb{C}^2$ in $\mathbb{P}^2$. The bottlenecks of X are the pairs $(p, q) \in X \times X$ with $p \neq q$ and $N_p X = N_q X$. We shall now consider the other double point pairs of g, that is distinct points $p, q \in \bar{X}$ such that $g(p) = g(q)$ and p or q lies on the line at infinity

H_∞. The latter corresponds to the point $(0,0,1) \in (\mathbb{P}^2)^*$. If $p = (x,y,z) \in H_\infty \cap \bar{X}$, that is $z = 0$, then $g(p) = (0,0,1)$. Conversely, if $q \in \bar{X}$ and $g(q) = (0,0,1)$ then $q \in H_\infty$ since q is a point on the line $g(q)$. The extraneous double points of g are thus exactly the d points $\bar{X}_\infty$, the intersection of $\bar{X}$ with the line at infinity. This gives rise to $d(d-1)$ extraneous double point pairs at infinity.

Proposition 2.2.21. *For a smooth affine variety $X \subset \mathbb{C}^n$ in general position,*

$$\mathrm{BND}(X) = \mathrm{BND}(\bar{X}) - \mathrm{BND}(\bar{X}_\infty).$$

Proof. By definition $\mathrm{BND}(\bar{X}_\infty) = \deg(\mathbb{D}(g_\infty))$ and so it remains to prove that $\mathrm{BND}(\bar{X}) = \deg(\mathbb{D}(g))$. In other words we need to show that $\deg(\mathbb{D}(f)) = \deg(\mathbb{D}(g))$ where f is the map

$$f : \mathscr{C}_{\bar{X}} \to \mathrm{Gr}(2, n+1) : (p,q) \mapsto \langle p, q \rangle.$$

By the double point formula it is enough to show that $f^* f_* [\mathscr{C}_{\bar{X}}] = g^* g_* [\mathscr{C}_{\bar{X}}]$ and $c(f^* T_G) = c(g^* T_G)$ where $G = \mathrm{Gr}(2, n+1)$. Since the Schubert classes generate $A_*(G)$ as a group the equality $c(f^* T_G) = c(g^* T_G)$ would follow after showing that $f^* \sigma_{a,b} = g^* \sigma_{a,b}$. We will do this first. As in the proof of Theorem 2.2.13, let $bl : \mathrm{Bl}_\Delta(\mathbb{P}^n \times \mathbb{P}^n) \to \mathbb{P}^n \times \mathbb{P}^n$ be the blow-up of $\mathbb{P}^n \times \mathbb{P}^n$ along the diagonal $\Delta \subset \mathbb{P}^n \times \mathbb{P}^n$ and let $E = bl^{-1}(\Delta)$. Let $\alpha, \beta \in A_*(\mathbb{P}^n \times \mathbb{P}^n)$ be the pullbacks of the hyperplane class of $\mathbb{P}^n$ under the two projections and let γ be as in Theorem 2.2.13. By (2.20)

$$\gamma^*(\sigma_{a,b}) = \sum_{i=0}^{a-b} bl^* \alpha^{b+i} bl^* \beta^{a-i} + R,$$

where $R = [E] \cdot \delta$ for some $\delta \in A_*(\mathrm{Bl}_\Delta(\mathbb{P}^n \times \mathbb{P}^n))$. Let $i : \mathscr{C}_{\bar{X}} \to \mathrm{Bl}_\Delta(\mathbb{P}^n \times \mathbb{P}^n)$ be the map induced by the inclusion $\mathscr{C}_{\bar{X}} \subset \mathbb{P}^n \times \mathbb{P}^n$ and let $j : \mathscr{C}_{\bar{X}} \to \mathrm{Bl}_\Delta(\mathbb{P}^n \times \mathbb{P}^n)$ be induced by the map $\mathscr{C}_{\bar{X}} \to \mathbb{P}^n \times \mathbb{P}^n$: $(p,q) \mapsto (p, v(q))$, where $v : \mathbb{P}^n \setminus \{o\} \to H_\infty$ is the linear projection. Note that $f = \gamma \circ i$ and $g = \gamma \circ j$. The map $bl \circ i$ is the identity on $\mathscr{C}_{\bar{X}}$ and $bl \circ j : \mathscr{C}_{\bar{X}} \to \mathbb{P}^n \times \mathbb{P}^n$ is the map $(p,q) \mapsto (p, v(q))$. It follows that $i^* bl^* \alpha = j^* bl^* \alpha$ and $i^* bl^* \beta = j^* bl^* \beta$. Since $\bar{X}$ and $\bar{X}_\infty$ are in general position, $i^* R = j^* R = 0$, and we conclude that $f^* \sigma_{a,b} = g^* \sigma_{a,b}$.

Now write $f_*[\mathscr{C}_{\bar{X}}] = \sum_i e_i \sigma_{n-1-i,i}$ and $g_*[\mathscr{C}_{\bar{X}}] = \sum_i e_i' \sigma_{n-1-i,i}$ where $e_i, e_i' \in \mathbb{Z}$. Note that $e_i = \deg(f_*[\mathscr{C}_{\bar{X}}] \cdot \sigma_{n-1-i,i}) = \deg([\mathscr{C}_{\bar{X}}] \cdot f^* \sigma_{n-1-i,i})$ and the same way $e_i' = \deg([\mathscr{C}_{\bar{X}}] \cdot g^* \sigma_{n-1-i,i})$. Since $f^* \sigma_{n-1-i,i} = g^* \sigma_{n-1-i,i}$, we have that $e_i = e_i'$ for all i. It follows that

$$f^* f_* [\mathscr{C}_{\bar{X}}] = \sum_i e_i f^* \sigma_{n-1-i,i} = \sum_i e_i' g^* \sigma_{n-1-i,i} = g^* g_* [\mathscr{C}_{\bar{X}}].$$

$\square$

Example 2.2.22. For a general curve $X \subset \mathbb{C}^2$ of degree d we have

$$\mathrm{BND}(X) = d^4 - 5d^2 + 4d.$$

Namely, the bottleneck degree of $\bar{X}$ is given in Corollary 2.2.14 and putting this together with Proposition 2.2.21 and Example 2.2.20 we get $\mathrm{BND}(X) = d^4 - 4d^2 + 3d - d(d-1) = d^4 - 5d^2 + 4d$.

Hence a general line in $\mathbb{C}^2$ has no bottlenecks, as one might expect. For $d = 2$ we get that a general conic has 4 bottlenecks, which corresponds to 2 pairs of points with coinciding normal lines. These lines can be real: Consider the case of a general real ellipse and its two principal axes, see Figure 2.11.
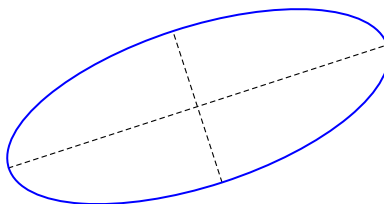

Figure 2.11: Ellipse with principal axes.

Remark 2.2.23. Let X be a smooth affine variety in general position. As we have seen, the bottleneck degrees of $\bar{X}$ and $\bar{X}_\infty$ are functions of the polar numbers of these varieties. If $i : \bar{X}_\infty \longrightarrow \bar{X}$ is the inclusion then the relation between the polar classes of $\bar{X}$ and those of its hyperplane section $\bar{X}_\infty$ is $p_j(\bar{X}_\infty) = i^* p_j(\bar{X})$. This is straightforward to verify using for example the adjunction formula [101, Example 3.2.12] and the relation between polar classes and Chern classes (2.14). This means that the polar numbers of $\bar{X}$ and $\bar{X}_\infty$ are the same in the sense that $\deg(p_1(\bar{X}_\infty)^{a_1} \ldots p_{m-1}(\bar{X}_\infty)^{a_{m-1}}) = \deg(p_1(\bar{X})^{a_1} \ldots p_{m-1}(\bar{X})^{a_{m-1}})$ for any $a_1, \ldots, a_{m-1} \in \mathbb{N}$ such that $\sum_{j=1}^{m-1} j \cdot a_j \leq m-1$. As a consequence, Proposition 2.2.21 may be used to express the bottleneck degree of $X \subset \mathbb{C}^n$ in terms of the polar numbers of its closure $\bar{X} \subset \mathbb{P}^n$.

Remark 2.2.24. Let $g_1, \ldots, g_k \in \mathbb{C}[x_1, \ldots, x_n]$ be a system of polynomials of degrees $d_1, \ldots, d_k$ which define a complete intersection $X \subset \mathbb{C}^n$. Suppose that the bottlenecks of X are known. If X is general enough to have the maximal number of bottlenecks, we may compute the isolated bottlenecks of any other complete intersection $Y \subset \mathbb{C}^n$ defined by polynomials $f_1, \ldots, f_k \in \mathbb{C}[x_1, \ldots, x_n]$ of the same degrees $d_1, \ldots, d_k$. We propose to do this by a parameter homotopy from X to Y. For background on homotopy methods, see Section 1.3. Suppose that both X and Y are smooth. Let $h_i(x) = (1-t)f_i(x) + \gamma t g_i(x)$ where $\gamma \in \mathbb{C}$ is random and t is the homotopy parameter. The homotopy paths are tracked from the bottlenecks of X at $t = 1$ to the bottlenecks at Y at $t = 0$. Introduce new variables $y_1, \ldots, y_n$ and $\lambda_1, \ldots, \lambda_k, \mu_1, \ldots, \mu_k$. The parameter homotopy is then the following square system of equations in $2(n+k)$ variables:

$$h_1(x) = \cdots = h_k(x) = 0,$$
$$h_1(y) = \cdots = h_k(y) = 0,$$
$$y - x = \sum_{i=1}^{k} \lambda_i \nabla h_i(x),$$
$$y - x = \sum_{i=1}^{k} \mu_i \nabla h_i(y).$$

For the starting points of the homotopy we need the bottleneck pairs (x, y) of X. To find the $\lambda_1, \ldots, \lambda_k$ and $\mu_1, \ldots, \mu_k$ corresponding to a bottleneck pair (x, y) one would need to solve the linear systems $y - x = \sum_{i=1}^{k} \lambda_i \nabla g_i(x)$ and $y - x = \sum_{i=1}^{k} \mu_i \nabla g_i(y) = 0$.

Along similar lines, [93] presents an efficient homotopy to compute bottlenecks of affine varieties.

Examples

Example 2.2.25. Consider the space curve in $\mathbb{C}^3$ given by the intersection of these two hypersurfaces:
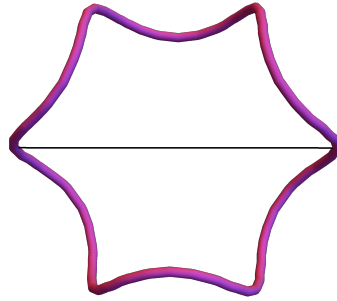
$$x^3 - 3xy^2 - z = 0$$
$$x^2 + y^2 + 3z^2 - 1 = 0.$$

Figure 2.12: A space curve of degree 6 shown with one of its bottleneck lines joining the points $(0, -1, 0)$ and $(0, 1, 0)$.

As computed in Macaulay2, the ideal of the bottleneck variety (with the diagonal removed) associated to this affine curve has dimension 0 and degree 480. The curve is the complete intersection of two surfaces of degrees $d_1 = 2$ and $d_2 = 3$.

Now consider a smooth complete intersection curve $X \subset \mathbb{C}^3$ cut out by surfaces of degree d_1 and d_2. Assume that X is in general position. By Corollary 2.2.14 the bottleneck degree of $\bar{X}$ is given by $\varepsilon_0^2 + d^2 - 5 \deg(p_1) - 2d$, where $\varepsilon_0 = d + \deg(p_1)$ and $d = d_1 d_2$. Using for example the adjunction formula, [101, Example 3.2.12], one can see that $c_1(T_X) = (4 - d_1 - d_2)h$, where $h \in A_0(X)$ is the hyperplane class. Also, by (2.14) we have $p_1 = 2h - c_1(T_X) = (d_1 + d_2 - 2)h$. Thus $\deg(p_1) = (d_1 + d_2 - 2)d_1 d_2$. By Proposition 2.2.21, to obtain the bottleneck degree of the affine variety X we subtract $\text{BND}(\bar{X}_\infty)$ from $\text{BND}(\bar{X})$. In this case, we have

$$\text{BND}(\bar{X}_\infty) = d_1 d_2 (d_1 d_2 - 1).$$

We obtain the following formula for the bottleneck degree of a smooth complete intersection curve $X \subset \mathbb{C}^3$ in general position:

$$\text{BND}(X) = d_1^4 d_2^2 + 2d_1^3 d_2^3 + d_1^2 d_2^4 - 2d_1^3 d_2^2 - 2d_1^2 d_2^3 + d_1^2 d_2^2 - 5d_1^2 d_2 - 5d_1 d_2^2 + 9d_1 d_2.$$

Substituting $d_1 = 2$ and $d_2 = 3$, we obtain $\text{BND}(X) = 480$, in agreement with the Macaulay2 computation for the sextic curve above.

Example 2.2.26. Let $X \subset \mathbb{C}^3$ be a general surface of degree d. Then

$$\text{BND}(X) = d^6 - 2d^5 + 3d^4 - 15d^3 + 26d^2 - 13d.$$

To see this use Proposition 2.2.21. Apply Corollary 2.2.14 to get $\text{BND}(\bar{X})$ and the bottleneck degree of the planar curve $\bar{X}_\infty$.

Example 2.2.27. Consider the quartic surface $X \subset \mathbb{C}^3$ defined by the equation

$$(0.3x^2 + 0.5z + 0.3x + 1.2y^2 - 1.1)^2 + (0.7(y - 0.5x)^2 + y + 1.2z^2 - 1)^2 = 0.3.$$

For a general quartic surface in $\mathbb{C}^3$, the bottleneck degree is 2220 by Example 2.2.26. In this case, $\text{BND}(X) = 1390$ was found using the Julia package *HomotopyContinuation.jl* [44]. Among the 1390 solutions are 49 distinct real bottleneck pairs. The quartic with its bottlenecks is shown in Figure 2.13.
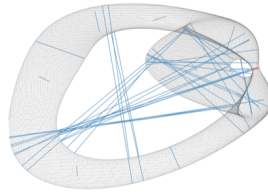

Figure 2.13: The quartic surface of Example 2.2.27 shown with its real bottleneck lines. The shortest bottleneck line is shown in red. The figure was produced by Sascha Timme using the Julia package *HomotopyContinuation.jl* [44].

Example 2.2.28. Consider the ellipsoid $X \subset \mathbb{C}^3$ defined by the equation

$$36x^2 + 9y^2 + 4z^2 = 36.$$

For a general quadric surface in $\mathbb{C}^3$, the bottleneck degree is 6 by Example 2.2.26. In this case, there are indeed three bottleneck pairs, all with real coordinates. The pairs occur on each of the coordinate axes, at $\{(-1,0,0),(1,0,0)\}$, $\{(0,-2,0),(0,2,0)\}$ and $\{(0,0,-3),(0,0,3)\}$.

If we set two axes to be the same length, as in the equation of the spheroid

$$4x^2 + y^2 + z^2 = 4,$$

then there is only one isolated bottleneck pair: $\{(-1,0,0),(1,0,0)\}$. The rest of the bottlenecks are part of an infinite locus. Intersecting with the plane $\{x = 0\}$ which is normal to the spheroid, we obtain the circle $\{y^2 + z^2 = 4\}$ and every antipodal pair of points of the circle is a bottleneck.

Conclusion

In this chapter, we gave algebraic formulations of the algebraic boundary of the Voronoi cell of a point on a variety and the bottleneck locus of a variety. Both of these objects are algebraic varieties that can be used to answer a distance optimization question about an underlying variety. In each case, we provided formulas for the algebraic degree of these varieties, characterizing the complexity of solving the corresponding distance optimization problems. In the next chapter, we shift our focus from distance to curvature but address similar questions.

Chapter 3

Algebraic Geometry of Curvature

Curvature is one of the most significant objects of study in differential geometry. This chapter takes an unusual approach to curvature in that we study its algebraic geometry and the algebraic varieties relevant to curvature. For each such variety, we study its defining equations and its degree. As discussed in the Introduction, this has applications to the computation of the reach of an algebraic variety.

Section 3.1 addresses critical curvature in the case of plane curves, providing a formula for the degree. This is adapted from the paper [35], which is joint work with Madeline Brandt. In Section 3.2, we seek to generalize this result to hypersurfaces in spaces of higher dimension. This is adapted from the manuscript [40], which is joint with Paul Breiding and Kristian Ranestad.

3.1 Curvature and the Evolute of a Plane Curve

Curvature of plane curves, osculating circles and evolutes have interested mathematicians since antiquity. As early as 200 BCE, Apollonius mentioned evolutes in Book V of *Conics* [69]. We refer readers to works of Salmon in the 19th century [166, 167] and to modern lectures by Fuchs and Tabachnikov outlining this history [99, Chapter 3].

We now discuss the minimal radius of curvature of a plane curve. This is one of the two quantities which determines the reach, see Equation (4.28). There are many ways to define the radius of curvature of a plane curve. We use the definition of Cauchy [54, 91].

Definition 3.1.1. Let $X \subset \mathbb{R}^2$ be an algebraic curve and $p \in X$ be a smooth point. The *center of curvature* at p is the intersection of the normal line to X at p and the normal line to X at a point infinitely close to p. The *radius of curvature* at p is the distance from p to its center of curvature. The (unsigned) *curvature* is the reciprocal of the radius of curvature. The *osculating circle* at p is the circle tangent to X at p centered at the center of curvature with radius equal to the radius of curvature.

Modern mathematicians may feel uncomfortable with the language of "infinitely close points." An alternative definition of center and radius of curvature can be given using envelopes.

Definition 3.1.2. The *envelope* of a one-parameter family of plane algebraic curves given implicitly by $F(x,y,t) = 0$ is a curve that touches every member of the family tangentially. The envelope is the variety defined by the ideal

$$\left\langle \frac{\partial F}{\partial t}, \; F(x,y,t) \right\rangle \cap \mathbb{R}[x,y].$$

The envelope of the family of normal lines parametrized by the points of the curve is called its *evolute*. A generalization of the evolute to all dimensions is called the *ED discriminant*, and is studied in [86]. They show that for general smooth plane algebraic curves, the degree of the evolute is $3d(d-1)$ [86, Example 7.4].

We now derive a formula for the center and radius of curvature of a plane curve at a point. Our derivation follows Salmon [167]. This can be taken as an equivalent definition of center and radius of curvature. The evolute is then the locus of the centers of curvature.

Proposition 3.1.3. *[167] Let $X = V(F(x,y)) \in \mathbb{R}^2$ be a smooth curve of degree d. The radius of curvature at a point $(x_0, y_0) \in V(F)$ is given by evaluating the following expression in terms of partial derivatives of F at (x_0, y_0):*

$$R = \frac{(F_x^2 + F_y^2)^{\frac{3}{2}}}{F_{xx}F_y^2 - 2F_{xy}F_xF_y + F_{yy}F_x^2}. \tag{3.1}$$

Proof. The equation of a normal line to X at a point $(x,y) \in X$ in the variables (α, β) is

$$F_y(\alpha - x) - F_x(\beta - y) = 0. \tag{3.2}$$

The total derivative of the equation for the normal line is

$$\left(F_{xy} + F_{yy}\frac{dy}{dx}\right)(\alpha - x_0) - \left(F_{xx} + F_{xy}\frac{dy}{dx}\right)(\beta - y) - F_y + F_x\frac{dy}{dx} = 0. \tag{3.3}$$

The total derivative of $F(x,y)$ is

$$F_x(x_0, y_0) + F_y\frac{dy}{dx} = 0. \tag{3.4}$$

The equations (3.2), (3.3) are a system of two linear equations in the unknowns $\{\alpha, \beta\}$. We solve this system to obtain expressions for α and β in terms of x, y, and $\frac{dy}{dx}$. We substitute in for $\frac{dy}{dx}$ the expression given by (3.4). The center of curvature of X at a point $(x,y) \in X$ is given by the coordinates (α, β), which are now expressions in x and y.

The radius of curvature R at a point (x,y) is its distance to its center of curvature (α, β), so we have $R = \sqrt{(\alpha - x)^2 + (\beta - y)^2}$. Substituting in the equations for α and β, we obtain the stated expression (3.1). $\qquad\square$

For curves in projective space, there is a modified formula for the radius of curvature.

Corollary 3.1.4. *[167] Let $X = V(F(x,y,z)) \subset \mathbb{P}^2_{\mathbb{R}}$ be a smooth curve of degree d defined by a homogeneous polynomial F. The radius of curvature at a point $(x_0, y_0, z_0) \in X$ is given by evaluating the following expression in terms of partial derivatives of F at (x_0, y_0, z_0):*

$$R = \frac{(d-1)^2(F_x^2 + F_y^2)^{\frac{3}{2}}}{z^2(F_{xx}F_{yy}F_{zz} - F_{xx}F_{yz}^2 - F_{yy}F_{xz}^2 - F_{zz}F_{xy}^2 + 2F_{yz}F_{xz}F_{xy})}. \tag{3.5}$$

Proof. For any homogeneous function $F(x,y,z)$ of degree d we have $xF_x + yF_y + zF_z = dF$. We use this equation to obtain expressions for F_x and F_y. Similarly, we find relations among the second derivatives. We substitute these expressions in to (3.1) to obtain our new formula. $\square$

We now analyze the critical points of curvature of a smooth algebraic curve $X \subset \mathbb{R}^2$. If X is a line, then for all $p \in X$ the radius of curvature is infinite and the curvature is 0. If X is a circle, then all points $p \in X$ have the same radius of curvature, equal to the radius of the circle. Thus the total derivative of the equation for the radius of curvature is identically 0. We exclude such curves from our analysis by requiring that X be irreducible of degree greater than or equal to 3.

Definition 3.1.5. The *degree of critical curvature* of a smooth algebraic curve $X \subset \mathbb{R}^2$ is the degree of the variety obtained by intersecting the Zariski closure $\overline{X} \subset \mathbb{P}^2_{\mathbb{C}}$ with the variety of the total derivative of the equation for the radius of curvature. If $X \subset \mathbb{R}^2$ is a smooth, irreducible algebraic curve of degree greater than or equal to 3, then the intersection consists of finitely many points, the points of critical curvature. Thus the degree of critical curvature of X gives an upper bound for the number of real points of critical curvature of X.

Theorem 3.1.6. *Let $X \subset \mathbb{R}^2$ be a smooth, irreducible algebraic curve of degree $d \geq 3$. Then the degree of critical curvature of X is $6d^2 - 10d$.*

Proof. To simplify notation, let $H = F_{xx}F_{yy}F_{zz} - F_{xx}F_{yz}^2 - F_{yy}F_{xz}^2 - F_{zz}F_{xy}^2 + 2F_{yz}F_{xz}F_{xy}$. We have assumed that the radius of curvature is finite, so H is nonzero. Dehomogenize Equation (3.5) by setting $z = 1$. Then take the total derivative and set the total derivative equal to 0. Then divide both sides of the equation by $\frac{(d-1)^2(F_x^2+F_y^2)^{\frac{1}{2}}}{2z^2H}$. We have already shown that the denominator of this fraction is nonzero. The numerator is nonzero as well because H is nonzero implies that F_x and F_y cannot both be zero. We obtain

$$(F_x^2 + F_y^2)(F_y H_x - F_x H_y) = 3H[(F_{xx} - F_{yy})F_x F_y + F_{xy}(F_y^2 - F_x^2)]. \tag{3.6}$$

The degree of F is d. So the degree of Equation (3.6) is $6d - 10$. We intersect the projective variety defined by the homogenization of Equation (3.6) (which has the same degree as the affine variety) with the projectivization of X. By Bézout's Theorem, the degree of critical curvature of the complex projectivization of X is $6d^2 - 10d$. $\square$

We remark that the critical points of curvature of X give cusps on the evolute [99, Lemma 10.1]. That is, if a normal line is drawn through a point of critical curvature on a curve, then the

normal line will pass through a cusp of the evolute. In addition, the evolute of a curve of degree d has d cusps at infinity. Thus the evolute of a plane curve of degree d has $6d^2 - 10d + d = 6d^2 - 9d$ cusps [167]. In Figure 3.1, we depict the quartic butterfly curve (4.29), its evolute, and pairs of critical curvature points on the butterfly curve with their corresponding cusps on the evolute.
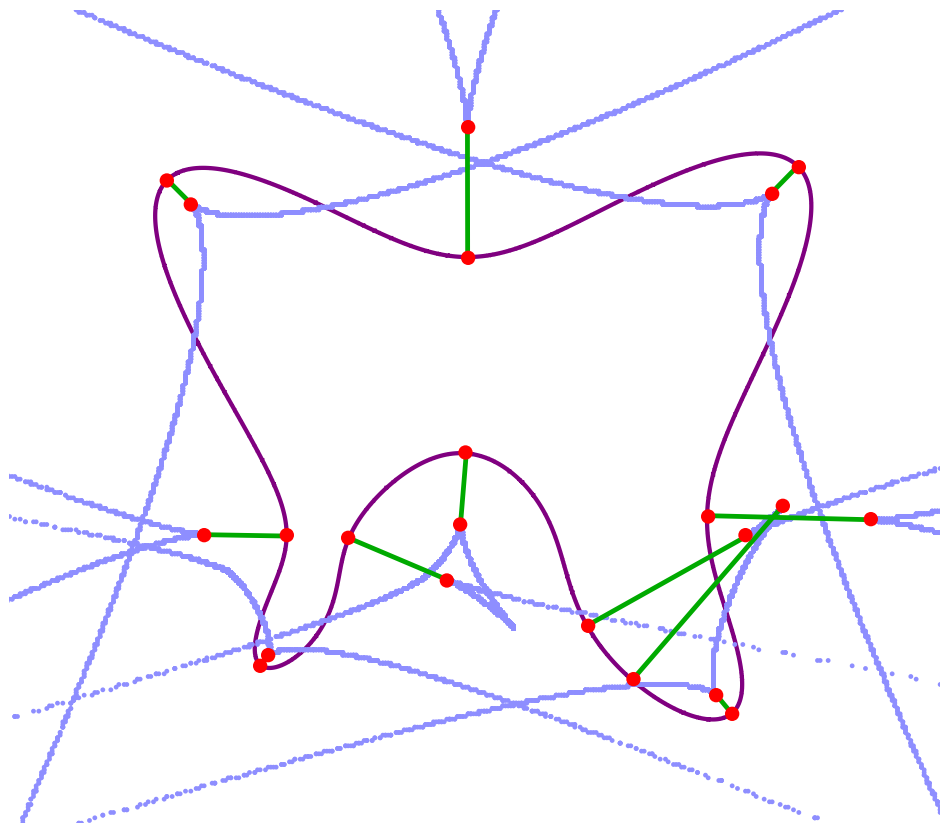

Figure 3.1: The eleven real points of critical curvature on the butterfly curve, computed in Example 3.1.7, joined by green line segments to their centers of curvature. These give cusps on the evolute, which is pictured here in light blue.

Example 3.1.7. Consider the butterfly curve (4.29). Using the above description, we can compute the 56 points of critical curvature using `JuliaHomotopyContinuation` [44]. Twelve of these points are real, and they are plotted in Figure 3.1. The maximal curvature is approximately 9.65. This is achieved at the lower left wing of the butterfly.

3.2   Algebraic Geometry of Curvature

In the previous section, we investigated the critical curvature locus of a plane curve. We now explore the same question for varieties of other dimensions. The definition of curvature for a plane

curve does not generalize easily to higher dimensions; there are several conceptions of curvature for varieties of higher dimension that coincide for plane curves. Thus we begin with the nuanced process of defining the notion of curvature relevant to the computation of the reach of an algebraic variety. While this definition is basic to differential geometry, effort is required to convert it to the language of algebraic geometry and polynomial systems.

The critical curvature degree of an algebraic variety was also discussed in [119]. In Section 3.1 of this dissertation, we describe a correspondence between the critical curvature points on a plane curve and the cusps on its evolute. The paper [119] generalizes this idea to varieties of higher dimension. It also provides Macaulay2 code for an ideal that contains the critical curvature locus of a hypersurface as a component.

Differential Geometry Formulation of Curvature

We now provide the background information on differential geometry necessary for a reader to understand the definitions we use for concepts related to curvature. We summarize the relevant parts of [82, Chapters 0-4] and [136, Chapters 5 and 8].

A *differentiable manifold* of dimension m is a set M and a family of injective mappings $\varphi_\alpha : U_\alpha \subset \mathbb{R}^m \to M$ of open sets U_α of $\mathbb{R}^m$ into M such that:

- $\cup_\alpha \varphi_\alpha(U_\alpha) = M$.

- For any pair α, β with $\varphi_\alpha(U_\alpha) \cap \varphi_\beta(U_\beta) = W \neq \emptyset$, the sets $\varphi_\alpha^{-1}(W)$ and $\varphi_\beta^{-1}(W)$ are open sets in $\mathbb{R}^m$ and the mappings $\varphi_\beta^{-1} \circ \varphi_\alpha$ are differentiable.

- The family $\{(U_\alpha, \varphi_\alpha)\}$ is maximal relative to the first two conditions.

Our setting is a special type of differentiable manifold called an *algebraic manifold*, which we now define.

Proposition 3.2.1. *Let $V = \{x \in \mathbb{C}^n \mid f_1(x) = \cdots = f_r(x) = 0\}$ be a smooth algebraic variety, where $f_1, \ldots, f_r$ are polynomials in n variables with real coefficients. We assume that $M := V \cap \mathbb{R}^n$ is nonempty. Then M is an embedded differentiable submanifold of $\mathbb{R}^n$. We call such an M an algebraic manifold, and V is called the complexification of M.*

Proof. This follows from [82, Chapter 0, Example 4.3], which uses the inverse function theorem to show that the inverse image of a differentiable mapping between Euclidean spaces is a differentiable manifold. The differentiable mapping is $F : \mathbb{C}^n \to \mathbb{C}^r$ given by $F(x) = (f_1(x), \ldots, f_r(x))$ and we take the inverse image of the regular value $(0, \ldots, 0)$. $\square$

In the following, we let M be an algebraic manifold. We write $F = (f_1, \ldots, f_r)$ and denote the *Jacobian* of F by

$$J_F(x) = \begin{bmatrix} \frac{\partial f_1}{\partial x_1} & \cdots & \frac{\partial f_1}{\partial x_n} \\ \vdots & & \vdots \\ \frac{\partial f_r}{\partial x_1} & \cdots & \frac{\partial f_r}{\partial x_n} \end{bmatrix} \in \mathbb{R}^{r \times n}.$$

A differentiable function $\alpha : (-\varepsilon, \varepsilon) \rightarrow M$ is called a *(differentiable) curve* in M. Suppose that $\alpha(0) = p \in M$. The *tangent vector to the curve* α at $t = 0$ is the derivative $\alpha'(0) = \frac{\mathrm{d}}{\mathrm{d}t} \alpha(t)|_{t=0}$. A *tangent vector at* p is the tangent vector at $t = 0$ of some curve $\alpha : (-\varepsilon, \varepsilon) \rightarrow M$ with $\alpha(0) = p$. The set of all tangent vectors to M at p constitute the tangent space $T_p M$. We note that $T_p M = \ker JF(p)^T$.

We can view $T_p M$ as a subspace of $\mathbb{R}^n$. The Euclidean metric on $\mathbb{R}^n$ induces a metric on each tangent space $T_p M$, making M a *Riemannian manifold*. We also define the normal space $N_p M := (T_p M)^\perp$.

A *vector field* X is a map $X : \mathbb{R}^n \rightarrow \mathbb{R}^n$. We also interpret X as a differential operator as follows: $X(g)(p) := \langle ((\frac{\partial g}{\partial x_i}(p))_{i=1}^n, X(p) \rangle$, where $g : \mathbb{R}^n \rightarrow \mathbb{R}$ is C^∞. We denote by $\mathscr{X}$ the set of all vector fields of class C^∞ on $\mathbb{R}^n$. We say that a vector field $X \in \mathscr{X}$ is tangent to M if for all $p \in M$ we have $X(p) \in T_p M$. We have the following characterization of tangential vector fields.

Lemma 3.2.1. *Let* $X \in \mathscr{X}$. *Then, for all* $p \in M$ *we have* $X(p) \in T_p M$ *if and only if* $X(f_i) = 0$ *for* $1 \leq i \leq r$.

Proof. Since $T_p M = \ker JF(p)^T$, we have that $X(p)$ is tangent to M at p if and only if $JF(p)X(p) = 0$. This is equivalent to $X(f_i)(p) = 0$ for all i. $\qquad \square$

The *Euclidean connection* $\overline{\nabla}$ on $\mathbb{R}^n$ is a map $\overline{\nabla} : \mathscr{X} \times \mathscr{X} \rightarrow \mathscr{X}, (X, Y) \mapsto \overline{\nabla}_X Y$ defined as follows:

$$(\overline{\nabla}_X Y)(p) = \sum_{i=1}^n X_i(p) \frac{\partial Y}{\partial x_i}(p). \tag{3.7}$$

In other words, $\overline{\nabla}_X Y$ is the directional derivative of Y in the direction X. The Euclidean connection is the *Levi-Civita connection* for the manifold $\mathbb{R}^n$; see, e.g., [136, Chapter 5]. As such it is *symmetric*, which means that for all $X, Y \in \mathscr{X}$ we have $\nabla_X Y - \nabla_Y X = [X, Y]$, where the Lie bracket $[X, Y]$ of two vector fields X, Y is defined to be the vector field $[X, Y](g) = X(Y(g)) - Y(X(g))$. The Euclidean connection is also *compatible* with the inner product on Euclidean space, meaning that $X(\langle Y, Z \rangle) = \langle \nabla_X Y, Z \rangle + \langle Y, \nabla_X Z \rangle$, for $X, Y, Z \in \mathscr{X}$.

The *Gauss formula* [136, Theorem 8.2] implies that the Levi-Civita connection ∇ on M is the tangential component of the Euclidean connection. Let X, Y be vector fields on $\mathbb{R}^n$ that are tangent to M. Then,

$$(\nabla_X Y)(p) = \mathrm{P}_{T_p M} (\overline{\nabla}_X Y)(p),$$

where $\mathrm{P}_{T_p M}$ is the orthogonal projection onto the tangent space $T_p M$. The *second fundamental form* of M at $p \in M$, on the other hand, is the vector field given by the normal component of $\overline{\nabla}$. That is, $\mathrm{II}_p(X, Y) := \mathrm{P}_{N_p M} (\overline{\nabla}_X Y)(p)$. The following is an important lemma for our study.

Lemma 3.2.2. *The second fundamental form* II_p *is symmetric in* X *and* Y *and is independent of the values of* X *and* Y *at points other than* p.

Proof. We recall the proof of [136, Lemma 8.1]. Let X, Y be vector fields on $\mathbb{R}^n$ that are tangent to M. By symmetry of the connection, we have $\overline{\nabla}_X Y - \overline{\nabla}_Y X = [X, Y]$. And for all $1 \leq i \leq r$, we have

$[X,Y](f_i) = X(Y(f_i)) - Y(X(f_i)) = X(0) - Y(0) = 0$ by Lemma 3.2.1. The lemma then implies that for all $p \in M$, the vector field $[X,Y]$ is tangent to M, so that $\mathrm{P}_{N_pM}[X,Y] = 0$. This shows that II_p is symmetric in X and Y. From (3.7) it follows immediately that $(\overline{\nabla}_X Y)(p)$ only depends on $X(p)$, which implies that $\mathrm{II}_p(X,Y)$ only depends on $X(p)$. By symmetry it also only depends on $Y(p)$. $\qquad\square$

The second fundamental form defines a quadratic form. We call it the *shape operator* in the normal direction $\eta \in N_pM$:

$$S_{p,\eta} : T_pM \rightarrow \mathbb{R}, \ v \mapsto \langle (\overline{\nabla}_X X)(p), \eta \rangle, \tag{3.8}$$

where X is a vector field on $\mathbb{R}^n$ tangent to M with $X(p) = v$. The shape operator allows us to define the main object of study in this article: curvature of unit-speed geodesics in M. A curve $\alpha(t)$ in M is called a *unit-speed curve* if $\|\alpha'(t)\| = 1$ for all t. It is called a *geodesic* if $\alpha''(t) \in N_pM$ for all t. The *curvature* of such a curve at $p = \alpha(0)$ is $\|\alpha''(0)\|$.

Lemma 3.2.3. *Let $\alpha(t)$ be a unit-speed geodesic. Let $v = \alpha'(0)$ and $\eta = \frac{\alpha''(0)}{\|\alpha''(0)\|}$. Then the curvature of $\alpha(t)$ is at $p = \alpha(0)$ is $S_{p,\eta}(v)$.*

Proof. Let X be a vector field tangent to M with $X(p) = v$. Following (3.7), we have $(\overline{\nabla}_X X)(p) = \alpha''(0)$. This implies $S_{p,\eta}(v) = \langle \alpha''(0), \eta \rangle = \|\alpha''(0)\|$. $\qquad\square$

The lemma implies that the critical curvatures of geodesics orthogonal to $\eta \in N_pM$ are the eigenvalues of the shape operator $S_{p,\frac{\eta}{\|\eta\|}}$. These eigenvalues are called the *principal curvatures* in the direction η.

Corollary 3.2.2. *The maximal curvature of a unit-speed geodesic passing through $p \in M$ is*

$$\max_{\substack{v \in T_pM, \eta \in N_pM, \\ \|v\|=\|\eta\|=1}} S_{p,\eta}(v).$$

From a different perspective, we can see the shape operator as a tensor in $T_pM \otimes T_pM \otimes N_pM$. The corollary says that the maximal curvature of a unit-speed geodesic passing through $p \in M$ is equal to the *spectral norm* of this tensor.

We say that a vector field $N \in \mathscr{X}$ is *normal* to M if for all $p \in M$ we have $N(p) \in N_pM$. The next lemma introduces the *Weingarten equation*, a useful alternative characterization of the shape tensor.

Lemma 3.2.4. *Let $(v, \eta) \in T_pM \times N_pM$. Let $X, N \in \mathscr{X}$ such that X is tangent to M and N is normal to M, and such that $X(p) = v$ and $N(p) = \eta$. Then we have $S_{p,\eta}(v) = -\langle (\overline{\nabla}_X N)(p), v \rangle$.*

Proof. We recall the proof of [136, Lemma 8.1]. Consider $g : \mathbb{R}^n \rightarrow \mathbb{R}, p \mapsto \langle X(p), N(p) \rangle$. By definition, g vanishes on M and so by Lemma 3.2.1, $X(g) = 0$. By the compatibility of the Euclidean connection, we have $X(g) = \langle \overline{\nabla}_X X, N \rangle + \langle X, \overline{\nabla}_X N \rangle$. Since $S_{p,\eta}(v) = \langle (\overline{\nabla}_X X)(p), N(p) \rangle$, we therefore have that $S_{p,\eta}(v) = -\langle X(p), (\overline{\nabla}_X N)(p) \rangle$. This proves the assertion. $\qquad\square$

Algebraic Geometry Formulation of Curvature

We will now give an algebraic expression for the shape operator (3.8) of an algebraic manifold M. Recall that we denote by V the complexification of M.

We consider a vector of polynomials

$$\mu(x) := \begin{bmatrix} \sum_{j=1}^{r} \lambda_j \frac{\partial f_j}{\partial x_1} \\ \vdots \\ \sum_{j=1}^{r} \lambda_j \frac{\partial f_j}{\partial x_n} \end{bmatrix} \in \mathrm{rowspan}(J_F(x)) \tag{3.9}$$

for some fixed vector of coefficients $\lambda \in \mathbb{R}^r$. Then $\mu(x)$ is a normal field. Let $J_\mu(x)$ be the Jacobian matrix of $\mu(x)$. By definition,

$$J_\mu(x) = \sum_{j=1}^{r} \lambda_j H f_j(x), \text{ where } H f_j(x) = \begin{bmatrix} \frac{\partial^2 f_j(x)}{\partial x_1 \partial x_1} & \cdots & \frac{\partial^2 f_j(x)}{\partial x_1 \partial x_n} \\ \vdots & & \vdots \\ \frac{\partial^2 f_j(x)}{\partial x_1 \partial x_n} & \cdots & \frac{\partial^2 f_j(x)}{\partial x_n \partial x_n} \end{bmatrix}$$

is the Hessian of $f_j(x)$. Let us denote the corresponding complex quadratic form as

$$S_{p,\lambda} : \mathbb{C}^n \longrightarrow \mathbb{C}, v \mapsto - \sum_{j=1}^{r} \lambda_j v^T H f_j(x) v. \tag{3.10}$$

Let $v \in T_p M$ be a tangent vector and X be a vector field tangent to M with $X(p) = v$. By (3.7), we have $(\overline{\nabla}_X \mu)(p) = J\mu(p)v$. The Weingarten equation from Lemma 3.2.4 implies that

$$S_{p,\eta}(v) = S_{p,\lambda}(v), \tag{3.11}$$

where $\eta := \mu(p)$.

That is, we have an equality of the shape operator $S_{p,\eta}$ applied to v with the *complex quadratic form* $S_{p,\lambda}$ applied to v.

Remark 3.2.3. A special case is when $r = 1$; that is, when M is a hypersurface defined by a single polynomial $f(x) = 0$. In this case, we have $J_\mu(p) = \lambda H f(p)$, where $Hf(x)$ is the Hessian of f at x. Equation (3.11) becomes $S_{p,\eta}(v) = \lambda v^T H f(x) v$.

Umbilics

On our way to a discussion of the critical curvature locus, we take a detour to study points where some or all of the principal curvatures are equal. For the principal curvatures $c_1(x), \ldots, c_m(x)$ to be smooth functions of x, we must avoid these points, called umbilics. In addition to being relevant to critical curvature, umbilics are geometrically interesting in their own right.

George Salmon studied umbilics of a surface, points where the two principal curvatures are equal and thus the best second-order approximation of the surface is a sphere. In 1865, he published

a formula for the degree of the variety of umbilics of a general surface of degree d in $\mathbb{R}^3$ [168]. We present his formula along with our own proof using complex projective geometry.

Definition 3.2.4. A point $p \in M$ is called an *umbilic* if there exists a normal direction η such that $S_{p,\eta}$ has one eigenvalue of multiplicity m (i.e. $S_{p,\eta}$ is a multiple of the identity). A point $p \in M$ is called an *umbilic of order k*, for $1 < k \leq m$, if there exists a normal direction η such that $S_{p,\eta}$ has an eigenvalue of order k.

Theorem 3.2.5 (Salmon). *The degree of the variety of umbilics of a general surface of degree d in $\mathbb{R}^3$ is $10d^3 - 28d^2 + 22d$.*

Proof. Let $S \in \mathbb{P}^3$ be the projective closure of the surface S_{affine} of degree d in $\mathbb{R}^3$. Let $H_S \in \mathbb{P}^3$ be the Hessian of S. Then H_S has degree $4(d-2)$ and defines a 3-dimensional subspace H_Q in the $\mathbb{P}^9$ of quadrics in $\mathbb{P}^3$, one for each point in the $\mathbb{P}^3$ of S. For each point p on S, consider the 4-space Y_p of quadrics spanned by the Hessian quadric at the point and the reducible quadrics that have the tangent plane to S at p as a component. The union

$$Y = \cup_p Y_p$$

is a 6-dimensional scroll in $\mathbb{P}^9$, a birational image of the projective bundle

$$\tilde{Y} = \mathbb{P}(O_S(d-2) \oplus 4O_S(d-1)).$$

We consider the subring of the intersection ring on $\tilde{Y}$ generated by H, the pullback of a hyperplane class from $\mathbb{P}^9$, and F, the pullback of a hyperplane class on S. The canonical class on $\tilde{Y}$ is then

$$K_{\tilde{Y}} = -5H + (5d - 6 + d - 4)F = -5H + (6d - 10)F.$$

Consider the 4-dimensional space L of spheres in $\mathbb{P}^9$ and in it the 3-dimensional subspace L_0 of reducible spheres, consisting of pairs of planes with the plane at infinity as a factor. Let $P \supset L$ be a general 5-dimensional space containing L. Then the pullback to $\tilde{Y}$ of the intersection $P \cap Y$ is reducible and contains two surface components: one component S_0 contained in L_0, and another component X_N which is a scroll of lines. The image of S_0 in Y is the dual surface to S, of degree $(d-1)^2 d$. The canonical divisor on S_0 is the restriction of $(d-4)F$, while the canonical divisor $K_{S_0 \cup X_N}$, by adjunction, is the restriction of $-H + (5d - 6 + d - 4)F = -H + (6d - 10)F$. Restricted to S_0, the divisor $K_{S_0 \cup X_N}$ is the sum of the canonical divisor on S_0 and the class of the curve of intersection $C_0 = S_0 \cap X_N$, so the class of C_0 on S_0 is $C_0 = -H + (5d - 6)F = (5d - 6 - (d - 1))F = (4d - 5)F$. The degree of the image of this curve in Y is $\deg C_0 = (4d - 5)(d - 1)d$. The degree of Y and hence also of $S_0 \cup X_N$ is

$$\deg Y = H^6 = ((5d - 6)^2 - (d - 1)(4d - 8 + 6d - 6))d = 15d^3 - 36d^2 + 22d.$$

So X_N has degree

$$\deg X_N = 15d^3 - 36d^2 + 22d - (d - 1)^2 d = 14d^3 - 34d^2 + 21d.$$

The intersection of X_N with L is now a hyperplane section H_N of X_N. It contains the intersection curve $C_N = L_0 \cap X_N$. The curve C_N is the union of C_0 and the lines in X_N that are contained in L_0. The latter lines are in one-to-one correspondence with inflection points on the curve at infinity on S, so their number is $3(d-2)d$. The residual $H_N - C_N$ is a set of lines that all meet C_0 but do not lie in L_0; they correspond one to one to the umbilical points on S. Thus the number of umbilics is

$$14d^3 - 34d^2 + 21d - (4d-5)(d-1)d - 3(d-2)d = 10d^3 - 28d^2 + 22d.$$

$\square$

The expected codimension of umbilics on a smooth m-dimensional variety equals the codimension of real symmetric $m \times m$-matrices with an eigenvalue of order k. In fact,the expected codimension is independent of m.

Lemma 3.2.5. *The variety of real symmetric matrices with an eigenvalue of order at least k has codimension $\binom{k+1}{2} - 1$.*

Proof. The variety of corank k symmetric matrices has codimension $\binom{k+1}{2}$. Any symmetric matrix which is a linear combination of a corank k matrix and the identity matrix has an eigenvalue of order k, and vice versa, any matrix with an eigenvalue of order k is a linear combination of a corank k matrix and the identity matrix. Therefore the set of matrices with an eigenvalue of order at least k is the join of the variety of matrices of corank at least k and the identity matrix, so the lemma follows. $\square$

We note that Section 5.2 contains further discussion of varieties of real symmetric matrices with repeated eigenvalues.

Critical Curvature

We now define the critical curvature locus outside of the locus of umbilics.

Definition 3.2.6. A point $p \in M$ is called a *point of critical curvature* if p is not an order-2 umbilic and if there exists a principal curvature $c = c(x, \lambda)$ such that the gradient of c vanishes in the tangent direction of the unit normal bundle $\{(x, \lambda) \in M \times \mathbb{R}^r \mid \lambda^T J_F(x) J_F(x)^T \lambda = 1\}$.

Let $M = Z(f) \subset \mathbb{R}^n$ be a hypersurface. We now describe a system of polynomial equations for the critical curvature locus of M in the $2n+3$ variables $\{x_1, \ldots, x_n, u_1, \ldots, u_n, \lambda, y_1, y_2\}$. The variables $\{x_1, \ldots, x_n\}$ are used for points of M, the variables $\{u_1, \ldots, u_n\}$ are used for points in T_pM, the variable λ is used to control the length of normal vectors, and the variables $\{y_1, y_2\}$ are used to specify a decomposition of a vector into components in T_pM and N_pM. Consider the following set of $n+4$ equations:

$$f = f(x_1, \ldots, x_n) = 0,$$

$$\alpha = \nabla f \cdot u = 0,$$

$$v = \sum_{i=1}^{n} u_i^2 - 1 = 0,$$

$$\beta = \lambda^2 (\nabla f \cdot \nabla f) - 1 = 0,$$

$$w = H_f \cdot u + y_1 u + y_2 \nabla f = 0.$$

The equations α and v establish that u is a unit tangent vector. The equation β allows us to normalize the gradient. The equation w states that u is a principal curvature vector of M: it is an eigenvalue of the Hessian in the tangent space, with an arbitrary component in the normal space. Let $K \subset \mathbb{R}^{2n+3}$ be the zero set of the equations. It projects onto the set of principal vectors of length 1 at a point on the hypersurface M. The curvature is then given by $g(x, u, \lambda) = \lambda u^t \cdot H_f \cdot u$, so the critical curvature locus is the projection of the critical points of g on K into M.

By the principle of Lagrange multipliers, the critical locus of g on K is the locus where the following $(2n+3) \times (n+5)$-matrix A of partial derivatives has rank at most $n+4$:

$$A = \begin{pmatrix}
f_{x_1} & \alpha_{x_1} & 0 & \beta_{x_1} & w_{1,x_1} & \cdots & w_{n,x_1} & g_{x_1} \\
\vdots & \vdots & \vdots & \vdots & \vdots & \vdots & \vdots & \vdots \\
f_{x_n} & \alpha_{x_n} & 0 & \beta_{x_n} & w_{1,x_n} & \cdots & w_{n,x_n} & g_{x_n} \\
0 & \alpha_{u_1} & u_1 & 0 & w_{1,u_1} & \cdots & w_{n,u_1} & g_{u_1} \\
\vdots & \vdots & \vdots & \vdots & \vdots & \vdots & \vdots & \vdots \\
0 & \alpha_{u_n} & u_n & 0 & w_{1,u_n} & \cdots & w_{n,u_n} & g_{u_n} \\
0 & 0 & 0 & \beta_{\lambda} & 0 & \cdots & 0 & g_{\lambda} \\
0 & 0 & 0 & 0 & w_{1,y_1} & \cdots & w_{n,y_1} & 0 \\
0 & 0 & 0 & 0 & w_{1,y_2} & \cdots & w_{n,y_2} & 0
\end{pmatrix}.$$

As explained in the discussion of Porteous' formula in Section 1.2 of this dissertation, this locus has codimension $n-1$. Thus the critical curvature locus has expected dimension 0.

In the fourth column, we may divide by the common factor λ, since it is nonzero on the critical locus. We use this system of polynomial equations to obtain an upper bound for the degree of the critical curvature locus.

Theorem 3.2.7. *Let $M \subset \mathbb{R}^3$ be a smooth surface of degree d. An upper bound for the degree of the critical curvature locus is $2796d^3 - 6444d^2 + 3696d$.*

Proof. We homogenize the above system of $n+4$ equations to obtain the projective closure

$$\bar{K} \subset \mathbb{P}^n \times \mathbb{P}^n \times \mathbb{P}^1 \times \mathbb{P}^2.$$

When we homogenize the entries of A, the multidegrees are given by the following matrix:

$$\begin{pmatrix}
(d-1,0,0,0) & (d-2,1,0,0) & 0 & (2d-3,0,1,0) & (d-2,1,0,1) & \cdots & (d-2,1,0,1) & (d-3,2,1,0) \\
\\
(d-1,0,0,0) & (d-2,1,0,0) & 0 & (2d-3,0,1,0) & (d-2,1,0,1) & \cdots & (d-2,1,0,1) & (d-3,2,1,0) \\
0 & (d-1,0,0,0) & (0,1,0,0) & 0 & (d-1,0,0,1) & \cdots & (d-1,0,0,1) & (d-2,1,1,0) \\
\vdots & \vdots & \vdots & \vdots & \vdots & \vdots & \vdots & \vdots \\
0 & (d-1,0,0,0) & (0,1,0,0) & 0 & (d-1,0,0,1) & \cdots & (d-1,0,0,1) & (d-2,1,1,0) \\
0 & 0 & 0 & (2d-2,0,0,0) & 0 & \cdots & 0 & (d-2,2,0,0) \\
0 & 0 & 0 & 0 & (d-1,1,0,0) & \cdots & (d-1,1,0,0) & 0 \\
0 & 0 & 0 & 0 & (d-1,1,0,0) & \cdots & (d-1,1,0,0) & 0
\end{pmatrix}.$$

Thus *A* is the matrix of the following map of vector bundles:

$$n\mathscr{O}(1,0,0,0) \oplus n\mathscr{O}(0,1,0,0) \oplus \mathscr{O}(0,0,1,0) \oplus 2\mathscr{O}(0,0,0,1) \rightarrow \mathscr{O}(d,0,0,0) \oplus \mathscr{O}(d-1,1,0,0)$$

$$\oplus \mathscr{O}(0,2,0,0) \oplus \mathscr{O}(2d-2,0,1,0) \oplus n\mathscr{O}(d-1,1,0,1) \oplus \mathscr{O}(d-2,2,1,0).$$

We apply Porteous' formula (Theorem 1.2.3) to obtain the class of the locus where the matrix *A* has rank at most $n+4$. Applying Bézout's formula for the intersection of this locus with the projective closure $\bar{K}$ of the zero locus of the above set of $n+4$ equations, we obtain the stated upper bound. □

Theorem 3.2.7 provides an upper bound for the degree of the critical curvature locus rather than an exact formula due to the presence of solutions to the homogenized system of equations that do not correspond to solutions of the original system of equations as well as other false solutions, including those where $\lambda = \nabla f \cdot \nabla f = 0$. The formula is stated in the case $n = 3$, but can be computed for any $n \geq 3$ using the same process. In future work, we hope to count and remove these false solutions so that we can provide an exact formula for the critical curvature degree.

Conclusion

In this chapter, we have investigated the critical curvature degree of an algebraic variety. This problem shows the necessity of building a bridge between differential geometry and algebraic geometry. The main difficulty of this chapter lies in reinterpreting the differential-geometric definition of curvature in a way that lends itself to a system of polynomial equations. Once we obtain this system of polynomial equations, we are able to use the tools of numerical algebraic geometry to compute these differential-geometric features. In future work, we hope to translate more concepts from differential geometry into the language of polynomial systems.

Chapter 4

Geometry of Data

A fundamental problem in data science is the following: Given a set of points in $\mathbb{R}^n$, find a model to describe these points. The standard technique used by many scientists is to fit a linear space or union of linear spaces to the points. However, data is often nonlinear. Here we will explore the idea of fitting algebraic varieties to data.

The original work in this chapter comes from three papers. Section 4.1 is based on [37], a joint paper with Paul Breiding, Sara Kališnik, and Bernd Sturmfels published in Revista Mathematica Complutense. Section 4.2 is based on the paper [120], joint with Emil Horobeţ and published in Computer Aided Geometric Design. Section 4.3 is based on the paper [35], joint with Madeline Brandt.

4.1 Modeling Point Clouds with Varieties

This section addresses a fundamental problem at the interface of data science and algebraic geometry. Given a sample of points $\Omega = \{u^{(1)}, u^{(2)}, \ldots, u^{(m)}\}$ from an unknown variety V in $\mathbb{R}^n$, our task is to learn as much information about V as possible. No assumptions on the variety V, the sampling, or the distribution on V are made. There can be noise due to rounding, so the points $u^{(i)}$ do not necessarily lie exactly on the variety from which they have been sampled. The variety V is allowed to be singular or reducible. We also consider the case where V lives in the projective space $\mathbb{P}_{\mathbb{R}}^{n-1}$. We are interested in questions such as:

1. What is the dimension of V?

2. Which polynomials vanish on V?

3. What is the degree of V?

4. What are the irreducible components of V?

5. What are the homology groups of V?

Figure 4.1: Sample of 27 points from an unknown plane curve.

Let us consider these five questions for the dataset with $m = 27$ and $n = 2$ shown in Figure 4.1. Here the answers are easy to see, but what to do if $n \geq 4$ and no picture is available?

1. The dimension of the unknown variety V is one.

2. The ideal of V is generated by one polynomial of the form $(x - \alpha)^2 + (y - \beta)^2 - \gamma$.

3. The degree of V is two. A generic line meets V in two (possibly complex) points.

4. The circle V is irreducible because it admits a parametrization by rational functions.

5. The homology groups are $H_0(V, \mathbb{Z}) = H_1(V, \mathbb{Z}) = \mathbb{Z}^1$ and $H_i(V, \mathbb{Z}) = 0$ for $i \geq 2$.

There is a considerable body of literature on such questions in statistics and computer science. The general context is known as *manifold learning*. One often assumes that V is smooth, i.e. a manifold, in order to apply local methods based on approximation by tangent spaces. Learning the true nature of the manifold V is not a concern for most authors. Their principal aim is *dimensionality reduction*, and V only serves in an auxiliary role. Manifolds act as a scaffolding to frame question 1. This makes sense when the parameters m and n are large. Nevertheless, the existing literature often draws its inspiration from figures in 3-space with many well-spaced sample points. For instance, the textbook by Lee and Verleysen [137] employs the "Swiss roll" and the "open box" for its running examples (cf. [137, Section 1.5]).

One notable exception is the work by Ma *et al.* [142]. Their *Generalized Principal Component Analysis* solves problems 1-4 under the assumption that V is a finite union of linear subspaces. Question 5 falls under the umbrella of *topological data analysis* (TDA). Foundational work by Niyogi, Smale and Weinberger [155] concerns the number m of samples needed to compute the homology groups of V, provided V is smooth and its *reach* is known.

Our perspective is that of *computational algebraic geometry*. We care deeply about the unknown variety V. Our motivation is the riddle: *what is V?* For instance, we may be given $m = 800$ samples in $\mathbb{R}^9$, drawn secretly from the group $\mathrm{SO}(3)$ of 3×3 rotation matrices. Our goal is to learn the true dimension, which is three, to find the 20 quadratic polynomials that vanish on V, and to conclude with the guess that V equals $\mathrm{SO}(3)$.

Our writing is organized as follows. First, we present basics of algebraic geometry from a data perspective. Building on [64], we explain some relevant concepts and offer a catalogue of varieties V frequently seen in applications. This includes our three running examples: the Trott curve, the rotation group $\mathrm{SO}(3)$, and varieties of low rank matrices.

Next we address the problem of estimating the dimension of V from the sample Ω. We study nonlinear PCA, box counting dimension, persistent homology curve dimension, correlation dimension and the methods of Levina-Bickel [139] and Diaz-Quiroz-Velasco [81]. Each of these notions depends on a parameter ε between 0 and 1. This determines the scale from local to global at which we consider Ω. Our empirical dimensions are functions of ε. We aggregate their graphs in the *dimension diagram* of Ω, as seen in Figure 4.2.

Then we link algebraic geometry to topological data analysis. To learn homological information about V from Ω, one wishes to know the *reach* of the variety V. This algebraic number is

used to assess the quality of a sample [1, 155]. We propose a variant of persistent homology that incorporates information about the tangent spaces of V at points in Ω.

A key feature of our setting is the existence of polynomials that vanish on the model V, extracted from polynomials that vanish on the sample Ω. Linear polynomials are found by Principal Component Analysis (PCA). However, many relevant varieties V are defined by quadratic or cubic equations. Below we discuss the computation of these polynomials.

Next we utilize the polynomials found earlier. These cut out a variety V' that contains V. We do not know whether $V' = V$ holds, but we would like to test this and certify it, using both numerical and symbolic algorithms. The geography of Ω inside V' is studied by computing dimension, degree, irreducible decomposition, real degree, and volume.

We then introduce our software package `LearningAlgebraicVarieties`. This is written in `Julia` [23], and implements all algorithms described in this section. It is available at

$$\text{https://github.com/PBrdng/LearningAlgebraicVarieties.git}.$$

To compute persistent homology, we use Henselman's package `Eirene` [117]. For numerical algebraic geometry we use `Bertini` [20] and `HomotopyContinuation.jl` [44]. We conclude with a detailed case study for the dataset in [3, Section 6.3]. Here, Ω consists of 6040 points in $\mathbb{R}^{24}$, representing conformations of the molecule cyclooctane C_8H_{16}, shown in Figure 4.10.

Many important aspects of learning varieties from samples are not addressed in this work. One is the issue of noise. Clearly, already the slightest noise in one of the points in Figure 4.1 will let no equation of the form $(x - \alpha)^2 + (y - \beta)^2 - \gamma$ vanish on Ω. But some will *almost* vanish, and these are the equations we are looking for. Based on our experiments, the methods we present for answering questions 1-5 can handle data that is approximate to some extent. However, we leave a qualitative stability analysis for future work. We also assume that there are no outliers in our data. Another aspect of learning varieties is optimization. We might be interested in minimizing a polynomial function f over the unknown variety V by only looking at the samples in Ω. This problem was studied by Cifuentes and Parrilo in [59], using the sum of squares (SOS) paradigm [26].

Varieties and Data

The mathematics of data science is concerned with finding low-dimensional needles in high-dimensional haystacks. The needle is the model which harbors the actual data, whereas the haystack is some ambient space. The paradigms of models are the d-dimensional linear subspaces V of $\mathbb{R}^n$, where d is small and n is large. Most of the points in $\mathbb{R}^n$ are very far from any sample Ω one might ever draw from V, even in the presence of noise and outliers.

The data scientist seeks to learn the unknown model V from the sample Ω that is available. If V is suspected to be a linear space, then she uses linear algebra. The first tool that comes to mind is Principal Component Analysis (PCA). Numerical algorithms for linear algebra are well-developed and fast. They are at the heart of scientific computing and its numerous applications. However, many models V occurring in science and engineering are not linear spaces. Attempts to replace V with a linear approximation are likely to fail.

This is the point where new mathematics comes in. Many branches of mathematics can help with the needles of data science. One can think of V as a topological space, a differential manifold, a metric space, a Lie group, a hypergraph, a category, a semi-algebraic set, and lots of other things. All of these structures are useful in representing and analyzing models.

In this work we focus on the constraints that describe V inside the ambient $\mathbb{R}^n$ (or $\mathbb{P}_{\mathbb{R}}^{n-1}$). The paradigm says that these are linear equations, revealed numerically by feeding Ω to PCA. But, if the constraints are not all linear, then we look for equations of higher degree.

Algebraic Geometry Basics

Our models V are algebraic varieties over the field $\mathbb{R}$ of real numbers. A *variety* is the set of common zeros of a system of polynomials in n variables. A priori, a variety lives in *Euclidean space* $\mathbb{R}^n$. In many applications two points are identified if they agree up to scaling. In such cases, one replaces $\mathbb{R}^n$ with the *real projective space* $\mathbb{P}_{\mathbb{R}}^{n-1}$, whose points are lines through the origin in $\mathbb{R}^n$. The resulting model V is a *real projective variety*, defined by homogeneous polynomials in n unknowns. In this section, we use the term *variety* to mean any zero set of polynomials in $\mathbb{R}^n$ or $\mathbb{P}_{\mathbb{R}}^{n-1}$. The following three varieties serve as our running examples.

Example 4.1.1 (Trott Curve). The Trott curve is the plane curve of degree four defined by

$$12^2(x^4+y^4) - 15^2(x^2+y^2) + 350x^2y^2 + 81 = 0. \tag{4.1}$$

This curve is compact in $\mathbb{R}^2$ and has four connected components (see Figure 4.3). The equation of the corresponding projective curve is obtained by homogenizing the polynomial (4.1). The curve is nonsingular. The Trott curve is quite special because all of its bitangent lines are all fully real. Plücker showed in 1839 that every plane quartic has 28 complex bitangents, Zeuthen argued in 1873 that the number of real bitangents is 28, 16, 8 or 4; see [163, Table 1].

Example 4.1.2 (Rotation Matrices). The group SO(3) consists of all 3×3-matrices $X = (x_{ij})$ with $\det(X) = 1$ and $X^T X = \mathrm{Id}_3$. The last constraint translates into 9 quadratic equations:

$$\begin{array}{ccc}
x_{11}^2+x_{21}^2+x_{31}^2-1 & x_{11}x_{12}+x_{21}x_{22}+x_{31}x_{32} & x_{11}x_{13}+x_{21}x_{23}+x_{31}x_{33} \\
x_{11}x_{12}+x_{21}x_{22}+x_{31}x_{32} & x_{12}^2+x_{22}^2+x_{32}^2-1 & x_{12}x_{13}+x_{22}x_{23}+x_{32}x_{33} \\
x_{11}x_{13}+x_{21}x_{23}+x_{31}x_{33} & x_{12}x_{13}+x_{22}x_{23}+x_{32}x_{33} & x_{13}^2+x_{23}^2+x_{33}^2-1
\end{array} \tag{4.2}$$

These quadrics say that X is an orthogonal matrix. Adding the cubic $\det(X) - 1$ gives 10 polynomials that define SO(3) as a variety in $\mathbb{R}^9$. Their ideal I is prime. In total, there are 20 linearly independent quadrics in I: the nine listed in (4.2), two from the diagonal of $XX^T - \mathrm{Id}_3$, and nine that express the right-hand rule for orientation, like $x_{22}x_{33} - x_{23}x_{32} - x_{11}$.

Example 4.1.3 (Low Rank Matrices). Consider the set of $m \times n$-matrices of rank $\leq r$. This is the zero set of $\binom{m}{r+1}\binom{n}{r+1}$ polynomials, namely the $(r+1)$-minors. These equations are homogeneous of degree $r+1$. Hence this variety lives naturally in the projective space $\mathbb{P}_{\mathbb{R}}^{mn-1}$.

A variety V is *irreducible* if it is not a union of two proper subvarieties. The above varieties are irreducible. A sufficient condition for a variety to be irreducible is that it has a parametrization by rational functions. This holds in Example 4.1.3 where V consists of the matrices $U_1^T U_2$ where U_1 and U_2 have r rows. It also holds for the rotation matrices

$$X = \frac{1}{1-a^2-b^2-c^2-d^2} \begin{pmatrix} 1-2b^2-2c^2 & 2ab-2cd & 2ac+2bd \\ 2ab+2cd & 1-2a^2-2c^2 & 2bc-2ad \\ 2ac-2bd & 2bc+2ad & 1-2a^2-2b^2 \end{pmatrix}. \tag{4.3}$$

However, smooth quartic curves in $\mathbb{P}_{\mathbb{R}}^2$ admit no such rational parametrization.

The two most basic invariants of a variety V are its *dimension* and its *degree*. The former is the length d of the longest proper chain of irreducible varieties $V_1 \subset V_2 \subset \cdots \subset V_d \subset V$. A general system of d linear equations has a finite number of solutions on V. That number is well-defined if we work over $\mathbb{C}$. It is the degree of V, denoted $\deg(V)$. The Trott curve has dimension 1 and degree 4. The group SO(3) has dimension 3 and degree 8. In Example 4.1.3, if $m = 3, n = 4$ and $r = 2$, then the projective variety has dimension 9 and degree 6.

There are several alternative definitions of dimension and degree in algebraic geometry. For instance, they are read off from the Hilbert polynomial, which can be computed by way of Gröbner bases. We refer to Chapter 9, titled *Dimension Theory*, in the textbook [64].

A variety that admits a rational parametrization is called *unirational*. Smooth plane curves of degree ≥ 3 are not unirational. However, the varieties V that arise in applications are often unirational. The reason is that V often models a generative process. This happens in statistics, where V represents some kind of (conditional) independence structure. Examples include graphical models, hidden Markov models and phylogenetic models.

If V is a unirational variety with given rational parametrization, then it is easy to create a finite subset Ω of V. One selects parameter values at random and plugs these into the parametrization. For instance, one creates rank one matrices by simply multiplying a random column vector with a random row vector. A naive approach to sampling from the rotation group SO(3) is plugging four random real numbers a, b, c, d into the parametrization (4.3). Another method for sampling from SO(3) will be discussed in Section 4.1.

Given a dataset $\Omega \subset \mathbb{R}^n$ that comes from an applied context, it is reasonable to surmise that the underlying unknown variety V admits a rational parametrization. However, from the vantage point of a pure geometer, such unirational varieties are rare. To sample from a general variety V, we start from its defining equations, and we solve $\dim(V)$ many linear equations on V. The algebraic complexity of carrying this out is measured by $\deg(V)$. See Dufresne *et al.* [90] for recent work on sampling by way of numerical algebraic geometry.

Example 4.1.4. One might sample from the Trott curve V in Example 4.1.1 by intersecting it with a random line. Algebraically, one solves $\dim(V) = 1$ linear equation on the curve. That line intersects V in $\deg(V) = 4$ points. Computing the intersection points can be done numerically, but also symbolically by using Cardano's formula for the quartic. In either case, the coordinates computed by these methods may be complex numbers. Such points are simply discarded if real samples are desired. This can be a rather wasteful process.

At this point, optimization and real algebraic geometry enter the scene. Suppose that upper and lower bounds are known for the values of a linear function ℓ on V. In that case, the equations to solve have the form $\ell(x) = \alpha$, where α is chosen between these bounds.

For the Trott curve, we might know that no real points exist unless $|x| \leq 1$. We choose x at random between -1 and $+1$, plug it into the equation (4.1), and then solve the resulting quartic in y. The solutions y thus obtained are likely to be real, thus giving us lots of real samples on the curve. Of course, for arbitrary real varieties, it is a hard problem to identify a priori constraints that play the role of $|x| \leq 1$. However, recent advances in polynomial optimization, notably in sum-of-squares programming [26], should be quite helpful.

At this point, let us recap and focus on a concrete instance of the riddles we seek to solve.

Example 4.1.5. Let $n = 6$, $m = 40$ and consider the following forty sample points in $\mathbb{R}^6$:

$(0,-2,6,0,-1,12)$	$(-4,5,-15,-12,-5,15)$	$(-4,2,-3,2,6,-1)$	$(0,0,-1,-6,0,4)$
$(12,3,-8,8,-12,2)$	$(20,24,-30,-25,24,-30)$	$(9,3,5,3,15,1)$	$(12,9,-25,20,-15,15)$
$(0,-10,-12,0,8,15)$	$(15,-6,-4,5,-12,-2)$	$(3,2,6,6,3,4)$	$(12,-8,9,9,12,-6)$
$(2,-10,15,-5,-6,25)$	$(5,-5,0,-3,0,3)$	$(-12,18,6,-8,9,12)$	$(12,10,-12,-18,8,-15)$
$(1,0,-4,-2,2,0)$	$(4,-5,0,0,-3,0)$	$(12,-2,1,6,2,-1)$	$(-5,0,-2,5,2,0)$
$(3,-2,-8,-6,4,4)$	$(-3,-1,-9,-9,-3,-3)$	$(0,1,-2,0,1,-2)$	$(5,6,8,10,4,12)$
$(2,0,-1,-1,2,0)$	$(12,-9,-1,4,-3,-3)$	$(5,-6,16,-20,-4,24)$	$(0,0,1,-3,0,1)$
$(15,-10,-12,12,-15,-8)$	$(15,-5,6,6,15,-2)$	$(-2,1,6,-12,1,6)$	$(3,2,0,0,-2,0)$
$(24,-20,-6,-18,8,15)$	$(-3,3,-1,-3,-1,3)$	$(-10,0,6,-12,5,0)$	$(2,-2,10,5,4,-5)$
$(4,-6,1,-2,-2,3)$	$(3,-5,-6,3,-6,-5)$	$(0,0,-2,3,0,1)$	$(-6,-4,-30,15,12,10)$

Where do these samples come from? Do the zero entries or the sign patterns offer any clue?

To reveal the answer we label the coordinates as $(x_{22}, x_{21}, x_{13}, x_{12}, x_{23}, x_{11})$. The relations

$$x_{11}x_{22} - x_{12}x_{21} = x_{11}x_{23} - x_{13}x_{21} = x_{12}x_{23} - x_{22}x_{13} = 0$$

hold for all 40 data points. Hence V is the variety of 2×3-matrices (x_{ij}) of rank ≤ 1. Following Example 4.1.3, we view this as a projective variety in $\mathbb{P}^5_{\mathbb{R}}$. In that ambient projective space, the determinantal variety V is a manifold of dimension 3 and degree 3. Note that V is homeomorphic to $\mathbb{P}^1_{\mathbb{R}} \times \mathbb{P}^2_{\mathbb{R}}$, so we can write its homology groups using the Künneth formula.

In data analysis, proximity between sample points plays a crucial role. There are many ways to measure distances. In this section we restrict ourselves to two metrics. For data in $\mathbb{R}^n$ we use the Euclidean metric, which is induced by the standard inner product $\langle u, v \rangle = \sum_{i=1}^{n} u_i v_i$. For data in $\mathbb{P}^{n-1}_{\mathbb{R}}$ we use the Fubini-Study metric. Points u and v in $\mathbb{P}^{n-1}_{\mathbb{R}}$ are represented by their homogeneous coordinate vectors. The *Fubini-Study distance* from u to v is the angle between the lines spanned by representative vectors u and v in $\mathbb{R}^n$:

$$\text{dist}_{\text{FS}}(u,v) = \arccos \frac{|\langle u,v \rangle|}{\|u\| \|v\|}. \tag{4.4}$$

This formula defines the unique Riemannian metric on $\mathbb{P}^{n-1}_{\mathbb{R}}$ that is orthogonally invariant.

A Variety of Varieties

In what follows we present some "model organisms" seen in applied algebraic geometry. Familiarity with a repertoire of interesting varieties is an essential prerequisite for those who are serious about learning algebraic structure from the datasets Ω they might encounter.

Rank Constraints. Consider $m \times n$-matrices with linear entries having rank $\leq r$. We saw the $r = 1$ case in Example 4.1.3. A *rank variety* is the set of all tensors of fixed size and rank that satisfy some linear constraints. The constraints often take the simple form that two entries are equal. This includes symmetric matrices, Hankel matrices, Toeplitz matrices, Sylvester matrices, etc. Many classes of structured matrices generalize naturally to tensors.

Example 4.1.6. Let $n = \binom{s}{2}$ and identify $\mathbb{R}^n$ with the space of skew-symmetric $s \times s$-matrices $P = (p_{ij})$. These satisfy $P^T = -P$. Let V be the variety of rank 2 matrices P in $\mathbb{P}^{n-1}_{\mathbb{R}}$. A parametric representation is given by $p_{ij} = a_i b_j - a_j b_i$, so the p_{ij} are the 2×2-minors of a $2 \times s$-matrix. The ideal of V is generated by the 4×4 *pfaffians* $p_{ij}p_{kl} - p_{ik}p_{jl} + p_{il}p_{jk}$. These $\binom{s}{4}$ quadrics are also known as the *Plücker relations*, and V is the *Grassmannian* of 2-dimensional linear subspaces in $\mathbb{R}^s$. The *r-secants* of V are represented by the variety of skew-symmetric matrices of rank $\leq 2r$. Its equations are the $(2r+2) \times (2r+2)$ pfaffians of P. We refer to [111, Lectures 6 and 9] for an introduction to these classical varieties.

Example 4.1.7. The space of $3 \times 3 \times 3 \times 3$ tensors $(x_{ijkl})_{1 \leq i,j,k,l \leq 3}$ has dimension 81. Suppose we sample from its subspace of symmetric tensors $m = (m_{rst})_{0 \leq r \leq s \leq t \leq 3}$. This has dimension $n = 20$. We use the convention $m_{rst} = x_{ijkl}$ where r is the number of indices 1 in (i,j,k,l), s is the number of indices 2, and t is the number of indices 3. This identifies tensors m with cubic polynomials $m = \sum_{i+j+k \leq 3} m_{ijk} x^i y^j z^k$, and hence with cubic surfaces in 3-space. Fix $r \in \{1,2,3\}$ and take V to be the variety of tensors m of rank $\leq r$. The equations that define the tensor rank variety V are the $(r+1) \times (r+1)$-minors of the 4×10 *Hankel matrix*

$$\begin{bmatrix} m_{000} & m_{100} & m_{010} & m_{001} & m_{200} & m_{110} & m_{101} & m_{020} & m_{011} & m_{002} \\ m_{100} & m_{200} & m_{110} & m_{101} & m_{300} & m_{210} & m_{201} & m_{120} & m_{111} & m_{102} \\ m_{010} & m_{110} & m_{020} & m_{011} & m_{210} & m_{120} & m_{111} & m_{030} & m_{021} & m_{012} \\ m_{001} & m_{101} & m_{011} & m_{002} & m_{201} & m_{111} & m_{102} & m_{021} & m_{012} & m_{003} \end{bmatrix}.$$

See Landsberg's book [133] for an introduction to the geometry of tensors and their rank.

Example 4.1.8. In *distance geometry*, one encodes finite metric spaces with p points in the *Schönberg matrix* $D = (d_{ip} + d_{jp} - d_{ij})$ where d_{ij} is the squared distance between points i and j. The symmetric $(p-1) \times (p-1)$ matrix D is positive semidefinite if and only if the metric space is Euclidean, and its embedding dimension is the rank r of D. See [75, Section 6.2.1] for a textbook introduction and derivation of Schönberg's esults. Hence the rank varieties of the Schönberg matrix D encode the finite Euclidean metric spaces with p points. A prominent dataset corresponding to the case $p = 8$ and $r = 3$ will be studied in Section 4.1.

Matrices and tensors with rank constraints are ubiquitous in data science. Make sure to search for such low rank structures when facing vectorized samples, as in Example 4.1.5.

Hypersurfaces. The most basic varieties are defined by just one polynomial. When given a sample Ω, one might begin by asking for hypersurfaces that contain Ω and that are especially nice, simple and informative. Here are some examples of special structures worth looking for.

Example 4.1.9. For $s = 6, r = 2$ in Example 4.1.6, V is the hypersurface of the 6×6-*pfaffian*:

$$
\begin{aligned}
& p_{16}p_{25}p_{34} - p_{15}p_{26}p_{34} - p_{16}p_{24}p_{35} + p_{14}p_{26}p_{35} + p_{15}p_{24}p_{36} \\
& - p_{14}p_{25}p_{36} + p_{16}p_{23}p_{45} - p_{13}p_{26}p_{45} + p_{12}p_{36}p_{45} - p_{15}p_{23}p_{46} \\
& + p_{13}p_{25}p_{46} - p_{12}p_{35}p_{46} + p_{14}p_{23}p_{56} - p_{13}p_{24}p_{56} + p_{12}p_{34}p_{56}.
\end{aligned}
\tag{4.5}
$$

The 15 monomials correspond to the matchings of the complete graph with six vertices.

Example 4.1.10. The *hyperdeterminant* of format $2 \times 2 \times 2$ is a polynomial of degree four in $n = 8$ unknowns, namely the entries of a $2 \times 2 \times 2$-tensor $X = (x_{ijk})$. Its expansion equals

$$
\begin{aligned}
& x_{110}^2 x_{001}^2 + x_{100}^2 x_{011}^2 + x_{010}^2 x_{101}^2 + x_{000}^2 x_{111}^2 + 4x_{000}x_{110}x_{011}x_{101} + 4x_{010}x_{100}x_{001}x_{111} - 2x_{100}x_{110}x_{001}x_{011} \\
& - 2x_{010}x_{110}x_{001}x_{101} - 2x_{010}x_{100}x_{011}x_{101} - 2x_{000}x_{110}x_{001}x_{111} - 2x_{000}x_{100}x_{011}x_{111} - 2x_{000}x_{010}x_{101}x_{111}.
\end{aligned}
$$

This hypersurface is rational and it admits several nice parameterizations, useful for sampling points. For instance, up to scaling, we can take the eight principal minors of a symmetric 3×3-matrix, with $x_{000} = 1$ as the 0×0-minor, $x_{100}, x_{010}, x_{001}$ for the 1×1-minors (i.e. diagonal entries), $x_{110}, x_{101}, x_{011}$ for the 2×2-minors, and x_{111} for the 3×3-determinant.

Example 4.1.11. Let $n = 10$, with coordinates for $\mathbb{R}^{10}$ given by the off-diagonal entries of a symmetric 5×5-matrix (x_{ij}). There is a unique quintic polynomial in these variables that vanishes on symmetric 5×5-matrices of rank ≤ 2. This polynomial, known as the *pentad*, plays a historical role in the statistical theory of *factor analysis* [87, Example 4.2.8]. It equals

$$
\begin{aligned}
& x_{14}x_{15}x_{23}x_{25}x_{34} - x_{13}x_{15}x_{24}x_{25}x_{34} - x_{14}x_{15}x_{23}x_{24}x_{35} + x_{13}x_{14}x_{24}x_{25}x_{35} \\
& + x_{12}x_{15}x_{24}x_{34}x_{35} - x_{12}x_{14}x_{25}x_{34}x_{35} + x_{13}x_{15}x_{23}x_{24}x_{45} - x_{13}x_{14}x_{23}x_{25}x_{45} \\
& - x_{12}x_{15}x_{23}x_{34}x_{45} + x_{12}x_{13}x_{25}x_{34}x_{45} + x_{12}x_{14}x_{23}x_{35}x_{45} - x_{12}x_{13}x_{24}x_{35}x_{45}.
\end{aligned}
$$

We can sample from the pentad using the parametrization $x_{ij} = a_i b_j + c_i d_j$ for $1 \leq i < j \leq 5$.

Example 4.1.12. The determinant of the $(p-1) \times (p-1)$ matrix in Example 4.1.8 equals the squared volume of the simplex spanned by p points in $\mathbb{R}^{p-1}$. If $p = 3$ then we get Heron's formula for the area of a triangle in terms of its side lengths. The hypersurface in $\mathbb{R}^{\binom{p}{2}}$ defined by this polynomial represents configurations of p points in $\mathbb{R}^{p-1}$ that are degenerate.

One problem with interesting hypersurfaces is that they often have a very high degree and it would be impossible to find that equation by our methods in Section 4.1. For instance, the *Lüroth hypersurface* [17] in the space of ternary quartics has degree 54, and the *restricted Boltzmann machine* [65] on four binary random variables has degree 110. These hypersurfaces are easy to sample from, but there is little hope to learn their equations from those samples.

Secret Linear Spaces. This refers to varieties that become linear spaces after a simple change of coordinates. Linear spaces V are easy to recognize from samples Ω using PCA.

Toric varieties become linear spaces after taking logarithms, so they can be learned by taking the coordinatewise logarithm of the sample points. Formally, a toric variety is the image of a monomial map. Equivalently, it is an irreducible variety defined by binomials.

Example 4.1.13. Let $n = 6, m = 40$ and consider the following dataset in $\mathbb{R}^6$:

$$
\begin{array}{cccc}
(91,130,169,70,91,130) & (4,2,1,8,4,2) & (6,33,36,11,12,66) & (24,20,44,30,66,55) \\
(8,5,10,40,80,50) & (11,11,22,2,4,4) & (88,24,72,33,99,27) & (14,77,56,11,8,44) \\
(70,60,45,84,63,54) & (143,13,78,11,66,6) & (182,91,156,98,168,84) & (21,98,91,42,39,182) \\
(5,12,3,20,5,12) & (80,24,8,30,10,3) & (3,5,5,15,15,25) & (10,10,11,10,11,11) \\
(121,66,88,66,88,48) & (45,81,63,45,35,63) & (48,52,12,156,36,39) & (45,50,60,45,54,60) \\
(143,52,117,44,99,36) & (56,63,7,72,8,9) & (10,55,20,11,4,22) & (91,56,7,104,13,8) \\
(24,6,42,4,28,7) & (18,10,18,45,81,45) & (36,27,117,12,52,39) & (3,2,2,3,3,2) \\
(40,10,35,8,28,7) & (22,10,26,55,143,65) & (132,36,60,33,55,15) & (98,154,154,77,77,121) \\
(55,20,55,44,121,44) & (24,30,39,40,52,65) & (22,22,28,121,154,154) & (6,3,6,4,8,4) \\
(77,99,44,63,28,36) & (30,20,90,6,27,18) & (1,5,2,5,2,10) & (26,8,28,26,91,28)
\end{array}
$$

Replace each of these forty vectors by its coordinate-wise logarithm. Applying PCA to the resulting vectors, we learn that our sample comes from a 4-dimensional subspace of $\mathbb{R}^6$. This is the row space of a 4×6-matrix whose columns are the vertices of a regular octahedron:

$$
A \;=\; \begin{pmatrix} 1 & 1 & 1 & 0 & 0 & 0 \\ 1 & 0 & 0 & 1 & 1 & 0 \\ 0 & 1 & 0 & 1 & 0 & 1 \\ 0 & 0 & 1 & 0 & 1 & 1 \end{pmatrix}.
$$

Our original samples came from the toric variety X_A associated with this matrix. This means each sample has the form (ab, ac, ad, bc, bd, cd), where a, b, c, d are positive real numbers.

Toric varieties are important in applications. For instance, in statistics they correspond to *exponential families* for discrete random variables. Overlap with rank varieties arises for matrices and tensors of rank 1. Those smallest rank varieties are known in geometry as the *Segre varieties* (for arbitrary tensors) and the *Veronese varieties* (for symmetric tensors). These special varieties are toric, so they are represented by an integer matrix A as above.

Example 4.1.14. Let $n = 6$ and take Ω to be a sample of points of the form

$$
\left((2a+b)^{-1}, (a+2b)^{-1}, (2a+c)^{-1}, (a+2c)^{-1}, (2b+c)^{-1}, (b+2c)^{-1}\right).
$$

The corresponding variety $V \subset \mathbb{P}^5_{\mathbb{R}}$ is a *reciprocal linear space V*; see [131]. In projective geometry, such a variety arises as the image of a linear space under the classical *Cremona transformation*. From the sample we can learn the variety V by replacing each data point by its coordinate-wise inverse. Applying PCA to these reciprocalized data, we learn that V is a surface in $\mathbb{P}^5_{\mathbb{R}}$, cut out by ten cubics like $2x_3x_4x_5 - x_3x_4x_6 - 2x_3x_5x_6 + x_4x_5x_6$.

Algebraic Statistics and Computer Vision. Model selection is a standard task in statistics. The models considered in algebraic statistics [87] are typically semi-algebraic sets, and it is customary to identify them with their Zariski closures, which are algebraic varieties.

Example 4.1.15. *Bayesian networks* are also known as directed graphical models. The corresponding varieties are parametrized by monomial maps from products of simplices. Here are the equations for a Bayesian network on 4 binary random variables [87, Example 3.3.11]:

$$(x_{0000}+x_{0001})(x_{0110}+x_{0111})-(x_{0010}+x_{0011})(x_{0100}+x_{0101}),$$
$$(x_{1000}+x_{1001})(x_{1110}+x_{1111})-(x_{1010}+x_{1011})(x_{1100}+x_{1101}),$$
$$x_{0000}x_{1001}-x_{0001}x_{1000}, x_{0010}x_{1011}-x_{0011}x_{1010}, x_{0100}x_{1101}-x_{0101}x_{1100}, x_{0110}x_{1111}-x_{0111}x_{1110}.$$

The coordinates x_{ijkl} represent the probabilities of observing the 16 states under this model.

Computational biology is an excellent source of statistical models with interesting geometric and combinatorial properties. These include hidden variable tree models for phylogenetics, and hidden Markov models for gene annotation and sequence alignment.

In the social sciences and economics, statistical models for permutations are widely used:

Example 4.1.16. Let $n = 6$ and consider the *Plackett-Luce model* for rankings of three items [179]. Each item has a model parameter θ_i, and we write x_{ijk} for the probability of observing the permutation ijk. The model is the surface in $\mathbb{P}^5_{\mathbb{R}}$ given by the parametrization

$$x_{123} = \theta_2\theta_3(\theta_1+\theta_3)(\theta_2+\theta_3), \quad x_{132} = \theta_2\theta_3(\theta_1+\theta_2)(\theta_2+\theta_3), \quad x_{213} = \theta_1\theta_3(\theta_1+\theta_3)(\theta_2+\theta_3),$$
$$x_{231} = \theta_1\theta_3(\theta_1+\theta_2)(\theta_1+\theta_3), \quad x_{312} = \theta_1\theta_2(\theta_1+\theta_2)(\theta_2+\theta_3), \quad x_{321} = \theta_1\theta_2(\theta_1+\theta_2)(\theta_1+\theta_3).$$

The prime ideal of this model is generated by three quadrics and one cubic:

$$x_{123}(x_{321}+x_{231})-x_{213}(x_{132}+x_{312}), \ x_{312}(x_{123}+x_{213})-x_{132}(x_{231}+x_{321}),$$
$$x_{231}(x_{132}+x_{312})-x_{321}(x_{123}+x_{213}), \quad x_{123}x_{231}x_{312}-x_{132}x_{321}x_{213}.$$

When dealing with continuous distributions, we can represent certain statistical models as varieties in moment coordinates. This applies to Gaussians and their mixtures.

Example 4.1.17. Consider the projective variety in $\mathbb{P}^6_{\mathbb{R}}$ given parametrically by $m_0 = 1$ and

$$
\begin{aligned}
m_1 &= \lambda\mu+(1-\lambda)\nu \\
m_2 &= \lambda(\mu^2+\sigma^2)+(1-\lambda)(\nu^2+\tau^2) \\
m_3 &= \lambda(\mu^3+3\mu\sigma^2)+(1-\lambda)(\nu^3+3\nu\tau^2) \\
m_4 &= \lambda(\mu^4+6\mu^2\sigma^2+3\sigma^4)+(1-\lambda)(\nu^4+6\nu^2\tau^2+3\tau^4) \\
m_5 &= \lambda(\mu^5+10\mu^3\sigma^2+15\mu\sigma^4)+(1-\lambda)(\nu^5+10\nu^3\tau^2+15\nu\tau^4) \\
m_6 &= \lambda(\mu^6+15\mu^4\sigma^2+45\mu^2\sigma^4+15\sigma^6)+(1-\lambda)(\nu^6+15\nu^4\tau^2+45\nu^2\tau^4+15\tau^6).
\end{aligned}
$$

These are the moments of order ≤ 6 of the mixture of two Gaussian random variables on the line. Here μ and ν are the means, σ and τ are the variances, and λ is the mixture parameter. It was shown in [9, Theorem 1] that this is a hypersurface of degree 39 in $\mathbb{P}^6$. For $\mu = 0$ we get the *Gaussian moment surface* which is defined by the 3×3-minors of the 3×6-matrix

$$
\begin{pmatrix}
0 & m_0 & 2m_1 & 3m_2 & 4m_3 & 5m_4 \\
m_0 & m_1 & m_2 & m_3 & m_4 & m_5 \\
m_1 & m_2 & m_3 & m_4 & m_5 & m_6
\end{pmatrix}.
$$

Example 4.1.18. Let $n = 9$ and fix the space of 3×3-matrices. An *essential matrix* is the product of a rotation matrix times a skew-symmetric matrix. In computer vision, these matrices represent the relative position of two calibrated cameras in 3-space. Their entries x_{ij} serve as invariant coordinates for pairs of such cameras. The variety of essential matrices is defined by ten cubics. These are known as the *Démazure cubics* [127, Example 2.2].

The article [127] studies camera models in the presence of distortion. For example, the model described in [127, Example 2.3] concerns *essential matrices plus one focal length unknown*. This is the codimension two variety defined by the 3×3-minors of the 3×4-matrix

$$\begin{pmatrix} x_{11} & x_{12} & x_{13} & x_{21}x_{31} + x_{22}x_{32} + x_{23}x_{33} \\ x_{21} & x_{22} & x_{23} & -x_{11}x_{31} - x_{12}x_{32} - x_{13}x_{33} \\ x_{31} & x_{32} & x_{33} & 0 \end{pmatrix}.$$

Learning such models is important for image reconstruction in computer vision.

Estimating the Dimension

The first question one asks about a variety V is "What is the dimension?". In what follows, we discuss methods for estimating $\dim(V)$ from the finite sample Ω, taken from V. We present six dimension estimates. They are motivated and justified by geometric considerations. For a manifold, dimension is defined in terms of local charts. This is consistent with the notion of dimension in algebraic geometry [64, Chapter 9]. The dimension estimates in this section are based on Ω alone. Later sections will address the computation of equations that vanish on V. These can be employed to find upper bounds on $\dim(V)$; see (4.23). In what follows, however, we do not have that information. All we are given is the input $\Omega = \{u^{(1)}, \ldots, u^{(m)}\}$.

Dimension Diagrams

There is an extensive literature (see e.g. [50, 51]) on computing an *intrinsic dimension* of the sample Ω from a manifold V. The intrinsic dimension of Ω is a positive real number that approximates the *Hausdorff dimension* of V, a quantity that measures the local dimension of a space using the distances between nearby points. It is a priori not clear that the algebraic definition of $\dim(V)$ agrees with the topological definition of Hausdorff dimension that is commonly used in manifold learning. However, this will be true under the following natural hypotheses. We assume that V is a variety in $\mathbb{R}^n$ or $\mathbb{P}_{\mathbb{R}}^{n-1}$ such that the set of real points is Zariski dense in each irreducible component of V. If V is irreducible, then its singular locus $\mathrm{Sing}(V)$ is a proper subvariety, so it has measure zero. The regular locus $V \backslash \mathrm{Sing}(V)$ is a real manifold. Each connected component is a real manifold of dimension $d = \dim(V)$.

The definitions of intrinsic dimension can be grouped into two categories: *local methods* and *global methods* [51, 124]. Definitions involving information about sample neighborhoods fit into the local category, while those that use the whole dataset are called global.

Instead of making such a strict distinction between local and global, we introduce a parameter $0 \le \varepsilon \le 1$. The idea behind this is that ε should determine the range of information that is used to compute the dimension from the local scale ($\varepsilon = 0$) to the global scale ($\varepsilon = 1$).

To be precise, for each of the dimension estimates, locality is determined by a notion of *distance*: the point sample Ω is a finite metric space. In our context we restrict extrinsic metrics to the sample. For samples $\Omega \subset \mathbb{R}^n$ we work with the *scaled Euclidean distance*

$$\text{dist}_{\mathbb{R}^n}(u,v) \ := \ \frac{\|u-v\|}{\max_{x,y \in \Omega} \|x-y\|}. \tag{4.6}$$

For samples Ω taken in projective space $\mathbb{P}^{n-1}_{\mathbb{R}}$ we use the *scaled Fubini-Study distance*

$$\text{dist}_{\mathbb{P}^{n-1}_{\mathbb{R}}}(u,v) \ := \ \frac{\text{dist}_{\text{FS}}(u,v)}{\max_{x,y \in \Omega} \text{dist}_{\text{FS}}(x,y)}. \tag{4.7}$$

Two points $u^{(i)}$ and $u^{(j)}$ in Ω are considered ε-*close* with respect to the parameter ε if $\text{dist}_{\mathbb{R}^n}(u,v) \leq \varepsilon$ or $\text{dist}_{\mathbb{P}^{n-1}_{\mathbb{R}}}(u,v) \leq \varepsilon$, respectively. Given ε we divide the sample Ω into clusters $\Omega^{\varepsilon}_1, \ldots, \Omega^{\varepsilon}_l$, which are defined in terms of ε-closeness, and apply the methods to each cluster separately, thus obtaining dimension estimates whose definition of being local depends on ε. In particular, for $\varepsilon = 0$ we consider each sample point individually, while for $\varepsilon = 1$ we consider the whole sample. Intermediate values of ε interpolate between the two.

Many of the definitions of intrinsic dimension are consistent. This means that it is possible to compute a scale ε from Ω for which the intrinsic dimension of each cluster converges to the dimension of V if m is sufficiently large and Ω is sampled sufficiently densely. By contrast, our paradigm is that m is fixed. For us, m does not tend to infinity. Our standing assumption is that we are given one fixed sample Ω. The goal is to compute a meaningful dimension from that fixed sample of m points. For this reason, we cannot unreservedly employ results on appropriate parameters ε in our methods. The sample Ω will almost never satisfy the assumptions that are needed. Our approach to circumvent this problem is to create a *dimension diagram*. Such diagrams are shown in Figures 4.2, 4.6, 4.8 and 4.11.

Definition 4.1.19. Let $\dim(\Omega, \varepsilon)$ be one of the subsequent dimension estimates. The *dimension diagram* of the sample Ω is the graph of the function $(0,1] \longrightarrow \mathbb{R}_{\geq 0}$, $\varepsilon \mapsto \dim(\Omega, \varepsilon)$.

Remark 4.1.20. The idea of using dimension diagrams is inspired by persistent homology. Our dimension diagrams and our persistent homology barcodes of Section 4.1 both use ε in the interval $[0,1]$ for the horizontal axis. This uniform scale for all samples Ω makes comparisons across different datasets easier.

The true dimension of a variety is an integer. However, we defined the dimension diagram to be the graph of a function whose range is a subset of the real numbers. The reason is that the subsequent estimates do not return integers. A noninteger dimension can be meaningful mathematically, such as in the case of a fractal curve which fills space densely enough that its dimension could be considered closer to 2 than 1. By plotting these diagrams, we hope to gain information about the true dimension d of the variety V from which Ω was sampled.

One might be tempted to use the same dimension estimate for $\mathbb{R}^n$ and $\mathbb{P}^{n-1}_{\mathbb{R}}$, possibly via the Euclidean distance on an affine patch of $\mathbb{P}^{n-1}_{\mathbb{R}}$. However, the Theorema Egregium by Gauss implies
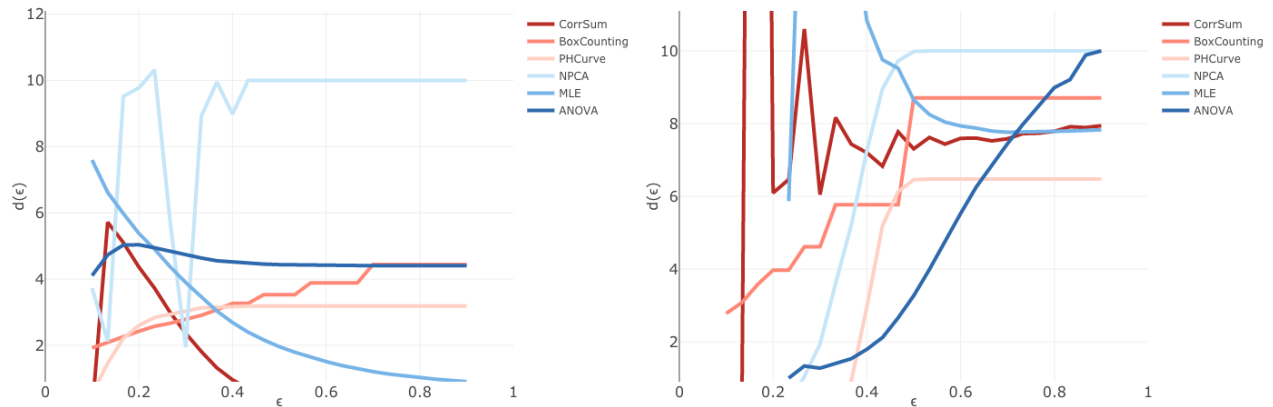
Figure 4.2: Dimension diagrams for 600 points on the variety of 3×4 matrices of rank 2. This is a projective variety of dimension 9. Its affine cone has dimension 10. The left picture shows dimension diagrams for the estimates in Euclidean space $\mathbb{R}^{12}$. The right picture shows those for projective space $\mathbb{P}^{11}_{\mathbb{R}}$. The projective diagrams yield better estimates. The 600 data points were obtained by independently sampling pairs of 4×2 and 2×3 matrices, each with independent entries from the normal distribution, and then multiplying them.

that any projection from $\mathbb{P}^{n-1}_{\mathbb{R}}$ to $\mathbb{R}^{n-1}$ must distort lengths. Hence, because we gave the parameter ε a metric meaning, we must be careful and treat real Euclidean space and real projective space separately.

Each of the curves seen in Figure 4.2 is a dimension diagram. We used six different methods for estimating the dimension on a fixed sample of 600 points. For the horizontal axis on the left we took the distance (4.6) in $\mathbb{R}^{12}$. For the diagram on the right we took (4.7) in $\mathbb{P}^{11}_{\mathbb{R}}$.

Six Dimension Estimates

In this section, we introduce six dimension estimates. They are adapted from the existing literature. Figures 4.2, 4.6, 4.8 and 4.11 show dimension diagrams generated by our implementation. Judging from those figures, the estimators CorrSum, PHCurve, MLE and ANOVA all perform well on each of the examples. By contrast, NPCA and BoxCounting frequently overestimate the dimension. In general, we found it useful to allow for a "majority vote" for the dimension. That is, we choose as dimension estimate the number which is closest to most of the estimators for a significant (i.e. "persistent") range of ε-values in $[0, 1]$.

NPCA Dimension. The gold standard of dimension estimation is PCA. Assuming that V is a linear subspace of $\mathbb{R}^n$, we perform the following steps for the input Ω. First, we record the *mean* $\bar{u} := \frac{1}{m} \sum_{i=1}^{m} u^{(i)}$. Let M be the $m \times n$-matrix with rows $u^{(i)} - \bar{u}$. We compute $\sigma_1 \geq \cdots \geq \sigma_{\min\{m,n\}}$, the *singular values* of M. The *PCA dimension* is the number of σ_i above a certain threshold. For instance, this threshold could be the same as in the definition of the numerical

rank in (4.21) below. Following [137, 30], another idea is to set the threshold as σ_k, where $k = \text{argmax}_{1 \le i \le \min\{m,n\}-1} |\log_{10}(\sigma_{i+1}) - \log_{10}(\sigma_i)|$. In our experiments we found that this improved the dimension estimates. In some situations it is helpful to further divide each column of M by its standard deviation. This approach is explained in [137, 26].

Using PCA on a local scale is known as *Nonlinear Principal Component Analysis* (NPCA). Here we partition the sample Ω into l clusters $\Omega_1^{\varepsilon}, \ldots, \Omega_l^{\varepsilon} \subset \Omega$ depending on ε. For each Ω_i^{ε} we apply the usual PCA and obtain the estimate $\dim_{\text{pca}}(\Omega_i^{\varepsilon})$. The idea behind this is that the manifold $V \setminus \text{Sing}(V)$ is approximately linear locally. We take the average of these local dimensions, weighted by the size of each cluster. The result is the *nonlinear PCA dimension*

$$\dim_{\text{npca}}(\Omega, \varepsilon) := \frac{1}{\sum_{i=1}^{l} |\Omega_i^{\varepsilon}|} \sum_{i=1}^{l} |\Omega_i^{\varepsilon}| \cdot \dim_{\text{pca}}(\Omega_i^{\varepsilon}). \tag{4.8}$$

Data scientists have many clustering methods. For our study we use *single linkage clustering*. This works as follows. The clusters are the connected components in the graph with vertex set Ω whose edges are the pairs of points having distance at most ε. We do this either in Euclidean space with metric (4.6), or in projective space with metric (4.7). In the latter case, the points come from the cone over the true variety V. To make Ω less scattered, we sample a random linear function l and scale each data point $u^{(i)}$ such that $l(u^{(i)}) = 1$. Then we use those affine coordinates for NPCA. We chose this procedure because NPCA detects linear spaces and the proposed scaling maps projective linear spaces to affine-linear spaces.

We next introduce the notions of box counting dimension, persistent homology curve dimension and correlation dimension. All three of these belong to the class of *fractal-based methods*, since they rest on the idea of using the fractal dimension as a proxy for $\dim(V)$.

Box Counting Dimension. Here is the geometric idea in $\mathbb{R}^2$. Consider a square of side length 1 which we cover by miniature squares. We could cover it with 4 squares of side length $\frac{1}{2}$, or 9 squares of side length $\frac{1}{3}$, etc. What remains constant is the log ratio of the number of pieces over the magnification factor. For the square: $\frac{\log(4)}{\log(2)} = \frac{\log(9)}{\log(3)} = 2$. If Ω only intersects 3 out of 4 smaller squares, then we estimate the dimension to be between 1 and 2.

In $\mathbb{R}^n$ we choose as a box the parallelopiped with lower vertex $u^- = \min(u^{(1)}, \ldots, u^{(m)})$ and upper vertex $u^+ = \max(u^{(1)}, \ldots, u^{(m)})$, where "min" and "max" are coordinatewise minimum and maximum. Thus the box is $\{x \in \mathbb{R}^n : u^- \le x \le u^+\}$. For $j = 1, \ldots, n$, the interval $[u_j^-, u_j^+]$ is divided into $R(\varepsilon)$ equally sized intervals, whose length depends on ε. A d-dimensional object is expected to capture $R(\varepsilon)^d$ boxes. We determine the number ν of boxes that contain a point in Ω. Then the *box counting dimension estimate* is

$$\dim_{\text{box}}(\Omega, \varepsilon) := \frac{\log(\nu)}{\log(R(\varepsilon))}. \tag{4.9}$$

How to define the function $R(\varepsilon)$? Since the number of small boxes is very large, we cannot iterate through all boxes. It is desirable to decide from a data point $u \in \Omega$ in which box it lies. To this end, we set $R(\varepsilon) = \lfloor \frac{\lambda}{\varepsilon} \rfloor + 1$, where $\lambda := \max_{1 \le j \le n} |u_j^+ - u_j^-|$. Then, for $u \in \Omega$ and $k = 1, \ldots, n$ we

compute the largest q_k such that $\frac{q_k}{R(\varepsilon)}|u_k^+ - u_k^-| \leq |u_k - u_k^-|$. The n numbers $q_1, \ldots, q_n$ completely determine the box that contains the sample u.

For the box counting dimension in real projective space, we represent the points in Ω on an affine patch of $\mathbb{P}_{\mathbb{R}}^{n-1}$. On this patch we do the same construction as above, the only exception being that "equally sized intervals" is measured in terms of scaled Fubini-Study distance (4.7).

Persistent Homology Curve Dimension. The underlying idea was proposed by the Pattern Analysis Lab at Colorado State University [160]. First we partition Ω into l clusters $\Omega_1^\varepsilon, \ldots, \Omega_l^\varepsilon$ using single linkage clustering with ε. On each subsample Ω_i we construct a minimal spanning tree. Suppose that the cluster Ω_i has m_i points. Let $l_i(j)$ be the length of the j-th longest edge in a minimal spanning tree for Ω_i. For each Ω_i we compute

$$\dim_{\text{PHcurve}}(\Omega_i, \varepsilon) = \left| \frac{\log(m_i)}{\log(\frac{1}{m_i - 1} \sum_{j=1}^{m_i - 1} l_i(j))} \right|.$$

The *persistent homology curve dimension estimate* $\dim_{()}\text{PHCurve}(\Omega, \varepsilon)$ is the average of the local dimensions, weighted by the size of each cluster:

$$\dim_{\text{PHcurve}}(\Omega, \varepsilon) := \frac{1}{\sum_{i=1}^l |\Omega_i^\varepsilon|} \sum_{i=1}^m |\Omega_i| \dim_{\text{PHcurve}}(\Omega_i, \varepsilon).$$

In the clustering step we take the distance (4.6) if the variety is affine and (4.7) if it is projective.

Correlation Dimension. This is motivated as follows. Suppose that Ω is uniformly distributed in the unit ball. For pairs $u, v \in \Omega$, we have $\text{Prob}\{\text{dist}_{\mathbb{R}^n}(u, v) < \varepsilon\} = \varepsilon^d$, where $d = \dim(V)$. We set $C(\varepsilon) := (1/\binom{m}{2}) \cdot \sum_{1 \leq i < j \leq m} \mathbf{1}(\text{dist}_{\mathbb{R}^n}(u^{(i)}, u^{(j)}) < \varepsilon)$, where $\mathbf{1}$ is the indicator function. Since we expect the empirical distribution $C(\varepsilon)$ to be approximately ε^d, this suggests using $\frac{\log(C(\varepsilon))}{\log(\varepsilon)}$ as dimension estimate. In [137, Section 3.2.6] it is mentioned that a more practical estimate is obtained from $C(\varepsilon)$ by selecting some small $h > 0$ and putting

$$\dim_{\text{cor}}(\Omega, \varepsilon) := \left| \frac{\log C(\varepsilon) - \log C(\varepsilon + h)}{\log(\varepsilon) - \log(\varepsilon + h)} \right|. \tag{4.10}$$

In practice, we compute the dimension estimates for a finite subset of parameters $\varepsilon_1, \ldots, \varepsilon_k$ and put $h = \min_{i \neq j} |\varepsilon_i - \varepsilon_j|$. The ball in $\mathbb{P}_{\mathbb{R}}^{n-1}$ defined by the scaled Fubini-Study distance (4.7) is a spherical cap of radius ε. Its volume relative to a cap of radius 1 is $\int_0^\varepsilon (\sin \alpha)^{d-1} d\alpha / \int_0^1 (\sin \alpha)^{d-1} d\alpha$, which we approximate by $\left(\frac{\sin(\varepsilon)}{\sin(1)}\right)^d$. Hence, the *projective correlation dimension estimate* is

$$\dim_{\text{cor}}(\Omega, \varepsilon) := \left| \frac{\log C(\varepsilon) - \log C(\varepsilon + h)}{\log(\sin(\varepsilon)) - \log(\sin(\varepsilon + h))} \right|,$$

with the same h as above and where $C(\varepsilon)$ is now computed using the Fubini-Study distance.

We next describe two more methods. They differ from the aforementioned in that they derive from estimating the dimension of the variety V locally at a *distinguished point* $u^{(\star)}$.

MLE Dimension. Levina and Bickel [139] introduced a maximum likelihood estimator for the dimension of an unknown variety V. Their estimate is derived for samples in Euclidean space $\mathbb{R}^n$. Let k be the number of samples $u^{(j)}$ in Ω that are within distance ε to $u^{(\star)}$. We write $T_i(u^{(\star)})$ for the distance from $u^{(\star)}$ to its i-th nearest neighbor in Ω. Note that $T_k(u^{(\star)}) \leq \varepsilon < T_{k+1}(u^{(\star)})$. The *Levina-Bickel formula* around the point $u^{(\star)}$ is

$$\dim_{\text{MLE}}(\Omega, \varepsilon, u^{(\star)}) := \left(\frac{1}{k} \sum_{i=1}^{k} \log \frac{\varepsilon}{T_i(u^{(\star)})} \right)^{-1}. \tag{4.11}$$

This expression is derived from the hypothesis that $k = k(\varepsilon)$ obeys a Poisson process on the ε-neighborhood $\{u \in \Omega : \text{dist}_{\mathbb{R}^n}(u, u^{(\star)}) \leq \varepsilon\}$, in which u is uniformly distributed. The formula (4.11) is obtained by solving the likelihood equations for this Poisson process.

In projective space, we model $k(\varepsilon)$ as a Poisson process on $\{u \in \Omega : \text{dist}_{\mathbb{P}^{n-1}_{\mathbb{R}}}(u, u^{(\star)}) \leq \varepsilon\}$. However, instead of assuming that u is uniformly distributed in that neighborhood, we assume that the orthogonal projection of u onto the tangent space $\text{T}_{u^{(\star)}}\mathbb{P}^{n-1}_{\mathbb{R}}$ is uniformly distributed in the associated ball of radius $\sin \varepsilon$. Then, we derive the formula

$$\dim_{\text{MLE}}(\Omega, \varepsilon, u^{(\star)}) := \left(\frac{1}{k} \sum_{i=1}^{k} \log \frac{\sin(\varepsilon)}{\sin(\widehat{T_i}(u^{(\star)}))} \right)^{-1},$$

where $\widehat{T_i}(u^{(\star)})$ is the distance from $u^{(\star)}$ to its i-th nearest neighbor in Ω measured for (4.7).

It is not clear how to choose $u^{(\star)}$ from the given Ω. We chose the following method. Fix the sample neighborhood $\Omega_i^{\varepsilon} := \{u \in \Omega : \text{dist}_{\mathbb{R}^n}(u, u^{(i)}) \leq \varepsilon\}$. For each i we evaluate the formula (4.11) for Ω_i^{ε} with distinguished point $u^{(i)}$. With this, the *MLE dimension estimate* is

$$\dim_{\text{MLE}}(\Omega, \varepsilon) := \frac{1}{\sum_{i=1}^{m} |\Omega_i^{\varepsilon}|} \sum_{i=1}^{m} |\Omega_i^{\varepsilon}| \cdot \dim_{\text{MLE}}(\Omega_i^{\varepsilon}, \varepsilon, u^{(i)}).$$

ANOVA Dimension. Diaz, Quiroz and Velasco [81] derived an analysis of variance estimate for the dimension of V. In their approach, the following expressions are important:

$$\beta_{2s-1} = \frac{\pi^2}{4} - 2 \sum_{j=0}^{s} \frac{1}{(2j+1)^2} \quad \text{and} \quad \beta_{2s} = \frac{\pi^2}{12} - 2 \sum_{j=0}^{s} \frac{1}{(2j)^2} \qquad \text{for} \quad s \in \mathbb{N}. \tag{4.12}$$

The quantity β_d is the variance of the random variable Θ_d, defined as the angle between two uniformly chosen random points on the $(d-1)$-sphere. We again fix $\varepsilon > 0$, and we relabel so that $u^{(1)}, \ldots, u^{(k)}$ are the points in Ω with distance at most ε from $u^{(\star)}$. Let $\theta_{ij} \in [0, \pi]$ denote the angle between $u^{(i)} - u^{(\star)}$ and $u^{(j)} - u^{(\star)}$. Then, the *sample covariance* of the θ_{ij} is

$$S = \frac{1}{\binom{k}{2}} \sum_{1 \leq i < j \leq k} \left(\theta_{ij} - \frac{\pi}{2} \right)^2. \tag{4.13}$$

The analysis in [81] shows that, for small ε and Ω sampled from a d-dimensional manifold, the angles θ_{ij} are approximately Θ_d-distributed. Hence, S is expected to be close to $\beta_{\dim(V)}$. The *ANOVA dimension estimate* of Ω is the index d such that β_d is closest to S:

$$\dim_{\mathrm{ANOVA}}(\Omega, \varepsilon, u^{(\star)}) \; := \; \mathrm{argmin}_d |\beta_d - S|. \qquad (4.14)$$

As for the MLE estimate, we average (4.14) over all $u \in \Omega$ being the distinguished point.

To transfer the definition to projective space, we revisit the idea behind the ANOVA estimate. For u close to $u^{(\star)}$, the secant through u and $u^{(\star)}$ is approximately parallel to the tangent space of V at $u^{(\star)}$. Hence, the unit vector $(u^{(\star)} - u)/\|u^{(\star)} - u\|$ is close to being in the tangent space $\mathrm{T}_{u^{(\star)}}(V)$. The sphere in $\mathrm{T}_{u^{(\star)}}(V)$ has dimension $\dim V - 1$ and we know the variances of the random angles Θ_d. To mimic this construction in $\mathbb{P}_{\mathbb{R}}^{n-1}$ we use the angles between geodesics meeting at $u^{(\star)}$. In our implementation, we orthogonally project Ω to the tangent space $\mathrm{T}_{u^{(\star)}}\mathbb{P}_{\mathbb{R}}^{n-1}$ and compute (4.13) using coordinates on that space.

We have defined all the mathematical ingredients inherent in our dimension diagrams. Figure 4.2 now makes sense. Our software and its applications will be discussed in Section 4.1.

Persistent Homology

This section connects algebraic geometry and topological data analysis. It concerns the computation and analysis of the *persistent homology* (see Section 1.4) of our sample Ω. Persistent homology of Ω contains information about the shape of the unknown variety V from which Ω originates.

Barcodes

Let us briefly review the idea. Given Ω, we associate a simplicial complex with each value of a parameter $\varepsilon \in [0, 1]$. Just like in the case of the dimension diagrams in the previous section, ε determines the scale at which we consider Ω from local ($\varepsilon = 0$) to global ($\varepsilon = 1$). The complex at $\varepsilon = 0$ consists of only the vertices and at $\varepsilon = 1$ it is the full simplex on Ω.

Persistent homology identifies and keeps track of the changes in the homology of those complexes as ε varies. The output is a *barcode,* i.e. a collection of intervals. Each interval in the barcode corresponds to a topological feature which appears at the value of a parameter given by the left hand endpoint of the interval and disappears at the value given by the right hand endpoint. These barcodes play the same role as a histogram does in summarizing the shape of the data, with long intervals corresponding to strong topological signals and short ones to noise. By plotting the intervals, we obtain a barcode, such as the one in Figure 4.3.

The most straightforward way to associate a simplicial complex to Ω at ε is by covering Ω with open sets $U(\varepsilon) = \bigcup_{i=1}^{m} U_i(\varepsilon)$ and then building the associated *nerve complex*. This is the simplicial complex with vertex set $[m] = \{1, 2, \ldots, m\}$, where a subset σ of $[m]$ is a face if and only if $\bigcap_{i \in \sigma} U_i(\varepsilon) \neq \emptyset$. If all nonempty finite intersections of $U_i(\varepsilon)$ are contractible topological spaces, then the Nerve Lemma guarantees that the homology groups of $U(\varepsilon)$ agree with those of its nerve
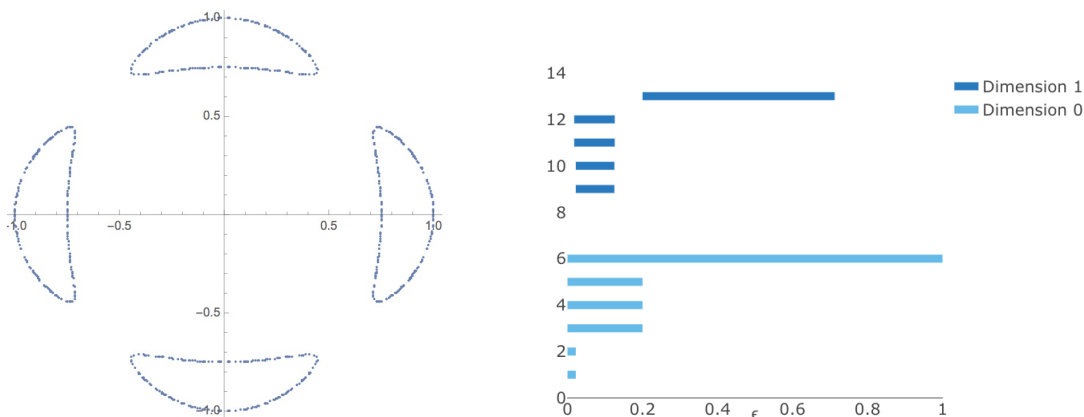
Figure 4.3: Persistent homology barcodes for the Trott curve.

complex. When $U_i(\varepsilon)$ are ε-balls around the data points, *i.e.*

$$U_i(\varepsilon) := \{v \in \mathbb{R}^n : \text{dist}_{\mathbb{R}^n}(u^{(i)}, v) < \varepsilon\} \text{ or } U_i(\varepsilon) := \{v \in \mathbb{P}^{n-1}_{\mathbb{R}} : \text{dist}_{\mathbb{P}^{n-1}_{\mathbb{R}}}(u^{(i)}, v) < \varepsilon\}, \quad (4.15)$$

the nerve complex is called the *Čech complex* at ε. Here $\text{dist}_{\mathbb{R}^n}$ and $\text{dist}_{\mathbb{P}^n_{\mathbb{R}}}$ are the distances from (4.6) and (4.7), respectively. Theorem 4.2.22 gives a precise statement for a sufficient condition under which the Čech complex of $U(\varepsilon)$ built on Ω yields the correct topology of V. However, in practice the hypotheses of the theorem will rarely be satisfied.

Čech complexes are computationally demanding as they require storing simplices in different dimensions. For this reason, applied topologists prefer to work with the *Vietoris-Rips complex*, which is the flag simplicial complex determined by the edges of the Čech complex. This means that a subset $\sigma \subset [m]$ is a face of the Vietoris-Rips complex if and only if $U_i(\varepsilon) \bigcap U_j(\varepsilon) \neq \emptyset$ for all $i, j \in \sigma$. With the definition in (4.15), the balls $U_i(\varepsilon)$ and $U_j(\varepsilon)$ intersect if and only if their centers $u^{(i)}$ and $u^{(j)}$ are less than 2ε apart.

Consider the sample from the Trott curve in Figure 4.3. Following Example 4.1.4, we sampled by selecting random x-coordinates between -1 and 1, and solving for y, or vice versa. The picture on the right shows the barcode. This was computed via the Vietoris-Rips complex. For dimensions 0 and 1 the six longest bars are displayed. The sixth bar in dimension 1 is so tiny that we cannot see it. In the range where ε lies between 0 and 0.2, we see four components. The barcode for dimension 1 identifies four persisting features for ε between 0.01 and 0.12. Each of these indicates an oval. Once these disappear, another loop appears. This corresponds to the fact that the four ovals are arranged to form a circle. So persistent homology picks up on both intrinsic and extrinsic topological features of the Trott curve.

The repertoire of algebraic geometry offers a fertile testing ground for practitioners of persistent homology. For many classes of algebraic varieties, both over $\mathbb{R}$ and $\mathbb{C}$, one has a priori information about their topology. For instance, the determinantal variety in Example 4.1.5 is the

3-manifold $\mathbb{P}^1_{\mathbb{R}} \times \mathbb{P}^2_{\mathbb{R}}$. Using Henselman's software `Eirene` for persistent homology [117], we computed barcodes for several samples Ω drawn from varieties with known topology.

Tangent Spaces and Ellipsoids

We underscore the benefits of an algebro-geometric perspective by proposing a variant of persistent homology that performed well in the examples we tested. Suppose that, in addition to knowing Ω as a finite metric space, we also have information on the tangent spaces of the unknown variety V at the points $u^{(i)}$. This will be the case after we have learned some polynomial equations for V. In such circumstances, we suggest replacing the ε-balls in (4.15) with *ellipsoids* that are aligned to the tangent spaces.

The motivation is that in a variety with a bottleneck (see Section 2.2), for example in the shape of a dog bone, the balls around points on the bottleneck may intersect for ε smaller than that which is necessary for the full cycle to appear. When V is a manifold, we design a covering of Ω that exploits the locally linear structure. Let $0 < \lambda < 1$. We take $U_i(\varepsilon)$ to be an ellipsoid around $u^{(i)}$ with principal axes of length ε in the tangent direction of V at $u^{(i)}$ and principal axes of length $\lambda \varepsilon$ in the normal direction. In this way, we allow ellipsoids to intersect with their neighbors and thus reveal the true homology of the variety before ellipsoids intersect with other ellipsoids across the medial axis. The parameter λ can be chosen by the user. We believe that λ should be proportional to the *reach* of V. This metric invariant is defined in the next subsection.

In practice, we perform the following procedure. Let $f = (f_1, \ldots, f_k)$ be a vector of polynomials that vanish on V, derived from the sample $\Omega \subset \mathbb{R}^n$ as described above. An estimator for the tangent space $\mathrm{T}_{u^{(i)}}V$ is the kernel of the Jacobian matrix of f at $u^{(i)}$. In symbols,

$$\widehat{\mathrm{T}}_{u^{(i)}}V := \ker Jf(u^{(i)}). \tag{4.16}$$

Let q_i denote the quadratic form on $\mathbb{R}^n$ that takes value 1 on $\widehat{\mathrm{T}}_{u^{(i)}}V \cap \mathbb{S}^{n-1}$ and value λ on the orthogonal complement of $\widehat{\mathrm{T}}_{u^{(i)}}V$ in the sphere $\mathbb{S}^{n-1}$. Then, the q_i specify the ellipsoids

$$E_i := \big\{ \sqrt{q_i(x)}\, x \in \mathbb{R}^n : \|x\| \leq 1 \big\}.$$

The role of the ε-ball enclosing the ith sample point is now played by $U_i(\varepsilon) := u^{(i)} + \varepsilon E_i$. These ellipsoids determine the covering $U(\varepsilon) = \bigcup_{i=1}^m U_i(\varepsilon)$ of the given point cloud Ω. From this covering we construct the associated Čech complex or Vietoris-Rips complex.

While using ellipsoids is appealing, it has practical drawbacks. Relating the smallest ε for which $U_i(\varepsilon)$ and $U_j(\varepsilon)$ intersect to $\mathrm{dist}_{\mathbb{R}^n}(u^{(i)}, u^{(j)})$ is not easy. For this reason we implemented the following variant of ellipsoid-driven barcodes. We use the simplicial complex on $[m]$ where

$$\sigma \text{ is a face iff } \frac{\mathrm{dist}_{\mathbb{R}^n}(u^{(i)}, u^{(j)})}{\frac{1}{2}\big(\sqrt{q_i(h)} + \sqrt{q_j(h)}\big)} < 2\varepsilon \text{ for all } i, j \in \sigma, \text{ where } h = \frac{u^{(i)} - u^{(j)}}{\|u^{(i)} - u^{(j)}\|}. \tag{4.17}$$

In (4.17) we weight the distance between $u^{(i)}$ and $u^{(j)}$ by the arithmetic mean of the radii of the two ellipsoids E_i and E_j in the direction $u^{(i)} - u^{(j)}$. If all quadratic forms q_i were equal to $\sum_{j=1}^n x_j^2$, then the simplicial complex of (4.17) equals the Vietoris-Rips complex from (4.15).
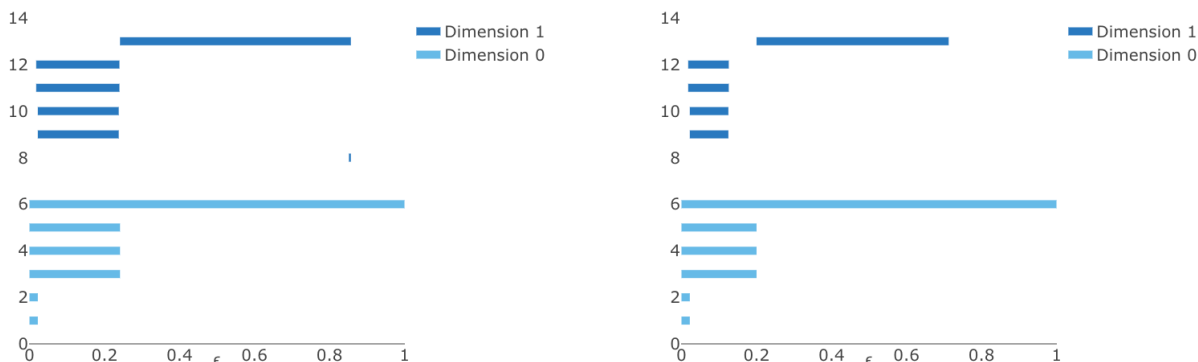
Figure 4.4: The left picture shows the barcode constructed from the ellipsoid-driven simplicial complex (4.17) with $\lambda = 0.01$, for the sample from the Trott curve used in Figure 4.3. For comparison we display the barcode from Figure 4.3 in the right picture. All relevant topological features persist longer in the left plot.

Figure 4.4 compares the barcodes for the classical Vietoris-Rips complex with those obtained from ellipsoids. It seems promising to further develop variants of persistent homology that take some of the defining polynomial equations for (Ω, V) into consideration.

Reaching the Reach

The Čech complex of a covering $U = \bigcup_{i=1}^{m} U_i$ has the homology of the union of balls U. But, can we give conditions on the sample $\Omega \subset V$ under which a covering reveals the true homology of V? A result due to Niyogi, Smale and Weinberger (Theorem 4.2.22 below) offers an answer in some circumstances. These involve the concept of the *reach*, which is an important metric invariant of a variety V. We here focus on varieties V in the Euclidean space $\mathbb{R}^n$.

Definition 4.1.21. The *medial axis* of V is the set M_V of all points $u \in \mathbb{R}^n$ such that the minimum distance from V to u is attained by two distinct points. The *reach* $\tau(V)$ is the infimum of all distances from points on the variety V to any point in its medial axis M_V. In formulas: $\tau(V) := \inf_{u \in V, w \in M_V} \|u - w\|$. If $M_V = \emptyset$, we define $\tau(V) = +\infty$.

Note that $\tau(V) = +\infty$, if and only if V is an affine-linear subspace. Otherwise, the reach is a non-negative real number. In particular, there exist varieties V with $\tau(V) = 0$. For instance, consider the union of two lines $V = \{(x, y) \in \mathbb{R}^2 : xy = 0\}$. All points in the diagonal $D = \{(x, y) \in \mathbb{R}^2 : x = y, x \neq 0\}$ have two closest points on V. Hence, D is a subset of the medial axis M_V, and we conclude that $0 \leq \tau(V) \leq \inf_{u \in V, w \in D} \|u - w\| = 0$. In general, any singular variety with an "edge" has zero reach.

To illustrate the concept of the reach, let V be a smooth curve in the plane, and draw the normal line at each point of V. The collection of these lines is the *normal bundle*. At a short distance from

the curve, the normal bundle is a product: each point u near V has a unique closest point u^* on V, and u lies on the normal line through u^*. At a certain distance, however, some of the normal lines cross. If u is a crossing point of minimal distance to V, then u has no unique closest point u^* on V. Instead, there are at least two points on V that are closest to u and the distance from u to each of them is the reach $\tau(V)$. Aamari *et al.* [1] picture this by writing that "*one can roll freely a ball of radius $\tau(V)$ around V*".

Niyogi, Smale and Weinberger refer to $\tau(V)^{-1}$ as the "condition number of V". Bürgisser *et al.* [47] relate $\tau(V)^{-1}$ to the condition number of a semialgebraic set. For the purposes of our survey it suffices to understand how the reach effects the quality of the covering $U(\varepsilon)$. The following result is a simplified version of [155, Theorem 3.1], suitable for low dimensions. Note that Theorem 4.2.22 only covers those varieties $V \subset \mathbb{R}^n$ that are smooth and compact.

Theorem 4.1.22 (Niyogi, Smale, Weinberger 2006). *Let $V \subset \mathbb{R}^n$ be a compact manifold of dimension $d \leq 17$, with reach $\tau = \tau(V)$ and d-dimensional Euclidean volume $v = \text{vol}(V)$. Let $\Omega = \{u^{(1)}, \ldots, u^{(m)}\}$ be i.i.d. samples drawn from the uniform probability measure on V. Fix $\varepsilon = \frac{\tau}{4}$ and $\beta = 16^d \tau^{-d} v$. For any desired $\delta > 0$, fix the sample size at*

$$m > \beta \cdot \left(\log(\beta) + d + \log(\frac{1}{\delta}) \right). \tag{4.18}$$

With probability $\geq 1 - \delta$, the homology groups of the following set coincide with those of V:

$$U(\varepsilon) = \bigcup_{i=1}^{m} \{ x \in \mathbb{R}^n : \|x - u^{(i)}\| < \varepsilon \}.$$

A few remarks are in order. First of all, the theorem is stated using the Euclidean distance and not the scaled Euclidean distance (4.6). However, scaling the distance by a factor t means scaling the volume by t^d, so the definition of β in the theorem is invariant under scaling. Moreover, the theorem has been rephrased in a manner that makes it easier to evaluate the right hand side of (4.18) in cases of interest. The assumption $d \leq 17$ is not important: it ensures that the volume of the unit ball in $\mathbb{R}^d$ can be bounded below by 1. Furthermore, in [155, Theorem 3.1], the tolerance ε can be any real number between 0 and $\tau/2$, but then β depends in a complicated manner on ε. For simplicity, we took $\varepsilon = \tau/4$.

Theorem 4.1.22 gives the asymptotics of a sample size m that suffices to reveal all topological features of V. For concrete parameter values it is less useful, though. For example, suppose that V has dimension 4, reach $\tau = 1$, and volume $v = 1000$. If we desire a 90% guarantee that $U(\varepsilon)$ has the same homology as V, so $\delta = 1/10$, then m must exceed $1,592,570,365$. In addition to that, the theorem assumes that the sample was drawn from the uniform distribution on V. But in practice one will rarely meet data that obeys such a distribution. In fact, drawing from the uniform distribution on a curved object is a non-trivial affair [80].

In spite of its theoretical nature, the Niyogi-Smale-Weinberger formula is useful in that it highlights the importance of the reach $\tau(V)$ for analyzing point samples. Indeed, the dominant quantity in (4.18) is β, and this grows to the power of d in $\tau(V)^{-1}$. It is therefore of interest to better understand $\tau(V)$ and to develop tools for estimating it.

We found the following formula by Federer [97, Theorem 4.18] to be useful. It expresses the reach of a manifold V in terms of points and their tangent spaces:

$$\tau(V) \;=\; \inf_{v \neq u \in V} \frac{||u-v||^2}{2\delta}, \quad \text{where} \;\; \delta = \min_{x \in T_v V} ||(u-v)-x||. \tag{4.19}$$

This formula relies upon knowing the tangent spaces at each point of $u \in V$.

Suppose we are given the finite sample Ω from V. If some equations for V are also known, then we can use the estimator $\widehat{T}_{u^{(i)}} V$ for the tangent space that was derived in (4.16). From this we get the following formula for the *empirical reach* of our sample:

$$\hat{\tau}(V) \;=\; \min_{\substack{u,v \in \Omega \\ u \neq v}} \frac{||u-v||^2}{2\widehat{\delta}}, \quad \text{where} \;\; \widehat{\delta} = \min_{x \in \widehat{T}_v V} ||(u-v)-x||.$$

A similar approach for estimating the reach was proposed by Aamari *et al.* [1, eqn. (6.1)].

Algebraicity of Persistent Homology

It is impossible to compute in the field of real numbers $\mathbb{R}$. Numerical computations employ floating point approximations. These are actually rational numbers. Computing in algebraic geometry has traditionally been centered around exact symbolic methods. In that context, computing with algebraic numbers makes sense as well. In this subsection we argue that, in the setting of this work, most numerical quantities in persistent homology, like the barcodes and the reach, have an algebraic nature. Here we assume that the variety V is defined over $\mathbb{Q}$.

We discuss the content of Section 4.2 of this dissertation which concerns metric properties of a given variety $V \subset \mathbb{R}^n$ that are relevant for its *true persistent homology*. Here, the true persistent homology of V, at parameter value ε, refers to the homology of the ε-neighborhood of V. Intuitively, the true persistent homology of the Trott curve is the limit of barcodes as in Figure 4.3, where more and more points are taken, eventually filling up the entire curve.

An important player is the *offset hypersurface* $\mathscr{O}_\varepsilon(V)$. This is the algebraic boundary of the ε-neighborhood of V. More precisely, for any positive value of ε, the offset hypersurface is the Zariski closure of the set of all points in $\mathbb{R}^n$ whose distance to V equals ε. If $n = 2$ and V is a plane curve, then the *offset curve* $\mathscr{O}_\varepsilon(V)$ is drawn by tracing circles along V.

Example 4.1.23. In Figure 4.5 we examine a conic V, shown in black. The light blue curve is its *evolute*. This is an *astroid* of degree 6. The evolute serves as the *ED discriminant* of V, in the context seen in [86, Figure 3]. The blue curves in Figure 4.5 are the offset curves $\mathscr{O}_\varepsilon(V)$. These have degree 8 and are smooth (over $\mathbb{R}$) for small values of ε. However, for larger values of ε, the offset curves are singular. The transition point occurs at the cusp of the evolute.

It is shown in Theorem 4.2.19 that the endpoints of bars in the true persistent homology of a variety V occur at numbers that are algebraic over $\mathbb{Q}$. The proof relies on results in real algebraic geometry that characterize the family of fibers in a map of semialgebraic sets.
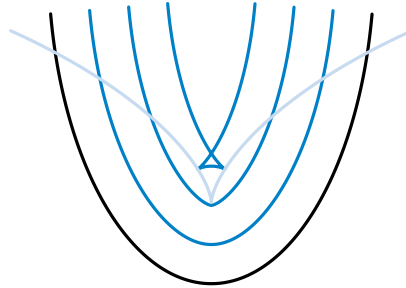
Figure 4.5: Offset curves (blue) and the evolute (light blue) of a conic (black).

Example 4.1.24. The bars of the barcode in Figure 4.3 begin and end near the numbers

$$\frac{1}{8} = 0.125, \quad \frac{\sqrt{24025 - 217\sqrt{9889}}}{248} = 0.19941426..., \quad \frac{3}{4} = 0.75.$$

These algebraic numbers delineate the true persistent homology of the Trott curve V.

The reach $\tau(V)$ of any real variety $V \subset \mathbb{R}^n$ is also an algebraic number. This follows from Federer's formula (4.19) which expresses $\tau(V)$ as the optimal value of a polynomial optimization problem. In principle, the reach can be computed in exact arithmetic from the polynomials that define V. It remains an open problem how to do this effectively in practice.

Finding Equations

Every polynomial in the ideal I_V of the unknown variety V vanishes on the sample Ω. The converse is not true, but it is reasonable to surmise that it holds among polynomials of low degree. The ideal I_Ω of the finite set $\Omega \subset \mathbb{R}^n$ can be computed using linear algebra. All our polynomials and ideals in this section lie in the ring $R = \mathbb{R}[x_1, x_2, \ldots, x_n]$.

Vandermonde Matrices

Let $\mathcal{M}$ be a finite linearly independent subset of R. We write $R_{\mathcal{M}}$ for the $\mathbb{R}$-vector space with basis $\mathcal{M}$ and generally assume that $\mathcal{M}$ is ordered, so that polynomials in $R_{\mathcal{M}}$ can be identified with vectors in $\mathbb{R}^{|\mathcal{M}|}$. Two primary examples for $\mathcal{M}$ are the set of monomials $\mathbf{x}^e = x_1^{e_1} x_2^{e_2} \cdots x_n^{e_n}$ of degree d and the set of monomials of degree at most d. We use the notation R_d and $R_{\leq d}$ for the corresponding subspaces of R. Their dimensions $|\mathcal{M}|$ are

$$\dim(R_d) = \binom{n+d-1}{d} \quad \text{and} \quad \dim(R_{\leq d}) = \binom{n+d}{d}.$$

We write $U_{\mathcal{M}}(\Omega)$ for the $m \times |\mathcal{M}|$ matrix whose i-th row consists of the evaluations of the polynomials in $\mathcal{M}$ at the point $u^{(i)}$. Instead of $U_{\mathcal{M}}(\Omega)$ we write $U_d(\Omega)$ when $\mathcal{M}$ contains all monomials of degree d and $U_{\leq d}(\Omega)$ when $\mathcal{M}$ contains monomials of degree $\leq d$.

For example, if $n = 1$, $m = 3$, and $\Omega = \{u, v, w\}$ then $U_{\leq 3}(\Omega)$ is the Vandermonde matrix

$$U_{\leq 3}(\Omega) = \begin{pmatrix} u^3 & u^2 & u & 1 \\ v^3 & v^2 & v & 1 \\ w^3 & w^2 & w & 1 \end{pmatrix}. \tag{4.20}$$

For $n \geq 2$, we call $U_{\mathscr{M}}(\Omega)$ a *multivariate Vandermonde matrix*. It has the following property:

Remark 4.1.25. The kernel of the multivariate Vandermonde matrix $U_{\mathscr{M}}(\Omega)$ equals the vector space $I_\Omega \cap R_{\mathscr{M}}$ of all polynomials that are linear combinations of $\mathscr{M}$ and that vanish on Ω.

The strategy for learning the variety V is as follows. We hope to learn the ideal I_V by making an educated guess for the set $\mathscr{M}$. The two desirable properties for $\mathscr{M}$ are:

(a) The ideal I_V of the unknown variety V is generated by its subspace $I_V \cap R_{\mathscr{M}}$.

(b) The inclusion of $I_V \cap R_{\mathscr{M}}$ in its superspace $I_\Omega \cap R_{\mathscr{M}} = \ker(U_{\mathscr{M}}(\Omega))$ is an equality.

There is a fundamental tension between these two desiderata: if $\mathscr{M}$ is too small then (a) will fail, and if $\mathscr{M}$ is too large then (b) will fail. But, of course, suitable sets $\mathscr{M}$ do always exist, since Hilbert's Basis Theorem ensures that all ideals in R are finitely generated.

The requirement (b) imposes a lower bound on the size m of the sample. Indeed, m is an upper bound on the rank of $U_{\mathscr{M}}(\Omega)$, since that matrix has m rows. The rank of any matrix is equal to the number of columns minus the dimension of the kernel. This implies:

Lemma 4.1.1. *If (b) holds, then* $m \geq |\mathscr{M}| - \dim(I_V \cap R_{\mathscr{M}})$.

In practice, however, the sample Ω is given and fixed. Thus, we know m and it cannot be increased. The question is how to choose the set $\mathscr{M}$. This leads to some interesting geometric combinatorics. For instance, if we believe that V is homogeneous with respect to some $\mathbb{Z}^r$-grading, then it makes sense to choose a set $\mathscr{M}$ that consists of all monomials in a given $\mathbb{Z}^r$-degree. Moreover, if we assume that V has a parametrization by sparse polynomials then we would use a specialized combinatorial analysis to predict a set $\mathscr{M}$ that works. A suitable choice of $\mathscr{M}$ can improve the numerical accuracy of the computations dramatically.

In addition to choosing the set of monomials $\mathscr{M}$, we face another problem: how to represent $I_\Omega \cap R_{\mathscr{M}}$? Computing a basis for the kernel of $U_{\mathscr{M}}(\Omega)$ yields a set of generators for $I_\Omega \cap R_{\mathscr{M}}$. But which basis to use and how to compute it? For instance, the right-singular vectors of $U_{\mathscr{M}}(\Omega)$ with singular value zero yield an *orthonormal basis* of $I_\Omega \cap R_{\mathscr{M}}$. But in applications one often meets ideals I that have sparse generators.

Example 4.1.26. Suppose that we obtain a list of 20 quadrics in nine variables as the result of computing the kernel of a Vandermonde matrix and each quadric looks something like this:

$$-0.037x_1^2 - 0.043x_1x_2 - 0.011x_1x_3 + 0.041x_1x_4 - 0.192x_1x_5 + 0.034x_1x_6 + 0.031x_1x_7 + 0.027x_1x_8 + 0.271x_1x_9 + 0.089x_2^2 - 0.009x_2x_3$$

$$+0.192x_2x_4 + 0.041x_2x_5 + 0.044x_2x_6 - 0.027x_2x_7 + 0.031x_2x_8 - 0.048x_2x_9 - 0.056x_3^2 - 0.034x_3x_4 - 0.044x_3x_5 + 0.041x_3x_6$$

$$-0.271x_3x_7 + 0.048x_3x_8 + 0.031x_3x_9 - 0.183x_4^2 - 0.043x_4x_5 - 0.011x_4x_6 + 0.039x_4x_7 + 0.004x_4x_8 + 0.019x_4x_9 - 0.057x_5^2$$

$$-0.009x_5x_6 - 0.004x_5x_7 + 0.039x_5x_8 - 0.35x_5x_9 - 0.202x_6^2 - 0.019x_6x_7 + 0.35x_6x_8 + 0.039x_6x_9 - 0.188x_7^2 - 0.043x_7x_8 - 0.011x_7x_9$$

$$-0.062x_8^2 - 0.009x_8x_9 - 0.207x_9^2 + 0.35x_1 + 0.019x_2 - 0.004x_3 - 0.048x_4 - 0.271x_5 + 0.027x_6 - 0.044x_7 + 0.034x_8 + 0.192x_9 + 0.302$$

This is the first element in an orthonormal basis for $I_\Omega \cap R_{\leq 2}$, where Ω is a sample drawn from a certain variety V in $\mathbb{R}^9$. From such a basis, it is very hard to guess what V might be.

It turns out that V is SO(3), the group of rotations in 3-space. After renaming the nine variables, we find the 20-dimensional space of quadrics mentioned in Example 4.1.2. However, the quadrics seen in (4.2) are much nicer. They are sparse and easy to interpret.

For this reason we aim to compute *sparse* bases of multivariate Vandermonde matrices. There is a trade-off between obtaining sparse basis vectors and stability of the computations. We shall discuss this issue in the next subsection. See Table 4.1 for a brief summary.

Numerical Linear Algebra

Computing kernels of matrices of type $U_{\mathcal{M}}(\Omega)$ is a problem in numerical linear algebra. One scenario where the methodology has been developed and proven to work well is the Generalized Principal Component Analysis of Ma *et al.* [142], where V is a finite union of linear subspaces in $\mathbb{R}^n$. For classical Vandermonde matrices, the Bjoerck-Pereyra algorithm [25] accurately computes a LU-decomposition of the Vandermonde matrix; see [118, Section 22]. This decomposition may then be used to compute the kernel. A generalization of this for multivariate Vandermonde matrices of the form $U_{\leq d}(\Omega)$ is given in [156, Theorem 4.4]. To date such a decomposition for $U_{\mathcal{M}}(\Omega)$ is missing for other subsets of monomials $\mathcal{M}$. Furthermore, [156, Theorem 4.4] assumes that the multivariate Vandermonde matrix is square and invertible, but this is never the case in our situation.

In the literature on numerical algebraic geometry, it is standard to represent varieties by point samples, and there are several approaches for learning varieties, and even schemes, from such numerical data. See e.g. [67, 108] and the references therein. From the perspective of commutative algebra, our interpolation problem was studied in e.g. [152, 153].

We developed and implemented three methods based on classical numerical linear algebra:

1. via the R from a QR-decomposition,
2. via a singular value decomposition (SVD), or
3. via the reduced row echelon form (RREF) of $U_{\mathcal{M}}(\Omega)$.

The goal is to compute a (preferably sparse) basis for the kernel of $U_{\mathcal{M}}(\Omega)$, with $N = |\mathcal{M}|$. All three methods are implemented in our software. Their descriptions are given below.

QR	slightly less accurate and fast than SVD, yields some sparse basis vectors.
SVD	accurate, fast, but returns orthonormal and hence dense basis.
RREF	no accuracy guarantees, not as fast as the others, gives a sparse basis.

Table 4.1: The three methods for computing the kernel of the Vandermonde matrix $U_{\mathcal{M}}(\Omega)$.

Algorithm 1 with_qr

Input: A multivariate Vandermonde matrix $U \in \mathbb{R}^{m \times N}$ and a tolerance value $\tau \geq 0$.

Output: A basis for the kernel of U.

    Compute the QR-decomposition $U = QR$, where Q is orthogonal and R is upper triangular;

    Put $I = \{i : 1 \leq i \leq N, |R_{ii}| < \tau\}$, $J = [N] \backslash I$, $R' = R^{[m] \times J}$ and $\mathscr{B} = \emptyset$;

    for $i \in I$ **do**

        Initialize $a \in \mathbb{R}^N$, $a = (a_1, \ldots, a_N)$ and put $a_i = 1$;

        Solve $R'y = R_i$ for y, where R_i is the i-th column of R;

        Put $(a_1, \ldots, a_{i-1}, a_{i+1}, \ldots, a_N) = y$;

        Update $\mathscr{B} \leftarrow \mathscr{B} \cup \{a\}$;

    end for

    Return $\mathscr{B}$.

Algorithm 2 with_svd

Input: A multivariate Vandermonde matrix $U \in \mathbb{R}^{m \times N}$ and a tolerance value $\tau \geq 0$.

Output: A basis for the kernel of U.

    Compute the singular value decomposition $U = X\Sigma Y$, where $\Sigma = \mathrm{diag}(\sigma_1, \ldots, \sigma_N)$;

    Let $k := \#\{1 \leq i \leq N : \sigma_i < \tau\}$;

    Return the last k columns of Y.

Algorithm 3 with_rref

Input: A multivariate Vandermonde matrix $U \in \mathbb{R}^{m \times N}$ and a tolerance value $\tau \geq 0$.

Output: A basis for the kernel of U.

    Compute the reduced row-echelon form A of U;

    Put $I = \{i : 1 \leq i \leq m, \|A_i\| > \sqrt{N}\tau\}$, where A_i is the i-th row of A;

    Put $B := A^{I \times [N]}$, $k := \#I$ and initialize $\mathscr{B} = \emptyset$;

    For $1 \leq i \leq k$ let j_i be the position of the first entry in the i-th row of B that has absolute value larger than τ and put $J := [N] \backslash \{j_1, \ldots, j_k\}$;

    for $j \in J$ **do**

        Put $J' := \{1 \leq i \leq N : i < j\}$;

        Initialize $a \in \mathbb{R}^N$, $a = (a_1, \ldots, a_N)$ and put $a_j = 1$ and $a_i = 0$ for $i \neq j$;

        for $i \in J'$ **do**

            $a_i = -B_{i,j}$;

            Update $\mathscr{B} \leftarrow \mathscr{B} \cup \{a\}$;

        end for

    end for

    Return $\mathscr{B}$.

Each of these three methods has its upsides and downsides. These are summarized in Table 4.1. The algorithms require a tolerance $\tau \geq 0$ as input. This tolerance value determines the *numerical rank* of the matrix. Let $\sigma_1 \geq \cdots \geq \sigma_{\min\{m,N\}}$ be the ordered singular values of the $m \times N$ matrix U. As above, the numerical rank of U is

$$r(U,\tau) := \#\{\, i \mid \sigma_i \geq \tau \,\}. \tag{4.21}$$

Using the criterion in [72, Section 3.5.1], we can set $\tau = \varepsilon\, \sigma_1 \max\{m,N\}$, where ε is the machine precision. The rationale behind this choice is [72, Corollary 5.1], which says that the round-off error in the σ_i is bounded by $\|E\|$, where $\|\cdot\|$ is the spectral norm and $U + E$ is the matrix whose singular values were computed. For backward stable algorithms we may use the bound $\|E\| = \mathcal{O}(\varepsilon)\sigma_1$. On the other hand, our experiments suggest that an appropriate value for τ is given by $\frac{1}{2}(\sigma_i + \sigma_{i+1})$, for which the jump from $\log_{10}(\sigma_i)$ to $\log_{10}(\sigma_{i+1})$ is significantly large. This choice is particularly useful for noisy data. In case of noise the first definition of τ will likely fail to detect the true rank of $U_{\leq d}(\Omega)$. The reason for this lies in the numerics of Vandermonde matrices, discussed below.

We apply all of the aforementioned to the multivariate Vandermonde matrix $U_{\mathscr{M}}(\Omega)$, for any finite set $\mathscr{M}$ in R that is linearly independent. We thus arrive at the following algorithm.

Algorithm 4 FindEquations

Input: A sample of points $\Omega = \{u^{(1)}, u^{(2)}, \ldots, u^{(m)}\} \subset \mathbb{R}^n$, a finite set $\mathscr{M}$ of monomials in n variables, and a tolerance value $\tau > 0$.
Output: A basis $\mathscr{B}$ for the kernel of $U_{\mathscr{M}}(\Omega)$;
Construct the multivariate Vandermonde matrix $U_{\mathscr{M}}(\Omega)$;
Compute a basis $\mathscr{B}$ for the kernel of $U_{\mathscr{M}}(\Omega)$ using Algorithm 1, 2 or 3;
Return $\mathscr{B}$.

Remark 4.1.27. Different sets of quadrics can be obtained by applying Algorithm 4 to a set Ω of 200 points sampled uniformly from the group $SO(3)$. The dense equations in Example 4.1.26 are obtained using Algorithm 2 (SVD) in Step 4. The more desirable sparse equations from (4.2) are found when using Algorithm 1 (with QR). In both cases the tolerance was set to be $\tau \approx 4 \cdot 10^{-14}\, \sigma_1$, where σ_1 is the largest singular value of the Vandermonde matrix $U_{\leq 2}(\Omega)$.

Running Algorithm 4 for a few good choices of $\mathscr{M}$ often leads to an initial list of non-zero polynomials that lie in I_Ω and also in I_V. Those polynomials can then be used to infer an upper bound on the dimension and other information about V. Of course, if we are lucky, we obtain a generating set for I_V after a few iterations.

If m is not too large and the coordinates of the points $u^{(i)}$ are rational, then it can be preferable to compute the kernel of $U_{\mathscr{M}}(\Omega)$ symbolically. Gröbner-based interpolation methods, such as the *Buchberger-Möller algorithm* [152], have the flexibility to select $\mathscr{M}$ dynamically. With this, they directly compute the generators for the ideal I_Ω, rather than the user having to worry about the

matrices $U_{\leq d}(\Omega)$ for a sequence of degrees d. In short, users should keep symbolic methods in the back of their minds when contemplating Algorithm 4.

In the remainder of this section, we discuss numerical issues associated with Algorithm 4. The key step is computing the kernel of the multivariate Vandermonde matrix $U_{\mathscr{M}}(\Omega)$. As illustrated in (4.20) for samples Ω on the line ($n = 1$), and $\mathscr{M}$ being all monomials up to a fixed degree, this matrix is a *Vandermonde matrix*. It is conventional wisdom that Vandermonde matrices are severely ill-conditioned [158]. Consequently, numerical linear algebra solvers are expected to perform poorly when attempting to compute the kernel of $U_d(\Omega)$.

One way to circumvent this problem is to use a set of *orthogonal polynomials* for $\mathscr{M}$. Then, for large sample sizes m, two distinct columns of $U_{\mathscr{M}}(\Omega)$ are approximately orthogonal, implying that $U_{\mathscr{M}}(\Omega)$ is well-conditioned. This is because the inner product between the columns associated to $f_1, f_2 \in \mathscr{M}$ is approximately the integral of $f_1 \cdot f_2$ over $\mathbb{R}^n$. However, a sparse representation in orthogonal polynomials does not yield a sparse representation in the monomial basis. Hence, to get sparse polynomials in the monomials basis from $U_{\mathscr{M}}(\Omega)$, we must employ other methods than the ones presented here. For instance, techniques from compressed sensing may help to compute sparse representations in the monomial basis.

We are optimistic that a numerically-reliable algorithm for computing the kernel of matrices $U_{\leq d}(\Omega)$ exists. The Bjoerck-Pereyra algorithm [25] solves linear equations $Ua = b$ for an $n \times n$ Vandermonde matrix U. There is a theoretical guarantee that the computed solution $\hat{a}$ satisfies $|a - \hat{a}| \leq 7n^5 \varepsilon + \mathcal{O}(n^4 \varepsilon^2)$; see [118, Corollary 22.5]. Hence, $\hat{a}$ is highly accurate – despite U being ill-conditioned. This is confirmed by the experiment mentioned in the beginning of [118, Section 22.3], where a linear system with $\kappa(U) \sim 10^9$ is solved with a relative error of 5ε. We suspect that a Bjoerck-Pereyra-like algorithm together with a thorough structured-perturbation analysis for multivariate Vandermonde matrices would equip us with an accurate algorithm for finding equations. Here, we stick with the three methods above, while bearing in mind the difficulties that ill-posedness can cause.

Learning from Equations

At this point we assume that the methods in the previous two sections have been applied. This means that we have an estimate d of what the dimension of V might be, and we know a set $\mathscr{P}$ of polynomials that vanish on the finite sample $\Omega \subset \mathbb{R}^n$. We assume that the sample size m is large enough so that the polynomials in $\mathscr{P}$ do in fact vanish on V. We now use $\mathscr{P}$ as our input.

Computational Algebraic Geometry

A finite set of polynomials $\mathscr{P}$ in $\mathbb{Q}[x_1, \ldots, x_n]$ is the typical input for algebraic geometry software. Traditionally, symbolic packages like `Macaulay2`, `Singular` and `CoCoA` were used to study $\mathscr{P}$. Buchberger's Gröbner basis algorithm is the workhorse underlying this approach. More recently, numerical algebraic geometry has emerged, offering lots of promise for innovative and accurate methods in data analysis. We refer to the textbook [20], which centers around the excellent software `Bertini`. Next to using `Bertini`, we also employ the `Julia` package

`HomotopyContinuation.jl` [44]. Both symbolic and numerical methods are valuable for data analysis. The questions we ask in this subsection can be answered with either.

In what follows we assume that the unknown variety V is equal to the zero set of the input polynomials $\mathscr{P}$. We seek to answer the following questions over the complex numbers:

1. What is the dimension of V?
2. What is the degree of V?
3. Find the irreducible components of V and determine their dimensions and degrees.

Here is an example that illustrates the workflow we imagine for analyzing samples Ω.

Example 4.1.28. The variety of Hankel matrices of size 4×4 and rank 2 has the parametrization

$$
\begin{bmatrix} a & b & c & x \\ b & c & x & d \\ c & x & d & e \\ x & d & e & f \end{bmatrix}
=
\begin{bmatrix} s_1^3 & s_2^3 \\ s_1^2 t_1 & s_2^2 t_2 \\ s_1 t_1^2 & s_2 t_2^2 \\ t_1^3 & t_2^3 \end{bmatrix}
\begin{bmatrix} s_1^3 & s_1^2 t_1 & s_1 t_1^2 & t_1^3 \\ s_2^3 & s_2^2 t_2 & s_2 t_2^2 & t_2^3 \end{bmatrix}.
$$

Suppose that an adversary constructs a dataset Ω of size $m = 500$ by the following process. He picks random integers s_i and t_j, computes the 4×4-Hankel matrix, and then deletes the antidiagonal coordinate x. For the remaining six coordinates he fixes some random ordering, such as (c, f, b, e, a, d). Using this ordering, he lists the 500 points. This is our input $\Omega \subset \mathbb{R}^6$.

We now run Algorithm 4 for the $m \times 210$-matrix $U_{\leq 4}(\Omega)$. The output of this computation is the following pair of quartics which vanishes on the variety $V \subset \mathbb{R}^6$ that is described above:

$$
\begin{aligned}
\mathscr{P} = \{ & acf^2 + ad^2f - 2ade^2 - b^2f^2 + 2bd^2e - c^2df + c^2e^2 - cd^3, \\
& a^2df - a^2e^2 + ac^2f - acd^2 - 2b^2cf + b^2d^2 + 2bc^2e - c^3d \}.
\end{aligned}
\tag{4.22}
$$

Not knowing the true variety, we optimistically believe that the zero set of $\mathscr{P}$ is equal to V. This would mean that V is a complete intersection, so it has codimension 2 and degree 16.

At this point, we may decide to compute a primary decomposition of $\langle \mathscr{P} \rangle$. We then find that there are two components of codimension 2, one of degree 3 and the other of degree 10. Since $3 + 10 \neq 16$, we learn that $\langle \mathscr{P} \rangle$ is not a radical ideal. In fact, the degree 3 component appears with multiplicity 2. Being intrigued, we now return to computing equations from Ω.

From the kernel of the $m \times 252$-matrix $U_5(\Omega)$, we find two new quintics in I_Ω. These only reduce the degree to $3 + 10 = 13$. Finally, the kernel of the $m \times 452$-matrix $U_6(\Omega)$ suffices. The ideal I_V is generated by 2 quartics, 2 quintics and 4 sextics. The mystery variety $V \subset \mathbb{R}^6$ has the same dimension and degree as the rank 2 Hankel variety in $\mathbb{R}^7$ whose projection it is.

Our three questions boil down to solving a system $\mathscr{P}$ of polynomial equations. Both symbolic and numerical techniques can be used for that task. Samples Ω seen in applications are often large, are represented by floating numbers, and have errors and outliers. In those cases, we use numerical algebraic geometry (see Section 1.3). For instance, in Example 4.1.28 we intersect (4.22) with a linear space of dimension 2. This results in 16 isolated solutions. Further numerical analysis in step 3 reveals the desired irreducible component of degree 10.

In the numerical approach to answering the three questions, one proceeds as follows:

1. We add s random (affine-)linear equations to $\mathscr{P}$ and we solve the resulting system in $\mathbb{C}^n$. If there are no solutions, then $\dim(V) < s$. If the solutions are not isolated, then $\dim(V) > s$. Otherwise, there are finitely many solutions, and $\dim(V) = s$.

2. The degree of V is the finite number of solutions found in step 1.

3. Using *monodromy loops* (cf. [20]), we can identify the intersection of a linear space L with any irreducible component of $V_{\mathbb{C}}$ whose codimension equals $\dim(L)$.

The dimension diagrams can be used to guess a suitable range of values for the parameter s in step 1. However, if we have equations at hand, it is better to determine the dimension s as follows. Let $\mathscr{P} = \{f_1, \ldots, f_k\}$ and u be any data point in Ω. Then, we choose the s from step 1 as the corank of the Jacobian matrix of $f = (f_1, \ldots, f_k)$ at u; i.e,

$$s := \dim \ker J f(u). \tag{4.23}$$

Note that $s = \dim V(\mathscr{P})$ as long as u is not a singular point of $V(\mathscr{P})$. In this case, s provides an upper bound for the true dimension of V. That is why it is important in step 3 to use higher-dimensional linear spaces L to detect lower-dimensional components of $V(\mathscr{P})$.

Example 4.1.29. Take $m = n = 3$ in Example 4.1.3. Let $\mathscr{P}$ consist of the four 2×2-minors that contain the upper-left matrix entry x_{11}. The ideal $\langle \mathscr{P} \rangle$ has codimension 3 and degree 2. Its top-dimensional components are $\langle x_{11}, x_{12}, x_{13} \rangle$ and $\langle x_{11}, x_{21}, x_{31} \rangle$. However, our true model V has codimension 4 and degree 6: it is defined by all nine 2×2-minors. Note that $\langle \mathscr{P} \rangle$ is not radical. It also has an embedded prime of codimension 5, namely $\langle x_{11}, x_{12}, x_{13}, x_{21}, x_{31} \rangle$.

Real Degree and Volume

The discussion in the previous subsection was about the complex points of the variety V. The geometric quantity $\deg(V)$ records a measurement over $\mathbb{C}$. It is insensitive to the geometry of the real points of V. That perspective does not distinguish between $\mathscr{P} = \{x^2 + y^2 - 1\}$ and $\mathscr{P} = \{x^2 + y^2 + 1\}$. That distinction is seen through the lens of *real algebraic geometry*.

In this subsection we study metric properties of a real projective variety $V \subset \mathbb{P}^n_{\mathbb{R}}$. We explain how to estimate the *volume* of V. Up to a constant depending on $d = \dim V$, this volume equals the *real degree* $\deg_{\mathbb{R}}(V)$, by which we mean the expected number of real intersection points with a linear subspace of codimension $\dim(V)$; see Theorem 4.1.30 below.

To derive these quantities, we use *Poincaré's kinematic formula* [121, Theorem 3.8]. For this we need some notation. By [138] there is a unique orthogonally invariant measure μ on $\mathbb{P}^n_{\mathbb{R}}$ up to scaling. We choose the scaling in a way compatible with the unit sphere $\mathbb{S}^n$:

$$\mu(\mathbb{P}^n_{\mathbb{R}}) = \frac{1}{2} \text{vol}(\mathbb{S}^n) = \frac{\pi^{\frac{n+1}{2}}}{\Gamma(\frac{n+1}{2})}.$$

This makes sense because $\mathbb{P}^n_{\mathbb{R}}$ is doubly covered by $\mathbb{S}^n$. The n-dimensional volume μ induces a d-dimensional measure of volume on $\mathbb{P}^n_{\mathbb{R}}$ for any $d = 1, 2, \ldots, n-1$. We use that measure for $d = \dim(V)$ to define the volume of our real projective variety as $\mathrm{vol}(V) := \mu(V)$.

Let $\mathrm{Gr}(k, \mathbb{P}^n_{\mathbb{R}})$ denote the Grassmannian of k-dimensional linear spaces in $\mathbb{P}^n_{\mathbb{R}}$. This is a real manifold of dimension $(n-k)(k+1)$. Because of the Plücker embedding it is also a projective variety. We saw this for $k = 1$ in Example 4.1.6, but we will not use it here. Again by [138], there is a unique orthogonally invariant measure ν on $\mathrm{Gr}(k, \mathbb{P}^n_{\mathbb{R}})$ up to scaling. We choose the scaling $\nu(\mathrm{Gr}(k, \mathbb{P}^n_{\mathbb{R}})) = 1$. This defines the *uniform probability distribution* on the Grassmannian. Poincaré's Formula [121, Theorem 3.8] states:

Theorem 4.1.30 (Kinematic formula in projective space)**.** *Let V be a smooth projective variety of codimension $k = n - d$ in $\mathbb{P}^n_{\mathbb{R}}$. Then its volume is the volume of $\mathbb{P}^d_{\mathbb{R}}$ times the real degree:*

$$\mathrm{vol}(V) = \frac{\pi^{\frac{d+1}{2}}}{\Gamma(\frac{d+1}{2})} \cdot \deg_{\mathbb{R}}(V) \quad where \quad \deg_{\mathbb{R}}(V) = \int_{L \in \mathrm{Gr}(k, \mathbb{P}^n_{\mathbb{R}})} \#(L \cap V) \, d\nu.$$

Note that in case of V being a linear space of dimension d, we have $\#(L \cap V) = 1$ for all $L \in \mathrm{Gr}(n-d, \mathbb{P}^n_{\mathbb{R}})$. Hence, $\mathrm{vol}(V) = \mathrm{vol}(\mathbb{P}^d_{\mathbb{R}})$, which verifies the theorem in this instance.

The theorem suggests an algorithm. Namely, we sample linear spaces $L_1, L_2, \ldots, L_N$ independently and uniformly at random, and compute the number $r(i)$ of real points in $V \cap L_i$ for each i. This can be done symbolically (using Gröbner bases) or numerically (using homotopy continuation). We obtain the following estimator for $\mathrm{vol}(V)$:

$$\widehat{\mathrm{vol}}(V) = \frac{\pi^{\frac{d+1}{2}}}{\Gamma(\frac{d+1}{2})} \cdot \frac{1}{N} \sum_{i=1}^{N} r(i).$$

We can sample uniformly from $\mathrm{Gr}(k, \mathbb{P}^n_{\mathbb{R}})$ by using the following lemma:

Lemma 4.1.2. *Let A be a random $(k+1) \times (n+1)$ matrix with independent standard Gaussian entries. The row span of A follows the uniform distribution on the Grassmannian $\mathrm{Gr}(k, \mathbb{P}^n_{\mathbb{R}})$.*

Proof. The distribution of the row space of A is orthogonally invariant. Since the orthogonally invariant probability measure on $\mathrm{Gr}(k, \mathbb{P}^n_{\mathbb{R}})$ is unique, the two distributions agree. $\square$

Example 4.1.31. Let $n = 2$, $k = 1$, and let V be the *Trott curve* in $\mathbb{P}^2_{\mathbb{R}}$. The area of the projective plane $\mathbb{P}^2_{\mathbb{R}}$ is half of the surface area of the unit circle: $\mu(\mathbb{P}^2_{\mathbb{R}}) = \frac{1}{2} \cdot \mathrm{vol}(\mathbb{S}^1) = \pi$. The real degree of V is computed with the method suggested in Lemma 4.1.2: $\deg_{\mathbb{R}}(V) = 1.88364$. We estimate the length of the Trott curve to be the product of these two numbers: 5.91763. Note that 5.91763 does *not* estimate the length of the affine curve depicted in Figure 4.3, but it is the length of the projective curve defined by the homogenization of the polynomial (4.1).

Remark 4.1.32. Our discussion in this subsection focused on real projective varieties. For affine varieties $V \subset \mathbb{R}^n$ there is a formula similar to Theorem 4.1.30. By [172, (14.70)],

$$\mathrm{vol}(V) = \frac{O_{n-d} \cdots O_1}{O_n \cdots O_{d+1}} \cdot \int_{L \cap V \neq \emptyset} \#(V \cap L) \, dL, \qquad d = \dim V,$$

where dL is the density of affine $(n-d)$-planes in $\mathbb{R}^n$ from [172, Section 12.2], vol$(\cdot)$ is Lebesgue measure in $\mathbb{R}^n$ and $O_m := \mathrm{vol}\,(\mathbb{S}^m)$. The problem with using this formula is that in general we do not know how to sample from the density dL given $L \cap V \neq \emptyset$. The reason is that this distribution depends on vol(V)–which we were trying to compute in the first place.

Suppose that the variety V is the image of a parameter space over which integration is easy. This holds for $V = \mathrm{SO}(3)$, by (4.3). For such cases, here is an alternative approach for computing the volume: pull back the volume form on V to the parameter space and integrate it there. This can be done either numerically or –if possible– symbolically. Note that this method is not only applicable to smooth varieties, but to any differentiable manifold.

Software and Experiments

Here, we demonstrate how the methods described previously work in practice. The implementations are available in our `Julia` package `LearningAlgebraicVarieties`. We offer a step-by-step tutorial. To install our software, start a `Julia` session and type

```
Pkg.clone("https://github.com/PBrdng/LearningAlgebraicVarieties.git")
```

After the installation, the next command is

```
using LearningAlgebraicVarieties
```

This command loads all the functions into the current session. Our package accepts a dataset Ω as a matrix whose *columns* are the data points $u^{(1)}, u^{(2)}, \ldots, u^{(m)}$ in $\mathbb{R}^n$.

To use the numerical algebraic geometry software `Bertini`, we must first download it from `https://bertini.nd.edu/download.html`. The `Julia` wrapper for `Bertini` is installed by

```
Pkg.clone("https://github.com/PBrdng/Bertini.jl.git")
```

The code `HomotopyContinuation.jl` accepts input from the polynomial algebra package `MultivariatePolynomials.jl`[1]. The former is described in [44] and it is installed using

```
Pkg.add("HomotopyContinuation")
```

We apply our package to three datasets. The first comes from the group $\mathrm{SO}(3)$, the second from the projective variety V of 2×3-matrices (x_{ij}) of rank 1, and the third from the conformation space of *cyclooctane*.

In the first two cases, we draw the samples ourselves. The introduction of [80] mentions algorithms to sample from compact groups. However, for the sake of simplicity we use the following algorithm for sampling from $\mathrm{SO}(3)$. We use `Julia`'s `qr()`-command to compute the QR-decomposition of a random real 3×3 matrix with independent standard Gaussian entries and take the Q of that decomposition. If the computation is such that the diagonal entries of R are all positive then, by [149, Theorem 1], the matrix Q is uniformly distributed in $\mathrm{O}(3)$. However, in our case, $Q \in \mathrm{SO}(3)$ and we do not know its distribution.

---

[1]`https://github.com/JuliaAlgebra/MultivariatePolynomials.jl`

Our sample from the *Segre variety* $V = \mathbb{P}^1_{\mathbb{R}} \times \mathbb{P}^2_{\mathbb{R}}$ in $\mathbb{P}^5_{\mathbb{R}}$ is drawn by independently sampling two standard Gaussian matrices of format 2×1 and 1×3 and multiplying them. This procedure yields the uniform distribution on V because the Segre embedding is an isometry under the Fubini-Study metrics on $\mathbb{P}^1_{\mathbb{R}}, \mathbb{P}^2_{\mathbb{R}}$ and $\mathbb{P}^5_{\mathbb{R}}$. The third sample, which is 6040 points from the conformation space of cyclooctane, is taken from Adams *et al.* [3, Section 6.3].

We provide the samples used in the subsequent experiments in the JLD[2] data format. After having installed the JLD package in `Julia` (`Pkg.add("JLD")`), load the datasets by typing

```
import JLD: load
s = string(Pkg.dir("LearningAlgebraicVarieties"),"/datasets.jld")
datasets = load(s)
```

Dataset 1: A Sample from the Rotation Group SO(3)

The group SO(3) is a variety in the space of 3×3-matrices. It is defined by the polynomial equations in Example 4.1.2. A dataset containing 887 points from SO(3) is loaded by typing

```
data = datasets["SO(3)"]
```

Now the current session should contain a variable `data` that is a 9×887 matrix. We produce the dimension diagrams by typing

```
DimensionDiagrams(data, false, methods=[:CorrSum,:PHCurve])
```

In this command, `data` is our dataset, the Boolean value is `true` if we suspect our variety is projective and `false` otherwise, and `methods` is any of the dimension estimates `:CorrSum`, `:BoxCounting` `:PHCurve`, `:NPCA`, `:MLE`, and `:ANOVA`. We can leave this unspecified and type

```
DimensionDiagrams(data, false)
```

This command plots all six dimension diagrams. Both outputs are shown in Figure 4.6.

Three estimates are close to 3, so we correctly guess the true dimension of SO(3). In our experiments we found that NPCA and Box Counting Dimension often overestimate.

We proceed by finding polynomials that vanish on the sample. The command we use is

```
FindEquations(data, method, d, homogeneous_equations)
```

where `method` is one of `:with_svd`, `:with_qr`, `:with_rref`. The degree d refers to the polynomials in R we are looking for. If `homogeneous_equations` is set to `false`, then we search in $R_{\leq d}$. If we look for a projective variety then we set it to `true`, and R_d is used. For our sample from SO(3) we use the `false` option. Our sample size $m = 887$ is large enough to determine equations up to $d = 4$. The following results are found by the various methods:
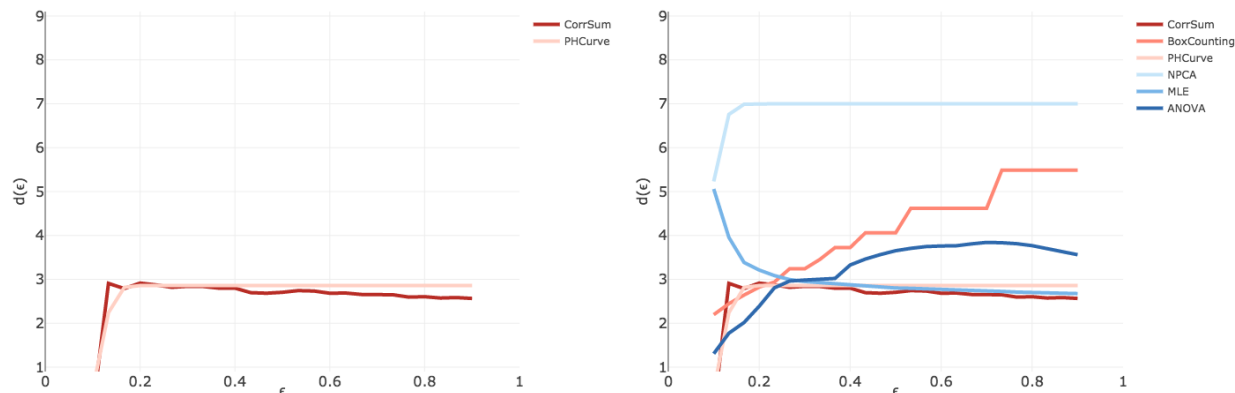
---

[2]https://github.com/JuliaIO/JLD.jl

Figure 4.6: Dimension diagrams for 887 points in $SO(3)$. The right picture shows all six diagrams described in Subsection 4.1. The left picture shows correlation sum and persistent homology curve dimension estimates.

d	method	number of linearly independent equations
1	SVD	0
2	SVD	20
2	QR	20
2	RREF	20
3	SVD	136
4	SVD	550

The correctness of these numbers can be verified by computing (*e.g.* using `Macaulay2`) the affine Hilbert function [64, Section 9.3] of the ideal with the generators in Example 4.1.2. If we type

```
f = FindEquations(data, :with_qr, 2, false)
```

then we get a list of 20 polynomials that vanish on the sample.

The output is often difficult to interpret, so it can be desirable to round the coefficients:

```
round.(f)
```

The precision can be specified, the default being to the nearest integer. We obtain the output

$$x_1 x_4 + x_2 x_5 + x_3 x_6,$$
$$x_1 x_7 + x_2 x_8 + x_3 x_9.$$

Let us continue analyzing the 20 quadrics saved in the variable `f`. We use the following command in `Bertini` to determine whether our variety is reducible and compute its degree:

```
import Bertini: bertini
bertini(round.(f), TrackType = 1, bertini_path = p1)
```

Here p1 is the path to the `Bertini` binary. `Bertini` confirms that the variety is irreducible of degree 8 and dimension 3 (cf. Figure 4.6).

Using `Eirene` we construct the barcodes depicted in Figure 4.7. We run the following commands to plot barcodes for a random subsample of 250 points in SO(3):

```
# sample 250 random points
i = rand(1:887, 250)
# compute the scaled Euclidean distances
dists = ScaledEuclidean(data[:,i])
# pass distance matrix to Eirene and plot barcodes in dimensions up to 3
C = eirene(dists, maxdim = 3)
barcode_plot(C, [0,1,2,3], [8,8,8,8])
```

The first array `[0,1,2,3]` of the `barcode_plot()` function specifies the desired dimensions. The second array `[8,8,8,8]` selects the 8 largest barcodes for each dimension. If the user does not pass the last array to the function, then all the barcodes are plotted. To compute barcodes arising from the complex specified in (4.17), we type

```
dists = EllipsoidDistances(data[:,i], f, 1e-5)
C = eirene(dists, maxdim = 3)
barcode_plot(C, [0,1,2,3], [8,8,8,8])
```

Here, `f = FindEquations(data, :with_qr, 2, false)` is the vector of 20 quadrics. The third argument of `EllipsoidDistances` is the parameter λ from (4.17). It is here set to 10^{-5}.
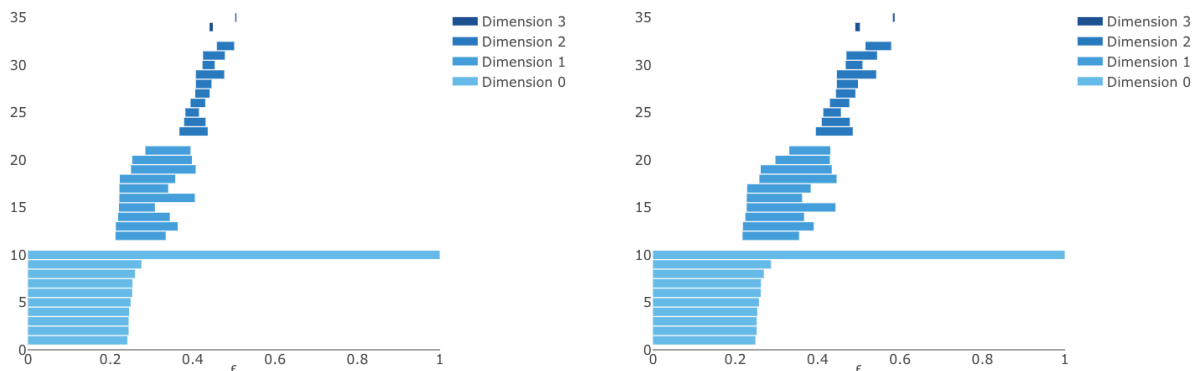
Figure 4.7: Barcodes for a subsample of 250 points from SO(3). The left picture shows the standard Vietoris-Rips complex, while that on the right comes from the ellipsoid-driven complex (4.17). Neither reveals any structures in dimension 3, though $V = \mathrm{SO}(3)$ is diffeomorphic to $\mathbb{P}^3_\mathbb{R}$ and has a non-vanishing $H_3(V, \mathbb{Z})$.

Our subsample of 250 points is not dense enough to reveal features except in dimension 0. Instead of randomly selecting the points in the subsample, one could also use the *sequential maxmin*

landmark selector [3, Section 5.2]. Subsamples chosen this way tend to cover the dataset and to be spread apart from each other. One might also improve the result by constructing different complexes, for example, the lazy witness complexes in [3, Section 5]. However, this is not implemented in `Eirene` at present.

Dataset 2: A Sample from the Variety of Rank One 2×3-Matrices

The second sample consists of 200 data points from the Segre variety $\mathbb{P}^1_{\mathbb{R}} \times \mathbb{P}^2_{\mathbb{R}}$ in $\mathbb{P}^5_{\mathbb{R}}$, that is Example 4.1.3 with $m = n = 3, r = 1$. We load our sample into the `Julia` session by typing

```
data = datasets["2x3 rank one matrices"]
```

We try the `DimensionDiagrams` command once with the Boolean value set to `false` (Euclidean space) and once with the value set to `true` (projective space). The diagrams are depicted in Figure 4.8. As the variety V naturally lives in $\mathbb{P}^5_{\mathbb{R}}$, the projective diagrams yield better estimates and hint that the dimension is either 3 or 4. The true dimension in $\mathbb{P}^5_{\mathbb{R}}$ is 3.
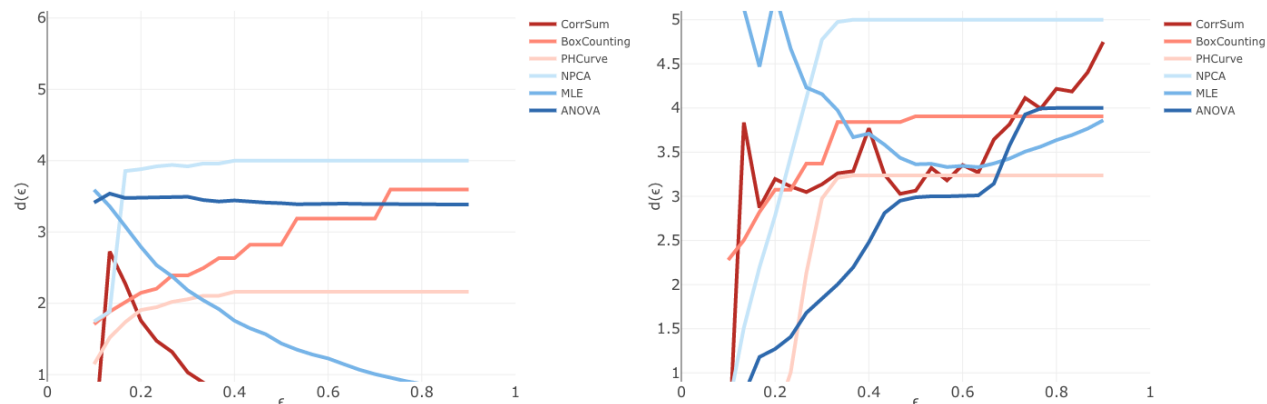
Figure 4.8: Dimension diagrams for 200 points on the variety of 2×3 matrices of rank 1. The left picture shows dimension diagrams for the estimates in $\mathbb{R}^6$. The right picture shows those for projective space $\mathbb{P}^5_{\mathbb{R}}$.

The next step is to find polynomials that vanish. We set `homogeneous_equations` to `true` and $d = 2$: `f = FindEquations(data, method, 2, true)`. All three methods, SVD, QR and RREF, correctly report the existence of three quadrics. The equations obtained with QR after rounding are as desired:

$$x_1x_4 - x_2x_3 = 0, \quad x_1x_6 - x_2x_5 = 0, \quad x_3x_6 - x_4x_5 = 0.$$

Running `Bertini` we verify that V is an irreducible variety of dimension 3 and degree 3.

We next estimate the volume of V using the formula in Theorem 4.1.30. We intersect V with 500 random planes in $\mathbb{P}^5_{\mathbb{R}}$ and count the number of real intersection points. We must initialize 500 linear functions with Gaussian entries involving the same variables as `f`:

```
import MultivariatePolynomials: variables
X = variables(f)
Ls = [randn(3, 6) * X for i in 1:500]
```

Now, we compute the real intersection points using `HomotopyContinuation.jl`.

```
using HomotopyContinuation
r = map(Ls) do L
  # we multiply with a random matrix to make the system square
  S = solve([randn(2,3) * f; L])
  # check which are solutions to f and return the real ones
  vals = [[fi(X => s) for fi in f] for s in solutions(S)]
  i = find(norm.(vals) .< 1e-10)
  return length(real(S[i]))
end
```

The command `pi^2 * mean(r)` reports an estimate of 19.8181 for the volume of V. The true volume of V is the length of $\mathbb{P}^1_\mathbb{R}$ times the area of $\mathbb{P}^2_\mathbb{R}$, which is $\pi \cdot (2\pi) = 19.7392$.
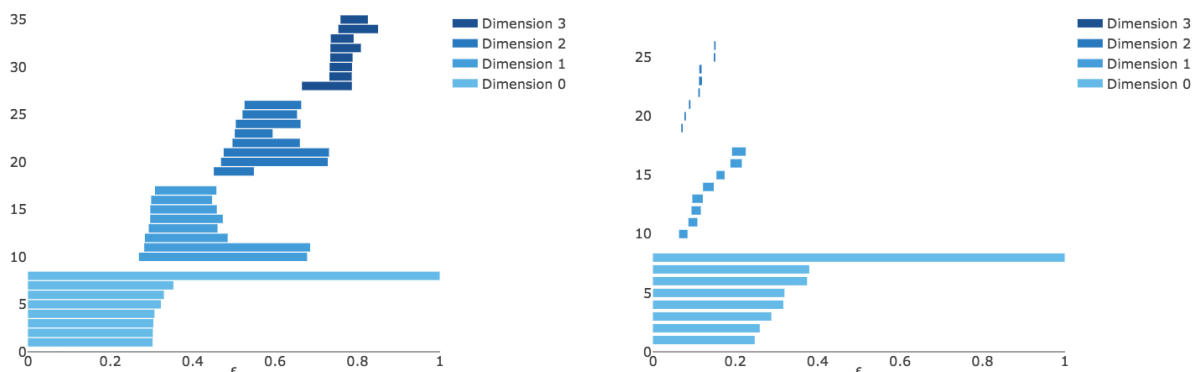
Figure 4.9: Barcodes for 200 points on the Segre variety of 2×3 matrices of rank 1. The true mod 2 Betti numbers of $\mathbb{P}^1_\mathbb{R} \times \mathbb{P}^2_\mathbb{R}$ are $1, 2, 2, 1$. The left picture shows the barcodes for the usual Vietoris-Rips complex computed using scaled Fubini-Study distance. The right picture is computed using the scaled Euclidean distance. Using the Fubini-Study distance yields better results.

Using `Eirene`, we construct the barcodes depicted in Figure 4.9. The barcodes constructed using Fubini-Study distance detect persistent features in dimensions 0, 1 and 2. The barcodes using Euclidean distance only have a strong topological signal in dimension 0.

Dataset 3: Conformation Space of Cyclooctane

Our next variety V is the conformation space of the molecule cyclooctane C_8H_{16}. We use the same sample Ω of 6040 points that was analyzed in [3, Section 6.3]. Cyclooctane consists of eight car-

bon atoms arranged in a ring and each bonded to a pair of hydrogen atoms (see Figure 4.10). The location of the hydrogen atoms is determined by that of the carbon atoms due to energy minimization. Hence, the conformation space of cyclooctane consists of all possible spatial arrangements, up to rotation and translation, of the ring of carbon atoms.
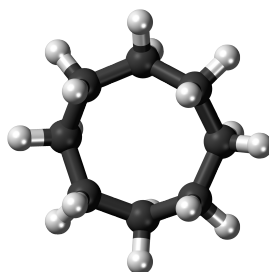

Figure 4.10: A cyclooctane molecule.

Each conformation is a point in $\mathbb{R}^{24} = \mathbb{R}^{8\cdot3}$, which represents the coordinates of the carbon atoms $\{z_0, \ldots, z_7\} \subset \mathbb{R}^3$. Every carbon atom z_i forms an isosceles triangle with its two neighbors with angle $\frac{2\pi}{3}$ at z_i. By the law of cosines, there is a constant $c > 0$ such that the squared distances $d_{i,j} = \|z_i - z_j\|^2$ satisfy

$$d_{i,i+1} = c \quad \text{and} \quad d_{i,i+2} = \frac{8}{3}c \quad \text{for all } i \pmod 8. \tag{4.24}$$

Thus we expect to find 16 quadrics from the given data. In our sample we have $c \approx 2.21$.

The conformation space is defined modulo translations and rotation; i.e., modulo the 6-dimensional *group of rigid motions* in $\mathbb{R}^3$. An implicit representation of this quotient space arises by substituting (4.24) into the Schönberg matrix of Example 4.1.8 with $p = 8$ and $r = 3$.

However, the given Ω lives in $\mathbb{R}^{24} = \mathbb{R}^{8\cdot3}$, *i.e.* it uses the coordinates of the carbon atoms. Since the group has dimension 6, we expect to find 6 equations that encode a *normal form*. That normal form is a distinguished representative from each orbit of the group action.

Brown *et al.* [45] and Martin *et al.* [143] show that the conformation space of cyclooctane is the union of a sphere with a Klein bottle, glued together along two circles of singularities. Hence, the dimension of V is 2, and it has Betti numbers $1, 1, 2$ in mod 2 coefficients.

To accelerate the computation of dimension diagrams, we took a random subsample of 420 points. The output is displayed in Figure 4.11. A dimension estimate of 2 seems reasonable:

```
i = rand(1:6040, 420)
DimensionDiagrams(data[:,i], false)
```

The dataset Ω is noisy: each point is rounded to 4 digits. Direct use of FindEquations() yields no polynomials vanishing on Ω. The reason is that our code sets the tolerance with the numerical rank in (4.21). For noisy samples, we must set the tolerance manually. To get a sense
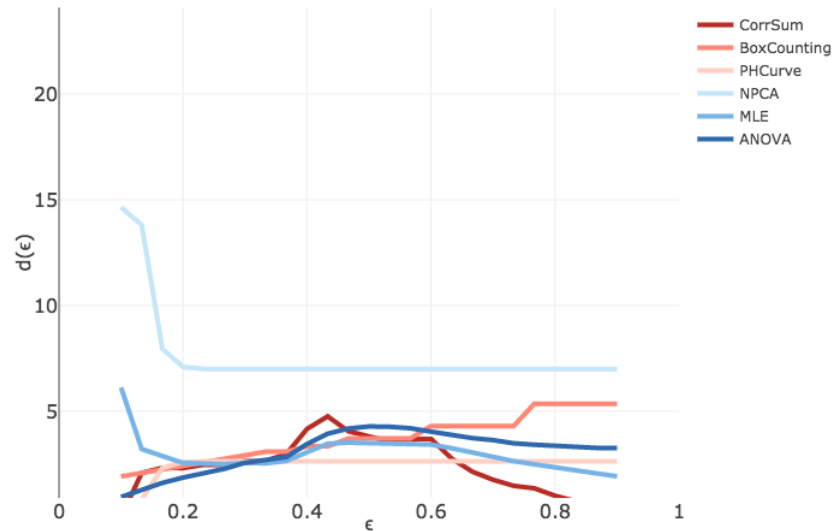
Figure 4.11: Dimension diagrams for 420 points from the cyclooctane dataset.

for adequate tolerance values, we first compute the multivariate Vandermonde matrix $U_{\leq d}(\Omega)$ and then plot the base 10 logarithms of its singular values. We start with $d = 1$.

```
import PlotlyJS
M = MultivariateVandermondeMatrix(data, 1, false)
s = log10.(svdvals(M.Vandermonde))
p = PlotlyJS.scatter(; y=s, mode="lines", line_width = 4)
PlotlyJS.Plot(p)
```

This code produces the left plot in Figure 4.12. This graph shows a clear drop from -0.2 to -2.5. Picking the in-between value -1, we set the tolerance at $\tau = 10^{-1}$. Then, we type

```
f = FindEquations(M, method, 1e-1)
```

where `method` is one of our three methods. For this tolerance value we find six linear equations. Computed using `:with_qr` and rounded to three digits, they are as follows:

1. $-1.2x_1 - 3.5x_2 + 1.2x_3 - 4.2x_4 - 4.1x_5 + 3.9x_6 - 5.4x_7 - 2.0x_8 + 4.9x_9 - 5.4x_{10} + 2.2x_{11} + 4.9x_{12}$
$- 4.2x_{13} + 4.3x_{14} + 3.8x_{15} - 1.1x_{16} + 3.6x_{17} + x_{18}$

2. $-0.6x_1 - 1.3x_2 - 2.0x_4 - 1.3x_5 - 2.5x_7 - 2.5x_{10} + x_{11} - 2.0x_{13} + 2.4x_{14} - 0.5x_{16} + 2.3x_{17} + x_{20}$

3. $2.5x_1 + 8.1x_2 - 4.0x_3 + 9.2x_4 + 9.6x_5 - 10.5x_6 + 11.4x_7 + 4.7x_8 - 11.5x_9 + 12.6x_{10} - 5.1x_{11}$
$- 10.5x_{12} + 9.4x_{13} - 10.0x_{14} - 6.5x_{15} + 1.9x_{16} - 8.3x_{17} - 1.1x_{19} + x_{21}$

4. $x_1 + x_4 + x_7 + x_{10} + x_{13} + x_{16} + x_{19} + x_{22}$

5. $0.6x_1 + 2.3x_2 + 2.0x_4 + 2.3x_5 + 2.5x_7 + x_8 + 2.5x_{10} + 2.0x_{13} - 1.4x_{14} + 0.5x_{16} - 1.3x_{17} + x_{23}$

6. $-1.3x_1 - 4.6x_2 + 3.8x_3 - 4.9x_4 - 5.5x_5 + 7.5x_6 - 6.0x_7 - 2.7x_8 + 7.5x_9 - 7.2x_{10} + 2.9x_{11} + 6.5x_{12}$
    $-5.2x_{13} + 5.7x_{14} + 3.7x_{15} - 0.8x_{16} + 4.7x_{17} + 1.1x_{19} + x_{24}$

We add the second and the fifth equation, and we add the first, third and sixth, by typing `f[2]+f[5]` and `f[1]+f[3]+f[6]` respectively. Together with `f[1]` we get the following:

$$
\begin{aligned}
x_1 + x_4 + x_7 + x_{10} + x_{13} + x_{16} + x_{19} + x_{22} \\
x_2 + x_5 + x_8 + x_{11} + x_{14} + x_{17} + x_{20} + x_{23} \\
x_3 + x_6 + x_9 + x_{12} + x_{15} + x_{18} + x_{21} + x_{24}
\end{aligned}
\tag{4.25}
$$

We learned that centering is the normal form for translation. We also learned that the columns in (4.25) represent the eight atoms. Since we found 6 linear equations, we believe that the three 3 remaining equations determine the normal form for rotations. However, we do not yet understand how the three degrees of rotation produce three linear constraints.
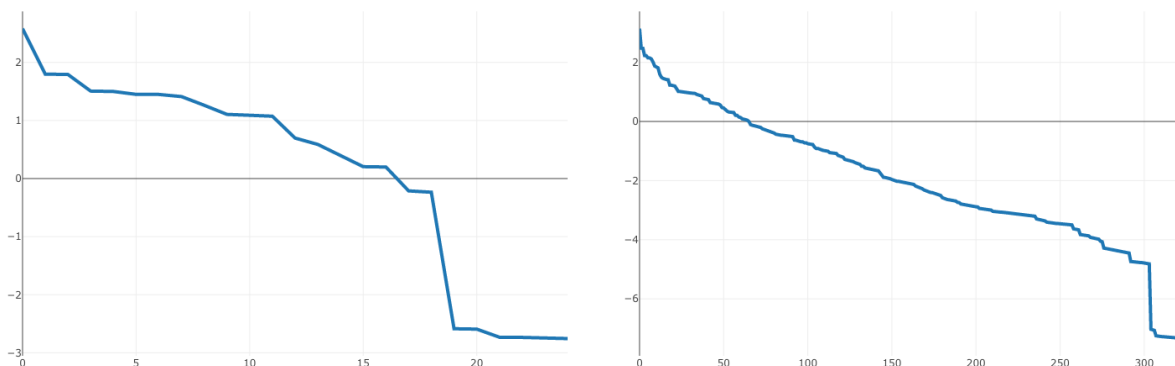
Figure 4.12: Logarithms (base 10) of the singular values of the matrices $U_{\leq 1}(\Omega)$ (left) and $U_{\leq 2}(\Omega)$ (right).

We next proceed to equations of degree 2. Our hope is to find the 16 quadrics in (4.24). Let us check whether this works. Figure 4.12 on the right shows the logarithms of the singular values of the multivariate Vandermonde matrix $U_{\leq 2}(\Omega)$. Based on this we set $\tau = 10^{-6}$.

The command `FindEquations(M, :with_svd, 2, 1e-6)` reveals 21 quadrics. However, these are the pairwise products of the 6 linear equations we found earlier. An explanation for why we cannot find the 16 distance quadrics is as follows. Each of the 6 linear equations evaluated at the points in Ω gives about 10^{-3} in our numerical computations. Thus their products equal about 10^{-6}. The distance quadrics equal about 10^{-3}. At tolerance 10^{-6}, we miss them. Their values are much larger than the 10^{-6} from the 21 redundant quadrics. By randomly rotating and translating each data point, we can manipulate the dataset such that `FindEquations` together with a tolerance value $\tau = 10^{-1}$ gives the 16 desired quadrics. The fact that no linear equation vanishes on the manipulated dataset provides more evidence that 3 linear equations are determining the normal form for rotations.
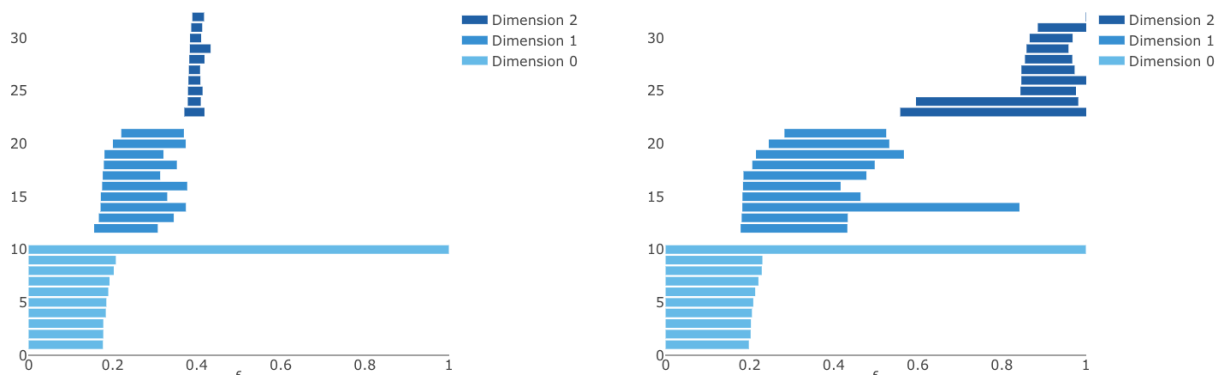
Figure 4.13: Barcodes for a subsample of 500 points from the cyclooctane dataset. The left plot shows the barcodes for the usual Vietoris-Rips complex. The right picture shows barcodes for the ellipsoid-driven simplicial complex in (4.17). The right barcode correctly captures the homology of the conformation space.

The cyclooctane dataset was used in [3, Section 6.3] to demonstrate that persistent homology can efficiently recover the homology groups of the conformation space. We confirmed this result using our software. We determined the barcodes for a random subsample of 500 points. In addition to computing with Vietoris-Rips complexes, we use the 6 linear equations and the 16 distance quadrics to produce the ellipsoid-driven barcode plots. The results are displayed in Figure 4.13. The barcodes from the usual Vietoris-Rips complex do not capture the correct homology groups, whereas the barcodes arising from our new complex (4.17) do.

4.2 Persistent Homology with the Offset Filtration

Experimental research is based on collecting and analyzing data. It is very important to understand the background mathematical model that defines a given phenomenon. One of the possibilities is that the data is driven by a geometric model, say an algebraic variety or a manifold. In this case, we would like to "learn the geometric object" from the data, as in Section 4.3. For example, we would like to understand the topological features of the underlying model. A common way to do this is by *persistent homology*, the topic of Section 1.4 of this dissertation, which studies the homology of the set of points within a range of distances from the data set, and considers features to be of interest if they persist through a wide range of the distance parameter.

This work is at the intersection of computational geometry, geometric design, topology and algebraic geometry, linking all of these topics together. In what follows, we study the *persistent homology of the offset filtration* of an algebraic variety, which we define to be the homology of its offsets. Related work includes [110] in which the notion of persistent homology is extended to the offsets of convex objects.

We show that the indicators (barcodes) of the persistent homology of the offset filtration of a variety defined over the rational numbers are algebraic and thus can be computed exactly (Theorem 4.2.19). Moreover, we connect persistent homology and algebraic optimization (Euclidean Distance Degree [86]) through the theory of offsets, bringing insights from each field to the other. Namely, we express the degree corresponding to the distance variable of the offset hypersurface in terms of the Euclidean Distance Degree of the original variety (Theorem 4.2.9), obtaining a new way to compute these degrees. A consequence of this result is a bound on the degree of the *ED discriminant* (Corollary 4.2.15) and on the degree of the closure of the medial axis (see 4.2.21). We describe the non-properness locus of the offset construction (Subsection 2.1) and use this to describe the set of points (Theorem 4.2.20) in the ambient space that are topologically interesting (the medial axis and center points of the bounded components of the complement of the variety) and relevant to the computation of persistent homology. Lastly, we show that the reach of a manifold, the quantity used to ensure the correctness of persistent homology computations, is algebraic (Proposition 4.2.23).

The section is structured as follows. The first subsection discusses offset hypersurfaces. We analyze the construction, dimension and degree of offsets and define the offset discriminant. The second subsection is about persistent homology. We define the persistent homology of the offset filtration of an algebraic variety and prove its algebraicity, connect the offset discriminant to topologically interesting points in the complement of the variety, and prove the algebraicity of the reach.

Offset Hypersurfaces of Algebraic Varieties

We devote this subsection to the algebraic study of offset hypersurfaces. Driven by real world applications, our starting variety $X_{\mathbb{R}} \subseteq \mathbb{R}^n$ is a real irreducible variety and we construct its ε-offset hypersurface, for any generic real positive ε. In order to use techniques from algebraic geometry, we consider the variety $X \subseteq \mathbb{C}^n$ that is the complexification of $X_{\mathbb{R}}$ and let ε be any complex number. In what follows, by the squared distance of two points $x, y \in \mathbb{C}^n$ we will mean the complex value of the function $d(x,y) = \sum_{i=1}^{n}(x_i - y_i)^2$. This is not the usual Hermitian distance function on $\mathbb{C}^n$, but rather the complexification of the real Euclidean distance function. It is not a metric on $\mathbb{C}^n$, but it is a metric when restricted to $\mathbb{R}^n$.

Offset Construction

Let $X \subseteq \mathbb{C}^n$ be an irreducible variety of codimension c and let ε be a fixed (generic) complex number. By an ε-hyperball centered at a point $y \in \mathbb{C}^n$, we mean the variety $V(d(x,y) - \varepsilon^2)$.

Definition 4.2.1. The *ε-offset hypersurface* is defined to be the union of the centers of ε-hyperballs that intersect the variety X non-transversally at some point $x \in X$. Equivalently the ε-offset hypersurface is the envelope of the family of ε-hyperballs centered on the variety. For a fixed ε we denote the ε-offset hypersurface by $\mathscr{O}_{\varepsilon}(X)$.
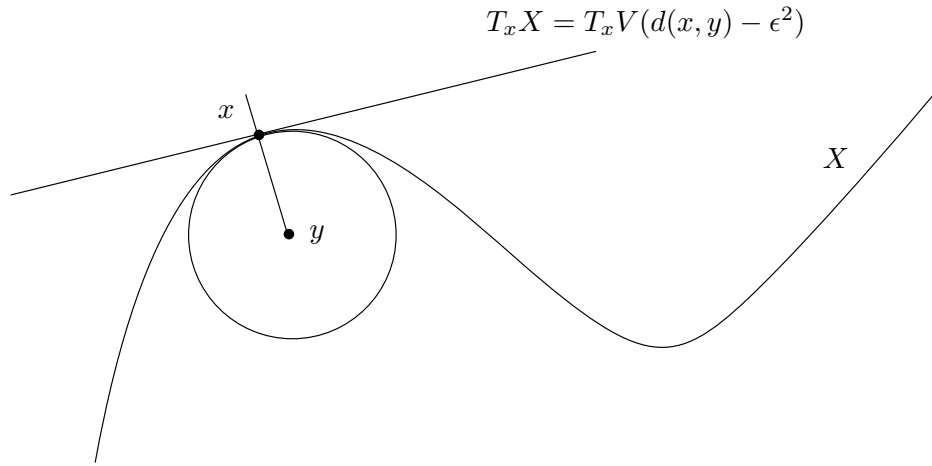
$$T_x X = T_x V(d(x,y) - \epsilon^2)$$

Figure 4.14: Non-transversal intersection of the variety with the ε-hyperball.

Let $y \in \mathscr{O}_\varepsilon(X)$, the above-defined ε-offset hypersurface. Then there exists an $x \in X_{reg}$, that is a regular (nonsingular) point of the variety, such that the squared distance $d(x,y)$ is exactly ε^2 and by the non-transversality $T_x X \subseteq T_x V(d(x,y) - \varepsilon^2)$. Hence

$$x - y \perp T_x X,$$

where $T_x X$ is the tangent space at x to X and $T_x V(d(x,y) - \varepsilon^2)$ is the tangent space at x to $V(d(x,y) - \varepsilon^2)$, the variety defined by the vanishing of the polynomial $d(x,y) - \varepsilon^2$, which is the ε-hyperball centered at y.

The latter condition can be described by polynomial equations as follows (see for example [86, Section 2]). The condition $x - y \perp T_x X$ is satisfied if and only if the rank of

$$\begin{pmatrix} x - y \\ \mathrm{Jac}_x(I) \end{pmatrix}$$

is less then $c + 1$, where $\mathrm{Jac}_x(X)$ is the Jacobian of the defining radical ideal of the variety X, at the point x (the matrix of all the partial derivatives of all the minimally defining polynomials of X). Namely $x - y \perp T_x X$ if and only if all the $(c+1) \times (c+1)$ minors of the matrix above vanish.

To capture the entire geometry behind the construction of the offset hypersurface we consider the closure of the set of all pairs $(x,y) \in \mathbb{C}^n \times \mathbb{C}^n$ such that $x \in X_{reg}$ and y satisfies the conditions above. We name this variety the *offset correspondence* of X and denote it by $\mathscr{OC}_\varepsilon(X)$. This correspondence is a variety in $\mathbb{C}^n_x \times \mathbb{C}^n_y$ and is equal to the closure of the intersection

$$(X_{reg} \times \mathbb{C}^n) \cap V\left((c+1) \times (c+1) \text{ minors of } \begin{pmatrix} x - y \\ \mathrm{Jac}_x(I) \end{pmatrix} \right) \cap V(d(x,y) - \varepsilon^2).$$

Observe that the intersection of the first two varieties is the *Euclidean Distance Degree correspondence*, $\mathscr{E}(X)$, that is the closure of the pair of points (x,y) in $\mathbb{C}^n_x \times \mathbb{C}^n_y$, such that $x \in X_{reg}$ and

$x - y \perp T_x X$. This correspondence contains pairs of "data points" $y \in \mathbb{C}_y^n$ and corresponding points on the variety $x \in X_{reg}$, such that x is a constrained critical point of the Euclidean distance function $d_y(x) = d(x, y)$ with respect to the constraint that $x \in X_{reg}$. For more details on this problem we direct the reader to [86, Section 2]. Using the terminology of the Euclidean Distance Degree problem, we have

$$\mathscr{OC}_\varepsilon(X) = \mathscr{E}(X) \cap V(d(x,y) - \varepsilon^2). \tag{4.26}$$

From the offset correspondence, we have the natural projections $\mathrm{pr}_x : \mathscr{OC}_\varepsilon(X) \to \mathbb{C}_x^n$ and $\mathrm{pr}_y : \mathscr{OC}_\varepsilon(X) \to \mathbb{C}_y^n$. The closure of the first projection is the variety X and the closure of the second projection is the offset hypersurface $\mathscr{O}_\varepsilon(X)$.

It follows that the *offset hypersurface* is

$$\mathscr{O}_\varepsilon(X) = \overline{\mathrm{pr}_y(\mathscr{OC}_\varepsilon(X))} \subseteq \mathbb{C}_y^n.$$

Remark 4.2.2. When X is a real variety, note that by the Tarski-Seidenberg Theorem (see Lemma 4.2.2) the offset hypersurface is defined over the same closed real (sub)field as X and ε are defined.

In the following example, we illustrate an algorithm to compute the defining polynomial of the offset hypersurface of an ellipse using `Macaulay2` [107].

Example 4.2.3 (**Computing the offset hypersurface of the ellipse**). Consider the ellipse $X \subseteq \mathbb{C}^2$ defined by the vanishing of the polynomial $f = x_1^2 + 4x_2^2 - 4$. The code below outputs the defining ideal of the offset hypersurface in terms of the parameter ε.

```
n=2;
kk=QQ[x_1..x_n,y_1..y_n,e];
f=x_1^2+4*x_2^2-4;
I=ideal(f);
c=codim I;
Y=matrix{{x_1..x_n}}-matrix{{y_1..y_n}};
Jac= jacobian gens I;
S=submatrix(Jac,{0..n-1},{0..numgens(I)-1});
Jbar=S|transpose(Y);
EX = I + minors(c+1,Jbar);
SingX=I+minors(c,Jac);
EXreg=saturate(EX,SingX);
distance=Y*transpose(Y)-e^2;
Offset_Correspondence=EXreg+ideal(distance);
Off_hypersurface=eliminate(Offset_Correspondence,toList(x_1..x_n))
```

The result is that $\mathcal{O}_\varepsilon(X)$ is the zero locus of the polynomial

$$
y_1^8 + 10y_1^6y_2^2 + 33y_1^4y_2^4 + 40y_1^2y_2^6 + 16y_2^8 + 4y_1^6\varepsilon^2 - 30y_1^4y_2^2\varepsilon^2 - 90y_1^2y_2^4\varepsilon^2
$$
$$
-56y_2^6\varepsilon^2 - 2y_1^4\varepsilon^4 + 62y_1^2y_2^2\varepsilon^4 + 73y_2^4\varepsilon^4 - 12y_1^2\varepsilon^6 - 42y_2^2\varepsilon^6 + 9\varepsilon^8 - 14y_1^6
$$
$$
-90y_1^4y_2^2 - 120y_1^2y_2^4 + 64y_2^6 - 62y_1^4\varepsilon^2 + 140y_1^2y_2^2\varepsilon^2 - 248y_2^4\varepsilon^2 - 90y_1^2\varepsilon^4
$$
$$
+270y_2^2\varepsilon^4 - 90\varepsilon^6 + 73y_1^4 + 248y_1^2y_2^2 - 32y_2^4 + 270y_1^2\varepsilon^2 - 360y_2^2\varepsilon^2
$$
$$
+297\varepsilon^4 - 168y_1^2 - 192y_2^2 - 360\varepsilon^2 + 144.
$$

The code above is designed to work in arbitrary dimensions and for any variety. For this reason, we saturate by the singular locus of the variety, even though this step is unnecessary in this example as the ellipse is smooth.

Example 4.2.4 (**Offset hypersurface of a space curve**). Let the variety X be the Viviani curve in $\mathbb{C}^3$, defined by the intersection of a sphere with a cylinder tangent to the sphere and passing through the center of the sphere. So X is defined by the vanishing of $f_1 = x_1^2 + x_2^2 + x_3^2 - 4$ and $f_2 = (x_1 - 1)^2 + x_2^2 - 1$. In Figure 4.15 the reader can see (on the left) the real part of the Viviani curve and (on the right) the $\varepsilon = 1$ offset surface of the curve. This surface is defined by a degree 10 irreducible polynomial consisting of 175 monomials.
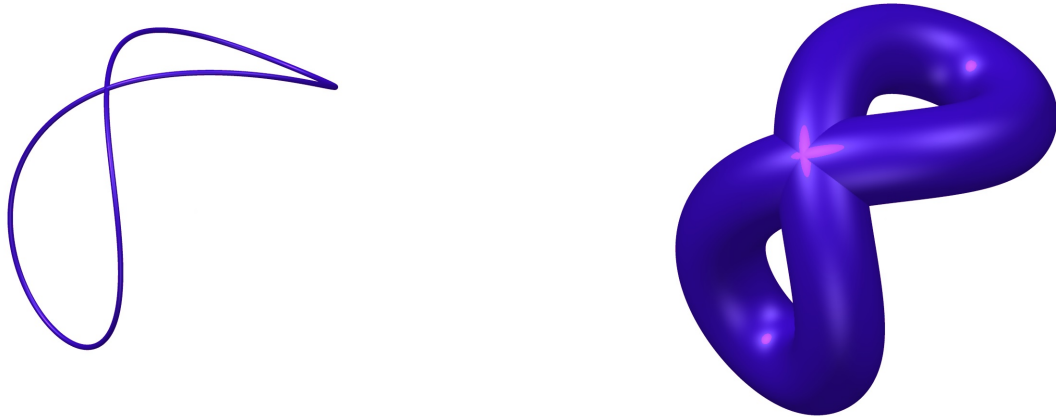

Figure 4.15: The Viviani curve (left) and its offset surface (right).

One could consider the family of all ε-offset hypersurfaces $\mathcal{O}_\varepsilon(X) \subseteq \mathbb{C}^n$ as ε varies over $\mathbb{C}$. This family is again a hypersurface in $\mathbb{C}_y^n \times \mathbb{C}_\varepsilon^1$ defined by the same ideal as is $\mathcal{O}_\varepsilon(X)$, but now ε is a variable.

Define the **offset family**, $\mathcal{O}(X)$, to be the closure of all offset hypersurfaces of X in the $n+1$ dimensional space $\mathbb{C}_y^n \times \mathbb{C}_\varepsilon^1$ defined by the same ideal as $\mathcal{O}_\varepsilon(X)$. More precisely, let

$$
\mathcal{O}(X) = \overline{\{(y, \varepsilon), \, y \in \mathcal{O}_\varepsilon(X)\}} \subseteq \mathbb{C}_y^n \times \mathbb{C}_\varepsilon^1.
$$

Example 4.2.5 (**The offset family of an ellipse**). A picture of the real part of $\mathscr{O}(X)$, where X is the ellipse defined by the vanishing of $x_1^2 + 4x_2^2 - 4 = 0$, can be seen below in Figure 4.16. It is the set of all points $(y_1, y_2, \varepsilon) \in \mathbb{C}^3$ that are zeros of the polynomial in Example 4.2.3.
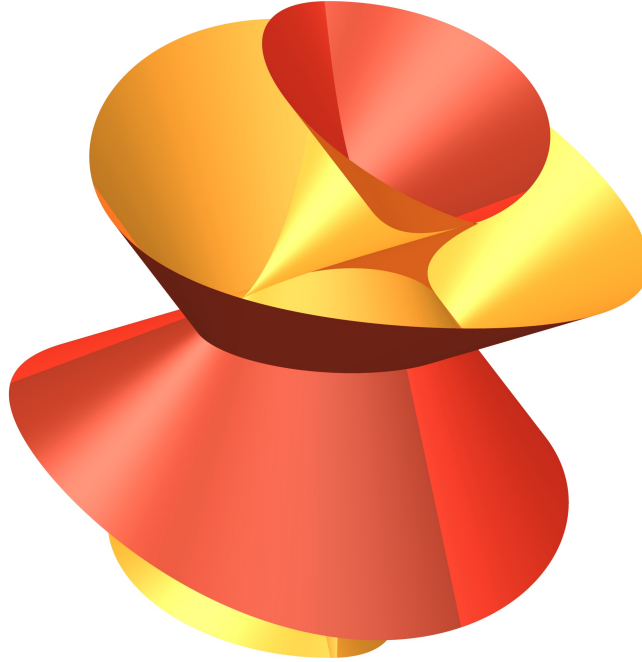

Figure 4.16: Offset family of an ellipse.

A horizontal cut (by a plane $\varepsilon = \varepsilon_0$) of the surface above is the ε_0-offset curve of the ellipse.

Offset Dimension and Degree

The degree and dimension are important invariants of an algebraic variety. These invariants of the offset hypersurface have been studied by many authors (for example by San Segundo and Sendra in [169–171]) in both the implicit and the parametric cases. To supplement the existing literature, in this subsection we relate the degree in ε (or ε-degree) of the defining polynomial of generic offset hypersurfaces to the ED degree of the original variety, for any irreducible variety X. In this way, we achieve a new method for computing both ED degrees of varieties and degrees of offsets.

We now recall a theorem crucial in further understanding the essence of the offset construction.

Theorem 4.2.6 (Theorem 4.1 from [86])**.** *The Euclidean Distance Degree correspondence $\mathscr{E}(X)$ (see Equation (4.26)) is an irreducible variety of dimension n inside $\mathbb{C}_x^n \times \mathbb{C}_y^n$. The first projection $\mathrm{pr}_x : \mathscr{E}(X) \to X \subseteq \mathbb{C}_x^n$ is an affine vector bundle of rank c over X_{reg}. Over generic $y_0 \in \mathbb{C}_y^n$, the second projection $\mathrm{pr}_y : \mathscr{E}(X) \to \mathbb{C}_y^n$ has finite fibers $\mathrm{pr}_y^{-1}(y_0)$ of cardinality equal (by definition) to the Euclidean Distance Degree (ED degree) of X.*

$$\mathscr{E}(X)$$

$$\mathrm{pr}_x \swarrow \qquad\qquad \searrow \mathrm{pr}_y$$

$$\mathbb{C}_x^n \qquad\qquad\qquad\qquad \mathbb{C}_y^n$$
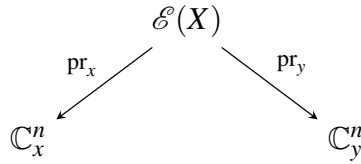
Remark 4.2.7. The second projection, pr_y, has a ramification locus which is generically a hypersurface in $\mathbb{C}_y^n$, by the Nagata-Zariski Purity Theorem [154], [187]. The *Euclidean Distance discriminant (ED discriminant)* is the closure of the image of the ramification locus of pr_y, (i.e. the points where the derivative of pr_y is not of full rank, under the projection pr_y). As in [86, Section 7], we denote the ED discriminant of the variety X by $\Sigma(X)$.

The offset correspondence is the intersection of the Euclidean Distance Degree correspondence with the hypersurface $V(d(x,y) - \varepsilon^2)$ in $\mathbb{C}_x^n \times \mathbb{C}_y^n$ (recall Equation 4.26). This intersection is $n-1$ dimensional because $\mathscr{E}(X)$ is not a subvariety of $V(d(x,y) - \varepsilon^2)$ (because not all pairs $(x,y) \in \mathscr{E}(X)$ are at ε^2 squared distance from each other). As a consequence the offset correspondence, $\mathscr{OC}_\varepsilon(X)$, is an $n-1$ dimensional variety in $\mathbb{C}_x^n \times \mathbb{C}_y^n$. But over generic $y_0 \in \mathbb{C}_y^n$, the projection

$$\mathrm{pr}_y : \mathscr{OC}_\varepsilon(X) \longrightarrow \mathbb{C}_y^n$$

has finite fibers, so the closure of the image, $\overline{\mathrm{pr}_y(\mathscr{OC}_\varepsilon(X))} = \mathscr{O}_\varepsilon(X)$ is $n-1$ dimensional as well, hence the name offset *hypersurface*. For a more detailed analysis of the dimension degeneration of components of the offset hypersurface see [173].

Remark 4.2.8. Observe that a fixed generic y_0 is an element of the offset hypersurface $\mathscr{O}_\varepsilon(X)$ for precisely two times ED degree many distinct ε. This is because y_0 has ED degree many critical points to X, say $\{x_1, \ldots, x_{EDdegree(X)}\}$ and then the corresponding offset hypersurfaces that include y_0, are the ones where ε is in

$$\left\{ \pm\sqrt{d(x_1,y_0)}, \ldots, \pm\sqrt{d(x_{EDdegree(X)},y_0)} \right\}.$$

Theorem 4.2.9. *The degree in ε (or ε-degree) of the defining polynomial of $\mathscr{O}(X)$ (the offset family) is equal to two times the Euclidean Distance degree of the variety X.*

Proof. Suppose that $\mathscr{O}(X)$ is defined by $f(y, \varepsilon)$. By Remark 4.2.8, a generic y_0 is an element of $\mathscr{O}_\varepsilon(X)$ for precisely two times ED degree many ε. This is equivalent to $f(y_0, \varepsilon)$ having exactly two times ED degree many roots. And these roots are

$$\left\{ \pm\sqrt{d(x_1,y_0)}, \ldots, \pm\sqrt{d(x_{EDdegree(X)},y_0)} \right\},$$

where x_i are critical points of the distance from y_0 to the variety. □

We note that San Segundo and Sendra [170] derived the ε-degree of plane offset curves in terms of resultants. In the light of Theorem 4.2.9 their result says the following.

Proposition 4.2.10 (Theorem 35 from [170])**.** *Let X be a plane curve defined by the polynomial* $f(x_1, x_2)$ *of degree d. The ED degree of X equals*

$$\deg_{x_1, x_2} \left(PP_{y_1, y_2} (\mathrm{Res}_{x_3} (F(x_H), N(x_H, y))) \right),$$

where $x_H = (x_1, x_2, x_3)$, $y = (y_1, y_2)$, $F(x_H)$ *is the homogenization of f with respect to a new variable* x_3, $N(x_H, y) = -F_2(x_H)(y_1 x_3 - x_1) + F_1(x_H)(y_2 x_3 - y_1)$, *where* F_1 *and* F_2 *are the homogenized partial derivatives of f and* PP_{y_1, y_2} *denotes the primitive part of the given polynomial with respect to* $\{y_1, y_2\}$.

Example 4.2.11 (**Determinantal varieties**)**.** Suppose $n \le m$ and let $M_{n,m}^{\le r}$ be the variety of $n \times m$ matrices over $\mathbb{C}$ of rank at most r. This variety is defined by the vanishing of all $(r+1) \times (r+1)$ minors of the matrix. For a fixed ε the construction of the offset hypersurface reduces to determining the set of matrices that have at least one critical rank r approximation at squared distance ε^2. By [86, Example 2.3] all the critical rank r approximations to a matrix U are of the form

$$T_1 \cdot \mathrm{Diag}(0, 0, ..., \sigma_{i_1}, ..., \sigma_{i_r}, 0, ..., 0) \cdot T_2,$$

where the singular value decomposition of U is equal to $U = T_1 \cdot \mathrm{Diag}(\sigma_1, ..., \sigma_n) \cdot T_2$, with $\sigma_1 > ... > \sigma_n$ singular values and T_1, T_2 orthogonal matrices of size $n \times n$ and $m \times m$. Now by [116, Corollary 2.3] the squared distance of such a critical approximation from U is exactly

$$\sigma_{i_1}^2 + \ldots + \sigma_{i_r}^2.$$

Recall that σ_i^2 are the eigenvalues of $U \cdot U^T$, so what we seek is that the sum of an r-tuple of the eigenvalues of $U \cdot U^T$ equals ε^2. Let us denote by $\bigwedge^{(r)}(U \cdot U^T)$ the r-th *additive compound matrix* of $U \cdot U^T$. For the construction of this object we refer to [98, P14]. The additive compound matrix is an $\binom{n}{r} \times \binom{n}{r}$ matrix with the property that its eigenvalues are the sums of r-tuples of eigenvalues of the original matrix [98, Theorem 2.1]. So the eigenvalues of $\bigwedge^{(r)}(U \cdot U^T)$ are exactly $\sigma_{i_1}^2 + \ldots + \sigma_{i_r}^2$. Putting this together we get that the offset hypersurface of $M_{n \times m}^{\le r}$ is defined by the vanishing of

$$\det \left(\overset{(r)}{\bigwedge}(U \cdot U^T) - \varepsilon^2 \cdot I_{\binom{n}{r}} \right).$$

Observe that the ε degree of this polynomial is $2 \cdot \binom{n}{r}$, which is indeed two times the ED degree of $M_{n \times m}^{\le r}$ (see [86, Example 2.3]).

Offset Discriminant

We now consider the restriction $\mathrm{pr}_y|_{\mathscr{OC}_\varepsilon(X)} : \mathscr{OC}_\varepsilon(X) \to \mathscr{O}_\varepsilon(X)$. We claim that, for generic ε, this restriction is one-to-one outside its branch locus. Indeed if we fix a generic $y_0 \in \mathscr{O}_\varepsilon(X)$, then the fiber above y_0 equals

$$\mathrm{pr}_y^{-1}(y_0) = \big(V(d(x,y) - \varepsilon^2) \cap (\mathbb{C} \times \{y_0\})\big) \cap (\mathscr{E}(X) \cap (\mathbb{C} \times \{y_0\}))\,.$$

By the definition of ED degree we have that

$$\mathscr{E}(X) \cap (\mathbb{C} \times \{y_0\}) = \{(x_1, y_0), \dots, (x_{EDdegree(X)}, y_0)\}.$$

Combining these we get,

$$\mathrm{pr}_y^{-1}(y_0) = \{(x_1, y_0), \dots, (x_{EDdegree(X)}, y_0)\} \cap \big(V(d(x,y) - \varepsilon^2) \cap (\mathbb{C} \times \{y_0\})\big)\,.$$

This means that the fiber consists of pairs (x, y_0), such that x is a critical point of the squared distance function from y_0 and is of squared distance ε^2 from y_0. For generic $y_0 \in \mathscr{O}_\varepsilon(X)$ and generic ε, there is exactly one such critical point. Otherwise a y_0 with at least two elements in the fiber would be a doubly covered point of the offset hypersurface, hence part of its singular locus, which is of strictly lower dimension than the offset hypersurface itself. Indeed the branch locus of the restriction of pr_y is (generically) a hypersurface inside $\mathscr{O}_\varepsilon(X)$ (by the Nagata-Zariski Purity theorem [154, 187]), hence a codimension two variety in $\mathbb{C}_y^n$, and it consists of points y for which there exist at least two $x_1, x_2 \in X_{reg}$, such that $(x_1, y), (x_2, y) \in \mathscr{OC}_\varepsilon(X)$, or one $(x_1, y) \in \mathscr{OC}_\varepsilon(X)$ with multiplicity greater than one. We denote the closure of the union of all branch loci, over ε in $\mathbb{C}$, by $B(X, X)$, which is the *bisector hypersurface of the variety X* (see for instance [95, 96]). Note that the variety itself is a component of $B(X, X)$ because for $\varepsilon = 0$ the variety is covered doubly under the projection pr_y. We call the set of doubly covered points such that $(x_1, y) \neq (x_2, y) \in \mathscr{OC}_\varepsilon(x)$, the *proper bisector locus*, and we denote it by $B_0(X, X)$. In summary, we have the following result.

Proposition 4.2.12. *For a fixed generic ε the projection $\mathrm{pr}_y|_{\mathscr{OC}_\varepsilon(X)} : \mathscr{OC}_\varepsilon(X) \longrightarrow \mathscr{O}_\varepsilon(X)$ is one-to-one outside the bisector hypersurface $B(X, X)$.*

Let us see how this relates to (not the union but) the collection of offset hypersurfaces for all ε. This collection is the offset family, $\mathscr{O}(X)$, and it is a hypersurface in $\mathbb{C}_y^n \times \mathbb{C}_\varepsilon^1$. Its defining polynomial is the same as of $\mathscr{O}_\varepsilon(X)$. Let us denote this polynomial by $f(y, \varepsilon)$. Now if we consider $f(y, \varepsilon)$ to be a univariate polynomial in the variable ε, then we can compute its discriminant $\mathrm{Discr}_\varepsilon(f)$, which is a polynomial in the variables y, with the property that $f(y_0, \varepsilon)$ has a double root (in ε) if and only if y_0 is in the zero set of $\mathrm{Discr}_\varepsilon(f)$.

Now $y_0 \in \mathrm{Discr}_\varepsilon(f)$ if and only if there are fewer than two times ED degree many distinct roots, not counting multiplicities, of $f(y_0, \varepsilon)$. By Theorem 4.2.9 this means that either y_0 has a non-generic number of critical points, meaning that y_0 is an element of the ED discriminant (for definition recall 4.2.7), or there are two critical points $x_i \neq x_j$, such that

$$d(x_i, y_0) = d(x_j, y_0),$$

meaning that the projection $\mathrm{pr}_y : \mathscr{OC}_\varepsilon(X) \rightarrow \mathscr{O}_\varepsilon(X)$ is not one-to-one over y_0, so y_0 in an element of the branch locus. To summarize this we have the following proposition.

Proposition 4.2.13. *Suppose that $\mathcal{O}(X)$ is defined by the vanishing of $f(y,\varepsilon)$. Then the zero locus of the ε-discriminant of f is the union of the ED discriminant of X and the bisector hypersurface of X. So we have that*

$$\text{Discr}_\varepsilon(f) = \Sigma(X) \cup B(X,X).$$

In what follows we call the union of the ED discriminant and the bisector hypersurface the *offset discriminant*, denoted $\Delta(X)$. And we recall that by construction, it is *the envelope of all the offset hypersurfaces* to X.

Example 4.2.14 (**Offset discriminant of an ellipse**). Let X be the ellipse defined by $x_1^2 + 4x_2^2 - 4$. The offset family of the ellipse is defined by the vanishing of the polynomial from Example 4.2.3. The ε-discriminant of this polynomial factors into five irreducible components. One of them is the defining polynomial of the sextic *Lamé curve*

$$64y_1^6 + 48y_1^4y_2^2 + 12y_1^2y_2^4 + y_2^6 - 432y_1^4 + 756y_1^2y_2^2 - 27y_2^4 + 972y_1^2 + 243y_2^2 - 729,$$

with zero locus $\Sigma(X)$, the ED discriminant (evolute) of X. The remaining four components comprise the bisector curve $B(X,X)$ of the ellipse. Two out of these four components of $B(X,X)$ are the x- and y- axes (the proper bisector locus $B_0(X,X)$), one of the components is the ellipse itself (because for $\varepsilon = 0$ the variety is doubly covered under the projection pr_y) and the remaining component is fully imaginary. A cartoon of the real part of $\Delta(X)$ can be seen in Figure 4.17. The ellipse is black, the proper bisector locus (the axis) is blue and the ED discriminant is red.
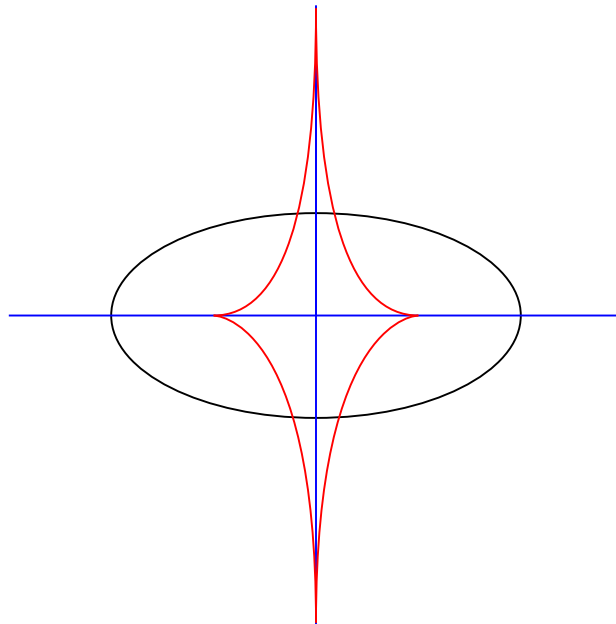

Figure 4.17: The ED discriminant and the bisector curve of the ellipse.

Corollary 4.2.15. *Let X be an irreducible variety in $\mathbb{C}^n$. The degree of its offset discriminant $\Delta(X)$ (hence also the degree of its ED discriminant $\Sigma(X)$ and the degree of the bisector hypersurface $B(X,X)$) is bounded from above by*

$$2 \cdot \deg_y(\mathscr{O}(X)) \cdot (4 \cdot \mathrm{EDdegree}(X) - 2).$$

Proof. Suppose that the offset family $\mathscr{O}(X)$ is the zero set of the polynomial $f(y,\varepsilon)$. The offset discriminant $\Delta(X)$ is the discriminant of the univariate polynomial

$$f(y,\varepsilon) = a_0(y) + \ldots + a_{d-1}(y) \cdot \varepsilon^{d-1} + a_d(y)\varepsilon^d$$

in the variable ε of degree $d = \deg_\varepsilon(f)$. So $\Delta(X)$ is a homogeneous polynomial in the coefficients $a_0(y), \ldots, a_d(y)$ of degree equal to $2 \cdot d - 2$. By Theorem 4.2.9 we have that $d = 2 \cdot \mathrm{EDdegree}(X)$. Now because the discriminant is a homogeneous polynomial in the coefficients we get the desired degree bound. $\qquad\square$

Example 4.2.16 (**Degree bounds of the offset discriminant**). The following table contains degree bounds of the offset discriminant based on the formula above and the total degree formulae, $\deg_{()}y(\mathscr{O}(X))$, by San Segundo and Sendra [170, Appendix. Table of offset degrees].

Name of X	Defining poly. of X	$\deg_y \mathscr{O}(X)$	$\deg_\varepsilon \mathscr{O}(X)$	$\deg_y \Delta(X) \leq$
Circle	$x_1^2 + x_2^2 - 1$	4	4	24
Parabola	$x_2 - x_1^2$	6	6	60
Ellipse	$x_1^2 + 4x_2^2 - 4$	8	8	112
Cardioid	$(x_1^2 + x_2^2 + x_1)^2 - x_1^2 - x_2^2$	10	8	140
Rose(3 petals)	$(x_1^2 + x_2^2)^2 + x_1(3x_2^2 - x_1^2)$	14	12	308

As the degree of an algebraic variety is a proxy for computational complexity, these degree bounds serve a reminder of the challenges of computing offsets, and thus persistence. We also see how the difficulty depends on the nature of the starting variety X.

Algebraicity of Persistent Homology

As an application of this knowledge of offset hypersurfaces, we study the persistent homology of the offset filtration of an algebraic variety. We define this to be the homology of the set of points within distance ε of the variety, which is bounded by the offset hypersurface. We define the persistent homology of the offset filtration in terms of the offset hypersurface. We prove the algebraicity of two quantities involved in computing persistent homology. We do not present a new algorithm to compute persistent homology. However, we do provide theoretical foundations to show that it is possible for an algorithm to compute persistent homology barcodes exactly. If the expected output of a computation is algebraic over the rational numbers, this means it can be computed using polynomials of finite degree, and thus it is possible for the algorithm to terminate. We also discuss the relevance of the offset discriminant to persistent homology. We refer the reader to Section 1.4 of this dissertation for an introduction to persistent homology.

Persistent Homology of the Offset Filtration of a Variety

Persistent homology is typically defined for a finite metric space. To compute the persistent homology of a variety X, one might sample a finite set of points from the variety and compute the Čech complex of those points. The equivalent of the Čech complex $C_X(\varepsilon)$ obtained from sampling every point on the variety would be the set of all points within ε of the variety. For this reason, we define the *persistent homology of the offset filtration of a variety X at parameter ε* as the homology of the subset

$$X_\varepsilon = \{x| \text{ there exists } y \in V \text{ with } ||x - y|| \leq \varepsilon\} \subset \mathbb{R}^n$$

consisting of all points within ε of the variety.

Since the ε-offset hypersurface is the envelope of a family of ε-hyperballs centered on the variety, we can define the the persistent homology of the offset filtration of a variety at parameter ε equivalently as the homology of the set bounded by $\mathscr{O}_\varepsilon(X)$.

To define barcodes with respect to this filtration, we use Hardt's theorem from real algebraic geometry. We now make the necessary definitions and state the theorem.

Definition 4.2.17 (Definition 9.3.1 from [29]). Let S, T and T' be semi-algebraic sets, $T' \subset T$, and let $f : S \longrightarrow T$ be a continuous semi-algebraic mapping. A *semi-algebraic trivialization of f over T'*, with fiber F, is a semi-algebraic homeomorphism $\theta : T' \times F \longrightarrow f^{-1}(T')$, such that $f \circ \theta$ is the projection mapping $T' \times F \longrightarrow T'$. We say that the semi-algebraic trivialization θ is *compatible with a subset S' of S* if there is a subset F' of F such that $\theta(T' \times F') = S' \cap f^{-1}(T')$.

Lemma 4.2.1 (Hardt's Theorem, 9.3.1 from [29]). *Let S and T be two semi-algebraic sets, $f : S \longrightarrow T$ a continuous semi-algebraic mapping, $(S_j)_{j=1,\ldots,q}$ a finite family of semi-algebraic subsets of S. There exist a finite partition of T into semi-algebraic sets $T = \cup_{l=1}^r T_l$ and, for each l, a semi-algebraic trivialization $\theta_l : T_l \times F_l \longrightarrow f^{-1}(T_l)$ of f over T_l, compatible with S_j, for $j = 1, \ldots, q$.*

Let $S = \{(X_\varepsilon, \varepsilon)| \varepsilon \in [0, \infty)\} \subset \mathbb{R}^{n+1}$ and let $\text{pr}_\varepsilon : S \longrightarrow \mathbb{R}$ be the projection to ε. By Hardt's theorem, there is a partition of $\mathbb{R}$ into finitely many intervals $I_l = [\delta_l, \varepsilon_l]$ for $l \in \{1, \ldots, j\}$ such that the fibers $\text{pr}_\varepsilon^{-1}(\varepsilon) = X_\varepsilon$ for all $\varepsilon \in [\delta_l, \varepsilon_l]$ are homeomorphic. Thus we can create the *offset filtration barcode* of X.

We show that $\{\delta_l\} \cup \{\varepsilon_l\}$ for $l \in \{1, \ldots, j\}$, the values of the persistence parameter ε at which a bar in the offset filtration barcode appears or disappears, are algebraic over the field of definition of a real affine variety X. As a consequence, the persistent homology of the offset filtration of X can be computed exactly.

The proof relies on two lemmas from real algebraic geometry. We describe the content of these lemmas. The setting of the results is a real closed field, which we now define.

Definition 4.2.18 (Definitions 1.1.9 and 1.2.1 from [29]). A field R is a *real field* if it can be ordered. A real field R is a *real closed field* if it has no nontrivial real algebraic extension.

The first lemma is Tarski-Seidenberg's Theorem, a fundamental result in real algebraic geometry which implies that quantifier elimination is possible over real closed fields. This means that for

every system of polynomial equations and inequalities that can described using logical quantifiers, there is an equivalent system without the quantifiers.

To state the result, we use the following notation, where R is a real closed field and $a \in R$.

$$\text{sign}(a) = 0 \qquad\qquad \text{if } a = 0$$
$$\text{sign}(a) = 1 \qquad\qquad \text{if } a > 0$$
$$\text{sign}(a) = -1 \qquad\qquad \text{if } a < 0$$

Lemma 4.2.2 (Tarski-Seidenberg's Theorem, 1.4.2 from [29]). *Let $f_i(X,Y) = h_{i,m_i}(Y)X^{m_i} + \cdots + h_{i,0}(Y)$ for $i = 1,\ldots,s$ be a sequence of polynomials in $n+1$ variables with coefficients in $\mathbb{Z}$, where $Y = (Y_1,\ldots,Y_n)$. Let ε be a function from $\{1,\ldots,s\}$ to $\{-1,0,1\}$. Then there exists a boolean combination $\mathscr{B}(Y)$ (i.e. a finite composition of disjunctions, conjunctions and negations) of polynomial equations and inequalities in the variables Y with coefficients in $\mathbb{Z}$ such that for every real closed field R and for every $y \in R^n$, the system*

$$\begin{cases} sign(f_1(X,y)) = \varepsilon(1) \\ \qquad\qquad \vdots \\ sign(f_s(X,y)) = \varepsilon(s) \end{cases}$$

has a solution x in R if and only if $\mathscr{B}(y)$ holds true in R.

The second result gives an isomorphism of homology groups of a variety and its restriction to the closed subfield of real algebraic numbers over $\mathbb{Q}$.

Lemma 4.2.3 (Theorem 4.2 from [71]). *Let $R \subset \tilde{R}$ be an inclusion of real closed fields. Let $\tilde{X} \subset \tilde{R}^n$ be a semialgebraic set and $X = \tilde{X} \cap R^n$. Then there are canonical isomorphisms*

$$H_q(X) \cong H_q(\tilde{X}),$$

$$H^q(X) \cong H^q(\tilde{X}).$$

The proof spans the first four sections of [71] and the first-named author Delfs' thesis. Tarski-Seidenberg's theorem is used to establish a base extension functor from the category of semial-gebraic maps and spaces over R to the corresponding category for $\tilde{R}$. Using base extension, a triangulation of $\tilde{X} \subset \tilde{R}^n$ can be obtained from a triangulation of $X \subset R^n$. This establishes the desired isomorphism of homology groups.

Theorem 4.2.19. *(Algebraicity of persistent homology barcodes.) Let $f_1,\ldots,f_s$ be polynomials in $\mathbb{Q}[x_1,\ldots,x_n]$ with $X_{\mathbb{R}} = V_{\mathbb{R}}(f_1,\ldots,f_s)$. Then the values of the persistence parameter ε at which a bar in the offset filtration barcode appears or disappears are real numbers algebraic over $\mathbb{Q}$.*

Proof. Let $\mathbb{R}_{alg}$ denote the closed subfield of real algebraic numbers over $\mathbb{Q}$. Let $S_{alg} = \{(X_\varepsilon \cap \mathbb{R}_{alg}^n, \varepsilon) | \varepsilon \in [0,\infty)\}$. Then S_{alg} is a semialgebraic subset of $\mathbb{R}_{alg}^{n+1}$ in the sense of [29, Definition 2.4.1] since S_{alg} is defined by polynomial equalities and inequalities with coefficients in $\mathbb{Q}$. Let $\text{pr}_\varepsilon : S_{alg} \rightarrow \mathbb{R}_{alg}$ be the projection to ε.

Since $\mathbb{R}_{alg}$ is a closed subfield of $\mathbb{R}$, by Hardt's theorem there is a partition of $\mathbb{R}_{alg}$ into finitely many sets $I_l = [\delta_l, \varepsilon_l] \cap \mathbb{R}_{alg}$ with $\delta_l, \varepsilon_l \in \mathbb{R}_{alg}$ for $l \in \{1, \ldots, j\}$ such that $\mathrm{pr}_{\varepsilon}^{-1}(\varepsilon) = X_{\varepsilon} \cap \mathbb{R}_{alg}^n$ for all $\varepsilon \in [\delta_l, \varepsilon_l]$ are homeomorphic.

By Lemma 4.2.3, there is an isomorphism of homology groups

$$H_q(X_{\varepsilon} \cap \mathbb{R}_{alg}^n) \cong H_q(X_{\varepsilon})$$

for each q and ε. So the partition by the sets $I_l = [a_l, b_l] \cap \mathbb{R}_{alg}$ given by Hardt's theorem corresponds to a partition of $\mathbb{R}$ by intervals $\tilde{I}_l = [\delta_l, \varepsilon_l] \subset \mathbb{R}$ such that X_{ε} for all $\varepsilon \in [\delta_l, \varepsilon_l]$ with $\delta_l, \varepsilon_l \in \mathbb{R}_{alg}$ are homeomorphic. Thus $\{\delta_l\}_{l \in \{1, \ldots, j\}} \cup \{\varepsilon_l\}_{l \in \{1, \ldots, j\}} \subset \mathbb{R}_{alg}$. $\square$

Using the Offset Discriminant to Identify Points of Interest for Persistent Homology

We now discuss the bisector hypersurface (a component of the offset discriminant) in the context of persistent homology of the offset filtration. We first show how the bisector hypersurface can help identify points where homological events occur. Then we discuss the medial axis, a subset of the proper bisector locus of X, which gives information about the density of sampling required to compute the persistent homology accurately.

Consider a bar in the offset filtration barcode corresponding to the top dimension Betti number. To each such bar, there corresponds a $y \in \Delta(X)$. Informally, this y is the center of the n-dimensional hole corresponding to the bar. We illustrate with the example of the circle $x_1^2 + x_2^2 = r^2 \subset \mathbb{R}^2$ in Figure 4.18. The persistent homology of the circle has $\beta_1 = 1$ for all $\varepsilon < r$, and a real component of the offset hypersurface is a smaller circle inside the circle. When $\varepsilon = r$, the offset hypersurface is simply the point at the center of the circle, and $\beta_1 = 0$.

Theorem 4.2.20. *(Geometric interpretation of endpoints in barcode.) Let $X \subset \mathbb{R}^{n+1}$ be a hypersurface. Let $J = \{[\delta_l, \varepsilon_l] | l \in \{1, \ldots, m\}\}$ be the set of intervals in the barcode for the top dimensional Betti number β_n. Then each interval endpoint ε_l corresponds to a point $y_l \in \mathcal{O}_{\varepsilon_l}(X)$ on the bisector hypersurface $B(X, X)$ such that y_l is the limit of a sequence of centers of hyperballs contained in the complement of $\mathcal{O}_{\varepsilon}(X)$ as $\varepsilon \longrightarrow \varepsilon_l$.*

We make the following observations. First, the correspondence does not assign each interval to a unique point on the offset discriminant. Consider the persistent homology of the Trott curve. In dimension 1, there is one interval corresponding to four cycles, and we do not specify to which cycle to assign the interval. Second, we note that the set of y_l corresponding to endpoint intervals may not be 0-dimensional. For example, let X be the torus. Then the set of y_l contains a circle.

We also comment on the topology of the real algebraic varieties involved. Suppose $X \subset \mathbb{R}^2$ is a curve. Then $\mathcal{O}_{\varepsilon}$ for $\varepsilon \in (\varepsilon_l - \varepsilon', \varepsilon_l)$ will have an oval component not present in $\mathcal{O}_{\varepsilon}$ for $\varepsilon > \varepsilon_l$, so y_l is an isolated real point of $\mathcal{O}_{\varepsilon_l}$.

Proof. Fix $[\delta_l, \varepsilon_l] \in J$. Then there exists $\varepsilon' > 0$ such that $\beta_n(X_{\varepsilon_l}) < \beta_n(X_{\varepsilon})$ for all $\varepsilon \in (\varepsilon_l - \varepsilon', \varepsilon_l)$.
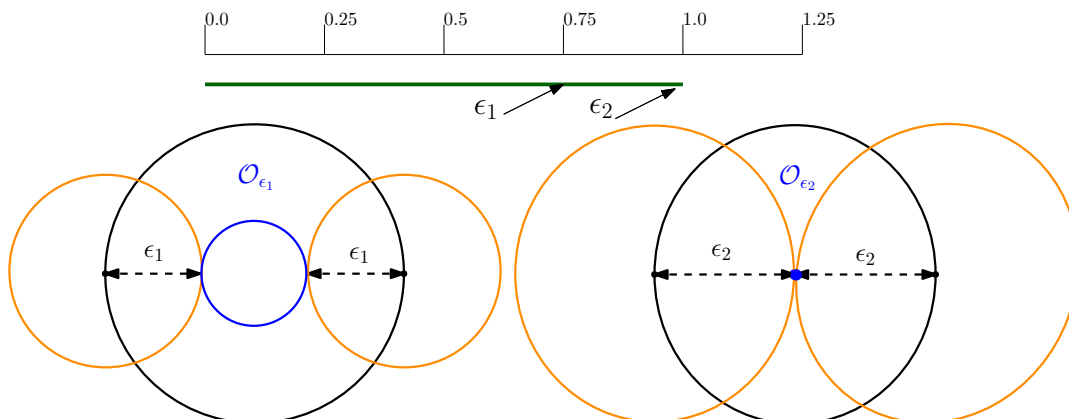
Figure 4.18: These pictures illustrate how the offset variety provides a geometric interpretation of the endpoints of a bar. The black circle is the variety X and the orange circles are ε-balls around X. When ε reaches the radius of the black circle, the blue offset hypersurface $\mathscr{O}_\varepsilon$ has an isolated real point.

Since $\beta_n(X_{\varepsilon_l}) < \beta_n(X_\varepsilon)$ for all $\varepsilon \in (\varepsilon_l - \varepsilon', \varepsilon_l)$, there is some $\varepsilon_1 \in (\varepsilon_l - \varepsilon', \varepsilon_l)$ such that there is a maximum $\delta_1 > 0$ such that there is a ball $B^{n+1}_{\delta_1}(z_{\varepsilon_1})$ such that $B^{n+1}_{\delta_1}(z_{\varepsilon_1}) \subset X_{\varepsilon_l}$ but $B^{n+1}_\delta(z_\varepsilon)$ is contained in a bounded connected component of $\mathbb{R}^{n+1} \setminus X_{\varepsilon_1}$. Furthermore, since $X_{\varepsilon_n} \supset X_{\varepsilon_{n-1}}$ for $\varepsilon_{n-1} < \varepsilon_n$, there is a monotonically increasing sequence of $\{\varepsilon_n\}_{n=1,2,\ldots}$ with $\varepsilon_1 < \varepsilon_{n-1} < \varepsilon_n < \varepsilon_l$ such that for each ε_n, there is a maximum δ_n such that there is a ball $B^{n+1}_{\delta_n}(z_{\varepsilon_n}) \subset B^{n+1}_{\delta_{n-1}}(z_{\varepsilon_{n-1}})$ with $B^{n+1}_{\delta_n}(z_{\varepsilon_n})$ contained in a bounded connected component of $\mathbb{R}^{n+1} \setminus X_\varepsilon$.

Let $\varepsilon_n \rightarrow \varepsilon_l$. The diameter of the bounded connected component of X_{ε_n} containing z_{ε_n} is less than that of $X_{\varepsilon_{n-1}}$ containing $z_{\varepsilon_{n-1}}$ for $\varepsilon_{n-1} < \varepsilon_n$ and $B^{n+1}_{\delta_1}(z_{\varepsilon_1}) \subset X_{\varepsilon_l}$, so $\delta_n \rightarrow 0$. So $\{z_{\varepsilon_n}\}$ is a Cauchy sequence in $\mathbb{R}^{n+1}$, so it converges. Let $y = \lim_{\varepsilon_n \rightarrow \varepsilon_l} z_{\varepsilon_n}$.

Since δ_n is the maximum radius of such a ball, $B^{n+1}_{\delta_n}(z_{\varepsilon_n}) \cap \mathscr{O}_{\varepsilon_n}$ contains at least two points $\{y_{1,\varepsilon_n}, y_{2,\varepsilon_n}\}$. Corresponding to these points in $\mathscr{O}_{\varepsilon_n}$ are at least two points in the offset correspondence $\mathscr{OC}_{\varepsilon_n}(X)$, say $\{(x_{1,\varepsilon_n}, y_{1,\varepsilon_n}), (x_{2,\varepsilon_n}, y_{2,\varepsilon_n})\}$.

As $\delta_n \rightarrow 0$, we have $||y_{1,\varepsilon_n} - y_{2,\varepsilon_n}|| \rightarrow 0$ since $||y_{1,\varepsilon_n} - y_{2,\varepsilon_n}|| \leq \delta_n$. Thus $y \in B(X,X)$. $\square$

Since the construction in the proof of the theorem is based on the limit of a converging sequence, the method above does not point to a new algorithm for computing barcodes or determining the reach. However, it shows how persistent homology barcodes can be studied in the algebraic geometry context of the bisector hypersurface.

Algebraicity of the Reach

The bisector hypersurface has further relevance to persistent homology because one of its components is the closure of the medial axis. The shortest distance from a manifold to its medial axis

is called the reach. The reach of a manifold is a very important quantity in the computation of its persistent homology as it determines the density of sample points required to obtain the correct homology. We now define the reach, describe its importance in the theory of persistent homology, and prove its algebraicity.

Definition 4.2.21. Let X be a real algebraic manifold in $\mathbb{R}^n$. The *medial axis* of X is the set M_X of all points $u \in \mathbb{R}^n$ such that the minimum Euclidean distance from X to u is attained by at least two distinct points in X. The *reach* $\tau(X)$ is the shortest distance between any point in the manifold X and any point in its medial axis M_X.

Observe that the closure of the medial axis is by our definition the proper bisector locus, hence the degree bound of the offset discriminant (see 4.2.15) gives upper bound on the degree of the closure of the medial axis as well.

We now state the theorem showing that sampling density depends on the reach. In particular, the smaller the reach (and thus, the curvier the manifold), the higher the density of sample points required to compute persistent homology accurately. We have adapted this from [155], where it is stated in terms of the reciprocal of a reach, a quantity which they call the condition number of the manifold.

Theorem 4.2.22 (Theorem 3.1 from [155]). *Let M be a compact submanifold of $\mathbb{R}^N$ of dimension k with reach τ. Let $\bar{x} = \{x_1, \ldots, x_n\}$ be a set of n points drawn in i.i.d fashion according to the uniform probability measure on M. Let $0 < \varepsilon < \frac{1}{2\tau}$. Let $U = \bigcup_{x \in \bar{x}} B_\varepsilon(x)$ be a corresponding random open subset of $\mathbb{R}^N$. Let $\beta_1 = \frac{vol(M)}{(\cos^k(\theta_1))vol(B_{\varepsilon/4}^k)}$ and $\beta_2 = \frac{vol(M)}{(\cos^k(\theta_2))vol(B_{\varepsilon/8}^k)}$ where $\theta_1 = \arcsin(\frac{\varepsilon\tau}{8})$ and $\theta_2 = \arcsin(\frac{\varepsilon\tau}{16})$. Then for all*

$$n > \beta_1 \left(\log(\beta_2) + \log\left(\frac{1}{\delta}\right) \right)$$

the homology of U equals the homology of M with high confidence (probability $> 1 - \delta$).

Studying a formulation for reach given by Federer with the tools of real algebraic geometry, we show the algebraicity of the reach.

Proposition 4.2.23. *(Algebraicity of reach). Let X be a real algebraic manifold in $\mathbb{R}^n$. Let $f_1, \ldots, f_s \in \mathbb{Q}[x_1, \ldots, x_n]$ with $X_\mathbb{R} = V_\mathbb{R}(f_1, \ldots, f_s)$. Then the reach of X is an algebraic number over $\mathbb{Q}$.*

Proof. Federer [97, Theorem 4.18] gives a formula for the reach τ of a manifold X in terms of points and their tangent spaces:

$$\tau(X) = \inf_{v \neq u \in X} \frac{||u - v||^2}{2\delta}, \quad \text{where } \delta = \min_{x \in T_vX} ||(u - v) - x||. \tag{4.27}$$

Equation 4.27 gives the following system of polynomial inequalities with rational coefficients

$$\begin{cases} x \in \mathrm{T}_v X \\ \delta^2 = \|(u-v)-x\|^2 \\ \delta > 0 \\ 2\delta\tau = \|u-v\|^2 \end{cases}$$

in unknowns $\{x, \delta, \tau, u, v\}$. This defines a semialgebraic set in $\mathbb{R}^{3n+2}$ in the sense of [29, Definition 2.4.1]. Consider the projection on to $\mathbb{R}^2$ with coordinates (δ, τ). By Tarski-Seidenberg's theorem ([29, Theorem 1.4.2]), the image is a semialgebraic set S.

Project S onto $\mathbb{R}$ with coordinate δ. The minimum δ_0 is attained in the closure of the image. Then $\overline{S} \cap \{\delta = \delta_0\} \subset \mathbb{R}$ is semialgebraic over $\mathbb{Q}$. It is bounded below by 0. The reach is the infimum of this set, and thus is an algebraic number over $\mathbb{Q}$.   □

4.3   Voronoi Cells in Metric Algebraic Geometry of Plane Curves

Metric algebraic geometry addresses questions about real algebraic varieties involving distances. For example, given a point x on a real plane algebraic curve $X \subset \mathbb{R}^2$, we may ask for the locus of points which are closer to x than to any other point of X. This is called the *Voronoi cell of X at x*, as defined in Section 2.1. The boundary of a Voronoi cell consists of points which have more than one nearest point to X. So we may ask, given a point in $\mathbb{R}^2$, how close must it be to X in order to have a unique nearest point on X? This quantity is called the *reach*, and was first defined by [97].

We use Voronoi cells to study metric features of plane curves. The following theorem makes precise the idea behind Figures 4.19 and 4.20.

Theorem 4.3.1. *Let X be a compact algebraic curve in $\mathbb{R}^2$ and $\{A_\varepsilon\}_{\varepsilon \searrow 0}$ be a sequence of finite subsets of X containing all singular points of X such that every point of X is within distance ε of some point in A_ε.*

1. *Every Voronoi cell is the Wijsman limit (see Definition 4.3.12) of a sequence of Voronoi cells of $\{A_\varepsilon\}_{\varepsilon \searrow 0}$.*

2. *If X is not tangent to any circle in four or more points, then every maximal Delaunay cell is the Hausdorff limit (see Definition 4.3.11) of a sequence of Delaunay cells of $\{A_\varepsilon\}_{\varepsilon \searrow 0}$.*

Voronoi diagrams of finite point sets are widely studied and have seen applications across science and technology, most notably in the natural sciences, health, engineering, informatics, civics and city planning. For example in Victoria, a state in Australia, students are typically assigned to the school to which they live closest. Thus, the catchment zones for schools are given by a Voronoi diagram [183]. Metric features of varieties, such as the medial axis and curvature of a point, can be detected from the Voronoi cells of points sampled densely from a variety. Computational geometers frequently use Voronoi diagrams to approximate these features and reconstruct varieties [6, 33, 34].
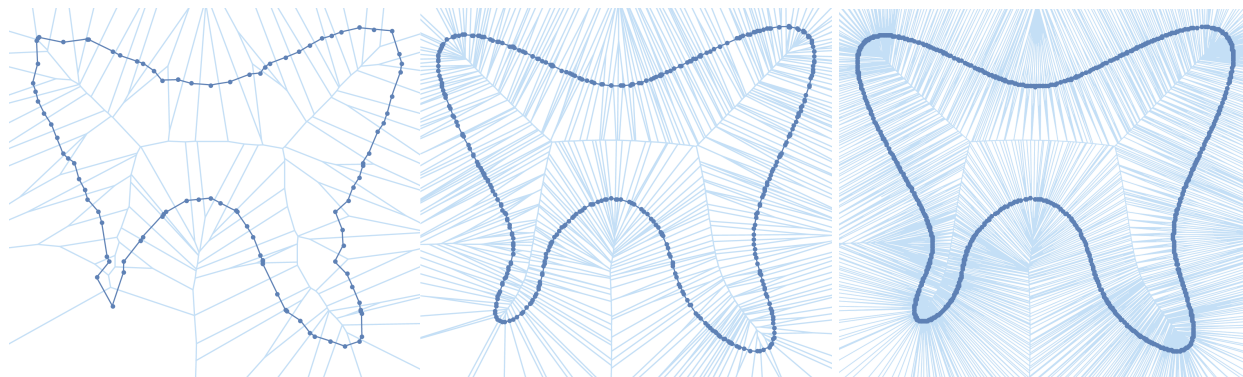
Figure 4.19: Voronoi cells of 101, 441, and 1179 points sampled from the butterfly curve 4.29.
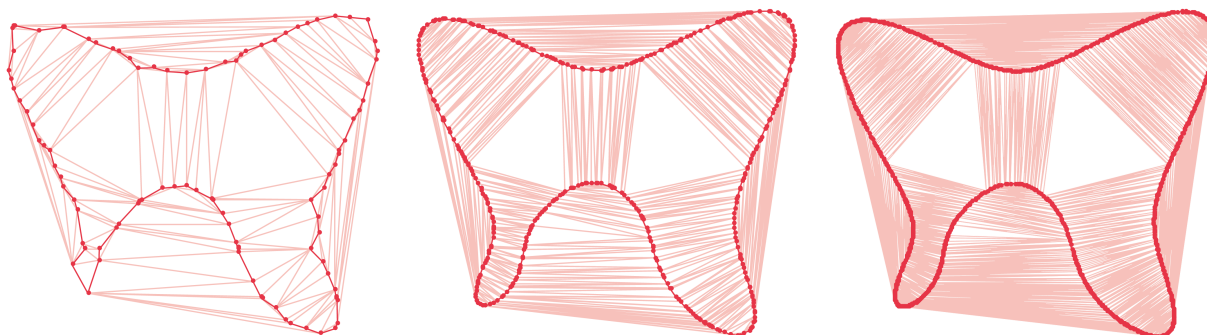

Figure 4.20: Delaunay cells of 101, 441, and 1179 points sampled from the butterfly curve 4.29. The two large triangles correspond to tritangent circles of the curve.

The reach of an algebraic variety, as discussed in the Introduction, is an invariant that is important in applications of algebraic topology to data science.The *medial axis* of a variety is the locus of points which have more than one nearest point on X. This gives the following definition of the reach.

Definition 4.3.2. The *reach* $\tau(X)$ of an algebraic variety $X \subset \mathbb{R}^n$ is the minimum distance from any point on X to a point on the medial axis of X.

The paper [1] describes how the reach is the minimum of two quantities. We have

$$\tau(X) = \min\left\{q, \frac{\rho}{2}\right\}, \tag{4.28}$$

where q is the minimum radius of curvature of points in X and ρ is the narrowest bottleneck distance. An example is depicted in Figure 4.21.
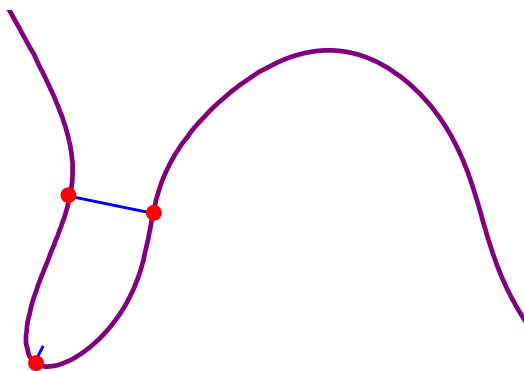
Figure 4.21: The reach of the butterfly curve is attained by the maximal curvature point in the lower left wing. The narrowest bottleneck is also shown. This figure is explained in Example 4.3.30.

This section is organized as follows. We begin with a systematic treatment in of convergence of Voronoi cells of increasingly dense point samples of a variety. This gives the proof of Theorem 4.3.1, split among Theorems 4.3.15 and 4.3.17, as well as Proposition 4.3.20, which treats the singular case separately. Theorem 4.3.1 is robust because it is not affected by the distribution of the point sample. Theorem 4.3.1 provides the theoretical foundations for estimating metric features of a variety from a point sample. We do this for the medial axis, curvature, evolute, bottlenecks, and reach. For each of these metric features, we first give defining equations and where possible a formula for the degree. We then turn our attention to detecting information about a real plane curve X from its Voronoi cells. For each metric feature, we state a theoretical result about how to detect the feature from the Voronoi cells of X or a subset of X. Corollaries to Theorem 4.3.1 provide convergence results for these features. The overall aim is to give a path to compute the metric features of a plane algebraic curve X from Voronoi cells of dense point samples of X. We use the *butterfly curve*

$$b(x,y) = x^4 - x^2y^2 + y^4 - 4x^2 - 2y^2 - x - 4y + 1 \tag{4.29}$$

in our examples. In computational geometry and data science, these problems are often considered when there is noise in the sample. We assume that our samples lie precisely on the curve X.

Voronoi and Delaunay Cells of Varieties and Their Limits

Let $X \subset \mathbb{R}^n$ be a real algebraic variety, and let $d(x,y)$ denote the Euclidean distance between two points $x, y \in \mathbb{R}^n$.

Definition 4.3.3. The *Voronoi cell of $x \in X$* is

$$Vor_X(x) = \{y \in \mathbb{R}^n \mid d(y,x) \leq d(y,x') \text{ for all } x' \in X\}.$$

An example of a Voronoi cell is given in Figure 4.22. This is a convex semialgebraic set whose dimension is equal to *codim*(X) so long as x is a smooth point of X. It is contained in the *normal space to X at x*:

$$N_X(x) = \{u \in \mathbb{R}^n \mid u - x \text{ is perpendicular to the tangent space of } X \text{ at } x\}.$$

The topological boundary of the Voronoi cell $Vor_X(x)$ consists of the points in $\mathbb{R}^n$ that have two or more closest points in X, one of which is x. The collection of boundaries of Voronoi cells is described as follows.

Definition 4.3.4. The *medial axis* $M(X)$ of an algebraic variety $X \subset \mathbb{R}^n$ is the collection of points in $\mathbb{R}^n$ that have two or more closest points in X. An example of the medial axis is given in Figure 4.22.

Let $B(p,r)$ denote the open disc with center $p \in \mathbb{R}^n$ and radius $r > 0$. We say this disc is *inscribed* with respect to X if $X \cap B(p,r) = \emptyset$ and we say it is *maximally inscribed* if no disc containing $B(p,r)$ shares this property. Each inscribed disc gives a Delaunay cell, defined as follows.

Definition 4.3.5. Given an inscribed disc B of an algebraic variety $X \subset \mathbb{R}^n$, the *Delaunay cell* $Del_X(B)$ is $conv(\overline{B} \cap X)$. An example of a Delaunay cell and the corresponding maximally inscribed disc is given in Figure 4.22.
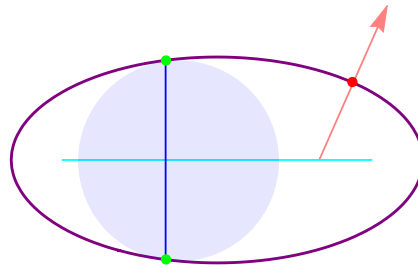

Figure 4.22: The ellipse $(x/2)^2 + y^2 - 1 = 0$ is shown in purple. The Voronoi cell of the red point $(\sqrt{7}/2, 3/4)$ is shown in pink. It is a ray starting at the point $(3\sqrt{7}/8, 0)$ in the direction $(\sqrt{7}/4, 3/2)$. The dark blue line segment between the points $(-1/2, \sqrt{15}/4)$ and $(-1/2, -\sqrt{15}/4)$ is a Delaunay cell defined by the light blue maximally inscribed circle with center $(-3/8, 0)$ and radius $\sqrt{61}/8$. The light blue line is the medial axis, which goes from $(-3/2, 0)$ to $(3/2, 0)$ because the curvature at the points $(-2, 0)$ and $(2, 0)$ is 2.

Remark 4.3.6. For plane curves, the collection of centers of all inscribed spheres which give maximal Delaunay cells (Delaunay cells which are not contained in any other Delaunay cell) is the Euclidean closure of the medial axis. Points of a plane algebraic curve X which are themselves

maximal Delaunay cells are points of X with locally maximal curvature. In this case, the maximally inscribed circle is an *osculating circle*, see Definition 3.1.1.

We now describe two convex sets whose face structures encode the Delaunay and Voronoi cells of X. We embed $\mathbb{R}^n$ in $\mathbb{R}^{n+1}$ by adding a coordinate. We usually imagine that this last coordinate points vertically upwards. So, we say that $x \in \mathbb{R}^{n+1}$ is below $y \in \mathbb{R}^{n+1}$ if $x_{n+1} \leq y_{n+1}$ and all other coordinates are the same. Let

$$U = \{x \in \mathbb{R}^{n+1} \mid x_{n+1} = x_1^2 + \cdots + x_n^2\}$$

be the *standard paraboloid* in $\mathbb{R}^{n+1}$. If $p \in \mathbb{R}^n$, then let $p_U = (p, \|p\|^2)$ denote its lift to U.

Given a convex set $C \subset \mathbb{R}^{n+1}$, a convex subset $F \subset C$ is called a *face* of C if for every $x \in F$ and every $y, z \in C$ such that $x \in conv(y,z)$, we have that $y, z \in F$. We say that a face F is *exposed* if there exists an *exposing hyperplane* H such that C is contained in one closed half space of the hyperplane and such that $F = C \cap H$. We call an exposed face F a *lower exposed face* of C if the exposing hyperplane lies below C.

Definition 4.3.7. The *Delaunay lift of an algebraic variety* $X \subset \mathbb{R}^n$ is the convex set

$$P_X^* = conv(x_u \mid x \in X) + \{(0, \ldots, 0, \lambda) \ : \ \lambda \in \mathbb{R}_{\geq 0}\} \subset \mathbb{R}^{n+1},$$

where we recall that $x_u = (x, \|x\|^2)$ and use $+$ to denote the Minkowski sum. The Delaunay lift of the butterfly curve is shown in Figure 4.23.
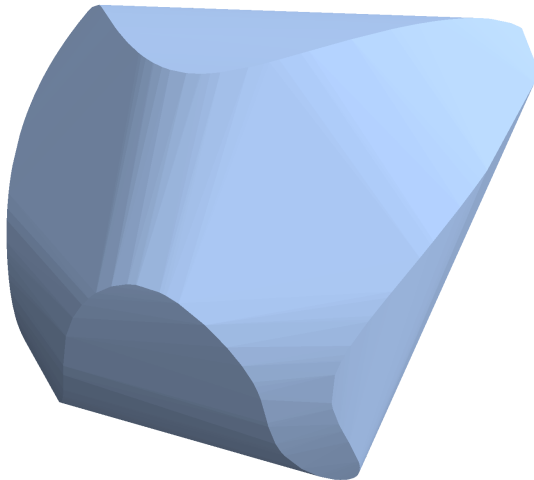

Figure 4.23: The Delaunay lift (Definition 4.3.7) of the butterfly curve, viewed from below.
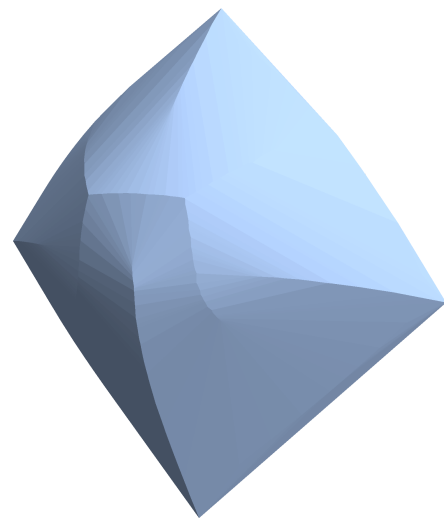
Figure 4.24: The Voronoi lift (Definition 4.3.9) of the butterfly curve, viewed from below.

We now study how the lower exposed faces of the Delaunay lift P_X^* project to $conv(X)$, and give the Delaunay cells of X.

Proposition 4.3.8. *Let $X \subset \mathbb{R}^n$ be an algebraic variety. Let $\pi : \mathbb{R}^{n+1} \to \mathbb{R}^n$ be the projection onto the first n coordinates. A subset $F \subset P_X^*$ is a lower exposed face if and only if $\pi(F)$ is a Delaunay cell of X. Furthermore, if H_F is the hyperplane exposing F, then $\pi(U \cap H_F)$ is an inscribed sphere of X and $\pi(F) = Del_X(\pi(U \cap H_F))$.*

Proof. The map from $\mathbb{R}^n \to \mathbb{R}^{n+1}$ defined by $x \mapsto x_U = (x, ||x||^2)$ lifts every sphere in $\mathbb{R}^n$ to the intersection of a hyperplane H with U [126, Proposition 7.17]. Moreover, the projection of the intersection of any hyperplane with U gives a sphere in $\mathbb{R}^n$ [126, Proposition 7.17].

Given a Delaunay cell $\text{Del}_X(B)$ for some inscribed sphere B, we have that P_X^* lies above the corresponding hyperplane H. This is because any points below H would project to points in X lying inside of B, contradicting the condition that $X \cap B = \emptyset$ for an inscribed disc B. So, H is the exposing hyperplane of the face $(Del_X(B))_U$.

Suppose $F \subset P_X^*$ is a lower exposed face with exposing hyperplane H_F. The interior of the sphere $\pi(H_F \cap U)$ contains no points of X, because if it did contain a point x, then x_U would lie in the lower half-space of H_F, which does not intersect P_X^*. Then $\pi(H_F \cap U)$ is the inscribed disc corresponding to a Delaunay cell.

Since $\pi(H_F \cap U)$ is a sphere, we have $\text{Del}_X(\pi(U \cap H_F)) = conv(\pi(U \cap H_F) \cap X)$. Let X_U denote the lift of X to $\mathbb{R}^{n+1}$. Then $\pi(U \cap H_F) \cap X = \pi(U \cap H_F \cap X_U) = \pi(H_F \cap X_U)$, and so $\text{Del}_X(\pi(U \cap H_F)) = conv(\pi(H_F \cap X_U)) = \pi(conv(H_F \cap X_U)) = \pi(F)$. $\square$

We may define a convex set whose faces project down to the Voronoi cells as follows. For any point $x \in X$, let $T(x)$ denote the plane in $\mathbb{R}^{n+1}$ through $x_U = (x, ||x||^2)$ tangent to the paraboloid U. Let $T(x)^+$ be the closed half-space consisting of all points in $\mathbb{R}^{n+1}$ lying above the plane $T(x)$.

Definition 4.3.9. The *Voronoi lift of an algebraic variety* $X \subset \mathbb{R}^n$ is the convex set $P_X = \cap_{x \in X} T(x)^+$. The Voronoi lift of the butterfly curve is shown in Figure 4.24.

The lower exposed faces of the Voronoi lift P_X project to Voronoi cells of X, as we now show.

Proposition 4.3.10. *Let $X \subset \mathbb{R}^n$ be an algebraic variety. Let $\pi : \mathbb{R}^{n+1} \to \mathbb{R}^n$ be the projection onto the first n coordinates. A subset F of the Voronoi lift P_X is an exposed face of P_X if and only if $\pi(F)$ is a Voronoi cell of X. Furthermore, if H_F is the hyperplane exposing F and $H_F \cap U \neq \emptyset$, then $H_F \cap U$ is a point and $\pi(F) = Vor_X(\pi(U \cap H_F))$.*

Proof. For some point $x \in X$, consider $P_X \cap T(x)$. Let $p \in \mathbb{R}^n$. There exists $p'_U \in T(x)$ with $\pi(p_U) = \pi(p'_U)$. The distance from p_U to the point p'_U is the distance $d_{\mathbb{R}^n}(\pi(p), \pi(x))$ [126, Lemma 6.11]. Therefore, $P_X \cap T(x)$ consists of those points p'_U for which the distance $d_{\mathbb{R}^n}(p, x)$ is minimal over all $x \in X$. In other words, $\pi(P_X \cap T(x)) = Vor_X(x)$.

Suppose $F \subset P_X$ is an exposed face with exposing hyperplane H_F such that $H_F \cap U \neq \emptyset$. Let $p \in H_F \cap U$. Since $U \subset P_X$ we have that $p \in P_X$. Then, $p \in F = H_F \cap P_X$. This implies H_F is the tangent hyperplane to U at the point p, so in particular, $p = U \cap H_F$. Since p is on the boundary

of P_x, we have $\pi(p) \in X$ and $T(\pi(p)) = H_F$. We have $\pi(F) = \pi(P_X \cap T(\pi(p))) = Vor_X(\pi(p)) = Vor_X(\pi(U \cap H_F))$, where in the second equality we use the result in the preceding paragraph. $\square$

There is a sense in which the Voronoi lift P_X and the Delaunay lift P_X^* are dual. We now describe this relationship. Suppose that X is not contained in any proper linear subspace of $\mathbb{R}^n$. This implies that P_X is pointed, meaning it does not contain a line. Therefore, it is projectively equivalent to a compact set [126, Theorem 3.36]. Embed $\mathbb{R}^{n+1}$ into $\mathbb{P}^{n+1}$ by the map

$$\iota(x_1, \ldots, x_{n+1}) = (1 : x_1 : \cdots : x_{n+1}).$$

Let l be the transformation of $\mathbb{P}^{n+1}$ defined by the following $(n+2) \times (n+2)$ matrix

$$\begin{bmatrix} 1 & 0 & \cdots & 0 & 1 \\ 0 & 2 & 0 & \cdots & 0 \\ \vdots & 0 & \ddots & 0 & \vdots \\ 0 & \cdots & 0 & 2 & 0 \\ -1 & 0 & \cdots & 0 & 1 \end{bmatrix}.$$

Then by [126, Lemma 7.1] the projective transformation l maps U to the sphere $S \subset \mathbb{R}^{n+1}$. The tangential hyperplane at the north pole $(1 : 0 : \cdots : 0 : 1)$ is the image of the hyperplane at infinity. Moreover, the topological closure of $l(P_X)$ is a compact convex body so long as the origin is in the interior of P_X^*. In this case, we call the convex body $l(P_X)$ the *Voronoi body*. The Voronoi body is full dimensional and contains the origin in its interior. Its polar dual

$$l(P_X)^\circ := \left\{ y \in \mathbb{R}^{n+1} : \sum_{i=1}^n x_i y_i \leq 1 \text{ for all } x \in p(P_X) \right\}$$

is also full dimensional and has the origin in its interior. If we apply l^{-1} to $l(P_X)^\circ$ we obtain an unbounded polyhedron, which is exactly the Delaunay lift P_X^* of X. For more details, see [126].

We now study convergence of Voronoi and Delaunay cells. More precisely, given a real algebraic curve X and a sequence of samplings $A_N \subset X$ with $|A_N| = N$, we show that Voronoi (or Delaunay) cells from the Voronoi (or Delaunay) cells of the A_N limit to Voronoi (or Delaunay) cells of X. We begin by introducing two notions of convergence which describe the limits.

The *Hausdorff distance* of two compact sets B_1 and B_2 in $\mathbb{R}^n$ is defined as

$$d_h(B_1, B_2) := \sup \left\{ \sup_{x \in B_1} \inf_{y \in B_2} d(x,y), \sup_{y \in B_2} \inf_{x \in B_1} d(x,y) \right\}.$$

More intuitively, we can define this distance as follows. If an adversary gets to put your ice cream on either set B_1 or B_2 with the goal of making you go as far as possible, and you get to pick your starting place in the opposite set, then $d_h(B_1, B_2)$ is the farthest the adversary could make you walk in order for you to reach your ice cream.

Definition 4.3.11. A sequence $\{B_v\}_{v\in\mathbb{N}}$ of compact sets is *Hausdorff convergent* to B if $d_h(B,B_v) \to 0$ as $v \to \infty$. Given a point $x \in \mathbb{R}^n$ and a closed set $B \subset \mathbb{R}^n$, define

$$d_w(x,B) = \inf_{b\in B} d(x,b).$$

Definition 4.3.12. A sequence $\{B_v\}_{v\in\mathbb{N}}$ of compact sets is *Wijsman convergent* to B if for every $x \in \mathbb{R}^n$, we have that

$$d_w(x,B_v) \to d_w(x,B).$$

An ε-*approximation* of a real algebraic variety X is a discrete subset $A_\varepsilon \subset X$ such that for all $y \in X$ there exists an $x \in A_\varepsilon$ so that $d(y,x) \leq \varepsilon$. By definition, when X is compact a sequence of ε-approximations is Hausdorff convergent to X, and for all X, a sequence of ε-approximations is Wijsman convergent to X. We use Wijsman convergence as a variation of Hausdorff convergence which is well suited for unbounded sets. Delaunay cells are always compact, while Voronoi cells may be unbounded.

We now study convergence of Delaunay cells of X, and introduce a condition on real algebraic varieties which ensures that the Delaunay cells are simplices.

Definition 4.3.13. We say that an algebraic variety $X \subset \mathbb{R}^n$ is *Delaunay-generic* if X does not meet any d-dimensional inscribed sphere at greater than $d+2$ points.

Example 4.3.14. The standard paraboloid U in any dimension $n+2$ is not Delaunay-generic because it contains n-spheres.

Although the focus of this work is on algebraic curves in $\mathbb{R}^2$, we state the following theorem for curves in $\mathbb{R}^n$ because the proof holds at this level of generality.

Theorem 4.3.15. *Let $X \subset \mathbb{R}^n$ be a Delaunay-generic compact algebraic curve, and let $\{A_\varepsilon\}_{\varepsilon\searrow 0}$ be a sequence of ε-approximations of X. Every maximal Delaunay cell is the Hausdorff limit of a sequence of Delaunay cells of A_ε.*

Proof. Consider a sequence $\{A_\varepsilon\}_{\varepsilon\searrow 0}$ of ε-approximations of X, where $\varepsilon \searrow 0$ indicates a decreasing sequence of positive real numbers ε_v for $v \in \mathbb{N}$. We will study the convex sets $P^*_{A_\varepsilon} = conv(a_U \mid a \in A_\varepsilon)$, where $a \mapsto a_U = (a,||a||^2)$ lifts a to the paraboloid U. The lower faces of $P^*_{A_\varepsilon}$ project to Delaunay cells of A_ε [126, Theorem 6.12, Theorem 7.7].

We now apply [61, Theorem 3.5] to our situation. This result says the following. Let C be a curve and B_ε be a sequence of ε-approximations of C. Suppose every point on C which is contained in the boundary of $conv(C)$ is an extremal point of $conv(C)$, meaning it is not contained in the open line segment joining any two points of $conv(C)$. Let F be a simplicial face of $conv(C)$ which is an exposed face of $conv(C)$ with a unique exposing hyperplane. Then F is the Hausdorff limit of a sequence of facets of $conv(B_\varepsilon)$. We apply this result in the case when $C = X_U = \{x_U \in \mathbb{R}^{n+1} \mid x \in X\}$ and $B_\varepsilon = (A_\varepsilon)_U = \{a_U \in \mathbb{R}^{n+1} \mid a \in A_\varepsilon\}$.

Since every point on U is extremal in $conv(U)$ and $conv(X_U) \subset conv(U)$, every point on X_U which is contained in the boundary of $conv(X_U)$ is also extremal in $conv(X_U)$. A maximal Delaunay

cell of X is a simplex because X is Delaunay-generic. Consider a maximal Delaunay cell of X which is not a vertex. It has a unique description as $Del_X(B)$ for a disc B. Proposition 4.3.8 establishes a one-to-one correspondence between such Delaunay cells and lower exposed faces of P_X^*, which are uniquely exposed by the hyperplane containing $(\partial \overline{B})_U$. In this case, [61, Theorem 3.5] holds, so the result is proved.

If a maximal Delaunay cell is a vertex, then it is a point $x \in X$. It is then also an extremal point of $conv(X_U)$. Since $conv(B_\varepsilon)$ is sequence of compact convex sets converging in the Hausdorff sense to P_X^*, by [61, Lemma 3.1] there exists a sequence of points of B_ε which are extremal points of $conv(B_\varepsilon)$ converging to x_U. So, their projections are Delaunay cells of A_ε converging to x, since every point in a finite point set is a Delaunay cell of that point set. □

We will now study limits of Voronoi cells, using results from [33], which studies convergence of Voronoi cells of *r-nice sets* (for a definition, see [33, 119]). In the plane, these are open sets whose boundary satisfies some properties. In particular, open sets whose boundaries are an algebraic curve with positive reach r satisfy the r-nice condition. For plane curves, having positive reach is equivalent to being smooth.

To study continuity and convergence of closed sets in the plane, J.W. Brandt uses the *hit-miss topology* [144, Section 1.2] $\mathscr{F}$ on closed subsets of the plane.

Definition 4.3.16. In the hit-miss topology, a sequence $\{F_n\}$ *converges* to F if and only if

1. for any $p \in F$, there is a sequence $p_n \in F_n$ such that $p_n \to p$; and

2. if there exists a subsequence $p_{n_k} \in F_{n_k}$ converging to a point p, then $p \in F$.

Then, to determine if a function with range in $\mathscr{F}$ is continuous, we need to examine the above conditions for sequences of sets obtained by applying the function to countable convergent sequences in $\mathbb{R}^2$. If all such sequences satisfy (1) then the function is *upper-semicontinuous*. If all such sequences satisfy (2) then it is *lower-semicontinuous*. If a function satisfies both then it is continuous.

Lemma 4.3.1. *Let $X \subset \mathbb{R}^2$ be a smooth plane algebraic curve. Then the function $Vor_X : X \to \mathscr{F}$ sending $x \mapsto Vor_X(x)$ is continuous in the hit-miss topology.*

Proof. By [33, Theorem 2.2], the Voronoi function $Vor_X : X \to \mathscr{F}$ is lower semicontinuous. By [33, Theorem 3.2], if the curve is C^2 and the *skeleton* (locus of centers of maximally inscribed discs) is closed, then the Voronoi function is continuous. A smooth algebraic curve is C^2. The skeleton is closed because a smooth curve satisfies the r-nice condition, and r-nice curves have closed skeletons [33]. □

By [144, 10], convergence in the hit-miss topology is equivalent to Wijsman convergence. In what follows, we rephrase the results from [33] in the setting of Wijsman convergence of Voronoi cells of plane curves, and extend it to singular curves.

Theorem 4.3.17. *Let X be a compact smooth algebraic curve in $\mathbb{R}^2$ and $\{A_\varepsilon\}_{\varepsilon \searrow 0}$ be a sequence of ε-approximations of X. Every Voronoi cell is the Wijsman limit of a sequence of Voronoi cells of A_ε.*

Proof. By Lemma 4.3.1, the function $Vor_X : X \to \mathscr{F}$ is continuous. Theorem 3.1 from [33] states that in this case, if x_ε is a sequence such that $x_\varepsilon \in A_\varepsilon$ and $x_\varepsilon \to x$, then $Vor_{A_\varepsilon}(x_\varepsilon) \to Vor_X(x)$. Such a sequence must exist because for all $y \in X$, there exists a $y_\varepsilon \in A_\varepsilon$ such that $d(y, y_\varepsilon) \le \varepsilon$. $\square$

We now investigate the structure of Voronoi cells of different types of singular points. In Figure 4.25, we give four examples of Proposition 4.3.18. First, we need a glueing lemma.

Lemma 4.3.2. *Let C and D be subsets of $\mathbb{R}^2$ containing a point $p \in C \cap D$. Then*

$$Vor_{C \cup D}(p) = Vor_C(p) \cap Vor_D(p).$$

Proof. A point $x \in Vor_{C \cup D}(p)$ is closer to p than it is to any other point of C or D. On the other hand, a point in $Vor_C(p) \cap Vor_D(p)$ is closer to p than it is to any other point of C or D. $\square$

**Proposition 4.3.18.** *Let $X \subset \mathbb{R}^2$ be a real plane algebraic curve and p be a singular point.*

1. *If p is an isolated point, its Voronoi cell is 2-dimensional;*

2. *If p is a node, then its Voronoi cell is 0-dimensional and equal to p;*

3. *If p is a tacnode, then its Voronoi cell is 1-dimensional.*

Proof.

1. Suppose p is an isolated point. Then there is a ball $B(p,r)$ centered at p such that the ball contains no other points of the curve X. Therefore, the ball $B(p, r/2)$ is entirely contained in $Vor_X(p)$, so it is 2-dimensional.

2. If p is a node, then we claim that the only point contained in $Vor_X(p)$ is p. At p, the curve meets in two branches which have distinct tangent directions at p. If we treat this as two separate 1-dimensional subsets X_1 and X_2 and apply Lemma 4.3.2, we see that $Vor_X(p) = Vor_{X_1}(p) \cap Vor_{X_2}(p)$. But, since p is a smooth point of X_1 and X_2, the Voronoi cells $Vor_{X_1}(p)$ and $Vor_{X_2}(p)$ are each contained in their respective normal directions, which are distinct. Therefore, $Vor_{X_1}(p) \cap Vor_{X_2}(p) = p$.

3. If p is a tacnode, then two or more osculating circles (see Definition 3.1.1) are tangent at p. We can choose $\varepsilon > 0$ so that we can separate $X \cap B(p, \varepsilon)$ into subsets $X_1, \ldots, X_n$ corresponding to the osculating circles at p such that $Vor_{X_i}(p)$ is a subset of the line from p to the center of the corresponding osculating circle. Then, we apply Lemma 4.3.2. We have $Vor_{X \cap B(p,\varepsilon)}(p) = \cap_{i=1}^n Vor_{X_i}(p)$. All of the $Vor_{X_i}(p)$ are contained in the normal line at p, so $Vor_{X \cap B(p,\varepsilon)}(p)$ is also a subset of this normal line. Since $Vor_X(p)$ is convex, and within $B(p, \varepsilon)$ the Voronoi cell is a line segment, $Vor_X(p)$ is 1-dimensional.
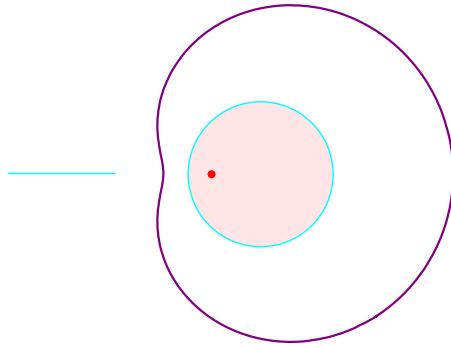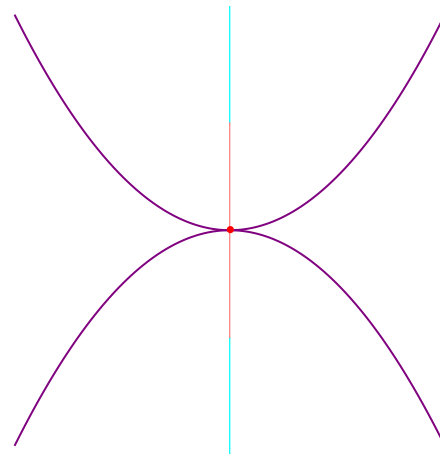
(a) $(x^2 + y^2 - x)^2 - (1.5)^2(x^2 + y^2) = 0$
An isolated singularity and its
2-dimensional Voronoi cell.
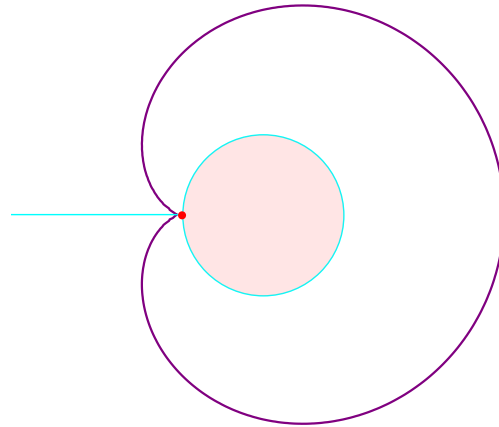
(b) $(x^2 + y^2 - x)^2 - (x^2 + y^2) = 0$
A cusp and its 2-dimensional Voronoi cell.
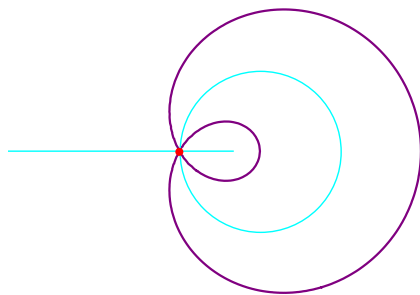
(c) $(x^2 + y^2 - x)^2 - (0.5)^2(x^2 + y^2) = 0$
A node and its 0-dimensional Voronoi cell.

(d) $x^4 - y^2 = 0$
A tacnode and its 1-dimensional Voronoi cell.

Figure 4.25: Four singular varieties with singular point $(0,0)$. In each case the medial axis is blue, the singular point is red, and its Voronoi cell is pink.

$\square$

Example 4.3.19. In this example we illustrate why Theorem 4.3.17 fails when the curve has a singular point. From this example it will be clear that the singular points must be included in the samples A_ε, and it turns out that this condition is enough to extend Theorem 4.3.17 to the singular

case.

Consider the curve defined by the equation $y^2 = x^3$. In [60, Remark 2.4] the authors give equations for the Voronoi cell of the cusp at the origin. This region is

$$Vor_{y^2=x^3}((0,0)) = \{(x,y) \in \mathbb{R}^2 \ : \ 27y^4 + 128x^3 + 72xy^2 + 32x^2 + y^2 + 2x \leq 0\}.$$

In Figure 4.26 we give three ε-approximations of the curve and the corresponding Voronoi decompositions. Let $\varepsilon = 1/n$. The points in the ε-approximation A_ε are given by:

$$A_\varepsilon = \left\{ \left(\frac{j}{n}, \pm \left(\frac{j}{n} \right)^{3/2} \right) \right\}_{j=1}^{\infty}.$$

As we can see in Figure 4.26, there is no sequence of cells converging to $Vor_{y^2=x^3}((0,0))$ because the x-axis, present due to the symmetrical nature of the sample, always divides the Voronoi cell.
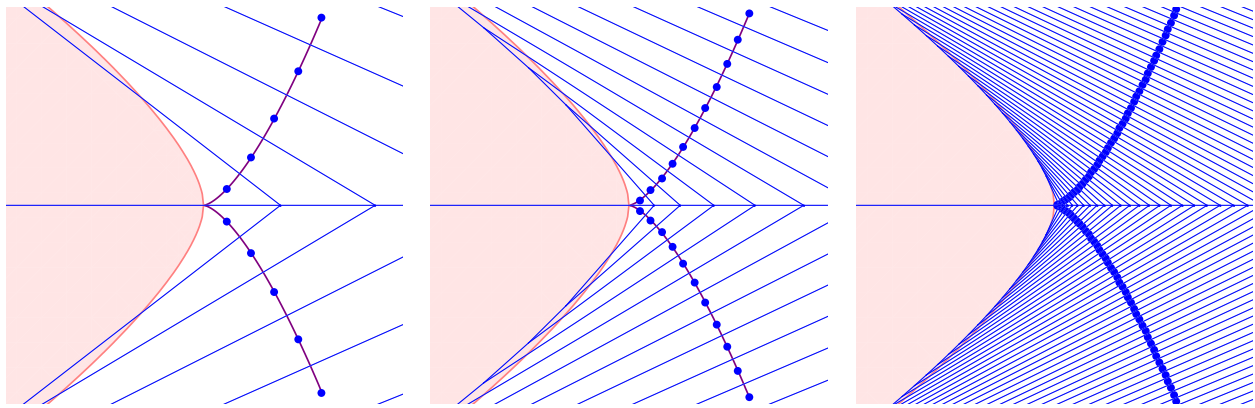

Figure 4.26: Some ε-approximations of the curve $y^2 = x^3$ and their Voronoi diagrams. The Voronoi cell of the cusp $(0,0)$ is shown in pink. This figure is discussed in Example 4.3.19.

We now are able to expand Theorem 4.3.17 to include singular varieties.

Proposition 4.3.20. *Let $X \subset \mathbb{R}^2$ be a compact smooth algebraic curve and $\{A_\varepsilon\}_{\varepsilon \searrow 0}$ a sequence of ε-approximations with the singular locus $Sing(X) \subset A_\varepsilon$ for all ε. Then every Voronoi cell of X is the Wijsman limit of a sequence of Voronoi cells of A_ε.*

Proof. By [33, Theorem 2.2], the Voronoi function is always lower-semicontinuous. So, we must show that condition (1) in Definition 4.3.16 holds. That is, we need that for all $p \in X$, there is a sequence $p_\varepsilon \in A_\varepsilon$ with $p_\varepsilon \to p$ such that for any $x \in Vor_X(p)$ there is an $x_\varepsilon \in Vor_{A_\varepsilon}(p_\varepsilon)$ with $x_\varepsilon \to x$. We distinguish the cases when p is smooth and singular.

If p is a smooth point on X, and $x \in Vor_X(p)$, there exists an ε such that x and p are both in the Voronoi cell $Vor_{A_\varepsilon}(p_\varepsilon)$ for some p_ε.

Suppose now that $p \in X$ is a singular point. We wish to show that there is a sequence of Voronoi cells converging to $Vor_X(p)$, and we take the sequence $Vor_{A_\varepsilon}(p)$. To establish convergence, it is now enough to show that for all $x \in Vor_X(p)$, there is an $x_\varepsilon \in Vor_{A_\varepsilon}(p)$ with $x_\varepsilon \to x$. Since $x \in Vor_X(p)$, we have that x is closer to p than it is to any other point in X. So, in particular, $x \in Vor_{A_\varepsilon}(p)$.

Now we have shown that for each $p \in X$, condition (1) in Definition 4.3.16 holds. Therefore, for each $p \in X$, we have sequences of Voronoi cells which are convergent to $Vor_p(X)$ in the hit-miss topology. Since convergence in the hit-miss topology and Wijsman convergence are equivalent, every Voronoi cell of X is the Wijsman limit of a sequence of Voronoi cells of the A_ε. □

This concludes the proof of Theorem 4.3.1.

Medial Axis

Let $X = V(F) \subset \mathbb{R}^2$ be a smooth plane algebraic curve. We now study the medial axis of X, as defined in Definition 4.3.4. The Zariski closure of the medial axis is an algebraic variety which has the same dimension as the medial axis. We can obtain equations in variables x, y for the ideal I of a variety containing the Zariski closure of the medial axis in the following way.

Let (s,t) and (z,w) be two points on X. Then, s, t, z, and w satisfy the equations

$$F(s,t) = 0 \text{ and } F(z,w) = 0.$$

If (x,y) is equidistant from (s,t) and (z,w) then

$$(x-s)^2 + (y-t)^2 = (x-z)^2 + (y-w)^2.$$

Furthermore, (x,y) must be a critical point of the distance function from both (s,t) and (z,w). Thus we require that the determinants of the following 2×2 augmented Jacobian matrices vanish:

$$\begin{bmatrix} x-s & y-t \\ F_s & F_t \end{bmatrix}, \quad \begin{bmatrix} x-z & y-w \\ F_z & F_w \end{bmatrix},$$

where F_s, F_t, F_z and F_w denote the partial derivatives of $F(s,t)$ and $F(z,w)$, respectively. Let

$$I = \langle F(s,t), F(z,w), (x-s)^2 + (y-t)^2 - (x-z)^2 - (y-w)^2,$$
$$(x-s)F_t - (y-t)F_t, (x-z)F_w - (y-w)F_z \rangle.$$

Then, $J = (I : (s-z, t-w)^\infty) \cap \mathbb{R}[x,y]$ is an ideal whose variety contains the Zariski closure of the medial axis.

We now study the medial axis from the perspective of Voronoi cells. It has been observed that an approximation of the medial axis arises as a subset of the Voronoi diagram of finitely many points sampled densely from a curve [74]. We now discuss theoretical results given in [33] about the convergence of medial axes. Let X be a compact smooth plane algebraic curve, and let A_ε be an ε-approximation of X. A Voronoi cell $Vor_{A_\varepsilon}(a_\varepsilon)$ for $a_\varepsilon \in A_\varepsilon$ is polyhedral, meaning it is an intersection of half-spaces.

Definition 4.3.21. For sufficiently small ε, exactly two edges of $Vor_{A_\varepsilon}(a_\varepsilon)$ will intersect X [33]. We call these edges the *long edges* of the Voronoi cell, and all other edges are called *short edges*. An example is given in Figure 4.27.
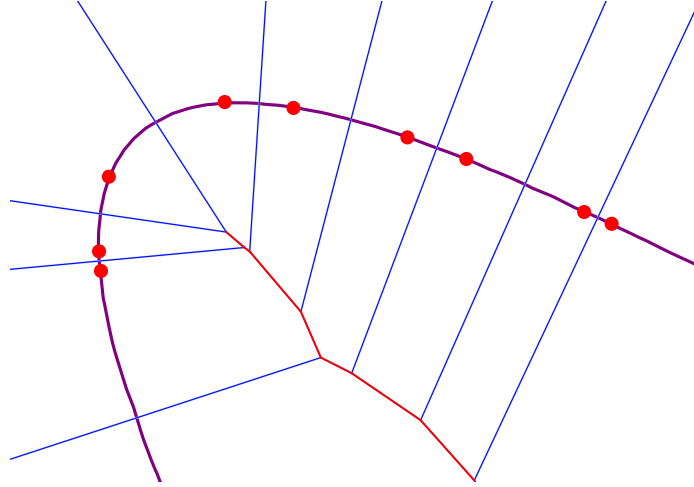

Figure 4.27: The long edges (blue) and short edges (red) of Voronoi cells of points sampled from the butterfly curve as in Definition 4.3.21.

In this case, let $\hat{S}_\varepsilon(a_\varepsilon)$ denote the union of the short edges and vertices of the Voronoi cell $Vor_{A_\varepsilon}(a_\varepsilon)$. An ε-*medial axis approximation* is the set of all short edges

$$\hat{S}_\varepsilon = \bigcup_{p \in A_\varepsilon} \hat{S}_\varepsilon(p).$$

Proposition 4.3.22. *([33, Theorem 3.4]) Let X be a compact smooth plane algebraic curve. The medial axis approximations $\hat{S}_\varepsilon$ converge to the Euclidean closure of the medial axis.*

Remark 4.3.23. The medial axis is the union of all endpoints of Voronoi cells $Vor_X(p)$ for $p \in X$. The medial axis is also the union of all centers of maximally inscribed circles of X.

The following corollary shows that the corresponding statements also hold for ε-approximations.

Corollary 4.3.24. *Let $\{A_\varepsilon\}_{\varepsilon \searrow 0}$ be a sequence of ε-approximations of a compact smooth algebraic curve $X \in \mathbb{R}^2$.*

1. *The collection of vertices of the Voronoi diagrams of the A_ε converge to the medial axis.*

2. *The collection of centers of maximally inscribed discs of the A_ε converge to the medial axis.*

Proof. This is a consequence of Theorem 4.3.15, Theorem 4.3.17, and Proposition 4.3.22. □

Example 4.3.25. In Figure 4.28 we display the centers of maximally inscribed circles, or equivalently circumcenters of the Delaunay triangles, for an ε-approximation of the butterfly curve where 898 points were sampled. In Figure 4.29 we show the short edges of Voronoi cells from an ε-approximation of the butterfly curve where 101 points were sampled.
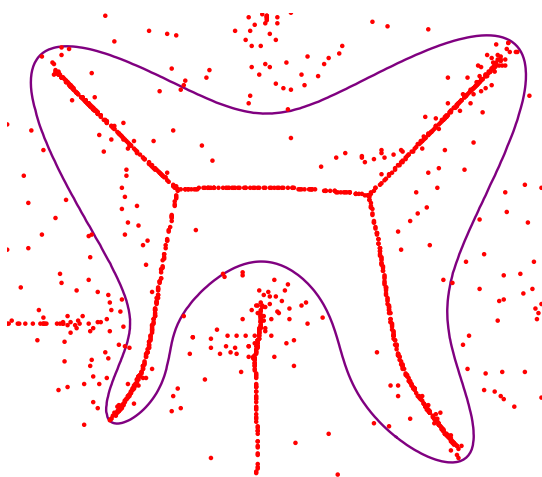

Figure 4.28: A medial axis approximation of the butterfly curve obtained from circumcenters of Delaunay triangles, which are shown in red.
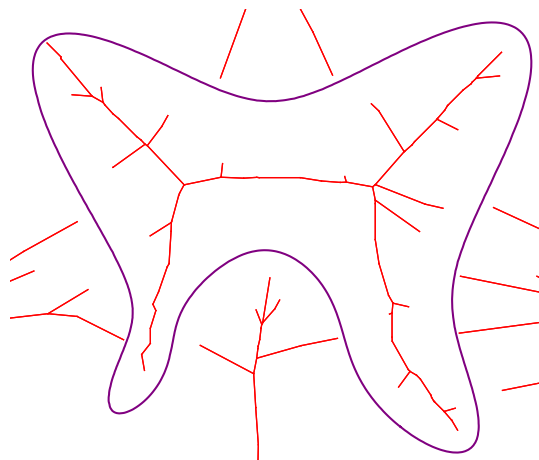
Figure 4.29: A medial axis approximation of the butterfly curve obtained from short edges of Voronoi cells, which are shown in red.

The medial axis plays an important role in applications for understanding the connected components and regions of a shape. As such, it is a very well-studied problem in computational geometry to find approximations of the medial axis from point clouds. A survey on medial axis computation is given in [13].

Curvature and the Evolute

In Section 3.1 of this dissertation, we defined and provided equations for the minimal radius of a curvature of a plane curve. We now describe how to recover the curvature at a point from the Voronoi cells of a subset of a curve X. In applications, Voronoi-based methods are used for obtaining estimates of curvature at a point. An overview of techniques for estimating curvature of a variety from a point cloud is given in [148]. Further, there are also Delaunay-based methods for estimating curvature of a surface in three dimensions [63].

Theorem 4.3.26. *Let X be a smooth plane curve of degree at least 3 and $p \in X$ a point. Let δ be less than the distance to the critical point of curvature nearest to p, and let $B(p, \delta)$ be a ball of radius δ centered at p. Then*

1. *The Voronoi cell $Vor_{X \cap B(p,\delta)}(p)$ is a ray. The distance from p to the endpoint of this ray is the radius of curvature of X at p.*

2. *Consider a sequence of ε-approximations A_ε of $X \cap B(p,\delta)$. Let a_ε be the point such that $p \in Vor_{A_\varepsilon}(a_\varepsilon)$, and let d_ε be the minimum distance from a_ε to a vertex of $Vor_{A_\varepsilon}(a_\varepsilon)$. Then, the sequence d_ε converges to the radius of curvature of X at p.*

Proof. The Voronoi cell $Vor_{X \cap B(p,\delta)}(p)$ is a subset of the line normal to $X \cap B(p,\delta)$ at p. This line has an endpoint either at the center of curvature of p or at a point where it intersects the normal space of a distinct point p' in $X \cap B(p,\delta)$. The point where the normals at p and p' intersect is contained in the Voronoi cell with respect to $X \cap B(p,\delta)$ of each of them, so in particular $X \cap B(p,\delta)$ has a nonempty medial axis. This medial axis has an endpoint which corresponds to a point of critical curvature [105]. This contradicts the constraint on δ. Therefore, the endpoint of the Voronoi cell $Vor_{X \cap B(p,\delta)}(p)$ is the center of curvature of p. This concludes the proof of (1).

For (2), we know that the sequence $Vor_{A_\varepsilon}(a_\varepsilon)$ is Wijsman convergent to $Vor_{X \cap B(p,\delta)}(p)$ by Theorem 4.3.17. Denote by V_ε the set of vertices of $Vor_{A_\varepsilon}(a_\varepsilon)$. By Corollary 4.3.24, we also have that the sets V_ε are Wijsman convergent to the endpoint of $Vor_{X \cap B(p,\delta)}(p)$, which we call p'. By the definition of Wijsman convergence, this means that for any $x \in \mathbb{R}^2$, $d_w(x, V_\varepsilon) \to d_w(x, p')$. By the definition of d_w, we have $d_w(p, V_\varepsilon) = d_\varepsilon$ and $d_w(p, p')$ is the radius of curvature of p. This concludes the second part of the proof. $\square$

The evolute E of a plane curve is the locus of all centers of curvature of the curve. Therefore, to find the evolute using Voronoi cells we may splice the curve into sections and apply Theorem 4.3.26. Let X be compact. Let $C \subset X$ denote the points of locally maximal curvature. Then $X \setminus C$ consists of finitely many components $X = X_1 \cup \cdots \cup X_n$. Let τ denote the reach of X, and cover each X_i by balls $B_{i,j}$ of radius less than τ. Let $E_{i,j}$ denote the collection of vertices of Voronoi cells of $X_i \cap B_{i,j}$. Then by Theorem 4.3.26, $E = \cup_{i,j} \overline{E_{i,j}}$. Furthermore, for ε-approximations $A_{\varepsilon,i,j}$ of $X_i \cap B_{i,j}$, the union over i, j of their Voronoi vertices will converge to E by Theorem 4.3.17.

Bottlenecks

Bottlenecks are the topic of Section 2.2 of this dissertation. We now study bottlenecks from the perspective of Voronoi cells. For a smooth point p in a algebraic curve $X \subset \mathbb{R}^2$, the Voronoi cell $Vor_X(p)$ is a 1-dimensional subset of the normal line to X at the point p. Therefore, the normal direction can be recovered from the Voronoi cell $Vor_X(p)$. For sufficiently small ε, an ε-approximation A_ε of X will have Voronoi cells whose long edges approximate the normal direction. More precisely, by Theorem 4.3.17, if $a_\varepsilon \in A_\varepsilon$ is the point such that $p \in Vor_{A_\varepsilon}(a_\varepsilon)$, then the directions of the long edges of $Vor_{A_\varepsilon}(a_\varepsilon)$ converge to the normal direction at p. We remark here that the problem of estimating normal directions from Voronoi cells is well-studied, and numerous efficient, robust algorithms exist [6, 10, 148].

Two points $x, y \in X$ form a bottleneck if their normal lines coincide. This implies that the line connecting them contains both $Vor_X(x)$ and $Vor_X(y)$.
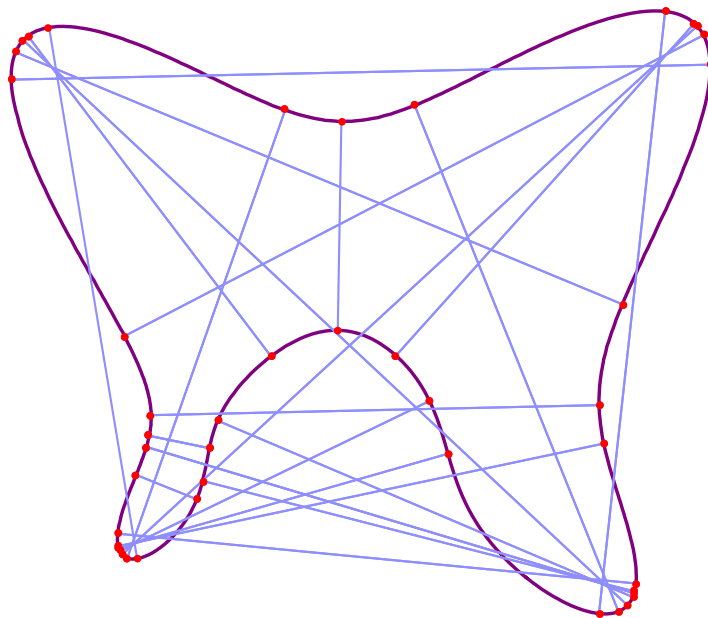
Figure 4.30: The real bottleneck pairs of the butterfly curve, computed in Example 4.3.28.

Definition 4.3.27. Let A_ε be an ε-approximation of an algebraic curve $X \subset \mathbb{R}^2$. We say a pair $x_\varepsilon, y_\varepsilon \in A_\varepsilon$ is an *approximate bottleneck reach candidate* if the line $\overline{x_\varepsilon y_\varepsilon}$ joining x_ε and y_ε meets each of $Vor_{A_\varepsilon}(x_\varepsilon)$ and $Vor_{A_\varepsilon}(y_\varepsilon)$ at short edges of those cells.

Example 4.3.28. We now compute the bottlenecks for the quartic butterfly curve $b(x,y) = 0$. The formula in 2.2 predicts that there are $192/2 = 96$ bottlenecks. Using the description above and `JuliaHomotopyContinuation` [44], we obtain the 96 bottleneck pairs. Of these, 22 are real. We show them in Figure 4.30.

In Figure 4.31, we show the approximate bottleneck reach candidates for 348 points sampled from the butterfly curve. The following result tells us that if the reach is achieved by a bottleneck pair, then this bottleneck pair is a limit of approximate bottleneck reach candidates.

Theorem 4.3.29. *Let $\{A_\varepsilon\}_{\varepsilon \searrow 0}$ be a sequence of ε-approximations of a smooth algebraic curve $X \subset \mathbb{R}^2$. If x,y is a bottleneck pair of X that achieves the reach, then there are sequences $x_\varepsilon, y_\varepsilon \in A_\varepsilon$ of approximate bottleneck reach candidates converging to x and y.*

Proof. Consider the line segment $\overline{xy}$ joining x and y. Since x and y are a bottleneck pair that achieves the reach, the midpoint of $\overline{xy}$ is on the medial axis of X. So $\overline{xy}$ intersects some short edge of two Voronoi cells $Vor_{A_\varepsilon}(x_\varepsilon)$ and $Vor_{A_\varepsilon}(y_\varepsilon)$ in a point v_ε. Then, x_ε and y_ε form an approximate bottleneck reach candidate by definition. We must then show that the sequence x_ε converges to x and the sequence y_ε converges to y.
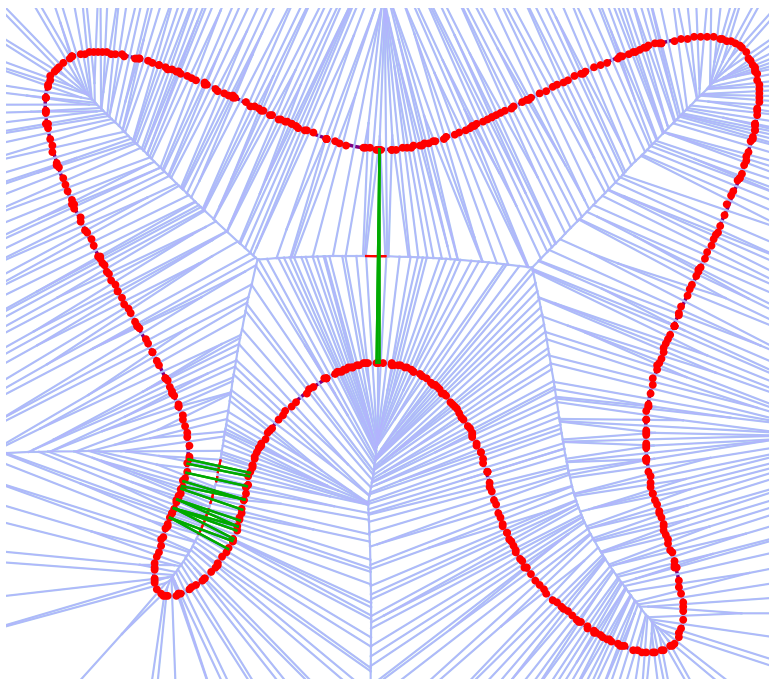
Figure 4.31: The approximate bottleneck reach candidates (see Definition 4.3.27) of 568 points sampled from the butterfly curve. The narrowest width of an approximate bottleneck reach candidate is approximately 0.495 while the true narrowest bottleneck width is approximately 0.503.

Since v_ε is in the normal space of x, there exists a neighborhood of x such that the nearest point of the intersection of this neighborhood and X to v_ε is x. So for ε smaller than the radius of this neighborhood, one of the two points in A_ε on either side of x as one moves along X must be the one whose Voronoi cell contains v_ε. Since x_ε is the point whose Voronoi cell contains v_ε, we have that x_ε is one of the two closest points in A_ε to x, meaning that $d(x,x_\varepsilon) \leq \varepsilon$. Hence, x_ε converges to x. Similarly, y_ε converges to y. $\qquad\square$

Reach

Example 4.3.30. We may find the reach of the butterfly curve by taking the minimum of half the narrowest bottleneck distance and the minimum radius of curvature. This is shown in Figure 4.21. From the computations in Example 4.3.28, we find that the narrowest bottleneck distance is approximately 0.251. Meanwhile, from Example 3.1.7, we find that the minimum radius of curvature is approximately 0.104. Therefore, the reach of the butterfly is approximately 0.104.

In previous sections, we describe how the reach is the minimum of the minimal radius of curvature and half of the narrowest bottleneck distance. We also give equations for the ideal of the bottlenecks and for the ideal of the critical points of curvature. We now give Macaulay 2 [107] code to compute these ideals for smooth algebraic curves $X \subset \mathbb{R}^2$. Finding the points in these

ideals, using for example `JuliaHomotopyContinuation` [44], and taking appropriate minimums gives the reach of X.

```
R=QQ[x_1,x_2,y_1,y_2]
f= x_1^4 - x_1^2*x_2^2 + x_2^4 - 4*x_1^2 - 2*x_2^2 - x_1 - 4*x_2 + 1
g=sub(f,{x_1=>y_1,x_2=>y_2})
augjacf=det(matrix{{x_1-y_1,x_2-y_2},{diff(x_1,f),diff(x_2,f)}})
augjacg=det(matrix{{y_1-x_1,y_2-x_2},{diff(y_1,g),diff(y_2,g)}})
bottlenecks=saturate(ideal(f,g,augjacf,augjacg),ideal(x_1-y_1,x_2-y_2))

R=QQ[x,y]
f=x^4 - x^2*y^2 + y^4 - 4*x^2 - 2*y^2 - x - 4*y + 1
num=(diff(x,f))^2 + (diff(y,f))^2
denom=-(diff(y,f))^2*diff(x,diff(x,f)) +
2*diff(x,f)*diff(y,f)*diff(y,diff(x,f)) -
(diff(x,f))^2*diff(y,diff(y,f))
crit=det(matrix({{num*diff(x,denom)- 3/2*denom*diff(x,num),
num*diff(y,denom)-3/2*denom*diff(y,num)},{diff(x,f),diff(y,f)}}))
criticalcurvature=ideal(f,crit)
```

Alternatively, one can estimate the reach from a point sample. The paper [1] provides a method to do so. We provide a substantially different method that relies upon computing Voronoi and Delaunay cells of points sampled from the curve. We have already discussed how to approximate bottlenecks and curvature using Voronoi cells. This gives the following Voronoi-based Algorithm 1 for approximating the reach of a curve.

Algorithm 1 Voronoi-Based Reach Estimation

Input: $A \subset X$ a finite set of points forming an $\varepsilon-$approximation for a compact, smooth algebraic curve $X \subset \mathbb{R}^2$.
Output: τ, an approximation of the reach.
  for $a \in A$ **do**
    Compute an estimate for the curvature ρ_a at a using a technique from [148].
  end for
  Set $\rho_{min} = \min_A(\rho_a)$.
  Set q to be the radius of any disk containing X.
  for $a,b \in A$ **do**
    if a,b form an approximate bottleneck reach candidate as in Definition 4.3.27 **then**
      Set $q = \min(q,d(a,b)/2)$
    end if
  end for
  Set $\tau = \min(q,\rho_{min})$.

The reach is equivalently defined as the minimum distance to the medial axis, which suggests the following Delaunay-based Algorithm 2 for estimating the reach. This algorithm is susceptible to sample error, and to give accurate results would require more sophisticated techniques.

Algorithm 2 Delaunay-Based Reach Estimation

Input: $A \subset X$ a finite set of points forming an $\varepsilon-$approximation for a compact, smooth algebraic curve $X \subset \mathbb{R}^2$.

Output: τ, an approximation of the reach.
  Compute a Delaunay triangulation D of A.
  Set $M = \emptyset$.
  for T a Delaunay triangle of D **do**
    Set c_T be the circumcenter of the Delaunay triangle T.
    Set $M = M \cup \{c_T\}$.
  end for
  Set $\tau = \min_{c \in M, a \in A} d(a, c)$.

The approximate methods can be used with curves of higher degree, while the symbolic methods are hard to compute for curves with degrees even as low as 4, but give a more accurate estimate for the reach. This suggests that more work can be done to develop fast and accurate methods to compute the reach of a variety.

Conclusion

In this chapter, we have explored the interplay between data analysis and algebraic geometry. We surveyed tools for modeling point sets with algebraic varieties and determining their dimension, degree, and homology. We showed how algebraic geometry and offset hypersurfaces can inform persistent homology. We proved that Voronoi diagrams of point sets converge to Voronoi cells of varieties and used this fact to develop algorithms for computing metric features, such as the reach, curvature, bottlenecks, and medial axis of plane curves. In the next chapter, we will see how numerical and computational tools can be used to explore algebraic varieties.

Chapter 5

Computational Algebraic Geometry

The past several years have seen rapid development in the speed and efficiency of software used for numerical algebraic geometry. These numerical techniques complement theoretical techniques and unlock possibilities for answering large computational and enumerative questions. In this chapter, we will demonstrate the strength of these numerical tools. In Section 5.1, we use software to show that the degree of a variety is 96120, a large number possible to compute only with recently developed technology. In Section 5.2, we show how computational techniques can be used to explore the variety of symmetric matrices with repeated eigenvalues, combining with theoretical techniques to study its implicit equations, degree, and dimension.

The original work in this chapter comes from two papers. Section 5.1 comes from the paper [46], which is joint work with Laura Brustenga i Moncusí and Sascha Timme. It is published in Le Matematiche. Section 5.2 comes from the single-authored paper [185].

5.1 Using Numerical Algebraic Geometry to Compute Degrees

Automorphism groups of varieties and group actions on varieties are of much interest to researchers of algebraic geometry, arithmetic, and representation theory [7, 48, 145, 181]. Here we study the action of the projective linear group $\mathrm{PGL}(\mathbb{C}, 4)$ on cubic surfaces parameterized by points in $\mathbb{P}_{\mathbb{C}}^{19}$. In particular, we compute the degree of the 15-dimensional projective variety in $\mathbb{P}_{\mathbb{C}}^{19}$ defined by the Zariski closure of the orbit of a general cubic surface under this action. This degree is also meaningful in enumerative geometry: It is the number of translates of a cubic surface that pass through 15 points in general position. This formulation provides an alternate method for obtaining the degree.

Aluffi and Faber considered the analogous problem for plane curves of arbitrary degree, first the smooth case in [7] and then the general case in [8]. They obtained a closed formula for the degree of the orbit closure of a plane curve under the action of $\mathrm{PGL}(\mathbb{C}, 3)$. This was a significant undertaking, involving long and detailed calculations in intersection rings using advanced techniques from intersection theory.

Instead of adopting the techniques developed by Aluffi and Faber, we use tools from *numerical*

algebraic geometry [113, 176]. We refer the reader to Section 1.3 of this dissertation for an introduction to these tools. The general idea is as follows. We fix a cubic surface f and 15 points in general position in $\mathbb{P}^3_{\mathbb{C}}$. The condition that a translate of f passes through these 15 points results in a polynomial system for which we compute all isolated numerical solutions by homotopy continuation and monodromy methods using the software `HomotopyContinuation.jl` [44]. The concept of an *approximate zero* [28] makes precise the definition of a numerical solution. We use Smale's α-theory and the software `alphaCertified` [114] to certify that the obtained numerical solutions indeed satisfy the system of polynomial equations. Finally, we use a *trace test* [141] to check that no solution is missing. With these techniques, we conclude that the number of numerical solutions we obtain, 96120, is in fact the degree of the orbit closure. This result is a "numerical theorem" rather a theorem in the classical sense.

Our presentation is organized as follows. First, we introduce the linear orbit problem in detail and derive the polynomial systems used in our computations. Next, we discuss the techniques used from numerical algebraic geometry and the computations performed to arrive at the result.

Linear Orbits and Polynomial Systems

A cubic surface in $\mathbb{P}^3_{\mathbb{C}}$ is defined by a cubic homogeneous polynomial in 4 variables with complex coefficients. The parameter space for cubic surfaces is $\mathbb{P}^{19}_{\mathbb{C}}$ and we fix coordinates $(c_0 : \cdots : c_{19}) \in \mathbb{P}^{19}_{\mathbb{C}}$.

The projective space $\mathbb{P}^{15}_{\mathbb{C}}$ of homogeneous 4×4 matrices $A = (a_{ij})_{1 \leq i,j \leq 4}$ is a compactification of the projective general linear group

$$\mathrm{PGL}(\mathbb{C}, 4) = \{A \in \mathbb{P}^{15}_{\mathbb{C}} \mid \det A \neq 0\} \subseteq \mathbb{P}^{15}_{\mathbb{C}}.$$

The group $\mathrm{PGL}(\mathbb{C}, 4)$ acts on a cubic surface $f \in \mathbb{P}^{19}_{\mathbb{C}}$, with $\varphi \in \mathrm{PGL}(\mathbb{C}, 4)$ sending f to the cubic surface $\varphi \cdot f$ defined by the equation

$$f(\varphi(x, y, z, w)) = 0.$$

This corresponds to a linear change of the coordinates x, y, z, w. We say that $\varphi \cdot f$ is the *translate* of f by φ. Then $\mathrm{PGL}(\mathbb{C}, 4) \cdot f$ is the orbit of f in $\mathbb{P}^{19}_{\mathbb{C}}$ and its Zariski closure $\Omega_f := \overline{\mathrm{PGL}(\mathbb{C}, 4) \cdot f}$ is a 15-dimensional projective variety.

Example 5.1.1. To illustrate this idea, we consider the action of $\mathrm{PGL}(\mathbb{C}, 2)$ on pairs of points defined by homogeneous polynomials

$$f(x, y) = b_0 x^2 + b_1 xy + b_2 y^2.$$

The parameter space for pairs of points is $\mathbb{P}^2_{\mathbb{C}}$, that is $f = (b_0 : b_1 : b_2) \in \mathbb{P}^2_{\mathbb{C}}$. Let

$$\varphi = \begin{pmatrix} a_{11} & a_{12} \\ a_{21} & a_{22} \end{pmatrix}.$$

Then

$$
\begin{aligned}
f(\varphi(x,y)) &= b_1(a_{11}x + a_{12}y)^2 + b_2(a_{11}x + a_{12}y)(a_{21}x + a_{22}y) + b_3(a_{21}x + a_{22}y)^2 \\
&= (b_1 a_{11}^2 + b_2 a_{11} a_{21} + b_3 a_{21}^2)x^2 + \\
&\quad (2b_1 a_{11} a_{12} + b_2(a_{11}a_{22} + a_{12}a_{21}) + 2b_3 a_{21}a_{22})xy + \\
&\quad (b_1 a_{12}^2 + b_2 a_{12} a_{22} + b_3 a_{22}^2)y^2.
\end{aligned}
$$

and thus

$$
\begin{aligned}
\varphi \cdot f = (&b_1 a_{11}^2 + b_2 a_{11} a_{21} + b_3 a_{21}^2 : \\
&2b_1 a_{11} a_{12} + b_2(a_{11}a_{22} + a_{12}a_{21}) + 2b_3 a_{21}a_{22} : \\
&b_1 a_{12}^2 + b_2 a_{12} a_{22} + b_3 a_{22}^2) \in \mathbb{P}^2_{\mathbb{C}}.
\end{aligned}
$$

To compute the degree of the orbit closure of a general cubic surface under the action of $PGL(\mathbb{C},4)$, we construct as follows polynomial systems whose number of isolated regular solutions correspond to the desired degree.

Fix a general cubic surface $f \in \mathbb{P}^{19}_{\mathbb{C}}$ and a general linear subspace $L \subseteq \mathbb{P}^{19}_{\mathbb{C}}$ of dimension 4, the codimension of Ω_f. Consider the rational map

$$
\Theta_f : \mathbb{P}^{15}_{\mathbb{C}} \longrightarrow \mathbb{P}^{19}_{\mathbb{C}}
$$

sending a 4×4 matrix φ to $\varphi \cdot f$. By definition, the image of Θ_f is Ω_f. By [145, Theorem 5], a generic hypersurface of degree at least three in at least four variables has a trivial stabilizer (we note that in [48, Propostion 7.5] it is stated that the argument in [145] has an error but that it does not affect the correctness of the statement). Hence, the map Θ_f is one-to-one, so the degrees of the zero-dimensional varieties $\Omega_f \cap L$ and $\Theta_f^{-1}(\Omega_f \cap L) = \Theta_f^{-1}(L)$ are equal.

Note that $\Theta_f^{-1}(L)$ includes non-invertible matrices whose kernel does not contain f. But since we assume $L \subseteq \mathbb{P}^{19}_{\mathbb{C}}$ to be general, $\Theta_f^{-1}(L)$ will not intersect the codimension 1 subvariety of $\mathbb{P}^{15}_{\mathbb{C}}$ of matrices with determinant equal to 0.

It follows that the degree of the orbit closure is the number of regular isolated solutions of the polynomial system

$$
\tilde{L}\,\varphi \cdot f = 0 \tag{5.1}
$$

in the entries of $\varphi \in \mathbb{P}^{15}_{\mathbb{C}}$, where $\tilde{L} \in \mathbb{C}^{15 \times 20}$ is a matrix representing the general linear subspace $L \subseteq \mathbb{P}^{19}_{\mathbb{C}}$ of dimension 4.

The degree of Ω_f can be thought of in enumerative terms as the number of translates of f that pass through 15 points $p_1, \dots, p_{15} \in \mathbb{P}^3_{\mathbb{C}}$ in general position. Consider the translated cubic surface $\varphi \cdot f$. Note that $\varphi \cdot f$ passes through a point $p \in \mathbb{P}^3_{\mathbb{C}}$ if and only if $f(\varphi(p)) = 0$. Therefore we obtain the polynomial system

$$
f(\varphi(p_i)) = 0 \,,\ i = 1, \dots, 15 \tag{5.2}
$$

in the entries of $\mathbb{P}^{15}_{\mathbb{C}}$. By Bertini's theorem, we may assume that the hypersurfaces $f(\varphi(p_i)) = 0$ intersect transversally. Hence, the degree of Ω_f is equal to the number of matrices satisfying (5.2).

Formulations (5.1) and (5.2) both result in a system of 15 homogeneous cubic polynomials in the 16 unknowns $(a_{ij})_{1 \leq i,j \leq 4}$, but they have different computational advantages. To perform numerical homotopy continuation, it is beneficial to pass to an affine chart of projective space. This can be done in formulation (5.1) by fixing a coordinate, say adding the polynomial $a_{11} - 1 = 0$. But this introduces artificial solutions. For example, for every solution $\phi \in \mathbb{C}^{16}$, we have that $e^{i\frac{2}{3}\pi}\phi$ and $e^{i\frac{4}{3}\pi}\phi$ are also solutions. The formulation (5.2) does not produce these undesired artificial solutions. However, the formulation (5.1) is better suited for applying the trace test than (5.2).

A Numerical Approach

In this section we explain our use of numerical algebraic geometry to obtain Theorem* 5.1.1 below. Reasonable mathematicians may differ as to whether it is appropriate to state this result as a theorem since we currently cannot certify the last step of our computation. We add the asterisk to acknowledge these differing opinions.

Theorem* 5.1.1. *The degree of the orbit closure of a general cubic surface under the action of* $\mathrm{PGL}(\mathbb{C}, 4)$ *is 96120.*

All computations performed to arrive at this result are available from the authors upon request.

To compute the degree of the orbit closure, we sample a general cubic surface $f \in \mathbb{P}_{\mathbb{C}}^{19}$ by drawing the real and imaginary parts of each of its coordinates independently from a univariate normal distribution. We then solve the polynomial system (5.2) encoding the enumerative geometry problem. A naive strategy is to sample 15 points $p_1, \ldots, p_{15} \in \mathbb{P}_{\mathbb{C}}^3$ in general position and use a total degree homotopy, but in this case the Bézout bound is $3^{15} = 14,348,907$. Here, the monodromy method is substantially more efficient.

To apply the monodromy method, we consider (5.2) as a polynomial system on the entries of φ parameterized by 15 points $p_1, \ldots, p_{15}$ in $\mathbb{P}_{\mathbb{C}}^3$. We consider the incidence variety

$$V = \{(\varphi, (p_1, \ldots, p_{15})) \in \mathbb{P}_{\mathbb{C}}^{15} \times (\mathbb{P}_{\mathbb{C}}^3)^{15} \mid F(\varphi(p_i)) = 0, i = 1, \ldots, 15\}$$

and we denote by π the projection $\mathbb{P}_{\mathbb{C}}^{15} \times (\mathbb{P}_{\mathbb{C}}^3)^{15} \longrightarrow (\mathbb{P}_{\mathbb{C}}^3)^{15}$ restricted to V.

We find a start pair $(\varphi_0; p_1, \ldots, p_{15}) \in V$ and then we use the monodromy action on the fiber $\pi^{-1}(p_1, \ldots, p_{15})$ to find all solutions in this fiber. Such a start pair can be found by exchanging the role of variables and parameters. First, we sample a $\varphi_0 \in \mathbb{P}_{\mathbb{C}}^{15}$ and the first three coordinates of 15 points $p_i \in \mathbb{P}_{\mathbb{C}}^3$ in general position. This yields a system of 15 polynomials each depending only on a unique variable: The *i*th polynomial depends only on the fourth coordinate of p_i. Such a system is easy to solve. Solving it yields a start pair $(\varphi_0; p_1, \ldots, p_{15}) \in V$, on which we run the monodromy method implemented in the software package `HomotopyContinuation.jl` [44]. In less than an hour on a single core, this method found 96120 approximate solutions corresponding to the start points $p_1, \ldots, p_{15} \in \mathbb{P}_{\mathbb{C}}^3$.

Next we apply Smale's α-theory as implemented in the software `alphaCertified` [114] to certify two conditions of our numerical approximations: First, we show that each is indeed an approximate zero to our original polynomial system, and second that all 96120 approximate zeros

have distinct associated zeros. Due to computational limits we were only able to obtain a certificate using (arbitrary precision) floating point arithmetic. Hauenstein and Sottile call this a "soft" certificate since it does not eliminate the possibility of floating point errors. It is preferable to use rational arithmetic for certification, but for a system of our size too much time is required to perform such a computation.

The certification process establishes a *lower* bound on the degree of the orbit closure. As a last step, we run a trace test to verify that we have indeed found *all* solutions. The trace test described in the previous section is only applicable to varieties $W \subset \mathbb{P}^n_{\mathbb{C}}$. In [141] the authors derive a trace test to certify the completeness of a *collection of partial multihomogeneous witness sets*. Our formulation (5.2) provides only one partial multihomogeneous witness set, namely $\pi^{-1}(p_1, \ldots, p_{15})$, and not the entire collection that would be necessary to run a trace test. To avoid these complications, we use formulation (5.1). We note that it is straightforward to construct a linear subspace L from the 15 points $p_1, \ldots, p_{15}$ such that our solutions from the monodromy computation are also solutions to (5.1), so translating formulation (5.2) to (5.1) is not difficult.

In the language of numerical algebraic geometry our 96120 solutions together with the linear subspace L constitute a *pseudo witness set* [112]. We construct a general pencil M_t of linear spaces with $M_0 = L$. Working with approximate solutions refined to around 38 digits of accuracy we obtain for $\text{tr}(1)$ a vector with norm of approximately 10^{-32}. Additionally, increasing the accuracy of the solutions decreases the norm of the trace test result. While this gives us very high certainty that we indeed obtained all solutions, we do not have a rigorous certificate that the trace test converges to zero when we increase the accuracy of the solutions. A certification of the trace test similar to Smale's α-theory for numerical solutions remains an open problem.

From the described computations we conclude that degree of the orbit closure of a general cubic surface under the action $\text{PGL}(\mathbb{C}, 4)$ is 96120.

We note that as a test of our methods, we confirmed known degrees of other varieties. In agreement with a theoretical result of Aluffi and Faber [7], we computed that the degree of the orbit closure of a general quartic curve in the plane is 14280. Additionally we computed that the degree of the orbit closure of the Cayley cubic, defined by the equation $yzw + xzw + xyw + xyz = 0$, is 305. Due to the symmetry of the variables in the Cayley cubic, there are 4! matrices corresponding to every polynomial in the orbit. As expected, we computed $7320 = 4! \cdot 305$ solutions. This coincides with a theoretical result of Vainsencher [181].

5.2 Real Symmetric Matrices with Partitioned Eigenvalues

Let $\lambda = (\lambda_1, \ldots, \lambda_m)$ be a partition of n. Let $\mathbb{R}^{\frac{n(n+1)}{2}}$ be the space of real symmetric $n \times n$ matrices. We define the **variety of λ-partitioned eigenvalues** $V_{\mathbb{R}}(\lambda) \subset \mathbb{R}^{\frac{n(n+1)}{2}}$ to be the Zariski closure of the locus of matrices with eigenvalue multiplicities determined by λ. Since we take the Zariski closure, these varieties include all matrices with eigenvalue multiplicities determined by partitions of n that are coarser than λ.

The space of real symmetric matrices has multiple advantages over the spaces of real square

matrices, complex square matrices, and complex symmetric matrices. Unlike other real matrices, real symmetric matrices have all real eigenvalues. Additionally, the real symmetric case has better properties with respect to diagonalizability than complex square or complex symmetric matrices.

We illustrate these properties with the example of $n = 2, \lambda = (2)$, the locus of 2×2 matrices with coinciding eigenvalues.

Example 5.2.1. Complex 2×2 matrices with the repeated eigenvalue μ can have two Jordan normal forms. The first is diagonal and the second is not. For convenience, call a 2×2 matrix with coinciding eigenvalues type A if its Jordan normal form (JNF) is diagonal and type B otherwise:

$$\text{JNF of a Type A matrix} : \begin{pmatrix} \mu & 0 \\ 0 & \mu \end{pmatrix} \qquad \text{JNF of a Type B matrix} : \begin{pmatrix} \mu & 1 \\ 0 & \mu \end{pmatrix}.$$

We examine the dimensions of the loci of type A and type B matrices in three cases: complex square, complex symmetric, and real symmetric. In each case, the dimension of the locus of type A matrices is 1 because scalar matrices are fixed by conjugation. For complex square matrices, the dimension of the Type B locus is 3. For complex symmetric matrices, the dimension of the Type B locus is 2. Conjugating the JNF of a Type B matrix by any invertible matrix of the form

$$\begin{pmatrix} a & b \\ c & d \end{pmatrix}$$

where $a^2 + c^2 = 0$ yields a symmetric matrix with coinciding eigenvalues. Real symmetric matrices are orthogonally diagonalizable, so the Type B locus for real symmetric matrices is empty.

The significance of these dimensions is as follows. A generic real symmetric matrix with coinciding eigenvalues is diagonalizable and a generic complex square matrix or complex symmetric matrix with coinciding eigenvalues is not. Real symmetric matrices can be studied through their diagonal restrictions.

Matrices with repeated eigenvalues have been studied in contexts from geometry [38] to classical invariant theory and linear algebra [83–85, 123, 135, 159, 164, 178]. Recently, they have come to focus in the study of curvature of algebraic varieties, as in Section 3.2. The *principal curvatures* of a variety are the eigenvalues of the *second fundamental form*. Coincidences of eigenvalues correspond to geometric features; for example, on a surface, a point where the eigenvalues of the second fundamental form coincide is called an *umbilic*. At an umbilic the best second-order approximation of a surface is given by a sphere.

A matrix is called *degenerate* if its eigenvalues are not all distinct. The locus of such matrices is a variety defined by the matrix discriminant. As a polynomial in the eigenvalues, the matrix discriminant is the product of the squared differences of each pair of eigenvalues, and thus it is zero exactly when the eigenvalues are not distinct. To study the variety of degenerate matrices, one considers the discriminant as a polynomial in the entries of the matrix. In [159], Parlett gives an equation for the discriminant of a matrix in its entries by describing it as the determinant of another matrix.

In a refinement of the study of degenerate matrices, some authors [84, 85, 164] have studied matrices by their number of distinct eigenvalues. In this situation, the role of the matrix discriminant is played by the sequence of *k-subdiscriminants*. The 0-subdiscriminant is the usual matrix discriminant. An $n \times n$ matrix has exactly $n - k$ distinct eigenvalues if and only if subdiscriminants 0 through $k - 1$ vanish and the k-subdiscriminant does not. In [164], Roy gives an explicit description of the k-subdiscriminant of the characteristic polynomial of a matrix A in terms of the entries of A. Furthermore, she expresses the k-subdiscriminant as a sum of squares with real coefficients.

In [85], Domokos studies the variety of matrices with a bounded number of distinct eigenvalues from the perspective of invariant theory. This variety can be characterized by its invariance under the action of conjugation by the special orthogonal group on the space of symmetric matrices. He describes the minimal degree homogeneous component of the space of invariants of the variety of matrices with a bounded number of distinct eigenvalues.

The variety of λ-partitioned eigenvalues appears in [24], where Bik and Draisma analyze its properties with respect to distance optimization. In [129], Kozhasov studies the open submanifold of the variety of λ-partitioned eigenvalues where the eigenvalue have exact multiplicities λ. Kozhasov proves that it is a *minimal submanifold* of the space of real symmetric $n \times n$ matrices. A minimal submanifold of a Riemannian manifold is one with zero mean curvature vector field; this generalizes the concept of surfaces in $\mathbb{R}^3$ that locally minimize area.

This section further investigates the variety of λ-partitioned eigenvalues, with each section addressing a different aspect. First, we give a parametrization. Second, we prove a formula for the dimension. Third, we put the parametrization to work to find equations and the degree of this variety for small n. We explain how representation theory can be used to extend these calculations to larger n. We also describe the ring of $SO(n)$-invariants. Lastly, we study the diagonal restriction, computing its degree. We show how the diagonal restriction provides a good model for distance optimization questions regarding the variety of λ-partitioned eigenvalues, presenting a theorem of Bik and Draisma for its Euclidean distance degree.

Parametrization

We now describe a parametrization of the variety of λ-partitioned eigenvalues $V_{\mathbb{R}}(\lambda) \subset \mathbb{R}^{\frac{n(n+1)}{2}}$ by rational functions. Real symmetric matrices are diagonalizable by orthogonal matrices. The orthogonal group is parametrized by the set of skew-symmetric matrices.

Proposition 5.2.2. *Let $\lambda = (\lambda_1, \ldots, \lambda_m)$ be a partition of n and let $Diag(\lambda)$ be a diagonal $n \times n$ matrix with diagonal entries $\mu_1, \ldots, \mu_m$ where each entry μ_i appears with multiplicity λ_i. Let B be a skew-symmetric $n \times n$ matrix. Let I be the $n \times n$ identity matrix. The map*

$$p : \mathbb{R}^{n \times n} \longrightarrow \mathbb{R}^{n \times n}$$

$$B \mapsto (I - B)(I + B)^{-1} Diag(\lambda)(I + B)(I - B)^{-1}$$

is a partial rational parametrization of $V_{\mathbb{R}}(\lambda)$.

Proof. Consider the Cayley transform map from the space $Skew(n)$ of real skew-symmetric $n \times n$ matrices to the orthogonal group $O(n)$ of real $n \times n$ matrices:

$$\text{Cay} : Skew(n) \longrightarrow O(n)$$
$$B \mapsto (I - B)(I + B)^{-1}$$

where I is the $n \times n$ identity matrix. Its image is the set $SO(n)$ of special orthogonal matrices minus those with -1 as an eigenvalue. See [11] for details. A real symmetric matrix A can be written in the form $A = PDP^{-1}$ where P is an orthogonal matrix and D is a diagonal matrix. The entries of D are the eigenvalues of A. □

As the image of the Cayley transform map is just the set $SO(n)$ of special orthogonal matrices minus those with -1 as an eigenvalue, to obtain a fuller parametrization of $V_{\mathbb{R}}(\lambda)$, we use Cay to parametrize $SO(n)$ and swap any two rows in the matrices in $SO(n)$ to obtain orthogonal matrices with determinant -1. The matrices excluded from this method form a subvariety of codimension 1 and thus can be ignored for most numerical calculations. We utilize such a parametrization in the next section.

Dimension

The dimension is an important invariant of any algebraic variety. We now give a formula for the dimension of the variety of λ-partitioned eigenvalues and show how it can be proved using the fact that this variety is the $O(n)$-orbit of a certain form of diagonal matrix. To use the algebraic definition of dimension, we study the complexification of $V_{\mathbb{R}}(\lambda)$, which is characterized by a parametrization.

Theorem 5.2.3. *The real algebraic variety $V_{\mathbb{R}}(\lambda) \subset \mathbb{R}^{\frac{n(n+1)}{2}}$ of $n \times n$ real symmetric matrices in $\mathbb{R}^{\frac{n(n+1)}{2}}$ with eigenvalue multiplicities corresponding to the partition $\lambda = (\lambda_1, \ldots, \lambda_m)$ of n has dimension $m + \binom{n}{2} - \sum_{i=1}^{m} \binom{\lambda_i}{2}$.*

Proof. Every real symmetric matrix A can be written in the form $A = PDP^{-1}$ where P is a real orthogonal matrix and D is a diagonal matrix with diagonal entries equal to the eigenvalues of A. The complexification of $V_{\mathbb{R}}(\lambda)$ consists of matrices of the form $A = PDP^{-1}$ where P is an orthogonal matrix with complex entries and D is a diagonal matrix with entries partitioned by λ. Choose m distinct eigenvalues. Arrange the matrix D so that repeated eigenvalues are grouped together along the diagonal. Scalar matrices commute with all matrices, so the scalar matrix block corresponding to each eigenvalue commutes with the corresponding blocks of P and P^{-1}. Thus any matrix P with orthogonal blocks for each eigenvalue stabilizes D. The dimension of the orthogonal group $O(n)$ is $\binom{n}{2}$. So the dimension of the block orthogonal stabilizer of D is $\sum_{i=1}^{m} \binom{\lambda_i}{2}$. By Proposition 21.4.3 of [180], the dimension of the orbit of a fixed diagonal matrix is $\binom{n}{2} - \sum_{i=1}^{m} \binom{\lambda_i}{2}$. Since there are m choices of eigenvalues, the dimension of the variety of matrices with multiplicities corresponding to λ is as stated. □

Having a formula for the dimension of this variety will help us to find its equations.

Equations

We now discuss how to find equations for the varieties $V_{\mathbb{R}}(\lambda)$. The case $n = 2$ was discussed in the introduction. For $n = 3$ and most partitions of $n = 4$, we use the parametrization from above to generate points on the variety and then use interpolation to find polynomials that vanish on these points. For larger n, the matrices used for interpolation become too large for both our symbolic and numerical methods. We discuss how representation theory can be used to make these computations more feasible. As a first step towards studying the relevant representations, we describe the ring of invariants.

In Examples 5.2.4, 5.2.5 and 5.2.6, we analyze the varieties $V_{\mathbb{R}}(\lambda)$ where λ is a partition of $n = 3$ or $n = 4$. By Theorem 5.2.3, we know the codimension of each variety. We generate points and use interpolation to find equations on those points. We use Macaulay2 [107] to verify that these equations generate a prime ideal of the expected codimension. This confirms that we have indeed found enough equations to generate the desired ideal.

For $n = 4$ and $\lambda = (2, 1, 1)$, our interpolation code found no polynomials of degree less than or equal to 5. As this partition is just the case of degenerate 4×4 matrices, it has been studied by other authors. The ideal is of codimension 2, generated by the (unsquared) summands in a sum of squares representation of the matrix discriminant. Parlett provides an algorithm using determinants for computing this discriminant and writing it as a sum of many squares [159]. Domokos gives a nonconstructive proof that it can be written as a sum of 7 squares [83].

Example 5.2.4. Let $n = 3$ and $\lambda = (2, 1)$. We confirm the findings of other authors that this ideal is of codimension 2 and degree 4 [178, Section 7.5]. It is generated by the following 7 cubic polynomials. The matrix discriminant is the sum of the squares of these polynomials.

$$-x_{11}x_{13}x_{22} + x_{11}x_{13}x_{33} + x_{12}^2 x_{13} - x_{12}x_{22}x_{23} + x_{12}x_{23}x_{33} - x_{13}^3 + x_{13}x_{22}^2 - x_{13}x_{22}x_{33}$$
$$-x_{12}^2 x_{23} + x_{12}x_{13}x_{22} - x_{12}x_{13}x_{33} + x_{13}^2 x_{23}$$
$$-x_{11}x_{13}x_{23} + x_{12}x_{13}^2 - x_{12}x_{23}^2 + x_{13}x_{22}x_{23}$$
$$x_{11}x_{12}x_{23} - x_{11}x_{13}x_{22} + x_{11}x_{13}x_{33} - x_{12}x_{22}x_{23} - x_{13}^3 + x_{13}x_{22}^2 - x_{13}x_{22}x_{33} + x_{13}x_{23}^2$$
$$-x_{11}x_{12}x_{22} + x_{11}x_{12}x_{33} - x_{11}x_{13}x_{23} + x_{12}^3 + x_{12}x_{22}x_{33} - x_{12}x_{23}^2 - x_{12}x_{33}^2 + x_{13}x_{23}x_{33}$$
$$-x_{11}^2 x_{23} + x_{11}x_{12}x_{13} + x_{11}x_{22}x_{23} + x_{11}x_{23}x_{33} - x_{12}^2 x_{23} - x_{12}x_{13}x_{33} - x_{22}x_{23}x_{33} + x_{23}^3$$
$$x_{11}^2 x_{22} - x_{11}^2 x_{33} - x_{11}x_{12}^2 + x_{11}x_{13}^2 - x_{11}x_{22}^2 + x_{11}x_{33}^2 + x_{12}^2 x_{22} - x_{13}^2 x_{33} + x_{22}^2 x_{33} - x_{22}x_{23}^2 - x_{22}x_{33}^2 + x_{23}^2 x_{33}$$

Example 5.2.5. Let $n = 4$ and $\lambda = (3, 1)$. The ideal is of codimension 5 and degree 8. It is generated by the following 10 quadrics:

$$-x_{12}x_{34} + x_{13}x_{24}$$
$$-x_{12}x_{24} + x_{13}x_{34} + x_{14}x_{22} - x_{14}x_{33}$$
$$-x_{12}x_{34} + x_{14}x_{23}$$
$$x_{12}x_{33} - x_{12}x_{44} - x_{13}x_{23} + x_{14}x_{24}$$
$$-x_{12}x_{23} + x_{13}x_{22} - x_{13}x_{44} + x_{14}x_{34}$$
$$x_{11}x_{34} - x_{13}x_{14} - x_{22}x_{34} + x_{23}x_{24}$$
$$x_{11}x_{24} - x_{12}x_{14} + x_{23}x_{34} - x_{24}x_{33}$$
$$-x_{11}x_{33} + x_{11}x_{44} + x_{13}^2 - x_{14}^2 + x_{22}x_{33} - x_{22}x_{44} - x_{23}^2 + x_{24}^2$$
$$x_{11}x_{23} - x_{12}x_{13} - x_{23}x_{44} + x_{24}x_{34}$$
$$-x_{11}x_{22} + x_{11}x_{44} + x_{12}^2 - x_{14}^2 + x_{22}x_{33} - x_{23}^2 - x_{33}x_{44} + x_{34}^2$$

Example 5.2.6. Let $n = 4$ and $\lambda = (2,2)$. The ideal is of codimension 4 and degree 6. It is generated by the following 9 quadrics:

$$x_{11}^2 + 4x_{13}^2 - x_{22}^2 - 4x_{24}^2 - 2x_{11}x_{33} + x_{33}^2 + 2x_{22}x_{44} - x_{44}^2$$
$$x_{11}x_{12} + x_{12}x_{22} + 2x_{13}x_{23} + 2x_{14}x_{24} - x_{12}x_{33} - x_{12}x_{44}$$
$$x_{11}x_{14} - x_{14}x_{22} + 2x_{12}x_{24} - x_{14}x_{33} + 2x_{13}x_{34} + x_{14}x_{44}$$
$$x_{11}x_{13} - x_{13}x_{22} + 2x_{12}x_{23} + x_{13}x_{33} + 2x_{14}x_{34} - x_{13}x_{44}$$
$$-x_{11}^2 - 4x_{14}^2 + x_{22}^2 + 4x_{23}^2 - 2x_{22}x_{33} + x_{33}^2 + 2x_{11}x_{44} - x_{44}^2$$
$$2x_{12}x_{14} - x_{11}x_{24} + x_{22}x_{24} - x_{24}x_{33} + 2x_{23}x_{34} + x_{24}x_{44}$$
$$2x_{12}x_{13} - x_{11}x_{23} + x_{22}x_{23} + x_{23}x_{33} + 2x_{24}x_{34} - x_{23}x_{44}$$
$$-x_{11}^2 - 4x_{12}^2 + 2x_{11}x_{22} - x_{22}^2 + x_{33}^2 + 4x_{34}^2 - 2x_{33}x_{44} + x_{44}^2$$
$$-x_{11}x_{34} + 2x_{13}x_{14} - x_{22}x_{34} + 2x_{23}x_{24} + x_{33}x_{34} + x_{34}x_{44}$$

Naive interpolation strategies, both symbolic and numerical, become infeasible as n increases. To reduce the dimensions of these matrices and make these linear algebra computations more feasible, we turn to representation theory. See [102] and [150, Chapter 10] for details.

The ideal $I(V_{\mathbb{R}}(\lambda))$ is stable under the action by conjugation of the real orthogonal group $SO(n)$ on the space $\mathbb{R}^{\frac{n(n+1)}{2}}$ of real symmetric $n \times n$-matrices. Thus the degree d homogeneous component $I(V_{\mathbb{R}}(\lambda))_d$ is a representation of $SO(n)$. So to find generators of $I(V_{\mathbb{R}}(\lambda))$, we find representations of $SO(n)$. Since $SO(n)$ is reductive, every representation has an *isotypic decomposition* into irreducible representations. While these irreducible representations may be of high dimension, they can be studied through their low-dimensional *highest weight spaces*. We refer the reader to [102, Chapter 26] or [150, Chapter 10] for details.

Here we examine the special case of one-dimensional representations of $SO(n)$. These vector spaces contain polynomials that are themselves invariant under the action of $SO(n)$, rather than simply generating an ideal which is $SO(n)$-stable as an ideal.

Denote by $I(V_{\mathbb{R}}(\lambda))^{SO(n)}$ the graded vector space of $SO(n)$-invariant polynomials in $I(V_{\mathbb{R}}(\lambda))$. Let $V_{\mathbb{R}}(D_\lambda)$ denote the intersection of $V_{\mathbb{R}}(\lambda)$ with the variety of diagonal matrices in $\mathbb{R}^{\frac{n(n+1)}{2}}$. We often identify $V_{\mathbb{R}}(D_\lambda)$ with a variety in $\mathbb{R}^n$. Let $I(V_{\mathbb{R}}(D_\lambda))^{S_n}$ be the graded vector space of S_n-invariant polynomials in $I(V_{\mathbb{R}}(D_\lambda))$.

Theorem 5.2.7. $I(V_{\mathbb{R}}(\lambda))^{SO(n)}$ and $I(V_{\mathbb{R}}(D_\lambda))^{S_n}$ are isomorphic as graded vector spaces.

Proof. Let Sym_n be the space of real symmetric $n \times n$ matrices and Diag_n the subspace of diagonal matrices. Denote by S_n the subgroup of $SO(n)$ of matrices which permute the diagonal entries. Consider the degree-preserving linear map from $\mathbb{R}[\mathrm{Sym}_n]^{SO(n)} \to \mathbb{R}[\mathrm{Diag}_n]^{S_n}$ given by restriction of functions. Every orbit of symmetric matrices under the action of $SO(n)$ contains a diagonal matrix. The stabilizer of the group of diagonal matrices under the action $SO(n)$ is S_n. Thus there is an isomorphism of quotient groups $\mathrm{Sym}_n/SO(n) \cong \mathrm{Diag}_n/S_n$. So the restriction of functions is an isomorphism of graded vector spaces $\mathbb{R}[\mathrm{Sym}_n]^{SO(n)} \cong \mathbb{R}[\mathrm{Diag}_n]^{S_n}$. It induces an isomorphism $I(V_{\mathbb{R}}(\lambda))^{SO(n)} \cong I(V_{\mathbb{R}}(D_\lambda))^{S_n}$. $\qquad \square$

This result is beneficial because $I(V_{\mathbb{R}}(D_\lambda))^{S_n}$ is easier to study than $I(V_{\mathbb{R}}(\lambda))^{SO(n)}$. We thus turn our study to $I(V_{\mathbb{R}}(D_\lambda))$.

Diagonal Matrices

We now study the intersection of the variety of λ-partitioned eigenvalues with the variety of diagonal matrices. Recall that $V_{\mathbb{R}}(D_\lambda)$ denotes the intersection of $V_{\mathbb{R}}(\lambda)$ with the variety of diagonal matrices in $\mathbb{R}^{\frac{n(n+1)}{2}}$. We identify this with the variety in $\mathbb{R}^n$ of points with coordinates that have multiplicities given by the partition λ. Then $V_{\mathbb{R}}(D_\lambda)$ is a union of the $\frac{n!}{\lambda_1!\cdots\lambda_m!}$ subspaces of dimension m given by permuting the coordinates of the subspace

$$V_1 = \{(a_1,\ldots,a_1,a_2,\ldots,a_2,\ldots,a_m,\ldots,a_m) \mid a_i \in \mathbb{R}\}$$

where the coordinate a_i is repeated λ_i times. Characterizing $V_{\mathbb{R}}(D_\lambda)$ as a union of linear spaces reveals its degree.

Proposition 5.2.8. *Let $\lambda = (\lambda_1,\ldots,\lambda_m)$ be a partition of n. The degree of the variety $V_{\mathbb{R}}(D_\lambda)$ of $n \times n$ diagonal matrices with eigenvalue multiplicities partitioned according to λ is*

$$\frac{n!}{\lambda_1!\cdots\lambda_m!}$$

One may ask how well the diagonal restriction of the variety of λ-partitioned eigenvalues models the variety as a whole. With regards to distance optimization, the diagonal restriction is a quite good model. Let $X \subset \mathbb{R}^n$ be a real algebraic variety and $X_{\mathbb{C}} \subset \mathbb{C}^n$ its complexification. Fix $u \in \mathbb{R}^n$. Then the *Euclidean distance degree (EDD)* of X is the number of complex critical points of the squared distance function $d_u(x) = \sum_{i=1}^{n}(u_i - x_i)^2$ on the smooth locus of $X_{\mathbb{C}}$ [86]. It can be shown that this number is constant on a dense open subset of data $u \in \mathbb{R}^n$. In [24], Bik and Draisma prove that the variety of λ-partitioned eigenvalues and its diagonal restriction have the same EDD. The diagonal restriction is a subspace arrangement, so its EDD is its number of distinct maximal subspaces.

Theorem 5.2.9 (Bik and Draisma). *Let $\lambda = (\lambda_1,\ldots,\lambda_m)$. The Euclidean distance degree of the variety $V_{\mathbb{R}}(\lambda)$ of λ-partitioned eigenvalues is $\frac{n!}{\lambda_1!\cdots\lambda_m!}$.*

Conclusion

In this chapter, we have seen how numerical algebraic geometry can be used to answer questions that are harder to approach with theoretical mathematics. We saw how certification techniques can yield numerical theorems. We also made a foray into the study of techniques to pair representation theory with numerical algebraic geometry to answer difficult computational questions.

Bibliography

[1] E. Aamari, F. Chazal, J. Kim, B. Michel, A. Rinaldo, and L. Wasserman: *Estimating the reach of a manifold*, Electronic Journal of Statistics 13(1) (2019) 1359–1399.

[2] E. Aamari and C. Levrard: *Stability and minimax optimality of tangential Delaunay complexes for manifold reconstruction*, Discrete and Computational Geometry 59(4) (2018) 923–971.

[3] H. Adams and A. Tausz: *JavaPlex Tutorial*, http://www.math.colostate.edu/~adams/research/javaplex_tutorial.pdf, Accessed: February 24, 2018.

[4] L. Alberti, G. Comte, and B. Mourrain: *Meshing implicit algebraic surfaces: the smooth case*, Mathematical Methods for Curves and Surfaces: Tromsø 2004, 2005.

[5] Y. Alexandr and A. Heaton: *Logarithmic Voronoi cells*, Algebraic Statistics 12(1) (2021) 75-95.

[6] P. Alliez, D. Cohen-Steiner, Y. Tong, and M. Desbrun: *Voronoi-based variational reconstruction of unoriented point sets*, Proceedings of the Fifth Eurographics Symposium on Geometry Processing, Switzerland, (2007) 39–48 .

[7] P. Aluffi and C. Faber: *Linear orbits of smooth plane curves*, Journal of Algebraic Geometry 2(1) (1993) 155–184.

[8] P. Aluffi and C. Faber: *Linear orbits of arbitrary plane curves*, Michigan Mathematical Journal 48(1) (2000) 1–37.

[9] C. Améndola, J.-C. Faugère, and B. Sturmfels: *Moment varieties of Gaussian mixtures*, Journal of Algebraic Statistics 7 (2016) 14–28.

[10] N. Amenta and M. Bern: *Surface reconstruction by Voronoi filtering*, Discrete and Computational Geometry 22 (4) (1999) 481–504.

[11] D. Andrica and O.L. Chender: *Rodrigues formula for the Cayley transform of groups SO(n) and SE(n)*, Studia Universitatis Babes-Bolyai 60 (2015) 31–38.

[12] E. Arias-Castro, B. Pateiro-López, and A.Rodríguez-Casal: *Minimax estimation of the volume of a set under the rolling ball condition*, Journal of the American Statistical Association 114(527) (2019) 1162–1173.

[13] D. Attali, J. Boissonnat, and H. Edelsbrunner: *Stability and computation of medial axes - a state-of-the-art report*, Springer Berlin Heidelberg, (2009) 109–125.

[14] S. Balakrishnan, A. Rinaldo, D. Sheehy, A. Singh, and L. Wasserman: *Minimax rates for homology inference*, Proceedings of the Fifteenth International Conference on Artificial Intelligence and Statistics, 64–72, Proceedings of Machine Learning Research 22, La Palma, Canary Islands, 2012.

[15] B. Bank, M. Giusti, J. Heintz, and G.M. Mbakop: *Polar varieties and efficient real elimination*, Mathematische Zeitschrift, 238(1) (2001) 115–144.

[16] R. G. Baraniuk and M. B. Wakin: *Random projections of smooth manifolds*, Foundations of Computational Mathematics, 9 (2009) 51–77.

[17] R. Basson, R. Lercier, C. Ritzenthaler, and J. Sijsling: *An explicit expression of the Lüroth invariant*, Proceedings of the 38th International Symposium on Symbolic and Algebraic Computation, 31–36, ACM, New York, 2013.

[18] D. J. Bates, W. Decker, J. D. Hauenstein, C. Peterson, G. Pfister, F. Schreyer, A. J. Sommese, and C. W.Wampler: *Comparison of probabilistic algorithms for analyzing the components of an affine algebraic variety*, Applied Mathematics and Computation, 231(C) (2014) 619–633.

[19] D. J. Bates, D. Eklund, and C. Peterson: *Computing intersection numbers of Chern classes*, Journal of Symbolic Computation 50 (2013) 493 – 507.

[20] D. Bates, J. Hauenstein, A. Sommese, and C. Wampler: *Numerically Solving Polynomial Systems with Bertini*, Software, Environments, and Tools, SIAM, Philadelphia, PA, 2013.

[21] D. Bates, J. Hauenstein, A. Sommese, and C. Wampler: *Bertini: Software for Numerical Algebraic Geometry*, available at `bertini.nd.edu`.

[22] U. Bauer: *Ripser*, available at `https://github.com/Ripser/ripser`.

[23] J. Bezanson, A. Edelman, S. Karpinski, and V. Shah: *Julia: A fresh approach to numerical computing*, SIAM Review 59 (2017) 65–98.

[24] A. Bik and J. Draisma: *A note on ED degrees of group-stable subvarieties in polar representations*, Israel Journal of Mathematics 228 (2018) 353–377.

[25] A. Bjoerck and V. Pereyra: *Solutions of Vandermonde systems of equations*, Mathematics of Computation 24 (1970) 893–903.

[26] G. Blekherman, P. Parrilo, and R. Thomas: *Semidefinite Optimization and Convex Algebraic Geometry*, MOS-SIAM Series on Optimization 13, 2012.

[27] A. Blum: *Random projection, margins, kernels, and feature-selection*, Subspace, Latent Structure and Feature Selection, 52–68, Springer Berlin Heidelberg, 2006.

[28] L. Blum, F. Cucker, M. Shub, and S. Smale: *Complexity and real computation*, Springer Science and Business Media, 1998.

[29] J. Bochnak, M. Coste and M. Roy: *Real Algebraic Geometry*, A Series of Modern Surveys in Mathematics, Springer Berlin Heidelberg, 1998.

[30] J. Boissonnat and A. Ghosh: *Triangulating smooth submanifolds with light scaffolding*, Mathematics in Computer Science 4(4) (2011) 431.

[31] J. Boissonnat and A. Ghosh: *Manifold reconstruction using tangential Delaunay complexes*, Discrete and Computational Geometry 51(1) (2014) 221–267.

[32] J. Boissonnat and S. Oudot: *Provably good sampling and meshing of surfaces*, Graphical Models 67(5) (2005) 405 – 451.

[33] J.W. Brandt: *Convergence and continuity criteria for discrete approximations of the continuous planar skeleton*, CVGIP: Image Understanding 59(1) (1994) 116 – 124.

[34] J.W. Brandt and V.R. Algazi: *Continuous skeleton computation by Voronoi diagram*, CVGIP: Image Understanding 55(3) (1992) 329 – 338.

[35] M. Brandt and M. Weinstein: *Voronoi cells in metric algebraic geometry of plane curves*, arXiv:1906.11337.

[36] M. Brandt and M. Weinstein: *MatheMaddies' ice cream map*, available at `https://www.youtube.com/watch?v=YxMsVByhk34`.

[37] P. Breiding, S. Kališnik, B. Sturmfels, and M. Weinstein: *Learning algebraic varieties from samples*, Revista Mathematica Complutense 31 (2018) 545-593.

[38] P. Breiding, K. Kozhasov, and A. Lerario: *On the geometry of the set of symmetric matrices with repeated eigenvalues*, Arnold Mathematical Journal 4 (2018) 423–443.

[39] P. Breiding and O. Marigliano: *Sampling from the uniform distribution on an algebraic manifold*, SIAM Journal on Mathematics of Data Science 2(2) (2020) 683-704.

[40] P. Breiding, K. Ranestad, and M. Weinstein: *Algebraic geometry of curvature*. In preparation.

[41] P. Breiding, K. Rose, and S. Timme: *Certifying zeros of polynomial systems using interval arithmetic*, arXiv:2011.05000.

[42] P. Breiding, B. Sturmfels, and S. Timme: *3264 conics in a second*, Notices of the American Mathematical Society 67 (2020) 30-37.

[43] P. Breiding and S. Timme: *The reach of a plane curve*, `https://www.JuliaHomotopyContinuation.org/examples/reach-curve/`. Accessed: October 24, 2019.

[44] P. Breiding and S. Timme: *HomotopyContinuation.jl: A package for homotopy continuation in Julia*, International Congress on Mathematical Software (2018) 458-465.

[45] M.W. Brown, S. Martin, S.N. Pollock, E.A. Coutsias, and J.P. Watson: *Algorithmic dimensionality reduction for molecular structure analysis*, Journal of Chemical Physics 129 (2008) 064118.

[46] L. Brustenga i Moncusí, S. Timme, and M. Weinstein: *96120: The Degree of the Linear Orbit of a Cubic Surface*, Le Matematiche 75 (2020) 425-437.

[47] P. Bürgisser, F. Cucker, and P. Lairez: *Computing the homology of basic semialgebraic sets in weak exponential time*, Journal of the Association for Computing Machinery 66(1) (2017).

[48] P. Bürgisser and C. Ikenmeyer: *Fundamental invariants of orbit closures*, Journal of Algebra 477 (2017) 390-434.

[49] P. Bürgisser and M. Lotz: *The complexity of computing the Hilbert polynomial of smooth equidimensonal complex projective varieties*, Foundations of Computational Mathematics 7(1) (2007) 59–86.

[50] F. Camastra: *Data dimensionality estimation methods: a survey*, Pattern Recognition 36 (2003) 2945–2954.

[51] F. Camastra and A. Staiano: *Intrinsic dimension estimation: Advances and open problems*, Information Sciences 328 (2016) 26–41.

[52] G. Carlsson: *Topology and data*, Bulletin of the American Mathematical Society 46 (2009) 255-308.

[53] E. Cartan: *Les Systèmes Extérieurs et leurs Applications Géométriques*, Hermann, 1945.

[54] A.L. Cauchy: *Leçons sur les applications du calcul infinitésimal à la géométrie*, De Bure (1826).

[55] T. Çelik, A. Jamneshan, G. Montúfar, B. Sturmfels, and L. Venturello: *Wasserstein Distance to Independence Models*, Journal of Symbolic Computation 104 (2021) 855-873.

[56] T.R. Chen, T.L. Lee, and T.Y. Li: *HOM4PS-3: A Numerical Solver for Polynomial Systems Using Homotopy Continuation Methods*, available at `hom4ps3.org`.

[57] D. Cifuentes, S. Agarwal, P. Parrilo, and R. Thomas: *On the local stability of semidefinite relaxations*, arXiv:1710.04287.

[58] D. Cifuentes, C. Harris, and B. Sturmfels: *The geometry of SDP-exactness in quadratic optimization*, Mathematical Programming 182 (2020) 399-428.

[59] D. Cifuentes and P. Parrilo: *Sampling algebraic varieties for sum of squares programs*, SIAM Journal on Optimization 27 (2017) 2381–2404.

[60] D. Cifuentes, K. Ranestad, B. Sturmfels, and M. Weinstein: *Voronoi Cells of Varieties*, Journal of Symbolic Computation (2021).

[61] D. Ciripoi, N. Kaihnsa, A. Löhne, and B. Sturmfels: *Computing convex hulls of trajectories*, Revista de la Unión Matemática Argentina 60 (2019) 637-662.

[62] K.L. Clarkson: *Tighter bounds for random projections of manifolds*, Proceedings of the Twenty-fourth Annual Symposium on Computational Geometry, 39–48, New York, 2008.

[63] D. Cohen-Steiner and J. Morvan: *Restricted Delaunay triangulations and normal cycle*, Proceedings of the Nineteenth Annual Symposium on Computational Geometry, 312–321, New York, 2003.

[64] D. Cox, J. Little, and D. O'Shea: *Ideals, Varieties, and Algorithms: An Introduction to Computational Algebraic Geometry and Commutative Algebra*, fourth edition, Undergraduate Texts in Mathematics, Springer, 2015.

[65] M.A. Cueto, J. Morton, and B. Sturmfels: *Geometry of the restricted Boltzmann machine*, Algebraic Methods in Statistics and Probability, American Mathematical Society, Contemporary Mathematics 516 (2010) 135-153.

[66] A. Cuevas, R. Fraiman, and A. Rodríguez-Casal: *A nonparametric approach to the estimation of lengths and surface areas*, Annals of Statistics 35 (3) (2007) 1031-1051.

[67] N. Daleo and J. Hauenstein: *Numerically deciding the arithmetically Cohen-Macaulayness of a projective scheme*, Journal of Symbolic Computation 72 (2016) 128–146.

[68] S. Dasgupta and A. Gupta: *An elementary proof of a theorem of Johnson and Lindenstrauss*, Random Structures and Algorithms 22(1) (2003) 60–65.

[69] Apollonius de Perge. *Apollonius de Perge, Coniques. Tome 3: Livre V*, volume 1/3 of *Scientia Graeco-Arabica*. Walter de Gruyter & Co., Berlin, 2008. Greek and Arabic text established, translated and annotated under the direction of Roshdi Rashed, Historical and mathematical commentary, edition and translation of the Arabic text by Rashed.

[70] A.M. del Campo and J.I. Rodriguez: *Critical points via monodromy and local methods*, Journal of Symbolic Computation 79(3) (2017) 559-574.

[71] H. Delfts and M. Knebusch: *On the homology of algebraic varieties over real closed fields*, Journal für die reine und angewandte Mathematik 335 (1982) 122-163.

[72] J.W. Demmel: *Applied Numerical Linear Algebra*, SIAM, Philadelphia, 1997.

[73] H. Derksen: *Hilbert series of subspace arrangements*, Journal of Pure and Applied Algebra 209 (2007) 91–98.

[74] T.K. Dey and W. Zhao: *Approximate medial axis as a Voronoi subcomplex*, Proceedings of the Seventh ACM Symposium on Solid Modeling and Applications, 356–366, New York, 2002.

[75] M. Deza and M. Laurent: *Geometry of Cuts and Metrics*, Algorithms and Combinatorics 15, Springer-Verlag, Berlin, 1997.

[76] S. Di Rocco, D. Eklund, and C. Peterson: *Numerical polar calculus and cohomology of line bundles*, Advances in Applied Mathematics 100 (2017) 148–162.

[77] S. Di Rocco, D. Eklund, C. Peterson, and A. J. Sommese: *Chern numbers of smooth varieties via homotopy continuation and intersection theory*, Journal of Symbolic Computation 46(1) (2011) 23–33.

[78] S. Di Rocco, D. Eklund, and M. Weinstein: *A Macaulay2 script to compute bottleneck degree*, available at https://bitbucket.org/daek/bottleneck_script.

[79] S. Di Rocco, D. Eklund, and M. Weinstein: *The bottleneck degree of algebraic varieties*, SIAM Journal of Applied Algebra and Geometry 4 (2020) 227-253.

[80] P. Diaconis, S. Holmes, and M. Shahshahani: *Sampling from a manifold*, Institute of Mathematical Statistics Collections 10 (2013) 102–125.

[81] M. Díaz, A. Quiroz, and M. Velasco: *Local angles and dimension estimation from data on manifolds*, Journal of Multivariate Analysis (2019) 229-247.

[82] M.P. do Carmo and F. Flaherty: *Riemannian Geometry*, Mathematics: Theory & Applications, Birkhäuser Boston, 2013.

[83] M. Domokos: *Discriminant of symmetric matrices as a sum of squares and the orthogonal group*, Communications of Pure and Applied Mathematics 64 (2011) 443–465.

[84] M. Domokos: *Hermitian matrices with a bounded number of eigenvalues*, Linear Algebra and its Applications 12 (2013) 3964–3979.

[85] M. Domokos: *Invariant theoretic characterization of subdiscriminants of matrices*, Linear and Multilinear Algebra 62 (2014) 63–72.

[86] J. Draisma, E. Horobeţ, G. Ottaviani, B. Sturmfels, and R. Thomas: *The Euclidean distance degree of an algebraic variety*, Foundations of Computational Mathematics 16 (2016) 99–149.

[87] M. Drton, B. Sturmfels, and S. Sullivant: *Lectures on Algebraic Statistics*, Oberwolfach Seminars, 39, Birkhäuser Verlag, Basel, 2009.

[88] D. Drusvyatskiy, H. Lee, G. Ottaviani, and R.R. Thomas: *The Euclidean distance degree of orthogonally invariant matrix varieties*, Israel Journal of Mathematics 221 (2017) 291–316.

[89] T. Duff, C. Hill, A. Jensen, K. Lee, A. Leykin, and J. Sommars: *Solving polynomial systems via homotopy continuation and monodromy*, IMA Journal of Numerical Analysis 39 (3) (2018) 1421-1446.

[90] E. Dufresne, P. Edwards, H. Harrington, and J. Hauenstein: *Sampling real algebraic varieties for topological data analysis*, 2019 18th IEEE International Conference on Machine Learning and Applications (ICMLA) 1531-1536 (2020).

[91] H. Edelsbrunner and J. Harer: *Computational Topology: An Introduction*, American Mathematical Society, 2010.

[92] D. Eisenbud and J. Harris: *3264 and All That: A Second Course in Algebraic Geometry*, Cambridge University Press, first edition, 2016.

[93] D. Eklund: *The numerical algebraic geometry of bottlenecks*, arXiv:1804.01015.

[94] D. Eklund, C. Jost, and C. Peterson: *A method to compute Segre classes of subschemes of projective space*, Journal of Algebra and Its Applications 12(02) (2013).

[95] G. Elber and K. Myung-Soo: *Bisector curves of planar rational curves*, Computer-Aided Design 30(14) (1998) 1089-1096.

[96] R.T. Farouki and J.K. Johnstone: *The bisector of a point and a plane parametric curve*, Computer Aided Geometric Design 1(2) (1994) 117-151.

[97] H. Federer: *Curvature measures*, Transactions of the American Mathematical Society 93 (1959) 418-491.

[98] M. Fiedler, *Additive compound matrices and an inequality for eigenvalues of symmetric stochastic matrices*, Czechoslovak Mathematical Journal 24(3) (1974) 392-402.

[99] D. Fuchs and S. Tabachnikov: *Mathematical Omnibus: Thirty Lectures on Classic Mathematics*, American Mathematical Society, 2007.

[100] W. Fulton: *Introduction to Toric Varieties*, Princeton University Press, 1993.

[101] W. Fulton: *Intersection Theory*, Springer, second edition, 1998.

[102] W. Fulton and J. Harris: *Representation Theory: A First Course*, Graduate Texts in Mathematics, Springer New York, 1991.

[103] C.R. Genovese, M. Perone-Pacifico, I. Verdinelli, and L. Wasserman: *Minimax manifold estimation*, Journal of Machine Learning Research 13 (2012) 1263–1291.

[104] R. Ghrist: *Barcodes: The persistent topology of data*, Bulletin of the American Mathematical Society 45 (2008) 61-75.

[105] P. Giblin and B.B. Kimia: *On the local form and transitions of symmetry sets, medial axes, and shocks*, International Journal of Computer Vision 54(1) (2003) 143-147.

[106] D. Grayson, M. Stillman, S.A. Strømme, D. Eisenbud, and C. Crissman: *Schubert2: computations of characteristic classes for varieties without equations. Version 0.7*, available at `https://github.com/Macaulay2/M2/tree/master/M2/Macaulay2/packages`.

[107] D. Grayson and M. Stillman: *Macaulay2, a software system for research in algebraic geometry*, available at `www.math.uiuc.edu/Macaulay2/`.

[108] Z. Griffin, J. Hauenstein, C. Peterson, and A. Sommese: *Numerical computation of the Hilbert function and regularity of a zero dimensional scheme*, Connections between Algebra, Combinatorics, and Geometry, 235–250, Springer Proceedings in Mathematics and Statistics 76, Springer, New York, 2014.

[109] P. Griffiths and J. Harris: *Algebraic Geometry and Local Differential Geometry*, Annales Scientifiques de l'École Normale Supérieure 12 (1979) 355-452.

[110] D. Halperin, M. Kerber, and D. Shaharabani, *The offset filtration of convex objects*, Algorithms-ESA 2015, Springer Berlin Heidelberg, 2015, 705–716.

[111] J. Harris: *Algebraic Geometry. A First Course*, Graduate Texts in Mathematics 133, Springer-Verlag, New York, 1992.

[112] J.D. Hauenstein and A.J. Sommese: *Witness sets of projections*, Applied Mathematics and Computation 217(7) (2010) 3349-3354.

[113] J.D. Hauenstein and A.J. Sommese: *What is numerical algebraic geometry?*, Journal of Symbolic Computation 79 (2017) 99-507.

[114] J.D. Hauenstein and F. Sottile: *Algorithm 921: alphaCertified: certifying solutions to polynomial systems*, ACM Transactions on Mathematical Software 38 (4) (2012).

[115] C. Hegde, M. Wakin, and R. Baraniuk: *Random projections for manifold learning*, Advances in Neural Information Processing Systems 20 (2008) 641–648.

[116] U. Helmke and M.A. Shayman: *Critical points of matrix least square distance functions*, System Structure and Control (1992) 116-118.

[117] G. Henselman and R. Ghrist: *Matroid filtrations and computational persistent homology*, arXiv:1606.00199.

[118] N. Higham: *Accuracy and Stability of Numerical Algorithms*, SIAM, second edition, 2002.

[119] E. Horobeţ: *The critical curvature degree of an algebraic variety*, arXiv:2104.01124.

[120] E. Horobeţ and M. Weinstein: *Offset hypersurfaces and persistent homology of algebraic varieties*, Computer-Aided Geometric Design 74 (2019) 101767.

[121] R. Howard: *The kinematic formula in Riemannian homogeneous spaces*, Memoirs of the American Mathematical Society 106 (1993) 509.

[122] J.E. Humphreys: *Introduction to Lie Algebras and Representation Theory*, Graduate Texts in Mathematics, Springer New York, 2012.

[123] N.V. Ilyushechkin: *The discriminant of the characteristic polynomial of a normal matrix*, Matematicheskie Zametki 51 (3) (1992) 16-23; translation in Mathematical Notes 51 (3-4) (1992) 230-235.

[124] A. Jain and R. Dubes: *Algorithms for Clustering Data*, Prentice-Hall, Upper Saddle River, NJ, 1998.

[125] K.W. Johnson: *Immersion and embedding of projective varieties*, Acta Mathematica 140 (1978) 49–74.

[126] M. Joswig and T. Theobald: *Polyhedral and algebraic methods in computational geometry*, Universitext, Springer, London, 2013. Revised and updated translation of the 2008 German original.

[127] J. Kileel, Z. Kukelova, T. Pajdla, and B. Sturmfels: *Distortion varieties*, Foundations of Computational Mathematics 18 (2018) 1043-1071.

[128] A. K. H. Kim and H. H. Zhou: *Tight minimax rates for manifold estimation under Hausdorff loss*, Electronic Journal of Statistics 9(1) (2015) 1562-1582.

[129] K. Kozhasov: *On minimality of determinantal varieties*, arXiv:2003.01049.

[130] Zuzana Kukelova, M. Byröd, K. Josephson, T. Pajdla, and K. Åström: *Fast and robust numerical solutions to minimal problems for cameras with radial distortion*, Computer Vision and Image Understanding 114(2) (2010) 234 – 244.

[131] M. Kummer and C. Vinzant: *The Chow form of a reciprocal linear space*, Michigan Mathematics Journal 68(4) (2019) 831-858.

[132] D. Laksov: *Residual intersections and Todd's formula for the double locus of a morphism*, Acta Mathematica 140 (1978) 75–92.

[133] J.M. Landsberg: *Tensors: Geometry and Applications*, Graduate Studies in Mathematics 128, American Mathematical Society, Providence, RI, 2012.

[134] J.B. Lasserre: *An Introduction to Polynomial and Semi-Algebraic Optimization*, Cambridge Texts in Applied Mathematics, Cambridge University Press, 2015.

[135] P.D. Lax: *On the discriminant of real symmetric matrices*, Communications of Pure and Applied Mathematics 51 (1998) 1387-1396.

[136] J.M. Lee: *Riemannian Manifolds: Introduction to Curvature*, Springer Verlag, 1997.

[137] J.A. Lee and M. Verleysen: *Nonlinear Dimensionality Reduction*, Information Science and Statistics, Springer Verlag, New York, 2007.

[138] K. Leichtweiss: *Zur Riemannschen Geometrie in Grassmannschen Mannigfaltigkeiten*, Mathematische Zeitschrift 76 (1961) 334–366.

[139] E. Levina and P. Bickel: *Maximum likelihood estimation of intrinsic dimension*, Advances in Neural Information Processing Systems 17 (2004) 777–784.

[140] A. Leykin: *Numerical Algebraic Geometry for Macaulay2*, available at `people.math.gatech.edu/~aleykin2/NAG4M2`.

[141] A. Leykin, J.I. Rodriguez, and F. Sottile: *Trace test*, Arnold Mathematical Journal 4(1) (2018) 113-125.

[142] Y. Ma, A. Yang, H. Derksen, and R. Fossum: *Estimation of subspace arrangements with applications in modeling and segmenting mixed data*, SIAM Review 50 (2008) 413–458.

[143] S. Martin, A. Thompson, E. A. Coutsias, and J. P. Watson: *Topology of cyclo-octane energy landscape*, Journal of Chemical Physics 132 (2010) 234115.

[144] G. Matheron: *Random sets and integral geometry*, Wiley Series in Probability and Mathematical Statistics, New York, Wiley, 1987.

[145] H. Matsumura and P. Monsky: *On the automorphisms of hypersurfaces*, Journal of Mathematics of Kyoto University 3 (1963/1964) 347-361.

[146] R.D. McKelvey and A. McLennan: *The maximal number of regular totally mixed Nash equilibria*, Journal of Economic Theory 72(2) (1997) 411 – 425.

[147] D. Mehta, T. Chen, T. Tang, and J.D. Hauenstein: *The loss surface of deep linear networks viewed through the algebraic geometry lens*, arXiv:1810.07716.

[148] Q. Merigot, M. Ovsjanikov, and L.J. Guibas: *Voronoi-based curvature and feature estimation from point clouds*, IEEE Transactions on Visualization and Computer Graphics 17(6) (2011) 743–756.

[149] F. Mezzadri: *How to generate matrices from the classical compact groups*, Notices of the American Mathematical Society 54 (2007) 592–604.

[150] M. Michałek and B. Sturmfels: *Invitation to Nonlinear Algebra*, Graduate Studies in Mathematics, American Mathematical Society, 2021.

[151] M. Minimair and M.P. Barnett: *Solving polynomial equations for chemical problems using Gröbner bases*, Molecular Physics 102(23-24) (2004) 2521–2535.

[152] H. Möller and B. Buchberger: *The construction of multivariate polynomials with preassigned zeros*, Computer Algebra (Marseille 1982), 24–31, Lecture Notes in Computer Science 144, Springer, Berlin, 1982.

[153] M. Mustaţă: *Graded Betti numbers of general finite subsets of points on projective varieties*, Pragmatic 1997, Matematiche (Catania) 53 (1998) 53–81.

[154] M. Nagata: *Remarks on a paper of Zariski on the purity of branch-loci*, Proceedings of the National Academy of Sciences 44 (8) (1958) 796-799.

[155] P. Niyogi, S. Smale, and S. Weinberger: *Finding the homology of submanifolds with high confidence from random samples*, Discrete and Computational Geometry 39 (2008) 419–441.

[156] P.J. Olver: *On multivariate interpolation*, Studies in Applied Mathematics 116 (2006) 201–240.

[157] G. Ottaviani and L. Sodomaco: *The distance function from a real algebraic variety*, Computer Aided Geometric Design 82 (2020) 101927.

[158] V.Y. Pan: *How bad are Vandermonde matrices?*, SIAM Journal on Matrix Analysis and Applications 37(2) (2016) 676–694.

[159] B. Parlett: *The (matrix) discriminant as a determinant*, Linear Algebra and its Applications 355 (2002) 85–101.

[160] The Pattern Analysis Lab at Colorado State University: *A fractal dimension for measures via persistent homology*, Preprint, 2018.

[161] R. Piene: *Polar classes of singular varieties*, Annales Scientifiques de l'École Normale Supérieure, 4(11) (1978) 247–276.

[162] R. Piene: *Polar varieties revisited*, Lecture Notes in Computer Science: Computer algebra and polynomials 8942 (2015) 139–150.

[163] D. Plaumann, B. Sturmfels, and C. Vinzant: *Quartic curves and their bitangents*, Journal of Symbolic Computation 46 (2011) 712–733.

[164] M.F. Roy: *Subdiscriminants of symmetric matrices are sums of squares*, Mathematics, Algorithms, Proofs, Dagstuhl Seminar Proceedings 05021, Internationales Begegnungs und Forschungszentrum für Informatik (IBFI), Schloss Dagstuhl, Germany, 2005.

[165] M. Safey El Din and P. Spaenlehauer: *Critical point computations on smooth varieties: Degree and complexity bounds*, Proceedings of the ACM on International Symposium on Symbolic and Algebraic Computation, 183–190, New York, 2016.

[166] G. Salmon: *A Treatise on Conic Sections Containing an Account of Some Important Algebraic and Geometric Methods*, Hodges and Smith, 1848.

[167] G. Salmon: *A Treatise on the Higher Plane Curves*, Hodges and Smith, 1852.

[168] G. Salmon: *A Treatise on the Analytic Geometry of Three Dimensions*, Hodges, Smith, and Company, 1865.

[169] F. San Segundo and J.R. Sendra: *Degree formulae for offset curves*, Journal of Pure and Applied Algebra 195(3) (2005) 301-335.

[170] F. San Segundo and J.R. Sendra: *Partial degree formulae for plane offset curves*, Journal of Symbolic Computation 44(6) (2009) 635-654.

[171] F. San Segundo and J.R. Sendra: *Total degree formula for the generic offset to a parametric surface*, International Journal of Algebra and Computation 22(2) (2012) 1250013.

[172] L. Santalo: *Integral Geometry and Geometric Probability*, Addison-Wesley, 1976.

[173] J.R. Sendra and J. Sendra: *Algebraic analysis of offsets to hypersurfaces*, Mathematische Zeitschrift 234(4) (2000) 697-719.

[174] M. Shub and S. Smale: *Complexity of Bézout's theorem. I. Geometric aspects*, Journal of the American Mathematical Society 6(2) (1993) 459-501.

[175] S. Smale: *Newton's Method Estimates from Data at One Point*, The Merging of Disciplines: New Directions in Pure, Applied, and Computational Mathematics, 185-196, Springer New York, 1986.

[176] A.J. Sommese and C.W. Wampler: *The Numerical Solution of Systems of Polynomials Arising in Engineering and Science*, World Scientific, 2005.

[177] E. Spanier: *Algebraic Topology*, Springer Verlag, 1966.

[178] B. Sturmfels: *Solving Systems of Polynomial Equations*, Conference Board of the Mathematical Sciences, 2002.

[179] B. Sturmfels and V. Welker: *Commutative algebra of statistical ranking*, Journal of Algebra 361 (2012) 264–286.

[180] P. Tauvel and R.W.T. Yu: *Lie Algebras and Algebraic Groups*, Springer Monographs in Mathematics, Springer Verlag, 2005.

[181] I. Vainsencher: *Hypersurfaces with up to Six Double Points*, Communications in Algebra 31 (8) (2003) 4107-4129.

[182] N. Verma: *A note on random projections for preserving paths on a manifold*, UC San Diego, Tech. Report CS2011-0971, 2011.

[183] Victoria school districts. http://melbourneschoolzones.com/.

[184] C.W. Wampler and A.J. Sommese: *Numerical algebraic geometry and algebraic kinematics*, Acta Numerica 20 (2011) 469–567.

[185] M. Weinstein: *Real symmetric matrices with partitioned eigenvalues*, arXiv:2008.08554.

[186] Wolfram Research, Inc. Mathematica, Version 12.0. Champaign, IL, 2019.

[187] O. Zariski: *On the purity of the branch locus of algebraic functions*, Proceedings of the National Academy of Sciences 44(8) (1958) 791-796.

[188] A. Zomorodian and G. Carlsson: *Computing persistent homology*, Discrete and Computational Geometry 33(2)(2005) 247-274.